UC Berkeley

UC Berkeley Electronic Theses and Dissertations

Title

Fine-scale Environmental Variation in Mountain Landscapes: Quantitative approaches, influences on tree recruitment, and implications for scientific visualization

Permalink

https://escholarship.org/uc/item/80142362

Author

Christianson, Danielle Svehla

Publication Date

2016

Supplemental Material

https://escholarship.org/uc/item/80142362#supplemental

Peer reviewed|Thesis/dissertation

eScholarship.org Powered by the California Digital Library
University of California

Fine-scale Environmental Variation in Mountain Landscapes: Quantitative approaches, influences on tree recruitment, and implications for scientific visualization

by

Danielle Svehla Christianson

A dissertation submitted in partial satisfaction of the

requirements for the degree of

Doctor of Philosophy

in

Energy and Resources

and the Designated Emphasis

in

New Media

in the

Graduate Division

of the

University of California, Berkeley

Committee in charge:

Professor John Harte, Chair
Doctor Lara M. Kueppers
Professor Cari G. Kaufman
Professor Abigail De Kosnik

Spring 2016

Abstract

Fine-scale Environmental Variation in Mountain Landscapes:
Quantitative approaches, influences on tree recruitment, and implications for scientific visualization

by

Danielle Svehla Christianson

Doctor of Philosophy in Energy and Resources with Designated Emphasis in New Media

University of California, Berkeley

Professor John Harte, Chair

Individual organisms respond to environmental conditions that they experience on fine spatial and temporal scales, on the order of meters and hours. For example, a tree seedling lives or dies depending on local conditions, such as freezing temperatures on a spring morning, dry soils and air in the late summer, or a gopher that finds newly grown leaf tissue tasty. The persistence of a species depends on the collective survival of individuals throughout time and at various locations in space. To be of practical use to resource managers and policy makers, tools that inform human action and non-action with regard to other species, and the ecological processes that connect us, must operate at coarse spatial (10-100s km) and temporal (years-decades) scales and be applicable to many species. A core task then is to link ecological phenomena across spatiotemporal scales.

An understanding of fine-scale environs and their influence on organisms is necessary to address this challenge, but it is lacking. A primary focus of my research is to characterize (1) the fine-scale environs (1-meter and hourly resolution) over relatively large extents (1 continuous hectare), and (2) their influence on individual organisms. I chose to study mountainous systems because fine-scale environmental descriptions in these highly complex landscapes are few. Additionally, I focused on spatiotemporal characterization of fine-scale heterogeneity as it is increasingly being used, with average conditions, to explain ecological phenomena.

In chapter 1, I systematically studied the effects of sampling designs and landscape features on a measure of fine-scale heterogeneity. I found that appropriate sampling designs can reduce error in estimating fine-scale heterogeneity on complex landscapes. In chapter 2, I report that temporal patterns in fine-scale spatial heterogeneity are consistent across four mountainous landscapes and are highly variable both daily and seasonally. For some environmental quantities, aggregated temporal metrics do not adequately represent fine-scale heterogeneity. In chapter 3, I investigated the influences of fine-scale environmental conditions on the occupancy patterns of tree seedlings. Individual tree seedlings are influenced by fine-scale abiotic and biotic environmental conditions. However, the mechanism for some biotic interactions may occur indirectly via fine-scale abiotic influences. I recommend making this distinction to enable advances in coarse-scale modeling tools. In chapter 4, I questioned how new visualizations of the natural world based on fine-scale data shape ecological practice. Such visualizations enable lively novel interactions that may lead to new insight. Ecologists should approach such practice with an understanding of how these new, often highly technical, visualizations shape knowledge generation for themselves individually and the community as a whole.

To my friends, the trees: may we humans understand you as companion species.

Table of Contents

Introduction: Toward an understanding of ecological phenomena across space and time 1

Chapter 1: Effects of sample design and landscape features on a measure of environmental heterogeneity 7

Chapter 2: Towards a biologically meaningful climate characterization: spatial heterogeneity of temperature at multiple temporal scales 28

Chapter 3: Untangling influences on tree seedling establishment at fine spatial scales: abiotic and biotic factors explain seedling occupancy patterns 45

Chapter 4: 01100110 01101111 01110010 01100101 01110011 01110100 [forest] 69

Conclusion: Projecting fine-scale heterogeneity in future climates 105

Appendix A: Supplemental information for Chapter 1 122

Appendix B: Supplemental information for Chapter 2 138

Appendix C: Supplemental information for Chapter 3 149

Appendix D: Supplemental information for Chapter 4 173

Appendix E: Supplemental information for Conclusions 175

Acknowledgements

This research was supported by US Department of Energy Office of Science (BER), National Park Service (NPS) Californian Cooperative Ecosystem Unit, a NPS George Melendez Wright Climate Change Fellowship, National Science Foundation Graduate Fellowship, Berkeley Atmospheric Science Center Graduate Fellowship, UC Berkeley Philomathia Graduate Student Fellowship in the Environmental Sciences, and Energy and Resources Group Block Grants. Maptek provided an educational license for its I-Site Studio Software. Sierra Nevada Research Institute proved logistical support at the Wolverton Field Station / Sequoia & Kings Canyon National Parks (SEKI). UC Davis KeckCAVES provided access to its CAVE.

I am indebted to many individuals whose support in the form of an encouraging word, a thoughtful critique, hours of mind-numbing data entry, loans of rare or prohibitively expensive equipment, physical exertion in trying mountain climates, or provision of chocolate has helped make this dissertation and my graduate studies possible. There are so many of you! Thank you! I would be remiss if I didn't recognize the specific contributions of the following wonderful colleagues, friends, and family.

Thank you to Nate Stephenson and Phil van Mantgem for encouraging my initial ideas in SEKI and setting me up with logistical support primarily in the form of Kim Bollens who can make anything happen. Also to Adrian Das who answered all my questions regarding the USGS's neighboring study and said "hi" back during my initial days in Hilgard Hall. Thank you to Angela Evenden, who provided critical funds. My thanks to Anne Hopkins Pfaff, Tyler Johnson, and Koren Nydick for additional logistical support at SEKI. A special thank you to Athena Demetry, who in addition to offering logistical support, kindly lent me her total station.

My research experience at SEKI is profoundly shaped by the SEKI trail crews, who welcomed me into their lives. Their laid-back perspectives, hard work, and occasional drama kept me sane for 8 summers. In particular, thank you to James Dukich, Daniel Reddick, and Sam Wellin for spending some of their time off helping me at my field site.

My crew of talented and dedicated undergraduate researchers was indispensible in helping with data entry and portions of analysis. Each kept me on my toes and brought new perspectives to my primary research questions. Thank you to Mina Choi, Levon Dovlatyan, Erin Gelfat, Quinn Miller, Marco Paliza-Carre, and Yekun Wang.

The research presented in this dissertation could absolutely not exist without several amazing individuals who agreed to help me at my SEKI field site. Their positive attitudes, tireless work ethics, and ability to persevere difficult environments kept me going. Thank you to Stacy and Keith Jackson, Yekun Wang, Cleo Woelfe-Erskine, and Adam B. Smith for weekend-long assistance. Thank you to Toby J. Minear for an intense three days scanning my study site with terrestrial laser scanning. Thank you to Travis Kay-Rugen, Jessica Simms, Vicki Zhuang, Oriana Chafe, and Meera Lee Sethi for your dedication over many, many long days during the course of the field seasons. A special thank you to Jack Gedney for enduring two seasons with me, teaching me how to be a better naturalist, and debating the best and worst of science fiction. And also a special thank you to Sarah Richmond, who was steadfast in her optimism, stamina, advice, and excellent conversation during the critical first year of setting up the project in the field.

Several colleagues were especially supportive: Maya Hayden, my weekly "just write a paragraph" writing buddy and partner in figuring out soil moisture calibration; Christina Castahna, who taught me about soil litter profiles and freeze dryers and how to be kick-ass in the field; Erin Conlisk, who

gave critical feedback on multiple drafts, helped me learn how to think more creatively, and provided a source of perspective and joy; Laurie Koteen, who took a chance on an engineer for a field assistant, taught me how to conduct quality field work, and has been a source of encouragement throughout my graduate career; Manisha Anantharaman, whose keen intellect I aspire to emulate and who was always available for advice and encouragement; Alenda Chang, who encouraged me to consider the New Media DE and validated my existence pursuing it; Meredith Tromble, who also encouraged me to critically examine the use of New Media in my ecological studies; and Cleo Woelfle-Erskine, who serves as constant inspiration to be an interdisciplinary scholar exploring ecological phenomena and questioning our ethical responsibilities in doing so.

A very special thank you to Anna and Joe Kantenbacher, who not only encouraged necessary breaks to toss a Frisbee or save the world from imminent pandemics, but also provided intellectual and nutritional substance and were excellent craftspersons in helping to make the potential evaporation radiation shields. Additionally, to Anna for helping me plan how to complete this dissertation successfully and for excellent critique of and suggestions for chapter 4.

Adam B. Smith also receives my gratitude not only for improving several chapters of this dissertation but also for his unconditional support throughout my graduate studies: the lively discussion about a new-to-us paper, hammering out an analysis approach, working through statistical conundrums, counting endless serpentine plants, a reassuring hug at the end of a tough day, and lots of dark chocolate M&Ms.

Thank you to the Harte Lab for providing a safe place to explore ideas and making excellent suggestions for improvement. Thank you to my Hilgard officemates in particular: Laurie Koteen, Asmeret Asefaw Berhe, Susan Cary, Erin Conlisk, Adam B. Smith, Uthara Srinivasan, and Teresa Chang during my early years in the lab, and to Jade Zheng, Andy Rominger, Chloe Lewis, Meredith Jabis, Manisha Anantharaman, and Lydia Vaughn in the latter. A particular thank you to Stacy Jackson for keeping me on the bike during the middle schlog and to Lydia Vaughn and Adrienne Marshall for keeping me hiking through this last push!

Thank you also to the ERG community at large. It is humbling to be a member, and I am inspired everyday by the work of my ERG colleagues. Thank you to ERG Women's group, which has been an important and special source of collegiality especially during the last few years of my graduate experience. Thank you to Dick Norggard and Isha Ray who through their advising made me feel like a valued member of ERG. Thank you to the incredible ERG staff, especially Jane Youn and Lee Borrowman who assisted with logistics of my field work, to Sandra Dovali who always put a smile on my face, and to Kay Burns whose support in navigating the University is unparalleled as is her tireless commitment to making sure we are succeeding as people in addition to scholars.

I thank Margaret Torn for mentoring me throughout my graduate studies, giving me my first GSR, supporting my SEKI project when I was out of funds in 2010, and providing a model for how to be a thoughtful and creative scientist. Thank you to Gail De Kosnik for taking me on in my final year and offering encouragement alongside practical strategic advise.

I made two pivotal decisions during my graduate career. One was to audit Cari Kaufman's spatial statistics class. I had no idea that it would lead to one of the most enjoyable collaborations of my life thus far. Thank you to Cari for patiently teaching me statistics, for listening to my nitpicky analysis concerns and helping find ways to solve them, for the super fun collaborative seed rain analysis, and for encouraging me to be my own scientist through thoughtful example.

The second was to seek out Lara Kueppers at UC Merced. She welcomed me into her group, suggested that her USGS collaborators talk with me about potential projects in SEKI, and along with Margaret offered me my first GSR. Thank you to Lara for thinking through the small details of field work with me while always keeping the overarching idea in focus, for always finding me a source of funding support, for exemplifying critical thinking across multiple disciplines, and for providing an example of the type of scientist I hope to be.

Thank you to John Harte for taking a chance on me, for never faltering in support of me academically or personally, for challenging me to think more critically and to improve my writing skills. And also for teaching me how to be an effective teacher and then offering me the chance to do so. I am honored to be of his academic lineage.

And to my family. Many thanks to my mother-in-law, Cherry, who encouraged me with letters, emails, and texts containing can-do pick-me-ups. And also to my father-in-law, Doug, who edited nearly all of this dissertation, for his genuine interest in the details of my research.

To my sister Breanne, who never let me forget that I could do this, who found time to enter data for me while bringing a beautiful new person into this world, and who continues to inspire me to be a smart, professional working woman.

Who knew that one's parents could be a critical component of completing graduate school and a dissertation? I'm incredibly grateful for their continued support in making me a better person and holding me up during the challenging moments. My parents, Rick and Bonnie, went far beyond, editing drafts, entering data, and coming to the field twice(!), which entailed hiking 3 miles 1000' elevation change each way to my site, recording pages of seedling measurement data as I yelled it out from the study plot, digging out soil moisture tubes in the snow, surviving bear encounters, and keeping me fed. I'm so grateful. Thank you.

To my life partner, Eric, who has supported this adventure from the start and endured the ups and downs. Thank you for diffusing several panicked situations with your keen perspective or an extra set of hands and for several trips to SEKI to help with various field tasks. I look forward to the next adventure with you at my side.

And finally, thank you to the organisms and land that I investigated in my SEKI project for tolerating my presence and prodding and for giving me some really beautiful moments.

Introduction: Toward an understanding of ecological phenomena across space and time

Ecology, the study of relationships between living organisms and the physical environment, is challenging in part because many interactions span multiple spatial and temporal scales [Levin 1992]. Ecologists often draw study boundaries in time and space to understand individual phenomenon, which can lead to different scale-specific conclusions [Wiens 1989]. Sub-disciplines, like macroecology, have made important progress in linking ecological phenomena across multiple spatial scales (*e.g.,* metabolic scaling theory [Brown *et al.* 2004] and maximum entropy theory of ecology [Harte 2011]). To link phenomena mechanistically across space and time, frameworks have been proposed [Denny and Benedetti-Cecchi 2012]; however, much work remains [Urban 2005, Jackson 2009, Clark *et al.* 2011, Potter *et al.* 2013].

Linking processes that occur at fine scales to emergent dynamics that can be measured at coarse scales is of particular interest for practical application [Urban 2005, Wiens and Blanchet 2010]. For example, current and future species geographical ranges over regional (10-100s km) and larger spatial extents are useful to resource managers for biodiversity conservation, resource availability, and cultural use [Watson *et al.* 2012, Guisan *et al.* 2013]. Several tools have been developed to estimate species ranges, including climate envelope, dynamic vegetation, and forest gap models[1] [Acevedo *et al.* 1995, Stich *et al.* 2005, Perry and Millington 2008, Franklin 2010, Snell *et al.* 2014]. All of these models take a coarse-scale, top-down approach with typical spatial resolutions at 1km (or larger) and temporal resolutions of months to years. In other words, they utilize coarse-scale observations to project coarse-scale dynamics, ignoring fine-scale processes. This methodology yields useful information but these methodologies have been widely critiqued [*e.g.,* Bugmann 2001, Thuiller *et al.* 2008, Wiens *et al.* 2009, Quillet *et al.* 2010, Pappas *et al.* 2015]. And recent studies suggest that inclusion of fine-scale processes changes projections of species ranges [Trivedi *et al.* 2008, Ashcroft *et al.* 2009, Randin *et al.* 2009, Gillingham *et al.* 2012].

Many commonly used mechanistic modeling approaches are based on niche theory, which postulates that a set of definable conditions determines where a viable species population can occur on the landscape. Current authors consider a species' niche to be defined by abiotic (physical environmental) characteristics, biotic (species) interactions, and dispersal limitations [Soberón 2007, Peterson *et al.* 2011]. According to niche theory, fine-scale environmental conditions as well as biotic interactions determine fine-scale occupancy patterns of individuals, while coarse-scale climatic conditions and dispersal limitations describe species geographic ranges over large spatial extents. Thus, approaches like climate envelope, dynamic vegetation, and forest gap models use coarse-scale climatic metrics to project current and future species geographical distributions.

A key element in linking ecological phenomena across scales is whether there is variation, or heterogeneity, in the phenomena themselves or its mechanistic components at finer scales. Continuing with the example of projecting species geographical ranges, heterogeneity in abiotic environmental conditions on the order of meters and hours is of interest for many species, like

[1] Multiple forest gap models are linked together in transition models to project change across large extents [Acevedo *et al.* 1995].

plants, that are thought to respond as individuals to these local conditions [Clarke *et al.* 2011]. If fine-scale heterogeneity does not occur in space or time, then coarse-scale climatic metrics may adequately represent fine scale conditions that influence individuals. However, the influence of climatic conditions may differ at different spatiotemporal scales. In this case, it is important to (1) determine the scales at which influences differ and (2) investigate why. On the other hand, if heterogeneity in fine-scale conditions does occur, the spatial and temporal patterns of the heterogeneity needs to be characterized. For example, refugia have provided locations for species persistence during climatic change because their fine-scale environmental conditions differ from typical surrounding conditions [Dobrowski 2011, Keppel and Wardell-Johnson 2012]. The potential for refugia, *i.e.,* heterogeneity in environmental conditions, to maintain species diversity in future climates is a motivating factor for conservation calls to preserve heterogeneous environs [Lawler *et al.* 2015]. To do so effectively, we need to first quantify environmental heterogeneity across spatial and temporal scales and also determine to what spatiotemporal scales species are responding.

With recent advances in sensor technologies, ecologists have begun to quantify finer scale environs. Researchers have documented differences from coarse-scale data products, like commonly used PRISM and DAYMET interpolated weather station data [*e.g.,* Ashcroft *et al.* 2009], and the influence of fine-scale conditions on species [*e.g.,* Fridley *et al.* 2009]. Despite finer sampling frequency, observational measurements are still discrete samples of continuous quantities that are often autocorrelated or contain gradient patterns. For example, near-surface temperatures in a forest are often patchy following the sun / shade patterns of the forest canopy*, i.e.,* the temperature values are autocorrelated within patches. Soil moisture often gradually increases more-or-less monotonically when approaching a stream, *i.e.,* there is a gradient pattern in the soil moisture. These types of patterns, illustrated here in space but that can also occur in time, are problematic for accurately quantifying heterogeneity. Commonly employed sampling designs and statistical tools separate heterogeneity in temperature, for example, due to autocorrelation and gradient patterns from metrics of variation like variance and standard deviation. However, to be ecologically useful, measures of heterogeneity should represent all temperature heterogeneity on the landscape, no matter what its source. In chapter 1, I investigate the effects of sampling design and landscape features on a measure of heterogeneity. I derive an analytical approach to estimating the expected sampling error and systematically explore different sampling designs with a simulation study.

Mountainous landscapes are ecosystems in which fine-scale environmental heterogeneity is likely to be high. Complex terrain with steep elevation gains and fine-scale topographic features (slope and aspect) affect the energy balance and hydrological dynamics of the physical system [Barry 1992, Geiger *et al.* 2009]. Fine-scale disconnections from macro-scale weather patterns also occur amongst the heterogeneous surface features (*e.g.,* cold air pooling) [Lunquist *et al.* 2008]. In addition, mountain vegetation, especially forests, influence fine-scale environmental conditions [Chen *et al.* 1999, Van Pelt and Franklin 2000, Geiger *et al.* 2009, de Frenne *et al.* 2013, Ford *et al.* 2013, von Arx *et al.* 2013]. While researchers have begun to characterize fine-scale heterogeneity, a useful framework for understanding temporal dynamics of heterogeneity as well as comparisons across mountain systems are lacking. I address these issues in chapter 2, using four empirical studies in the Colorado Rocky Mountains and Californian Sierra Nevada.

Since ecologists are only now beginning to quantify fine-scale conditions, the next steps are to determine if heterogeneity in these conditions matters to organisms and ecological processes. It is thought that individual organisms respond to their local fine-scale environments [Clark *et al.* 2011, Potter *et al.* 2013, Harwood *et al.* 2014]. The fine-scale environment is especially important for sessile species such as plants that cannot avoid unfavorable conditions through movement. Additionally, all

plant species must survive fine-scale conditions, at least at the early life stages that are often most sensitive. Thus, the regeneration niche may differ than that of the adult individual [Grubb 1977]. Many tree species, with vast size differences between seedling and adult individuals, not only have different life history niches [Lenoir *et al.* 2009, McLaughlin and Zavaleta 2012, Bell *et al.* 2013, Dobrowski *et al.* 2015] but also likely experience environmental conditions at different spatial scales. Thus, understanding how tree seedlings are influenced by fine-scale abiotic conditions is critical to better understand current landscape patterns of tree species, in addition to projecting future patterns. In chapter 3, I begin this work with an observational study in the red fir forest of the Californian Sierra Nevada. I measured fine-scale environmental conditions at 225 locations within a hectare study site and tracked 3,500 red fir seedlings over 5 years to understand fine-scale abiotic influences on current seedling occupancy patterns.

With newly available technologies and goals of quantifying fine-scale ecological phenomena, ecologists are starting to collect "big data" both in time and space [Hampton *et al.* 2013]. My research follows this trend as I collected over 2 million empirical observations using established ecological field-based methods in a spatially dense sampling design. Additionally, I collected approximately 87 million observations with terrestrial laser scanning, a relatively new technology with which I created a 3D representation of my forest study site. As this trend of big data grows, new ways of collecting, analyzing, and visualizing such massive amounts of data will become common methodologies. It is likely that most new methodologies will be highly technical and include new forms of representation, such as the laser scanning technologies and associated digital 3D analysis and visualization platforms. How will these new practices change the study of ecology? Will all the changes be advantageous? Science Technology Studies (STS) scholars have described the importance of representation, especially visual representation, in scientific study [Latour 1990, Bowker 2008, Vertesi 2014, Myers 2014]. As these representations have become more technologically based, STS scholars have critiqued their use, urging scientists to engage in ethical ways that lead to more objective perspectives and ultimately richer understandings [Haraway 1991, Barad 2003]. In chapter 4, using terrestrial laser scanning as a case study of a new scientific visualization practice, I assess the potential for new ecological insights as well as the potential risks that the ecological community will eventually need to address to fully harness the advantages of new scientific representations.

My overarching aim with my dissertation research is to link ecological phenomena across spatiotemporal scales. I have laid a foundation for this endeavor through my study of fine-scale environmental heterogeneity in mountain landscapes. In the concluding chapter, I conduct a thought experiment in which I link fine-scale climatic heterogeneity to coarse-scale heterogeneity. In doing so, I generate hypotheses about the fate of fine-scale heterogeneity over large extents in future climates. Additionally, I map out a framework for future work to more fully link fine-scale interactions between individuals and their local environs with coarse-scale patterns of species geographical distributions.

References

Acevedo, M.F., Urban, D.L. & Ablan, M. (1995). Transition and gap models of forest dynamics. *Ecological Applications*.

Arx, von, G., Graf Pannatier, E., Thimonier, A. & Rebetez, M. (2013). Microclimate in forests with varying leaf area index and soil moisture: potential implications for seedling establishment in a changing climate. *Journal of Ecology*, **101**, 1201–1213.

Ashcroft, M.B., Chisholm, L.A. & French, K.O. (2009). Climate change at the landscape scale: predicting fine-grained spatial heterogeneity in warming and potential refugia for vegetation. *Global Change Biology*, **15**, 656–667.

Barad, K. (2003). Posthumanist Performativity: Toward an Understanding of How Matter Comes to Matter. *Signs: Journal of Women in Culture and Society*, **28**, 801–831.

Barry, R.G. (1992). *Mountain Weather and Climate*, 2nd edn. Routledge.

Bell, D.M., Bradford, J.B. & Lauenroth, W.K. (2013). Early indicators of change: divergent climate envelopes between tree life stages imply range shifts in the western United States. *Global Ecology and Biogeography*, **23**, 168–180.

Bowker, G.C. (2008). *Memory Practices in the Sciences*. MIT Press (MA).

Brown, J.H., Gillooly, J.F., Allen, A.P., Savage, V.M. & West, G.B. (2004). Toward a metabolic theory of ecology. *Ecology*.

Bugmann, H. (2001). A review of forest gap models. *Climatic Change*.

Chen, J.Q., Saunders, S.C., Crow, T.R., Naiman, R.J., Brosofske, K.D., Mroz, G.D., Brookshire, B.L. & Franklin, J.F. (1999). Microclimate in forest ecosystem and landscape ecology - Variations in local climate can be used to monitor and compare the effects of different management regimes. *Bioscience*, **49**, 288–297.

Clark, J.S., Bell, D.M., Hersh, M.H., Kwit, M.C., Moran, E., Salk, C., Stine, A., Valle, D. & Zhu, K. (2011). Individual-scale variation, species-scale differences: inference needed to understand diversity. *Ecology Letters*, **14**, 1273–1287.

De Frenne, P., Rodríguez-Sánchez, F., Coomes, D.A., Baeten, L., Verstraeten, G., Vellend, M., Bernhardt-Roemermann, M., Brown, C.D., Brunet, J., Cornelis, J., Decocq, G.M., Dierschke, H., Eriksson, O., Gilliam, F.S., Hedl, R., Heinken, T., Hermy, M., Hommel, P., Jenkins, M.A., Kelly, D.L., Kirby, K.J., Mitchell, F.J.G., Naaf, T., Newman, M., Peterken, G., Petřík, P., Schultz, J., Sonnier, G., Van Calster, H., Waller, D.M., Walther, G.-R., White, P.S., Woods, K.D., Wulf, M., Graae, B.J. & Verheyen, K. (2013). Microclimate moderates plant responses to macroclimate warming. *Proceedings of the National Academy of Sciences*, **110**, 18561–18565.

Denny, M. & Benedetti-Cecchi, L. (2012). Scaling Up in Ecology: Mechanistic Approaches. *Annual Review of Ecology, Evolution, and Systematics*, **43**, 1–22.

Dobrowski, S.Z. (2011). A climatic basis for microrefugia: the influence of terrain on climate. *Global Change Biology*, **17**, 1022–1035.

Ford, K.R., Ettinger, A.K., Lundquist, J.D., Raleigh, M.S. & Hille Ris Lambers, J. (2013). Spatial Heterogeneity in Ecologically Important Climate Variables at Coarse and Fine Scales in a High-Snow Mountain Landscape (F. de Bello, Ed.). *PLoS ONE*, **8**, e65008–13.

Franklin, J. (2010). *Mapping Species Distributions*. Cambridge University Press.

Fridley, J.D. (2009). Downscaling Climate over Complex Terrain: High Finescale (<1000 m) Spatial Variation of Near-Ground Temperatures in a Montane Forested Landscape (Great Smoky

Mountains). *Journal of Applied Meteorology and Climatology*, **48**, 1033–1049.

Geiger, R., Aron, R.H. & Todhunter, P. (2009). *The Climate Near the Ground*. Rowman & Littlefield Publishers, Inc, Plymouth, United Kindom.

Gillingham, P.K., Huntley, B., Kunin, W.E. & Thomas, C.D. (2012). The effect of spatial resolution on projected responses to climate warming. *Diversity and Distributions*, **18**, 990–1000.

Grubb, P.J. (1977). Maintenance of Species-Richness in Plant Communities - Importance of Regeneration Niche. *Biological Reviews of the Cambridge Philosophical Society*, **52**, 107–145.

Guisan, A., Tingley, R., Baumgartner, J.B., Naujokaitis-Lewis, I., Sutcliffe, P.R., Tulloch, A.I.T., Regan, T.J., Brotons, L., McDonald-Madden, E., Mantyka-Pringle, C., Martin, T.G., Rhodes, J.R., Maggini, R., Setterfield, S.A., Elith, J., Schwartz, M.W., Wintle, B.A., Broennimann, O., Austin, M., Ferrier, S., Kearney, M.R., Possingham, H.P. & Buckley, Y.M. (2013). Predicting species distributions for conservation decisions (H. Arita, Ed.). *Ecology Letters*, **16**, 1424–1435.Hampton, S.E., Strasser, C.A., Tewksbury, J.J., Gram, W.K., Budden, A.E., Batcheller, A.L., Duke, C.S. & Porter, J.H. (2013). Big data and the future of ecology. *Frontiers in Ecology and the Environment*, **11**, 156–162.

Haraway, D.J. (2013). Situated Knowledges. *Simians, Cyborgs, and Women*, pp. 183–202. The Science Question in Feminism and the Privelege of Partial Perspective. Routledge.

Harte, J. (2011). *Maximum Entropy and Ecology*. Oxford University Press.

Harwood, T.D., Mokany, K. & Paini, D.R. (2014). Microclimate is integral to the modeling of plant responses to macroclimate: Fig. 1. *Proceedings of the National Academy of Sciences*, **111**, E1164–E1165.

Jackson, S.T., Betancourt, J.L., Booth, R.K. & Gray, S.T. (2009). Ecology and the ratchet of events: Climate variability, niche dimensions, and species distributions. *Proceedings of the National Academy of Sciences*, **106**, 19685–19692.

Keppel, G. & Wardell-Johnson, G.W. (2012). Refugia: keys to climate change management. *Global Change Biology*, **18**, 2389–2391.

Latour, B. (1990). Drawing things together. *Representation in Scientific Practice* (eds M. Lynch & S. Woolgar), pp. 19–68. MIT Press.

Lawler, J.J., Ackerly, D.D., Albano, C.M., Anderson, M.G., Dobrowski, S.Z., Gill, J.L., Heller, N.E., Pressey, R.L., Sanderson, E.W. & Weiss, S.B. (2015). The theory behind, and the challenges of, conserving nature's stage in a time of rapid change. *Conservation Biology*, **29**, 618–629.

Lenoir, J., Gégout, J.-C., Pierrat, J.-C., Bontemps, J.-D. & Dhôte, J.-F. (2009). Differences between tree species seedling and adult altitudinal distribution in mountain forests during the recent warm period (1986-2006). *Ecography*, **32**, 765–777.

Levin, S.A. (1992). The Problem of Pattern and Scale in Ecology. *Ecology*, **73**, 1943–1967.

Lundquist, J.D., Pepin, N. & Rochford, C. (2008). Automated algorithm for mapping regions of cold-air pooling in complex terrain. *Journal of Geophysical Research*, **113**, D22107–15.

Mclaughlin, B.C. & Zavaleta, E.S. (2012). Predicting species responses to climate change: demography and climate microrefugia in California valley oak (Quercus lobata). *Global Change Biology*, **18**, 2301–2312.

Myers, N. (2014). Rendering Machinic Life. *Representation in Scientific Practice Revisited*, pp. 153–175. MIT Press.

Pappas, C., Fatichi, S., Rimkus, S., Burlando, P. & Huber, M.O. (2015). The role of local-scale heterogeneities in terrestrial ecosystem modeling. *Journal of Geophysical Research: Biogeosciences*, **120**,

341–360.

Perry, G.L.W. & Millington, J.D.A. (2008). Spatial modelling of succession-disturbance dynamics in forest ecosystems: Concepts and examples. *Perspectives in Plant Ecology, Evolution and Systematics*, **9**, 191–210.

Peterson, A.T., Soberón, J., Pearson, R.G., Anderson, R.P., Martínez-Meyer, E., Nakamura, M. & Araújo, M.B. (2011). *Ecological Niches and Geographic Distributions (MPB-49)*. Princeton University Press.

Potter, K.A., Arthur Woods, H. & Pincebourde, S. (2013). Microclimatic challenges in global change biology. *Global Change Biology*, **19**, 2932–2939.

Quillet, A., Peng, C. & Garneau, M. (2010). Toward dynamic global vegetation models for simulating vegetation–climate interactions and feedbacks: recent developments, limitations, and future challenges. *Environmental Reviews*, **18**, 333–353.

Randin, C.F., Engler, R., Normand, S., Zappa, M., Zimmermann, N.E., Pearman, P.B., Vittoz, P., Thuiller, W. & Guisan, A. (2009). Climate change and plant distribution: local models predict high-elevation persistence. *Global Change Biology*, **15**, 1557–1569.

Sitch, S., Huntingford, C., Gedney, N., Levy, P.E., Lomas, M., Piao, S.L., Betts, R., Ciais, P., Cox, P., Friedlingstein, P., Jones, C.D., Prentice, I.C. & Woodward, F.I. (2008). Evaluation of the terrestrial carbon cycle, future plant geography and climate-carbon cycle feedbacks using five Dynamic Global Vegetation Models (DGVMs). *Global Change Biology*, **14**, 2015–2039.

Snell, R.S., Huth, A., Nabel, J.E.M.S., Bocedi, G., Travis, J.M.J., Gravel, D., Bugmann, H., Gutiérrez, A.G., Hickler, T., Higgins, S.I., Reineking, B., Scherstjanoi, M., Zurbriggen, N. & Lischke, H. (2014). Using dynamic vegetation models to simulate plant range shifts. *Ecography*, **37**, 1184–1197.

Soberón, J. (2007). Grinnellian and Eltonian niches and geographic distributions of species. *Ecology Letters*, **10**, 1115–1123.

Thuiller, W., Albert, C., Araújo, M.B., Berry, P.M., Cabeza, M., Guisan, A., Hickler, T., Midgley, G.F., Paterson, J., Schurr, F.M., Sykes, M.T. & Zimmermann, N.E. (2008). Predicting global change impacts on plant species' distributions: Future challenges. *Perspectives in Plant Ecology, Evolution and Systematics*, **9**, 137–152.

Trivedi, M.R., Berry, P.M., Morecroft, M.D. & Dawson, T.P. (2008). Spatial scale affects bioclimate model projections of climate change impacts on mountain plants. *Global Change Biology*, **14**, 1089–1103.

Van Pelt, R. & Franklin, J.F. (2000). Influence of canopy structure on the understory environment in tall, old-growth, conifer forests. *Canadian Journal of Forest Research-Revue Canadienne De Recherche Forestiere*, **30**, 1231–1245.

Vertesi, J. (2014). Drawing as: Distinctions and Disambiguation in Digital Images of Mars. *Representation in Scientific Practice Revisited*, pp. 15–35. MIT Press.

Watson, J.E.M., Rao, M., Ai-Li, K. & Yan, X. (2012). Climate Change Adaptation Planning for Biodiversity Conservation: A Review. *Advances in Climate Change Research*, **3**, 1–11.

Wiens, J.A. (1989). Spatial scaling in ecology. *Functional Ecology*, **3**, 385.

Wiens, J.A. & Bachelet, D. (2010). Matching the Multiple Scales of Conservation with the Multiple Scales of Climate Change. *Conservation Biology*, **24**, 51–62.

Wiens, J.A., Stralberg, D., Jongsomjit, D., Howell, C.A. & Snyder, M.A. (2009). Niches, models, and climate change: Assessing the assumptions and uncertainties. *Proceedings of the National Academy of Sciences*, **106**, 19729–19736.

Chapter 1: Effects of sample design and landscape features on a measure of environmental heterogeneity

1.1 Environmental heterogeneity, an important influence on organisms and ecological processes, can be quantified by the variance of an environmental characteristic over all locations within a study extent. However on landscapes with autocorrelation and gradient patterns, estimating this variance from a sample of locations may lead to errors that cannot be corrected with statistical techniques.

1.2 We analytically derived the relative expected sampling error of sample designs on landscapes with particular gradient pattern and autocorrelation features. We applied this closed-form approach to temperature observations from an existing study. The expected heterogeneity differed, both in magnitude and direction, amongst sample designs over the study site's likely range of autocorrelation and gradient features.

1.3-1.4 We conducted a simulation study to understand the effects of (1) landscape variability and (2) design variability on an average sampling error. On 10,000 simulated landscapes with varying gradient and autocorrelation features, we compared estimates of variance from a variety of structured and random sample designs. While gradient patterns and autocorrelation cause large errors for some designs, others yield near-zero average sampling error. Sample location spacing is a key factor in sample design performance. Random designs have larger range of possible sampling errors than structured designs due to the potential for sample arrangements that over- and under-sample certain areas of the landscape.

1.5 When implementing a new sample design to quantify environmental heterogeneity via variance, we recommend using a simple structured design with appropriate sample spacing. For existing designs, we recommend calculating the relative expected sampling error via our analytical derivation.

1.1 Introduction

Environmental heterogeneity, a measure of variability in abiotic and biotic conditions, is important to many areas of ecological study, such as species diversity via niche theory [Holdridge 1947, Whitaker 1956], microbial biogeochemical processes [*e.g.,* Fierer *et al.* 2006, Sierra *et al.* 2011], and population dynamics [*e.g.,* Garcia-Carreras and Reuman 2013]. Increasingly, ecologists use environmental heterogeneity to understand how organisms and ecological processes may respond to a warmer future [*e.g.,* Jentsch *et al.* 2011, Clark *et al.* 2013, Thornton *et al.* 2014]. For example, heterogeneity in climate over small spatial scales results in climate refugia that may be of critical importance to the persistence of species with limited options for range expansion [Dobrowski 2011, Keppel and Wardell-Johnson 2012]. Additionally, while many organisms optimize for average conditions, heterogeneity is important for understanding when and how likely thresholds (*e.g.,* frost tolerances, heat stress, *etc.*) may be breached [Meehl *et al.* 2000, Jentsch and Beierkuhnlein 2008].

This chapter was written in a style for publication with advisor Cari G. Kaufman. Thus, I use "we."
All Tables and Figures with prefix "A" can be found in Appendix A.

There are many definitions of heterogeneity. Some authors simply define a range of values, while others include aspects of scale, quantify spatial features such as clumping, or qualitatively describe composition [Kolasa and Rollo 1991, Wiens 2000]. Quantitative metrics include coefficient of variance (standard deviation/mean), variance/mean ratio, variograms and others [reviewed by Downing 1991]. To be useful in many ecological applications, such a metric must describe the range of available environmental conditions, either in space or time. For example, consider a population of trees whose seeds disperse on the landscape. To maintain a viable population, there must be an adequate number of locations on the landscape through time that have environmental conditions suitable for the seeds to germinate and the resulting seedlings to survive. By quantifying the available set of environmental conditions, we can determine whether the environments for successful germination and establishment exist and thus predict whether early life history stages will limit population viability.

Accurately estimating heterogeneity, however, is not straightforward when sampling autocorrelated quantities that may also have gradient patterns, a gradual directional change. To account for autocorrelation or gradients, ecologists employ a combination of sample designs [Dutilleul 2011] and well-developed statistical tools, including techniques such as analysis of variance [Dutilleul 1993, Legendre *et al.* 2004], spatial regression analysis [reviewed by Beale *et al.* 2010], and the classical geostatistic metrics like Moran's I, correlograms, and variograms [Legendre 1993]. Researchers also employ methods from spatial statistics, modeling the distribution of an environmental characteristic with heterogeneity due to gradient patterns modeled in the mean and heterogeneity due to autocorrelation modeled in an autocorrelation matrix [Cressie 1993]. However, these traditional methods that *account* for autocorrelation and gradient patterns are not sufficient to *quantify* the metric of our choice, which we will now describe.

Consider an environmental characteristic, Y, that varies across the landscape, for example air temperature at 2m height. Although Y may vary continuously across a broad region, we restrict our attention to a particular geographical area and spatial scale. We call the geographical area the *extent* and define the spatial scale by dividing the landscape into gridcells, whose resolution we refer to as the *grain*. The grain is ideally chosen such that heterogeneity at the chosen scale is appropriate to the organism or process under study, *i.e.,* heterogeneity on a finer spatial scale is not practically important. In reality, however, the appropriate spatial scale may be unknown or variable, for example due to multiple scales of influence [Dutilleul 2011] and life history change [Wiens 2000]. For the purposes of this paper, we assess spatial heterogeneity only, defining Y as a representative value (*e.g.,* mean, minimum, *etc.*) over a period of time or at a single point in time. More broadly, the same exercise and issues can be applied to temporal heterogeneity.

To quantify the variability of available conditions on the landscape, we define heterogeneity as the variance of Y across all gridcells, which we call the complete variance, V_N. We can calculate V_N if we observe Y at all N gridcell locations. In addition, this calculation assumes that measurement error is negligible relative to variation across the landscape, so that V_N is essentially the "true" quantification of the heterogeneity. This quantity might also be thought of as the variance of an "empirical distribution" consisting of all values across the grid, as illustrated in Figure 1.1a. For specific landscape parameterizations used in this and all subsequent figures see Table A1. Measuring environmental quantities at every gridcell location, however, is rarely possible, and we typically cannot calculate the complete variance exactly. Instead, we observe the environmental characteristic at a restricted set of locations in a sample design, estimating the complete variance, V_N,

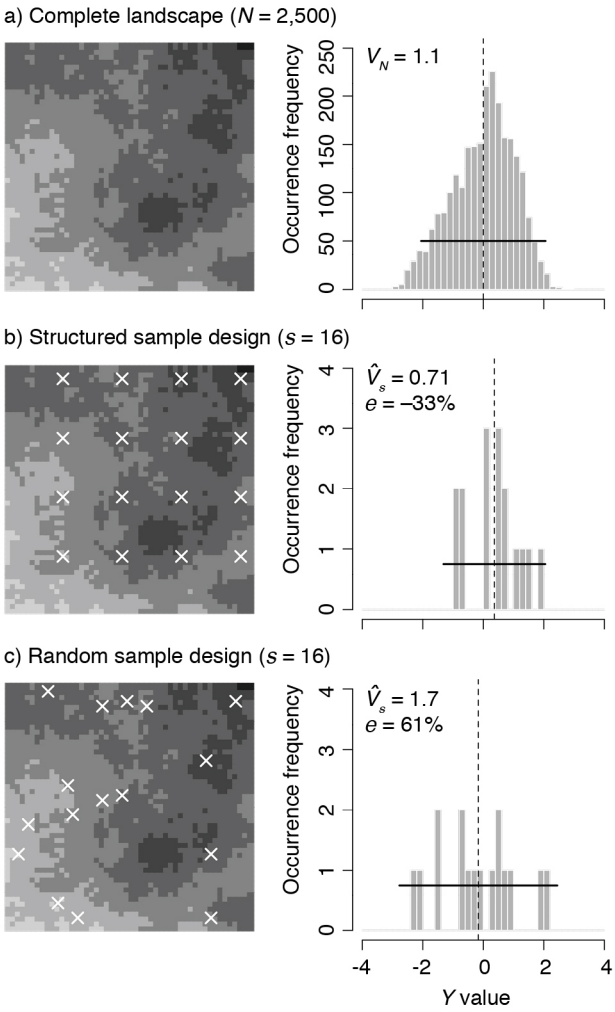


Figure 1.1: Landscapes with gradient patterns and/or spatial autocorrelation, as in this example landscape that has both, can cause significant error in estimates of the complete variance V_N. In panel a, the empirical distribution for all gridcells within the extent is shown, with the mean as the dotted line and ± twice the standard deviation as the solid horizontal line. The sample variance, $\widehat{V}_s$, of the structured sample design in panel b underestimates the complete variance by 33%, while that of the random sample design in panel c overestimates the complete variance by 61%.

by the sample variance $\widehat{V}_s$. As shown in Figure 1.1b–c, different sample designs can over- or underestimate the complete variance on landscapes with autocorrelation and gradient patterns.

Why, then, are traditional ecological methods insufficient? Whereas many sample design recommendations and statistical tools are designed to account for the effects of autocorrelation and gradients separately, we want a description of heterogeneity that includes them. Additionally, statistical tools that account for autocorrelation and gradients, such as analysis of variance and others mentioned earlier, do not estimate the complete variance. In spatial statistics models, Y is considered

a random variable drawn from an underlying stochastic process. However, none of the model parameters describing this process straightforwardly corresponds to the complete variance of the particular landscape that is observed.

Thus, we are interested in how the sample variance performs as an estimator of the complete variance. The average error (bias) can be calculated directly in closed form. We develop this analytical approach and illustrate its use with a forested study in Section 1.2. To find the spread around the average error due to variability in landscape features, which cannot be calculated analytically, we use simulated landscapes to compare a variety of structured and random sampling designs in Section 1.3–1.4. Using the results from these two approaches, we make recommendations for (1) implementing a new sample design to best quantify heterogeneity, and (2) quantifying sampling error from existing sample designs.

1.2 Analytical derivation of expected sampling error

1.2.1 Modeling landscape characteristics

Suppose that the environmental characteristic Y on a gridded landscape with N gridcells can be described by a multivariate normal distribution:

$$\boldsymbol{Y_N} \sim MVN(\boldsymbol{\mu_N}, \boldsymbol{\Sigma}), \qquad \text{eqn 1.1}$$

where $\boldsymbol{Y_N}$ is the vector of Y values at gridcells 1 to N, and $\boldsymbol{\mu_N}$ is a vector of mean values at gridcells 1 to N (see Table 1.1 for a summary of notations). The N x N covariance matrix $\boldsymbol{\Sigma}$ (gridcells 1 to N across the columns and 1 to N down the rows) describes the pairwise relationship between gridcells. We used a multivariate normal distribution for conceptual ease; however, this derivation holds with any distribution.

For landscapes without a gradient, $\boldsymbol{\mu_N}$ has the same value, μ, for all N locations. For landscapes with a gradient, $\boldsymbol{\mu_N}$ has different values and can be modeled by multiplying the gridcell coordinates by a vector $\boldsymbol{\beta} = [\beta_o, \beta_x, \beta_y]$. We decomposed the covariance $\boldsymbol{\Sigma}$ into a variance term, σ^2, and an autocorrelation matrix, $\boldsymbol{K}$: $\boldsymbol{\Sigma} = \sigma^2\boldsymbol{K}$. By doing this we assumed a constant variance across the landscape. We fixed $\sigma^2 = 1$ without loss of generality because σ^2 is a scaling factor.

We modeled autocorrelation with the exponential function in our example:

$$\boldsymbol{K} = e^{-\boldsymbol{d_N}/\rho}, \qquad \text{eqn 1.2}$$

where $\boldsymbol{d_N}$ is an N x N matrix of the pairwise distance between all gridcells, and $\rho > 0$ is a range parameter that determines the distance at which gridcells no longer have strong influence on one another. While we chose the commonly-used exponential function [Zimmerman and Stein 2010], we derive the analytical solution for a general $\boldsymbol{K}$ in which other autocorrelation functions can be used. We report spatial autocorrelation in terms of ρ as measured in gridcells rather than distance units for interpretability given our unitless landscape.

Table 1.1 Notation Definitions

N, s	locations	N = number of total locations within extent s = number of sample locations
$Y, \boldsymbol{Y_N}, \boldsymbol{Y_s}$	environmental characteristic	Y = an environmental characteristic $\boldsymbol{Y_N}$ = vector of Y at N grid locations $\boldsymbol{Y_s}$ = vector of Y at s grid locations
$\mu, \boldsymbol{\mu_N}, \bar{Y}_N, \bar{Y}_s$	mean	μ = model mean (same for all N if no gradient) $\boldsymbol{\mu_N}$ = vector of μ for all locations N $\bar{Y}_N$ = mean across all locations N $\bar{Y}_s$ = sample mean
$\sigma^2, V_N, \hat{V}_s$	variance	σ^2 = model variance V_N = complete variance $\hat{V}_s$ = sample variance
$SD_N, \widehat{SD}_s$	standard deviation	SD_N = complete standard deviation $\widehat{SD}_s$ = sample standard deviation
$\boldsymbol{\Sigma}, \boldsymbol{K}, \boldsymbol{d_N}$	covariance, autocorrelation, & distance matrices	$\boldsymbol{\Sigma}$ = model covariance matrix $\boldsymbol{K}$ = model autocorrelation matrix $\boldsymbol{d_N}$ = matrix of pairwise distances between all N locations
$\boldsymbol{\beta}, \rho$	landscape parameters	$\boldsymbol{\beta}$ = vector of gradient parameters ($\beta_o, \beta_x, \beta_y$) = (intercept, x, y) ρ = autocorrelation range parameter
$\boldsymbol{I_N}, \boldsymbol{J_N}, \boldsymbol{H}$	analytical derivation	$\boldsymbol{I_N}$ = N x N identity matrix ($\boldsymbol{I_s}$ = s x s identity matrix) $\boldsymbol{J_N}$ = N x N matrix of all ones ($\boldsymbol{J_s}$ = s x s matrix of all ones) $\boldsymbol{H}$ = s x N matrix that samples s locations from N
$e_{jk}^{(i)}, \bar{e}_{jk}, R_s$	error	$e_{jk}^{(i)}$ = sampling error $\bar{e}_{jk}$ = average error R_s = relative expected sampling error
i, j, k	error indices	i = index for simulated landscapes j = index for a single design k = index for design configuration

1.2.2 Expected value of complete and sample variance

We define the complete variance according to the standard equation:

$$V_N = \frac{1}{N}\sum_{i=1}^{N}(Y_i - \bar{Y}_N)^2 \quad \text{with} \quad \bar{Y}_N = \frac{1}{N}\sum_{i=1}^{N} Y_i. \qquad \text{eqn 1.3}$$

In Appendix A.1, we show that the expected value of the complete variance is

$$\mathrm{E}[V_N] = \frac{1}{N}\left[\sigma^2 tr\left\{\left(\boldsymbol{I_N} - \frac{1}{N}\boldsymbol{J_N}\right)\boldsymbol{K}\right\} + \boldsymbol{\mu_N^T}\left(\boldsymbol{I_N} - \frac{1}{N}\boldsymbol{J_N}\right)\boldsymbol{\mu_N}\right], \qquad \text{eqn 1.4}$$

where $\boldsymbol{I_N}$ is an N x N identity matrix and $\boldsymbol{J_N}$ is an N x N matrix with all entries equal to one.

The observations under a given sample design are a subset of the $\boldsymbol{Y_N}$ vector, which we call $\boldsymbol{Y_s}$. We write $\boldsymbol{Y_s} = \boldsymbol{H}\boldsymbol{Y_N}$, where $\boldsymbol{H}$ is a s x N matrix consisting mostly of zeros and single entries in each row,

equal to one, that correspond to the elements of $\boldsymbol{Y_N}$ to be selected (Appendix A.1). Thus, $\boldsymbol{Y_s} = \boldsymbol{HY_N} \sim MVN(\boldsymbol{H\mu_N}, \sigma^2 \boldsymbol{HKH}^T)$. With sample variance defined as

$$\widehat{V_s} = \frac{1}{s-1}\sum_{i=1}^{s}(Y_i - \overline{Y_s})^2 \text{ with } \overline{Y_s} = \frac{1}{s}\sum_{i=1}^{s} Y_i, \qquad \text{eqn 1.5}$$

the expected value of the sample variance is

$$\mathrm{E}[V_s] = \frac{1}{s-1}\left[\sigma^2 tr\left\{\left(\boldsymbol{I_s} - \frac{1}{s}\boldsymbol{J_s}\right)\boldsymbol{HKH}^T\right\} + \boldsymbol{\mu_N^T H}^T\left(\boldsymbol{I_s} - \frac{1}{s}\boldsymbol{J_s}\right)\boldsymbol{H\mu_N}\right], \qquad \text{eqn 1.6}$$

where $\boldsymbol{I_s}$ is an s x s identity matrix and $\boldsymbol{J_s}$ is an s x s matrix with all entries equal to one. For landscapes with no gradient, calculation of the expected variances is simplified as the term containing $\boldsymbol{\mu_N}$ is zero:

$$\mathrm{E}[V_N] = \frac{\sigma^2}{N} tr\left\{\left(\boldsymbol{I_N} - \frac{1}{N}\boldsymbol{J_N}\right)\boldsymbol{K}\right\} \text{ and } \mathrm{E}[V_S] = \frac{\sigma^2}{s-1} tr\left\{\left(\boldsymbol{I_s} - \frac{1}{s}\boldsymbol{J_s}\right)\boldsymbol{HKH}^T\right\}. \qquad \text{eqn 1.7, 1.8}$$

1.2.3 Relative expected sampling error

We calculated a relative expected sampling error for each sample design as the percent difference between the complete and sample expected variances:

$$relative\ expected\ sampling\ error = \ R_s = 100\% \times \frac{E[V_s] - E[V_N]}{E[V_N]}. \qquad \text{eqn 1.9}$$

We explored the general usefulness of this framework with sample designs in 1D space for landscapes with no gradient (Appendix A.2). As expected, we found that amongst structured designs with the same sample size and fixed relative sampling locations, R_s was the same regardless of placement within the extent. However, R_s for random designs with the same sample size varied significantly as the sample locations changed from design to design. Additionally, we found that average sample spacing between sample locations was a key factor in determining the magnitude and direction of R_s. We explore this point more fully in our simulation study (Section 1.3–1.4) and focus next on the practical application of R_s.

1.2.4 An example case: Alpine Treeline Warming Experiment (ATWE)

As an example, we applied the analytical derivation to temperature measurements from an existing sample design employed in the Alpine Treeline Warming Experiment (ATWE). ATWE is located along Niwot Ridge in the Eastern Colorado Rockies, USA (40°3' N, 105°36' W). The Forest study site (elev. 3100m) is located in a mature subalpine forest, primarily composed of conifer trees. Details of the study are described in Reinhardt *et al.* [2011]. Five control plots each contained four soil temperature probes arranged in a 1m square. Commensurate with this distance, we chose a grain of 1m for our analysis. The five plots were chosen to span a range of landscape features including sun/shade, topography, and rockiness within the ~100x50m site extent (Figure 1.2 inset). We compared the expected sampling error, R_s, between this Clustered Random design, as is, to a Simple Random version with only 1 measurement per plot. To carry out the analysis, we used equation 1.6, calculating $\boldsymbol{H}$ by matching the geo-located positions of the temperature probes with a 100x50 gridded landscape.

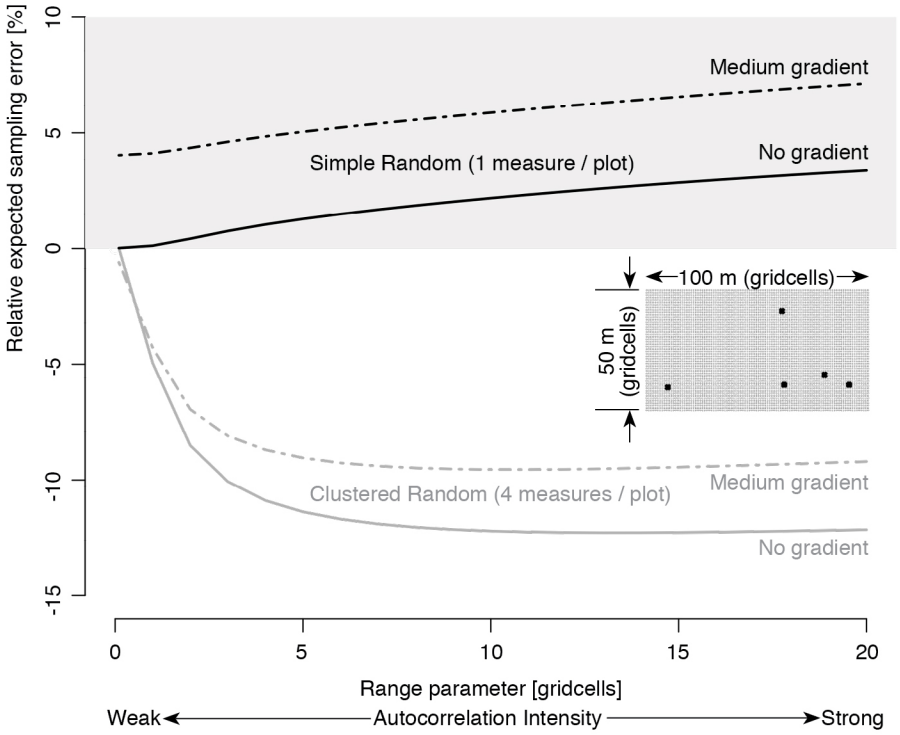


Figure 1.2: Assessment of soil temperature heterogeneity in existing design at ATWE study site by calculating the relative expected sampling error, R_s, via our analytical derivation. The inset figure illustrates the study site, as a 100x50 gridcell landscape with 1 gridcell = 1m and the five measurement plots in black.

With so few data, we were not able to assess spatial autocorrelation or gradient patterns via statistical methods to calculate $\boldsymbol{K}$ or $\boldsymbol{\mu_N}$. Rather, we identified a range of likely autocorrelation intensities, 5–20m, based on the sun-shade patterns from the semi-open canopy. While other factors influence the soil temperature such as topography and soil properties, direct radiation is likely a primary driver. Potential drivers of a gradient pattern at this site are topographical: a gradual east-west elevation change of 15m with minimal change in aspect. Thus, we suspect there to be essentially no gradient effect ($\boldsymbol{\beta} = [0,0,0]$); however we investigate a medium gradient to be conservative ($\boldsymbol{\beta} = [0,0,2]$).

As shown in Figure 1.2, the relative expected sampling error, R_s, differs in both magnitude and direction between the Simple Random design (1 measure / plot) and the Clustered Random design (4 measures / plot) over the range of autocorrelation intensities expected at the site. The simple design overestimates the complete variance while the clustered design underestimates it. On landscapes both with and without a gradient, the simple design, with smaller absolute R_s, yields a better estimate. When a gradient is included in the analysis, the magnitude of R_s for the simple design increases, while that for the clustered design decreases; however not enough to recommend it over the simple design. These results counter the common intuition that collecting more data is always better, which is only guaranteed to be true when the environmental characteristic at different sample locations can be thought of as independent of each other. This is not the case on landscapes with gradient patterns and spatial autocorrelation, which we explore further in the following simulation study.

1.3 Simulation study

While the analytical derivation is a useful tool to quickly assess the expected sampling error of a specific design, we completed a simulation study to systematically investigate the performance of a number of structured and random sample designs on landscapes with varying gradient patterns and spatial autocorrelation. In particular, this numerical approach allowed us to quantify the spread around R_s due to landscape variability. In addition, we assessed the importance of design variability in the case of random sample designs. We will demonstrate that sample designs estimate complete variance differently on different landscape types, sample spacing is a key factor in design performance, and design variability significantly affects random designs. We performed the analysis using R, version 3.0.2 [2013].

1.3.1 Simulation of landscape patterns

We simulated 10,000 landscapes for each of 185 landscape types varying in gradient pattern and spatial autocorrelation. We used a square grid with 50x50 gridcells, yielding 2,500 total locations, N. With edge length of 1 distance unit, the grain is 1 gridcell and the extent is 50 gridcells in each direction. By expressing the distance between two locations in units of gridcells, our results can be scaled to any real distance.

As in the analytical derivation, we simulated landscapes according to a multivariate normal distribution: $\boldsymbol{Y_N} \sim \text{MVN}(\boldsymbol{\mu_N}, \sigma^2\boldsymbol{K})$, which allowed us to vary gradient patterns via $\boldsymbol{\mu_N}$ and spatial autocorrelation via $\boldsymbol{K}$. We modeled landscapes with a 1D gradient in the y-direction by multiplying the y coordinates by a constant, taking values $\beta_y = 0$, 0.1, 2, or 10. The case $\beta_y = 0$ corresponds to no gradient. We again fixed $\sigma^2 = 1$ and used an exponential function with range parameter ρ to model spatial autocorrelation (eqn 1.2). We expected that the strength of autocorrelation, determined by ρ, would have a significant effect on efficacy of the sample designs. Thus, we varied ρ widely, from 0.1 to 100 gridcells (Figure A4). With $\rho = 0.1$, the elements of $\boldsymbol{Y_N}$ can be considered nearly independent and identically distributed, because neighboring gridcells have essentially zero correlation. At the opposite extreme, $\rho = 100$, each location is strongly influenced by all other locations.

1.3.2 Sample designs

We tested a series of structured and random sample designs types, which we call:

- *Simple Structured* – single samples located in a regularly spaced grid
- *Clustered Structure*d – groups of samples located in a regularly spaced grid
- *Nested Structured* – single samples located in two regularly spaced grids, one embedded within the other
- *Simple Random* – single samples randomly located on the landscape
- *Clustered Random* – groups of samples randomly located on the landscape.

In Figure A6, we illustrate the sample designs and define the nomenclature used.

All sample designs have a *sample size* equal to the total number of sampled locations within the extent. The *spacing* is the distance in gridcells between sampled locations. For Clustered Structured designs the spacing describes the distance between the clusters. For designs that have clusters or nested groups (Nested Structured), the *cluster size* is equal to the number of sample locations in each cluster or nest, and the *cluster spacing* describes the spacing between sample locations in each cluster

or nest. While we present our results using a few representative configurations, we illustrate all designs configurations that we investigated in Figure A7.

1.3.3 Calculation of complete and sample standard deviation

For a single simulated landscape of a given landscape type and for each sample design, we calculated:

$$SD_N = \sqrt{V_N} = \sqrt{\frac{1}{N}\sum_i^N (Y_i - \bar{Y}_N)^2} \text{ and } \widehat{SD_s} = \sqrt{\widehat{V_s}} = \sqrt{\frac{1}{s-1}\sum_i^s (Y_i - \bar{Y}_s)^2}, \quad \text{eqn 1.10, 1.11}$$

where as before N is the total number of locations, and s is the number of sample locations. We refer to SD_N as the complete standard deviation (what we cannot observe and wish to estimate) and to $\widehat{SD_s}$ as the sample standard deviation (our estimate based on s sample locations). We used standard deviation rather than variance as a metric describing heterogeneity because it has the same units as the environmental characteristic Y.

We report error between SD_N and $\widehat{SD_s}$at two levels for each design configuration. First, we quantified a relative sampling error, e, defined as percent difference between SD_N and $\widehat{SD_s}$:

$$sampling\ error = e_{jk}^{(i)} = 100\% \times \frac{\widehat{SD}_{s,jk}^{(i)} - SD_n^{(i)}}{SD_n^{(i)}}, \quad \text{eqn 1.12}$$

where i represents a single simulated landscape (1 to 10,000) within a landscape type and j represents a specific design within the design configuration k. A negative sampling error means $\widehat{SD_s}$ underestimates SD_N, while a positive sampling error indicates that $\widehat{SD_s}$ is an overestimate. Then, we calculated an average error, $\bar{e}_{jk}$, for each design by averaging the sampling error over the 10,000 simulated landscapes:

$$average\ error = \bar{e}_{jk} = \frac{1}{10{,}000}\sum_{i=1}^{10{,}000} e_{jk}^{(i)}. \quad \text{eqn 1.13}$$

Recall that this average error is the average of relative rather than absolute sampling errors. We examined the spread around average error from landscape variation by varying i in $e_{jk}^{(i)}$. Likewise, we vary j in $\bar{e}_{jk}$ within a design configuration k to examine the effects of design variation. For example, within the Simple Random configuration with sample size 16, we compare specific designs, each with a unique set of 16 sample locations.

To understand the impact of design variation, we randomly-selected 100 specific designs for each random configuration and compared the average error for each of these 100 designs. To verify the results from our analytical derivation, we computed the average error of 20 randomly-selected specific designs for each structured configuration. The differences in average error are indeed small (Figure A8). Thus, for structured configurations, we show results for a single representative structured design.

1.4 Simulation results

Our simulation results illustrate three main findings: (1) Sampling error can be significant in the presence of autocorrelation and especially gradients; (2) Sample spacing indicates how the landscape is sampled and thus is a key factor in the sampling error observed; (3) the range of possible sampling errors for random designs is large due to landscape and design variability.

1.4.1 Sampling error can be significant

1.4.1.1 Structured sample designs: Autocorrelation can cause significant average error

The effect of autocorrelation is striking, as shown in Figure 1.3-1. As autocorrelation intensity increases, the average error, $\bar{e}_{jk}$, can become quite large, varying from –38% to 12%. This increase in error occurs rapidly over range parameter values of 0–20 gridcells, approximately 25% of the maximum distance. Increasing the sample size without changing the sample spacing reduces the $\bar{e}_{jk}$ (d-e in Figure 1.3-1); however $\bar{e}_{jk}$ may still be significant. Moreover, the configuration determines the sign of $\bar{e}_{jk}$. In the majority of design configurations the sample standard deviation, $\widehat{SD}_s$, underestimates the complete standard deviation, SD_N, *i.e.,* the error is negative (b-e in Figure 1.3-1). However, $\widehat{SD}_s$ overestimates SD_N for a configuration in which the sample spacing is maximized across the extent (a in Figure 1.3-1).

1.4.1.2 Structured sample designs: Gradients increase average error

As shown in Figure 1.3-2, medium and strong gradient patterns degrade performance for all structured sample designs, the magnitude depending on both the strength of the gradient and the design configuration. In particular, design configurations that perform well without gradients (*e.g.,* b) continued to do well. Design configurations that had poor performance without gradients (*e.g.,* a and c) have even larger average error, $\bar{e}_{jk}$, on landscapes with gradients. For these configurations, medium strength gradients roughly double $\bar{e}_{jk}$, while strong gradients triple $\bar{e}_{jk}$. In Appendix A.4.2 and A.4.3, we examine clustered and nested designs. In summary, we find that these strategies generally lead to worse estimates of SD_N.

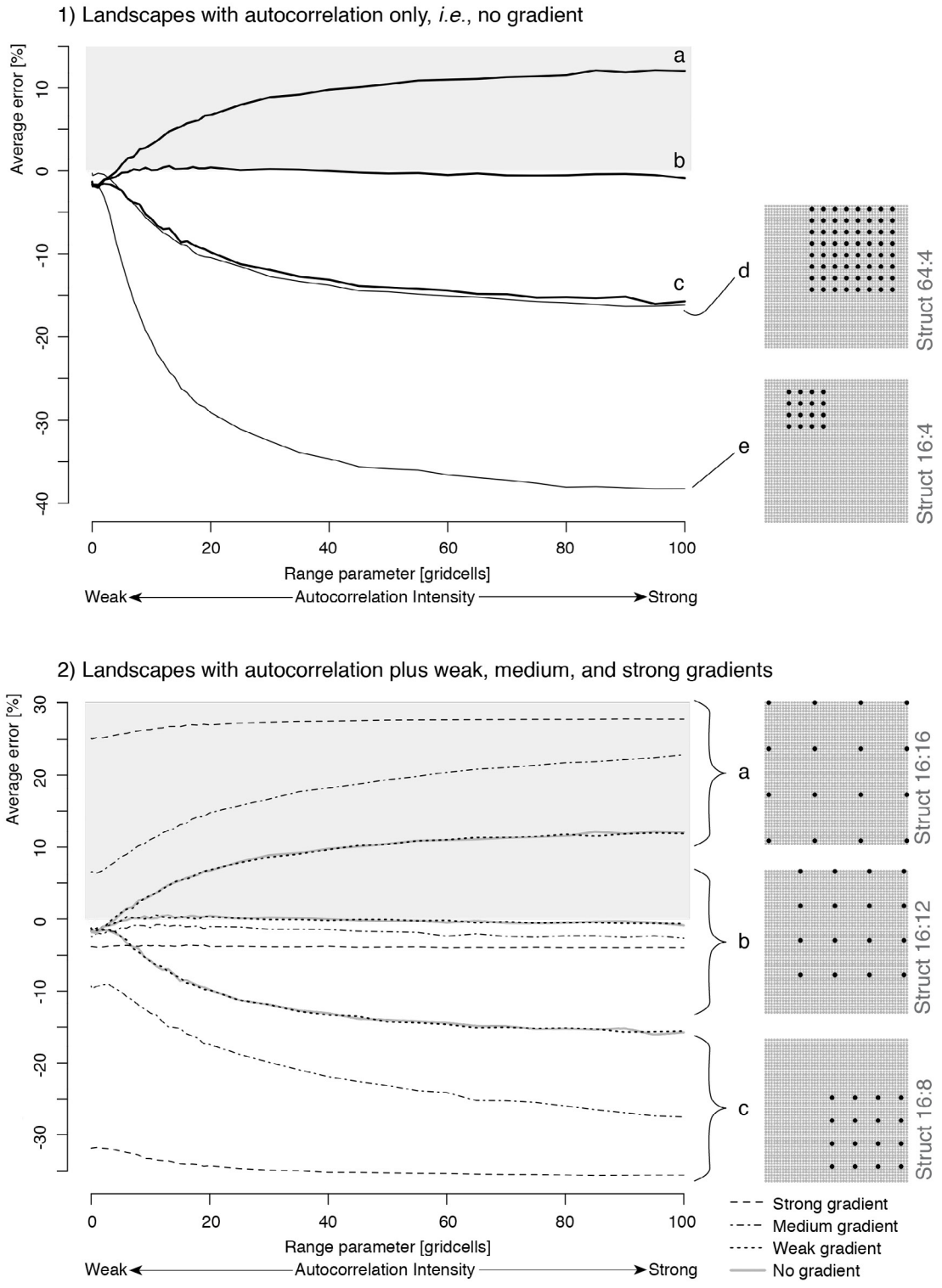


Figure 1.3: Average error, $\bar{e}_{jk}$, for structured design configurations on landscapes with autocorrelation only, *i.e.,* no gradient (panel 1) and additionally with a series of weak to strong gradients (panel 2). The $\bar{e}_{jk}$ reported is for the representative design shown.

1.4.1.3 Random designs: Effects of autocorrelation and gradients differ dependent on design

As shown in Figure 1.4, random design configurations perform differently on landscapes with varying autocorrelation intensities and gradient patterns. By comparing the difference between Simple Random 4 and Simple Random 16 (b to a) and between Random 4 and Clustered Random 16-4 (b to c), it is clear that increasing the sample size via a Simple Random configuration (*i.e.,* not in clusters) leads to a greater decrease in the magnitude of error.

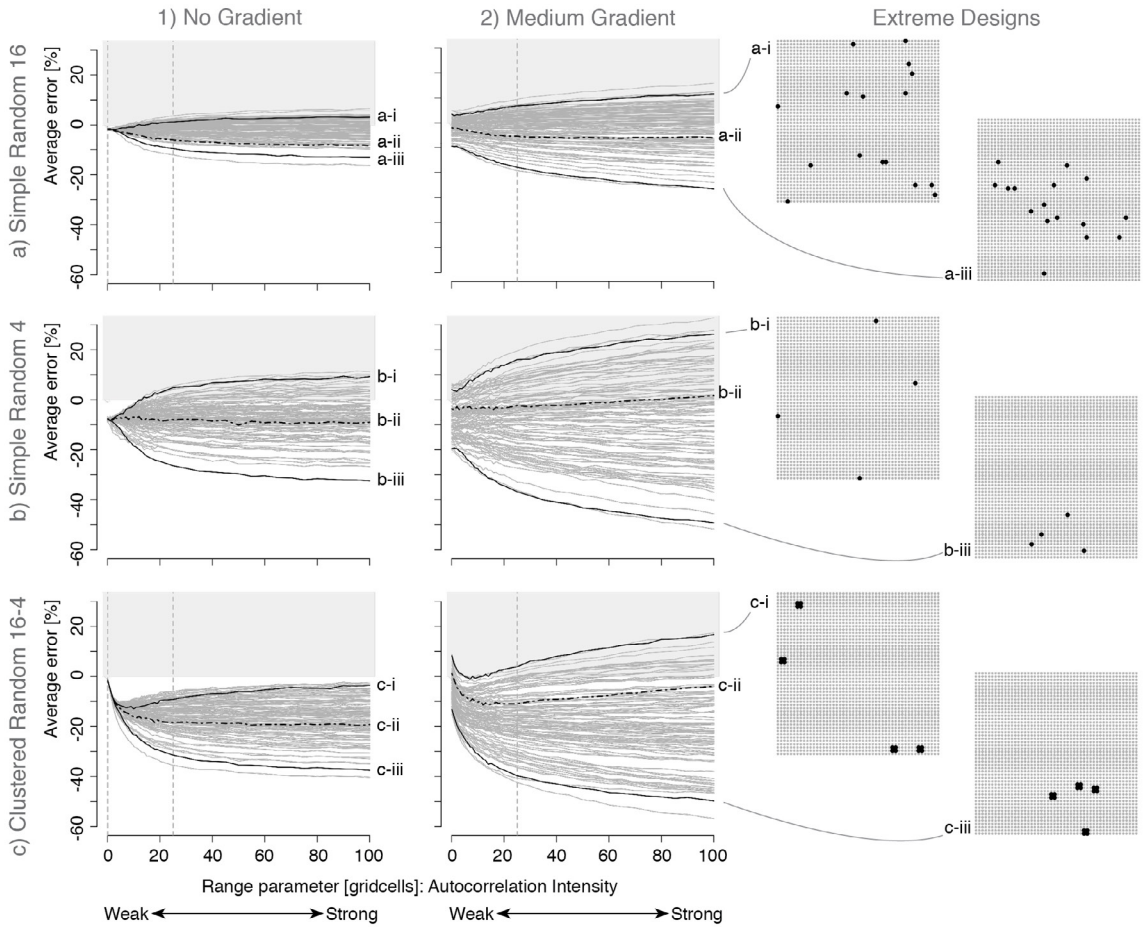


Figure 1.4: Spread in average error, $\bar{e}_{jk}$, for random designs due to design variation. Each line is $\bar{e}_{jk}$ for a single design within each configuration: Random 16, 4, and 16-4 (rows a–c, respectively). For each design configuration, examples of extreme designs (i and iii) are highlighted in solid black. Examples of designs (ii) that have generally better estimates of the complete standard deviation on landscapes with gradients are shown in the dashed black line. Landscapes with no gradient (column 1) and with a medium gradient (column 2) are the same landscapes used in Figure 1.3. The vertical lines are the representative landscapes used in subsequent Figure 1.6.

Additionally, the effects of autocorrelation and gradient patterns are complicated. For example design c-i on landscapes with no gradient in Figure 1.4, $\bar{e}_{jk}$ worsens initially then improves as autocorrelation increases. Furthermore, significant change in $\bar{e}_{jk}$ can happen rapidly over weak autocorrelation intensities (0–20 gridcells). Gradients can also have beneficial (*e.g.,* a-ii, b-ii, and c-ii) or detrimental (*e.g.,* all extreme designs) effects on $\bar{e}_{jk}$. Overall, increasing both autocorrelation intensity and gradient strengths increases the variability of $\bar{e}_{jk}$ across designs within a random

configuration. It is this design variability that led us to investigate what design characteristics yield near-zero $\bar{e}_{jk}$ across autocorrelation intensities and gradient pattern strengths. As discussed in the next result, sample spacing is a key factor.

1.4.2 Sample spacing is a key factor in observed sampling error

For landscapes with autocorrelation, we observed a positive linear relationship between a design's average error, $\bar{e}_{jk}$, and its average distance between sampling locations. That is, for a given sample size, the average distance seems to determine the bias in $\bar{e}_{jk}$. As shown in Figure 1.5, this relationship holds for autocorrelated landscapes with and without gradients and for both random and structured design configurations. For a sample size of 16, designs with average spacing of 25–30 gridcells consistently show $\bar{e}_{jk}$ near zero, where as designs with lower or higher average spacing have a non-zero $\bar{e}_{jk}$ that becomes more extreme as the autocorrelation intensity increases (not shown). Average spacing greater than 25–30 gridcells results in overestimates of SD_N (positive $\bar{e}_{jk}$), while average spacing less than 25–30 gridcells result in underestimates (negative $\bar{e}_{jk}$). Clustered designs almost always underestimate SD_N, with clusters reducing the average sample spacing (Appendix A.4.2). We performed a similar analysis for the spread around $\bar{e}_{jk}$ due to landscape variation. We did not find strong relationships (Figure A11). We discuss the importance of sample spacing further in the discussion section.

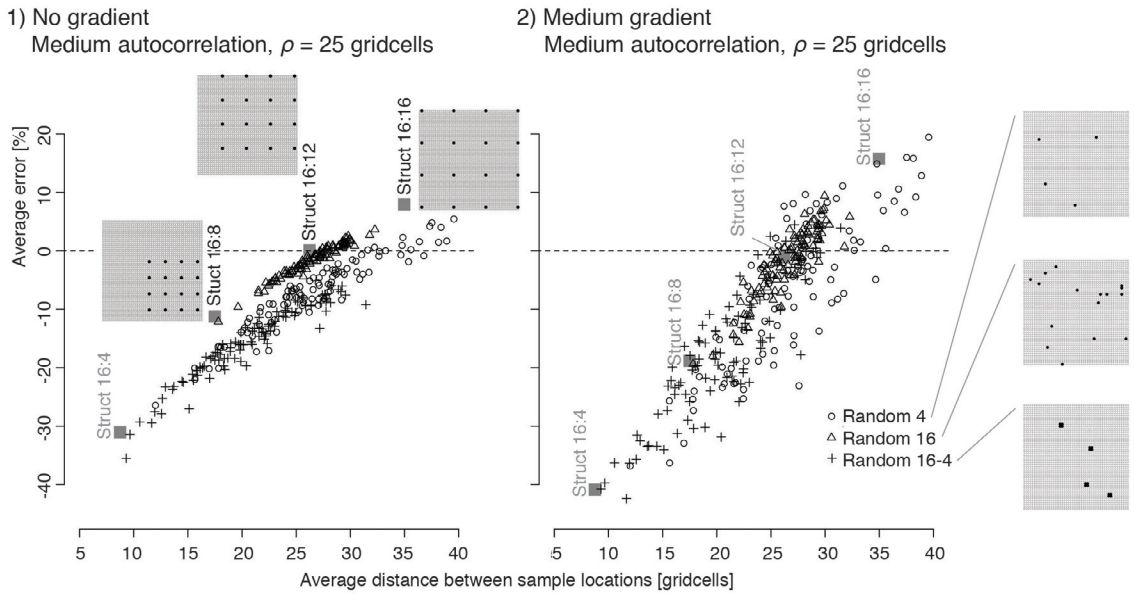


Figure 1.5: Average error, $\bar{e}_{jk}$, versus average distance between sampling locations. Designs for the random design configurations Random 16, 4, and 16-4 are shown with circles, triangles, and crosses, respectively. These are the same random designs for which results are reported in Figure 1.4. Average error, $\bar{e}_{jk}$, for simple structured designs with increasing spacing are reported with gray squares for comparison.

1.4.3 Random designs have a large range of sampling error due to the combination of design and landscape variability

When a random design configuration is chosen for a study's sample design, only one design is implemented. Therefore, the sampling error of the implemented design is a combination of both the design and landscape variability of that random design configuration. Thus, as we will show, the range of possible sampling error for a randomly-selected random design is much larger than that of a structured design with the same sample size. This finding holds for environmental quantities, $\boldsymbol{Y_N}$, that do not repeat in a regular pattern on the landscape at multiples of the structured design frequency.

In Figure 1.6, we illustrate the range of possible sampling error due to both design and landscape variation. For three representative landscape types, we show kernel estimates of the density of raw sampling error, $e_{jk}^{(i)}$, that underlie average errors for designs within (1) the best performing Simple Structured configuration Struct 16:12; (2) the Simple Random configuration Random 16, and (3) the Clustered Random configuration Random 16-4 (rows 1-3 respectively).

For landscapes with no autocorrelation or gradient (Figure 1.6 column 1), little difference exists in the sampling errors between the three design configurations. These results are expected, as this landscape type is essentially a random surface. However, on landscapes with medium autocorrelation (column 2), as we saw in Figure 1.4, design variability affects both the Simple and Clustered Random configurations, *i.e.,* the densities shift apart. Landscape variability also significantly affects the clustered configuration, *i.e.* the densities' widths increase. On landscapes with both autocorrelation and a medium gradient (column 3), the effect of design variability is exacerbated for the random designs, while the effect of landscape variability on the structured design is reduced as shown by a decrease in the density width.

When we consider the implications of the combined effects of design and landscape variability on landscapes with autocorrelation and gradients, the Simple Structured configuration clearly has a significantly smaller range of possible sampling errors than either of the random configurations. While any one Simple Random design may have a sampling error comparable to that of a Simple Structured design, the possible sampling error is considerably larger when choosing a design randomly.

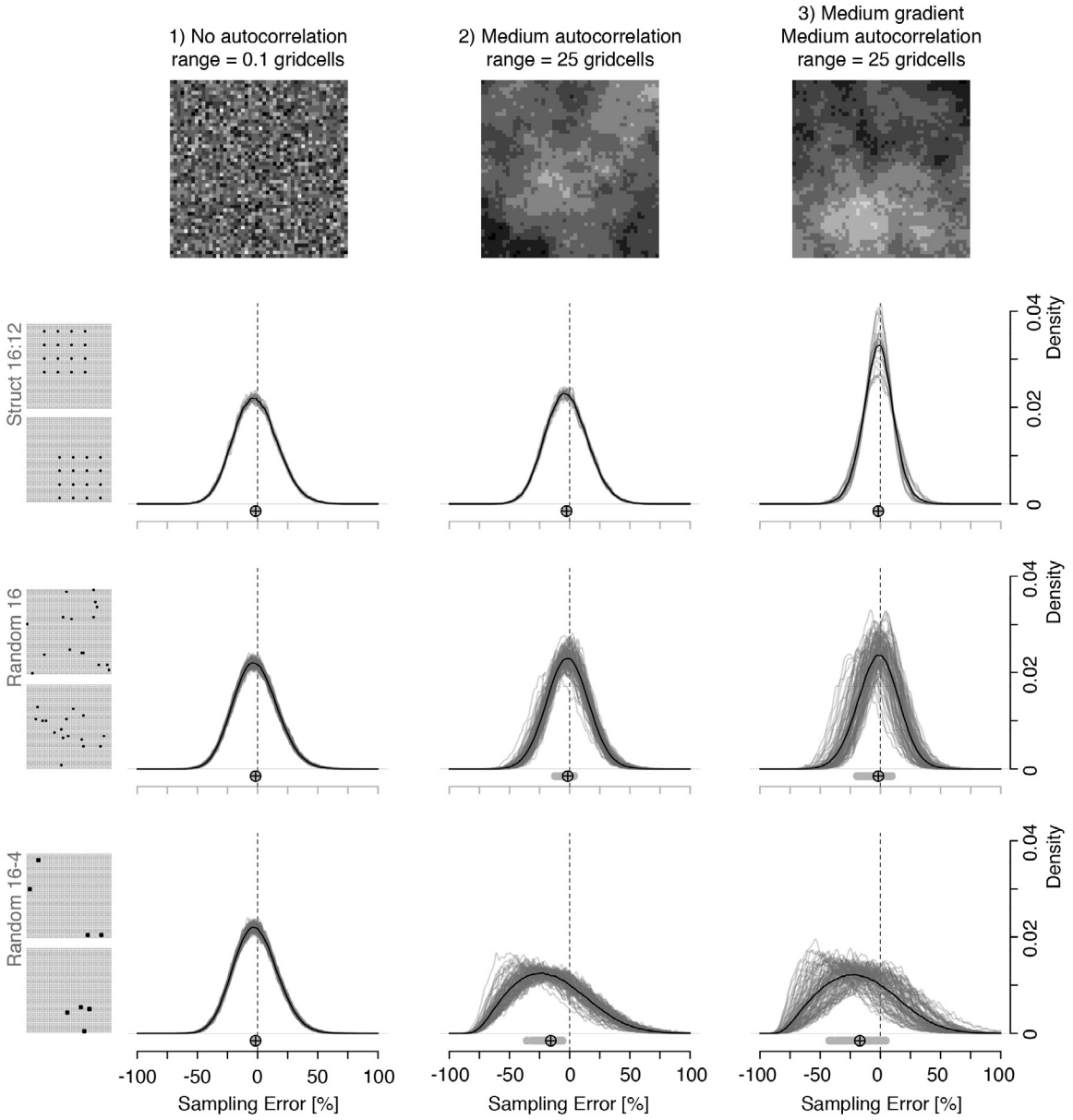


Figure 1.6: The combined effects of landscape and design variation is shown by comparing the kernel estimates of the density of raw sampling error, $e_{jk}^{(i)}$, for structured and random designs calculated over the 10,000 simulated landscapes. Results are shown in columns for three landscapes types indicated by vertical dotted lines in Figure 1.4. Each gray line is a single design within each of three configuration types shown in rows, each with sample size 16. The black line is the combined density distribution of raw sampling error for designs within each configuration type. The mean of the density, which is the average error, $\bar{e}_{jk}$, is represented by a gray dot below the densities. The black cross-haired dot is the mean of the average errors.

1.5 Discussion

Our simulation study shows that good estimates of heterogeneity as measured by complete variance can be obtained with a well-chosen sample design over a range of gradient strengths and autocorrelation intensities. We have identified sample spacing as a key factor in determining designs with good estimation. The question then becomes what characteristics of sample designs are associated with optimal spacing. Additionally, how should a researcher practically apply an understanding of sample design to quantify heterogeneity when: (1) implementing a new sample design; (2) using data from an existing sample design?

As shown in Figure 1.5, for a given sample size, an ideal range of average sample spacing, which holds across gradients, leads to near-zero average sampling error. The same range holds across autocorrelation intensities (not shown). Because the proportion of the landscape covered and the evenness of that coverage determine the average sample spacing, the average sample spacing can be considered a proxy for adequate sampling of the landscape within a given sample size. In general, larger average spacing, up to a distance constrained by the sample size, typically leads to greater landscape coverage. For structured designs, coverage increases evenly in both directions as average spacing increases; however for random designs, the evenness may not be constant in both directions. Thus, the problem is that random designs, as well as clusters and nests, can have particular spatial arrangements that over or under-sample certain regions of the extent, leading to larger sampling errors.

The combined effects of sample size and sample spacing determine a threshold sample size above which there are essentially no differences between Simple Structured and Simple Random designs' complete variance estimates, *i.e.,* the densities of raw sampling error $e_{jk}^{(i)}$, like those illustrated in Figure 1.6, look similar. For random designs, the possibility for spatial sampling arrangements that over- or under-sample certain regions of the extent decreases as the sample size increases. Additionally, average sample spacing necessarily approaches the ideal spacing in which a large portion of the landscape is sampled in a more-or-less evenly spaced fashion. Below the threshold sample size in a random design, too many possibilities exist for sampling arrangements that lead to poor complete variance estimates. An appropriately-spaced Simple Structured design, with both adequate landscape coverage and even spacing within that covered portion, provides a better estimate.

Finally, as the strength of both gradient patterns and spatial autocorrelation increases, errors in estimating the complete variance can become quite large. Thus, when implementing a new sample design or evaluating a proposed design, it is helpful to have a sense of how strong a gradient or autocorrelation pattern may be. When sufficient data are not available, expert knowledge can be used to identify a range of autocorrelation strengths to consider, as employed in the ATWE example. In the case when existing data are used, some sample designs, such as structured or stratified random, may allow for estimation of gradient patterns [Dutilleul 1993, Dutilleul 2011]. For datasets with sufficiently large sample sizes, geo- and spatial statistical techniques can be used to estimate the autocorrelation strength [Isaaks and Srivastava 1989, Zimmerman 2010].

In Figure 1.7, we summarize our recommendations for practical application of our results. When implementing a new design to quantify heterogeneity via complete variance, we recommend a

Simple Structured design when landscape features do not repeat at multiples of the appropriate sample spacing. We make this recommendation regardless of the sample size for 2 reasons: (1) an appropriately-space Simple Sturctured design ensures a good estimate as discussed above, and (2) the sample size threshold is complicated to determine as we discuss further below. Although motivated by a different purpose, authors have made a similar recommendation for using systematic sample designs to estimate spatial gradient and autocorrelation patterns [Zidek and Zimmerman 2010, Dutilleul 2011]. In contrast, Zhu & Stein [2005] report that structured (regular) designs are outperformed by other non-random designs when estimating the autocorrelation parameters of a statistical model of the landscape.

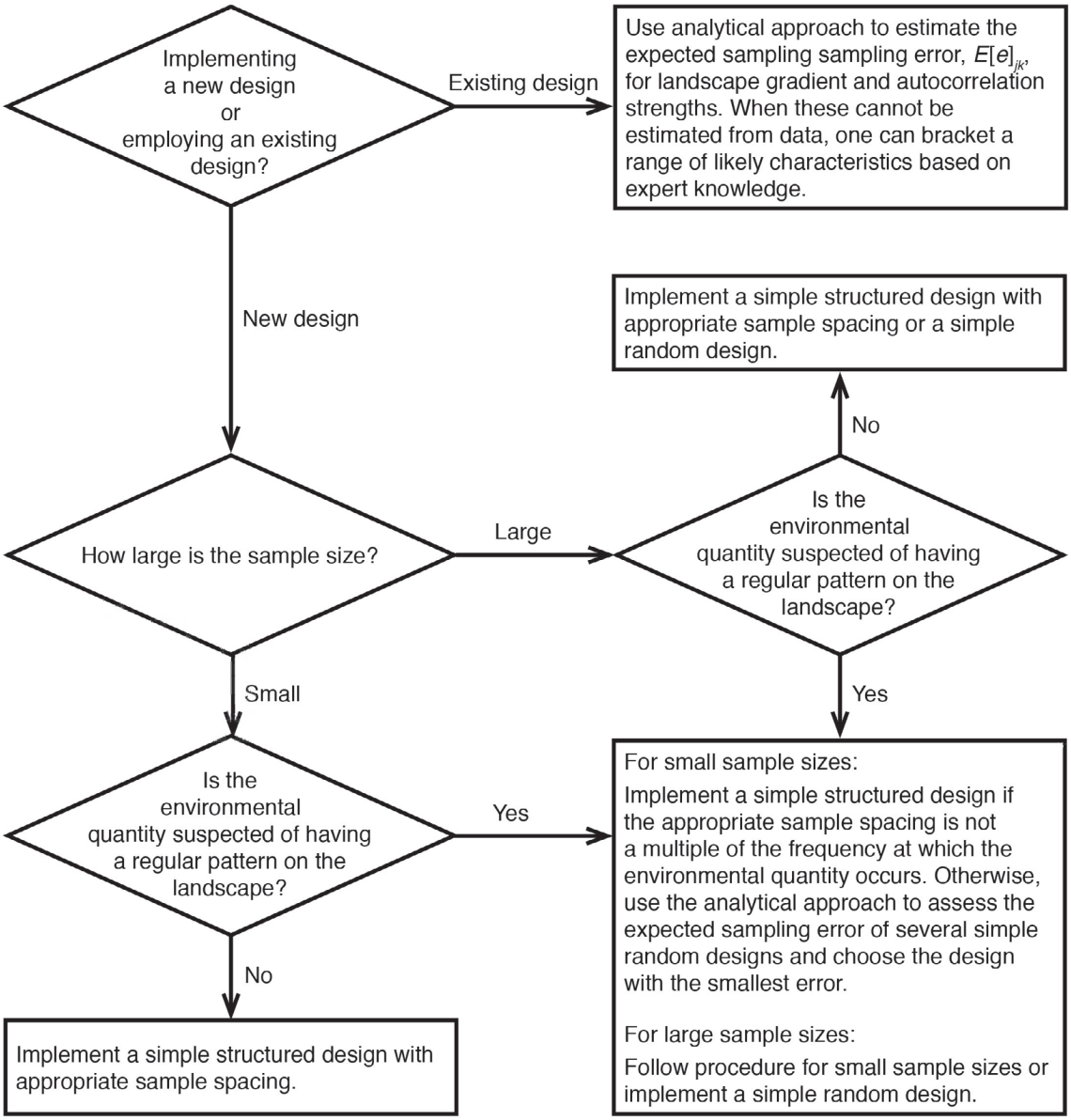


Figure 1.7: Recommendations for quantifying environmental heterogeneity via complete variance when gradient patterns and spatial autocorrelation occur on the landscape.

We recommend the following rule of thumb to determine the appropriate spacing for Simple Structured designs on roughly square-shaped extents based on our results for multiple Simple Structured configurations (Appendix A.3 and A.4). Divide the length of a side by the number of sample locations in each row (or column), and then truncate the resulting number to get the sample spacing. For the example of our 50x50 gridded landscape and a sample size of 16 (4x4), a spacing of 12 (50/4 = 12.5 → 12) gives the best estimate of the complete standard deviation, *i.e.,* sampling error is closest to zero for all gradient and autocorrelation intensities.

As previously discussed, above a sample size threshold there is essentially no difference between an appropriately-spaced Simple Structured design and a Simple Random design. A general threshold is difficult to determine because it depends on strength of the gradient and autocorrelation intensities, total number of locations (gridcells) within the extent, and potentially the extent shape. For our simulated 50x50 gridded landscape with no gradient, we estimate a threshold of ~1%, which is a sample size of 25. Sample sizes in ecological research are often smaller than this threshold, which we expect to increase with stronger gradients. Additionally, we expect extent shape to matter because we observed different thresholds between the 50x50 gridded landscape from the simulation study and the 1D gridded line from the analytical derivation.

Researchers, however, may have objectives other than heterogeneity when selecting a sample design. Random designs are often employed to avoid unintentional sampling bias and to satisfy criteria of inferential statistical methods [Zidek and Zimmerman 2010]. As mentioned earlier, structured designs can be problematic for sampling landscape features that repeat at multiple of the sample spacing [Dutilleul 2011]. Such patterns do occur in natural systems and care must be taken to implement an appropriate design. Fortunately, a number of particular Simple Random designs with near-zero sampling error across a range of autocorrelation intensities and gradient strengths do exist. Thus if desired, one can select a particular design by iteratively evaluating it with our analytical derivation, as exemplified in the ATWE example. Additionally, while we did not include a stratified random sample design in our analysis, we expect that it would provide good estimates as the stratification criteria would likely limit over and under-sampling.

To estimate the sampling error from a proposed design or existing data, we suggest using the analytical derivation to calculate the expected sampling error for the particular sample design at hand. The expectation can be calculated for a set of autocorrelation intensities and gradient strengths. We suggest bracketing these landscape features with a low and high value in cases where the value cannot be directly estimated, as illustrated in the ATWE example. This method allows a relatively quick assessment of the expected sampling error direction and magnitude. To quantify the range of sampling errors around the expected sampling error, the simulation methodology employed in this paper can be modified for specific study details. This error range due to landscape variability may be especially important for designs with low sample sizes.

We have begun a description of how different sample designs estimate heterogeneity via complete variance. In addition, we identified a tool to estimate the expected sampling error for landscapes with gradient patterns and spatial autocorrelation. Environmental heterogeneity is increasingly used in assessments of ecological pattern and function, in particular in climate change studies. To better represent this heterogeneity, future work should investigate more complex landscapes, for example those in which variance or autocorrelation is not constant (*i.e.,* landscapes with non-stationary features). Metrics other than variance, such as skew and kurtosis are also important descriptors of environmental conditions. The influence of gradients and autocorrelation on estimates of such metrics should be examined. Finally, given the interest in heterogeneity across ecological disciplines,

a summary of the different methods of defining and quantifying heterogeneity would serve as a guide to researchers, improving a common set of tools and enabling increased collaborative effort.

1.6 Acknowledgements

We thank Erin Conlisk, John Harte, Lara Kueppers, Lydia Smith, and Cleo Woelfle-Erskine for helpful comments. A UC Berkeley Philomathia Graduate Student Fellowship in the Environmental Sciences supported DSC while conducting this work.

1.7 References

Beale, C.M., Lennon, J.J., Yearsley, J.M., Brewer, M.J. & Elston, D.A. (2010) Regression analysis of spatial data. *Ecology Letters*, 13, 246–264.

Clark, J.S., Melillo, J., Mohan, J. & Salk, C. (2013) The seasonal timing of warming that controls onset of the growing season. *Global Change Biology*, 20, 1136–1145.

Cressie, N.A.C. (1993) *Statistics for spatial data*, revised edition. Wiley-Interscience, New York.

Dobrowski, S.Z. (2011) A climatic basis for microrefugia: the influence of terrain on climate. *Global Change Biology*, 17, 1022–1035.

Downing, J.A. (1991) Biological Heterogeneity in Aquatic Ecosystems. *Ecological Heterogeneity* (eds J. Kolasa & S.T.A. Pickett), pp. 160–180. Springer New York, New York.

Dutilleul, P. (1993) Spatial Heterogeneity and the Design of Ecological Field Experiments. *Ecology*, 74, 1646–1658.

Dutilleul, P. (2011) *Spatio-Temporal Heterogeneity*. Cambridge University Press, Cambridge.

Fierer, N., Colman, B.P., Schimel, J.P. & Jackson, R.B. (2006) Predicting the temperature dependence of microbial respiration in soil: A continental-scale analysis. *Global Biogeochemical Cycles*, 20, GB3026.

García-Carreras, B. & Reuman, D.C. (2013) Are Changes in the Mean or Variability of Climate Signals More Important for Long-Term Stochastic Growth Rate? (I. Gudelj, Ed.). *PLoS ONE*, 8, e63974.

Holdridge, L.R. (1947) Determination of World Plant Formations From Simple Climatic Data. *Science*, 105, 367–368.

Isaaks, E.H. & Srivastava, R.M. (1989) *An Introduction to Applied Geostatistics*. Oxford University Press, New York.

Jentsch, A. & Beierkuhnlein, C. (2008) Research frontiers in climate change: Effects of extreme meteorological events on ecosystems. *Comptes Rendus Geoscience*, 340, 621–628.

Jentsch, A., Kreyling, J., Elmer, M., Gellesch, E., Glaser, B., Grant, K., Hein, R., Lara, M., Mirzae, H., Nadler, S.E., Nagy, L., Otieno, D., Pritsch, K., Rascher, U., Schädler, M., Schloter, M., Singh, B.K., Stadler, J., Walter, J., Wellstein, C., Wöllecke, J. & Beierkuhnlein, C. (2011) Climate extremes initiate ecosystem-regulating functions while maintaining productivity. *Journal of Ecology*, 99, 689–702.

Keppel, G. & Wardell-Johnson, G.W. (2012) Refugia: keys to climate change management. *Global Change Biology*, 18, 2389–2391.

Kolasa, J. & Rollo, C.D. (1991) Introduction: The Heterogeneity of Heterogeneity: A Glossary. *Ecological Heterogeneity* (eds J. Kolasa & S.T.A. Pickett), pp. 1–23. Springer, New York.

Legendre, P. (1993) Spatial autocorrelation: trouble or new paradigm? *Ecology*, 74, 1659.

Legendre, P., Dale, M., Fortin, M.J., Casgrain, P. & Gurevitch, J. (2004) Effects of spatial structures on the results of field experiments. *Ecology*, 85, 3202–3214.

Meehl, G.A., Karl, T., Easterling, D.R., Changnon, S., Pielke, R., Changnon, D., Evans, J., Groisman, P.Y., Knutson, T.R., Kunkel, K.E., Mearns, L.O., Parmesan, C., Pulwarty, R., Root, T., Sylves, R.T., Whetton, P. & Zwiers, F. (2000) An introduction to trends in extreme weather and climate events: Observations, socioeconomic impacts, terrestrial ecological impacts, and model projections. *Bulletin of the American Meteorological Society*, 81, 413–416.

R Development Core Team (2013) *R: A Language and Environment for Statistical Computing*. R

Foundation for Statistical Computing, Vienna. URL http://www.R-project.org [accessed 25 September 2013]

Reinhardt, K., Castanha, C., Germino, M.J. & Kueppers, L.M. (2011) Ecophysiological variation in two provenances of Pinus flexilis seedlings across an elevation gradient from forest to alpine. *Tree Physiology*, 31, 615–625.

Sierra, C.A., Harmon, M.E., Thomann, E., Perakis, S.S. & Loescher, H.W. (2011) Amplification and dampening of soil respiration by changes in temperature variability. *Biogeosciences*, 8, 951–961.

Thornton, P.K., Ericksen, P.J., Herrero, M. & Challinor, A.J. (2014) Climate variability and vulnerability to climate change: a review. *Global Change Biology*, 20, 3313–3328.

Whittaker, R.H. (1956) Vegetation of the Great Smoky Mountains. *Ecological Monographs*, 26, 1–69.

Wiens, J.A. (2000) Ecological heterogeneity: an otogeny of concepts and approaches. *The Ecological Consequences of Environmental Heterogeneity* (eds M.J. Hutchings, A.J. Libby & A.J.A. Stewart). Cambridge University Press, Cambridge.

Zhu, Z. & Stein, M.L. (2005) Spatial sampling design for parameter estimation of the covariance function. *Journal of Statistical Planning and Inference*, 134, 583–603.

Zidek, J.V. & Zimmerman, D.L. (2010) Monitoring Network Design. *Handbook of Spatial Statistics* (eds A. Gelfand, P. Diggle, M. Fuentes & P. Guttorp). CRC Press, Boca Raton.

Zimmerman, D.L. (2010) Likelihood-Based Methods. *Handbook of Spatial Statistics* (eds A. Gelfand, P. Diggle, M. Fuentes & P. Guttorp). CRC Press, Boca Raton.

Zimmerman, D.L. & Stein, M.L. (2010) Classical Geostatistic Methods. *Handbook of Spatial Statistics* (eds A. Gelfand, P. Diggle, M. Fuentes & P. Guttorp). CRC Press, Boca Raton.

Chapter 2: Towards a biologically meaningful climate characterization: spatial heterogeneity of temperature at multiple temporal scales

Heterogeneity in fine-scale abiotic conditions is important to many organisms and ecological processes. While the mechanisms influencing fine-scale abiotic conditions have been described, characterization of heterogeneity in these fine-scale conditions is lacking, especially in complex mountainous landscapes that are thought to have high heterogeneity. Thus, we use soil temperature observations from 4 studies at high elevations in the Colorado Rockies and Californian Sierra Nevada (USA) to characterize fine-scale spatial heterogeneity, quantified by standard deviation, through time. We found that heterogeneity differs diurnally and throughout the growing season. Spatial heterogeneity in maximum daily soil temperatures is larger than projected future temperatures. Additionally, maximum daily temperatures have higher heterogeneity on warmer days, while minimum daily temperatures have consistent heterogeneity throughout the growing season. Our results also suggest that canopy complexity is an important factor in heterogeneity differences amongst mountainous landscapes. Furthermore, temporal dynamics are generally not adequately represented by temporally aggregated or bioclimatic metrics. Finally, heterogeneity in air temperature as typically measured at 2m height does not capture the temporal dynamics observed at the near surface where many organisms live. For organisms and ecological processes that are influenced by fine-scale spatiotemporal environmental conditions, better ways to quantify and incorporate these dynamic patterns will be needed.

2.1 Introduction

All plant individuals that eventually become adults must survive fine-scale environmental conditions, at least during early life history stages. The set of conditions describing suitable habitat for maintenance of a species' population, *i.e.,* the niche, is conceptualized as the intersection of abiotic (physical) conditions, biotic (species) interactions, and dispersal limitations [Soberón 2007, Peterson *et al.* 2011]. The species niche can differ across its life history stages, with often the earliest being the most sensitive [Grubb 1977]. Traditionally, abiotic factors at coarse spatial scales on the order of approximately 1km and temporal scales of months to years are generally assumed to characterize a species' niche [Soberón 2007, Peterson *et al.* 2011]. However, authors have recently questioned this framework because individuals respond to their immediate, fine-scale abiotic conditions on the scale of meters and hours [Clark *et al.* 2011, Potter *et al.* 2013, Harwood *et al.* 2014].

Heterogeneity in these fine-scale abiotic conditions is ecologically important. Fine-scale abiotic influences, in addition to coarse scale climatic conditions, affect the current and likely the future geographical distribution of species [Gillingham *et al.* 2012, de Frenne *et al.* 2013]. At geographical range limits, a species is more likely to persist in a location with fine-scale conditions that differ from a coarse-scale value that presumably is the average across all fine-scale conditions. Fine-scale heterogeneity describes the extent of this difference. Additionally, heterogeneity in fine-scale

This chapter was written in a style for publication with advisors Lara M. Kueppers and John Harte. Thus, I use "we." All Tables and Figures with prefix "B" can be found in Appendix B.

conditions may provide refugia for species throughout their current geographical ranges under future climates [Dobrowski 2011, Keppel and Wardell-Johnson 2012]. Abiotic fine-scale heterogeneity is also important for maintaining plasticity and genetic variability within a population because more environmental heterogeneity allows for more opportunities for selection of successful genetic combinations [Harper 1977].

A recent idea for maintaining biodiversity in future climates is to preserve "nature's stage" or areas with heterogeneous abiotic conditions [Lawler *et al.* 2015]. Conservation of coarse scale heterogeneity is tractable with coarse-scale interpolated climate information and coarse scale remote sensing data. However, targeting fine-scale abiotic heterogeneity (*e.g.,* near surface temperature and moisture within a plant's rooting zone) for conservation is more difficult as few studies characterize fine-scale conditions, and those that do cover small spatial extents. Furthermore, many abiotic influences, like frost and heat stress, occur at different times during the day and within a growing season. Thus, it is important to have a temporal understanding of spatial heterogeneity patterns and to know if these patterns are adequately represented in temporally aggregated and bioclimatic metrics that are more commonly used to describe abiotic conditions.

Geographic location, topographic characteristics (*e.g.,* slope, aspect, cold air drainages), vegetation type and pattern, and edaphic factors influence local energy balance and hydrology, which determine abiotic factors like soil temperature and moisture [reviewed in Geiger *et al.* 2009]. Empirical studies have demonstrated that fine-scale abiotic conditions can vary over distances on the order of meters [*e.g.,* Wolfe *et al.* 1949, Urban *et al.* 2000, Bond-Lamberty *et al.* 2005]. Complex mountainous terrain with its different vegetation communities is thought to have highly heterogeneous fine-scale abiotic conditions [Geiger *et al.* 2009]. A few studies have directly assessed the heterogeneity of fine scale climatic conditions in mountainous forest systems, reporting heterogeneity in several factors such as air and soil temperature, relative humidity, wind speed, and solar radiation, as well as diurnal patterns in the heterogeneity [Reifsnyder *et al.* 1971, Chen and Franklin 1997, Bond-Lamberty *et al.* 2005].

The results of these empirical heterogeneity assessments are often described using semivariograms and coefficient of variation. However, these metrics are not easily interpretable for assessing relevant processes such as the persistence of species on the landscape. The semivariogram describes the spatial similarity of conditions on the landscape but does not describe the magnitude of the heterogeneity itself. The coefficient of variation, the standard deviation of a set of observations divided by the mean of those observations, normalizes the variability across a wide range of observations. This is useful for comparisons of quantities where the variance should be compared as a ratio to the mean. The coefficient of variation is not appropriate for abiotic factors to which an individual organism responds because the importance of heterogeneity relative to the mean value may differ across change in the mean. For plants, for example, heterogeneity in soil moisture may be most important at low moisture values when avoiding drought stress is critical. Heterogeneity in temperature may be critical at both cooler and warmer average conditions, as both frost damage and heat stress can be fatal. Thus, absolute, rather than relative, heterogeneity should be examined across the entire range of conditions that a plant may experience on the landscape. While we consider heterogeneity primarily as it relates to plants in this paper, many similar issues pertain to animals living in the near surface. Previous studies fail to compare heterogeneity patterns across ecosystems [but see Chen *et al.* 1999], and they do not report if aggregation in time adequately captures the temporal dynamics of heterogeneity.

Here, we compare fine-scale heterogeneity patterns across four sites in complex mountain landscapes (the Colorado Rockies and the California Sierra Nevada of the western United States). We ask: (1) What are the temporal patterns in fine-scale soil temperature spatial heterogeneity? (2)

How do these patterns vary across mountainous areas with different canopy and landscape characteristics? (3) How do they change when observations are aggregated in time or combined into bioclimatic metrics? (4) Are near-surface patterns similar to those observed in air temperature, a measure commonly used to represent coarse spatial scales? We address these questions using the standard deviation as our metric of heterogeneity. Since we only calculate the standard deviation across space, all further discussion of heterogeneity is referring to spatial heterogeneity.

2.2 Methods

2.2.1 Study sites

We drew upon four fine-scale empirical studies located at alpine, subalpine, and montane elevations in the Colorado Rocky and Sierra Nevada Mountains. We focused our analysis on soil temperature, which is important to plant species itself (*e.g.,* affecting root growth rate, regulating plant available nitrogen via decomposition), and is representative of near-surface temperatures [Kolb and Robberecht 1996, Moyes *et al.* 2015], which is also critical to many plants via direct temperature stress and via indirect influence on water dynamics. We also include air temperatures measured at 2m height above the land surface because it is the standard micrometeorology air temperature observation used in weather forecasts [Geiger *et al.* 2009]. As such, it is one of the most commonly used climatic measurements [Daly *et al.* 2000, Franklin 2010, Oyler *et al.* 2014].

ATWE: The Alpine Treeline Warming Experiment (ATWE) is located on Niwot Ridge in the Eastern Colorado Rocky Mountains [Reinhardt *et al.* 2011, Moyes *et al.* 2012, Castanha *et al.* 2013]. Three sites are located along an elevational gradient in subalpine conifer "Forest" (3060m), alpine "Treeline" ecotone (3430m), and "Alpine" meadow (3540m). The Forest site is mature conifer forest primarily composed of Engelmann spruce, Limber pine, and Lodgepole pine. The Treeline site is an open herbaceous meadow surrounded by krummholz and flag trees in the alpine treeline ecotone. The Alpine site is composed of low-lying perennial herbaceous plants. We randomly selected 1 of 4 sensors in each of 5, 5, and 10 control plots (5, 5, 10 total) within the Forest, Treeline, and Alpine sites, respectively. The sensors [ECTM or 5TM, Decagon, Pullman, WA, USA] recorded soil temperature at 5-10cm depths every 15 minutes from 2010-2013. These sensors sampled an area approximately 2,500m^2, 2,500m^2, and 5,000m^2 for the Forest, Treeline, and Alpine sites, respectively. Although this study had warming and watering treatments, only the control plots are used in this analysis. Data quality was verified through automated and manual quality assessments, and data gaps were filled with Multi-channel Single Spectrum Analysis [Kondrashov and Ghil 2006], subject to gap-filling quality assessment protocols.

RMBL: This site is located at the Rocky Mountain Biological Laboratory (RMBL) on the Western slope of the Colorado Rocky Mountains (2920m) [Harte *et al.* 1995]. This site is a subalpine meadow composed of perennial shrubs (*Artemisia tridentada* Nutt. ssp. *vaseyana* Rydb. and *Dasiphora fruticosa* (L.) Rydb.) and herbaceous species. At peak biomass, the canopy is ~0.8m tall. Three sensors [copper-constantan thermocouples] per plot in 5 control plots (15 total) recorded soil temperature at 12cm depth every 2 hours from 1991–1997. These sensors collectively sampled an area approximately 600m^2. Although this study had warming treatments, only the five control plots are used in this analysis. Data quality was verified with manual quality assessment.

REV: The REV study is a series of elevational sites near the Rocky Mountain Biological Laboratory on the western slope of the Colorado Rocky Mountains [Saleska *et al.* 2002, Dunne *et al.* 2003]. The Lower (2770m), Middle (2940m), and Upper (3190m) sites are subalpine meadows dominated by

mountain big sagebrush *Artemisia tridentada* ssp. *vaseyana*. At each elevational site, 1 sensor [copper-constantan thermocouples] per plot in 5 control plots (5 total) measured soil temperature at 12cm depth every 2 hours from 1996-1998. At each elevational site, these sensors represented an area approximately 1,000m^2. Although this study had a snow manipulation treatment, only the control plots are used in this analysis.

SEKI and SEKI-A: The SEKI (soil temperature) and SEKI-A (air temperature) site is located in Sequoia National Park on the Western slope of the Californian Sierra Nevada (2500m). This site is red fir forest, a semi-open conifer forest composed of 99% red fir trees (*Abies magnifica* Andr. Murray). Two hundred and fifty sensors [DS1921G, Thermocron iButton, Dallas Semiconductor, Maxim Integrated, San Jose, CA, USA] measured soil temperature at 5cm depth every 4 hours form 2010-2013. Additionally, 21 sensors [DS1923, Hydrocron iButton, Dallas Semiconductor, Maxim Integrated, San Jose, CA, USA] with radiation shields [R3, Onset, Bourne, MA, USA] recorded air temperature at 2m height every hour from 2011-2014. To compare with the soil temperature we only use air temperature measurements every 4th hour. Both the soil and air sensors sample the same 12,000m^2 area. Data quality was verified through manual inspection.

Table 2.1 summarizes the data used in each analysis. See Appendix B.1 for site schematics and additional details. All analyses were performed using R version 3.0.2 [R Core Development Team 2013]. The heterogeneity calculated at each site is representative of the area (extent) sampled, which differs at each site (600m^2–12,000m^2). We might expect that larger extents have larger heterogeneity. It is also possible that in a location like the RMBL montane meadow that the majority of heterogeneity across the meadow is captured in the relatively small sample size. Unfortunately, we cannot assess whether this is the case since we would need to sample a larger area within the meadow. Furthermore, the other sites, excepting SEKI, do not have a large enough sample size to assess the scaling relationship. As such, we leave the issue for future work.

Table 2.1: Data used in each temporal analysis. For analyses using aggregated or bioclimatic versions, more than 75, 75, 95, and 50% (ATWE, RMBL, REV, and SEKI, respectively) of the sensor locations at given time step had to be snow-free and error-free for that time step to be included in the analyses. 80% of the SEKI-A locations had to have valid data to be included in the analyses.

Analysis	Temporal Observations / Metrics$^+$	ATWE	RMBL	REV	SEKI	SEKI-A
Raw	Observations in GS*	x	x	x	x	x
	Daily MIN, MAX	x	x	x	x	x
Aggregated	Average monthly daily MIN, MAX	x	x	x	x	
	Average daily MAX of warmest month	x	x		x	
	Average daily MIN of coolest month	x	x	x	x	
	GS average	x	x		x	
Bioclimatic	Soil Degree Days**	x	x		x	
	Snowmelt date***	x	x		x	

$^+$ GS = Growing season; MIN = Minimum; MAX = Maximum

* The ATWE growing season is defined at each sensor location as the period between the first and last day with a diel difference greater than 1.5°C and a mean daily temperature greater than 3°C [Moyes *et al.* 2015]. For RMBL, REV, and SEKI, the growing season for each sensor location is defined as the period between the first and last day of the year with a diel difference greater than 5, 5, and 3.5°C, respectively. Snow-free days during the winter were excluded by requiring the growing season to fall between days of year 90-240, 90-240, and 55-292 for RMBL, REV, and SEKI, respectively. The SEKI-A growing season is defined by first day and last day of installation at the site as determined by access.

** Soil Degree Days is the sum of the positive differences between each day's mean temperature and 5°C during the growing season, *i.e.,* if the daily mean is below 5°C it is not included in the sum.

*** Snowmelt date is the first day of the growing season calculated as described above.

2.2.2 Characterizing spatial heterogeneity

We are interested in the fine-scale heterogeneity of the climatic conditions available to plant species on the landscape at a given point or period of time. We considered these available conditions as a probability density (PDF) with a mean value (Figure 2.1). As a measure of the width of the PDF, the standard deviation (SD) represents the range of conditions observed on the landscape. Thus, we used SD as a measure of the heterogeneity for temperature observations and derived temperature-based metrics across the landscape. If we assume that the spatial distribution is more-or-less normal, we can estimate a range of expected temperature conditions across 95% of the study area by multiplying the SD by 4 (Appendix B.1.6).

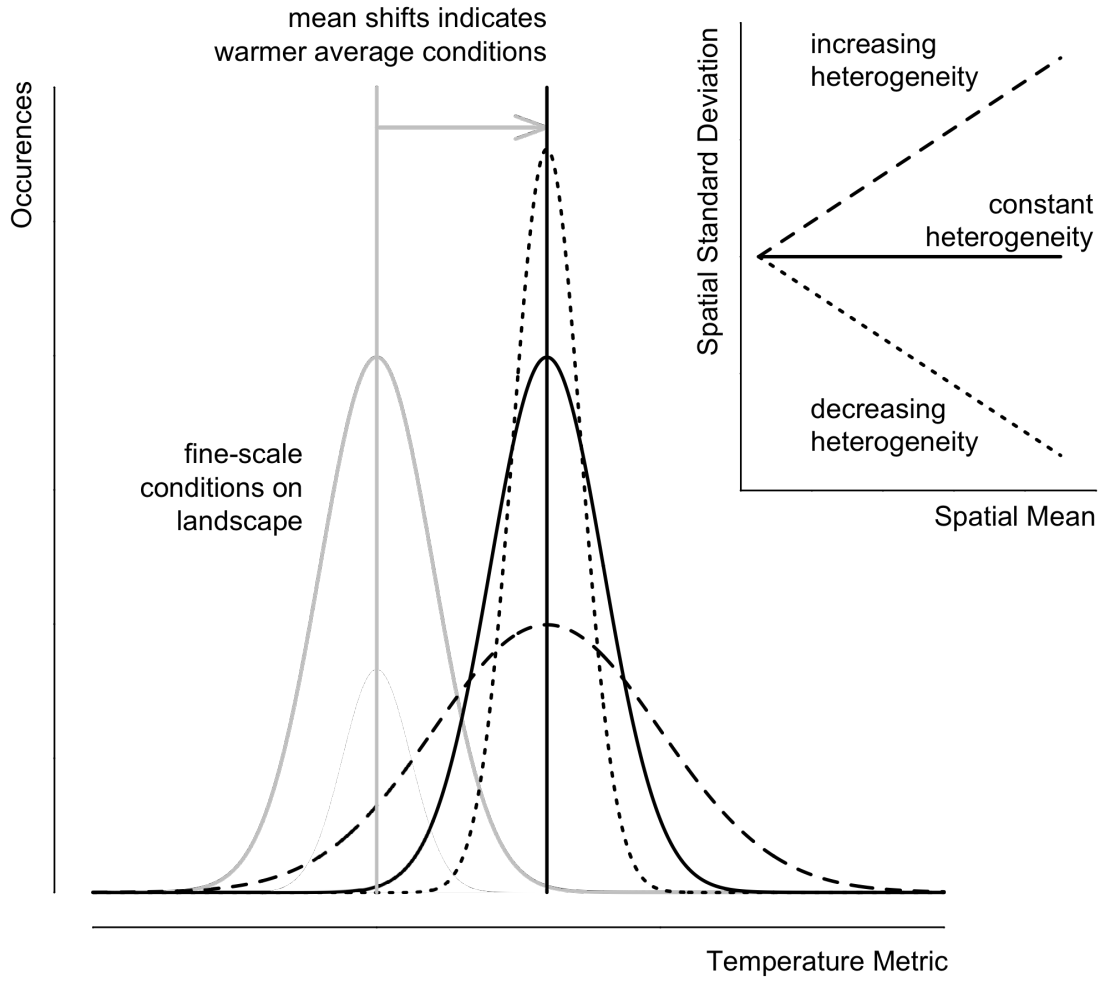


Figure 2.1: The fine scale conditions on a landscape can be considered as probability density. Both the mean (average conditions) and shape of the probability density (heterogeneity) may change in time (*e.g.,* time 1 in gray and time 2 in black). The relationship between spatial standard deviation, as a measure of the shape of the probability density, and the spatial mean indicates increasing, constant, or decreasing heterogeneity with warmer conditions.

For each temperature metric (daily maximum and minimum temperature, average monthly maximum and minimum daily temperatures, snowmelt date, soil degree days, and average growing season temperature), we first calculated the metric at each observation location and then calculated the heterogeneity (SD) over locations. For studies with relatively few sample locations (ATWE,

RMBL, and REV), we calculated the expected error in estimating heterogeneity due to the specific sampling designs implemented in each study (using techniques from chapter 1). In the ATWE, RMBL, and REV sites, the spatial SD calculated from the samples locations are likely underestimates of the true standard deviation, and thus our results are likely conservative (Appendix B.1).

To further assess heterogeneity, we compared the spatial SD to the spatial mean graphically [Famiglietti *et al.* 2008, Rosenbaum *et al.* 2012, Li and Rodell 2013] for snow-free days (Table 2.1). By finding the relationship between the spatial SD and the spatial mean, we characterized how the heterogeneity of fine-scale conditions changed as the average conditions, as described by the spatial mean, changed (Figure 2.1). Positive relationships indicate increasing heterogeneity with warming; no relationship indicates no change in heterogeneity with warming; and negative relationships indicate decreasing heterogeneity with warming. Although we illustrate this framework with a normal probability density, our framework applies to any distribution. Similarly, non-linear relationships between the spatial SD and mean are possible instead of the linear relationships that we used for conceptual illustration.

2.3 Results

2.3.1 Diurnal cycle in soil temperature heterogeneity; daily maximum most heterogeneous

At all of our study sites, there was a strong diurnal cycle in soil temperature heterogeneity, as exemplified by the SEKI site (Figure 2.2). Daily minimum temperatures show very little heterogeneity (1.4°C SD, 5.6°C difference across 95% of the study site) once the snow is completely melted out at the study site (~Day of year 150 in Figure 2.2a). As soon as snowmelt starts in earnest (~Day of year 110 in Figure 2.2a), there is significant heterogeneity in daily maximum temperatures (up to 5°C SD, 20°C across 95% of the study site). While soil temperature is important to plants directly, it has been shown to be correlated with the very near surface (< 5cm) [Kolb and Robberecht 1996, Moyes *et al.* 2015]. If the soil to very near surface temperature relationship at SEKI is similar to that in other temperate forests, heterogeneity in the very near surface temperature is 30-50°C over 95% of the study sites. The diurnal heterogeneity dynamics that we observed in all sites are similar to temporal patterns found in other studies [Chen and Franklin 1997, Xu *et al.* 1997]. These diurnal dynamics are lost when aggregating to daily average temperatures (Figure 2.2b). Additionally, the amplitude of the diurnal heterogeneity pattern is much less for air temperature at 2m height compared to that of the soil temperature at the SEKI site (Figure 2.2c).

2.3.2 Warmer days have higher maximum soil temperature heterogeneity at the near surface

In all of our mountainous sites, the spatial standard deviation of daily maximum soil temperatures is positively related to the spatial mean over time, *i.e.,* heterogeneity in soil daily maximum temperature is greater on warmer days (Figure 2.3). We do not observe this relationship for daily minimum temperatures (Figure B9) or for daily maximum SEKI air temperatures (compare Figure 2.3a to 2.3b). Subalpine forests in the Sierra Nevada (2.3a) and Rocky Mountains (2.3c) have similar positive relationships between heterogeneity and warmer conditions. Both alpine meadows (3d) and subalpine meadows (2.3f) in the Rockies show a positive relationship; however, the relationship is stronger for subalpine meadows (slope=0.11) than alpine (slope=0.08), and both are weaker than for subalpine forests (slope=0.16 SEKI and slope=0.18 A-Forest). At the REV sites (3e), the relationship is twice as strong for the upper elevational site (U) than at the middle (M) and lower (L) sites. Saleska *et al.* 2002 report total above ground biomass increases from U to M to L (from 49, 76

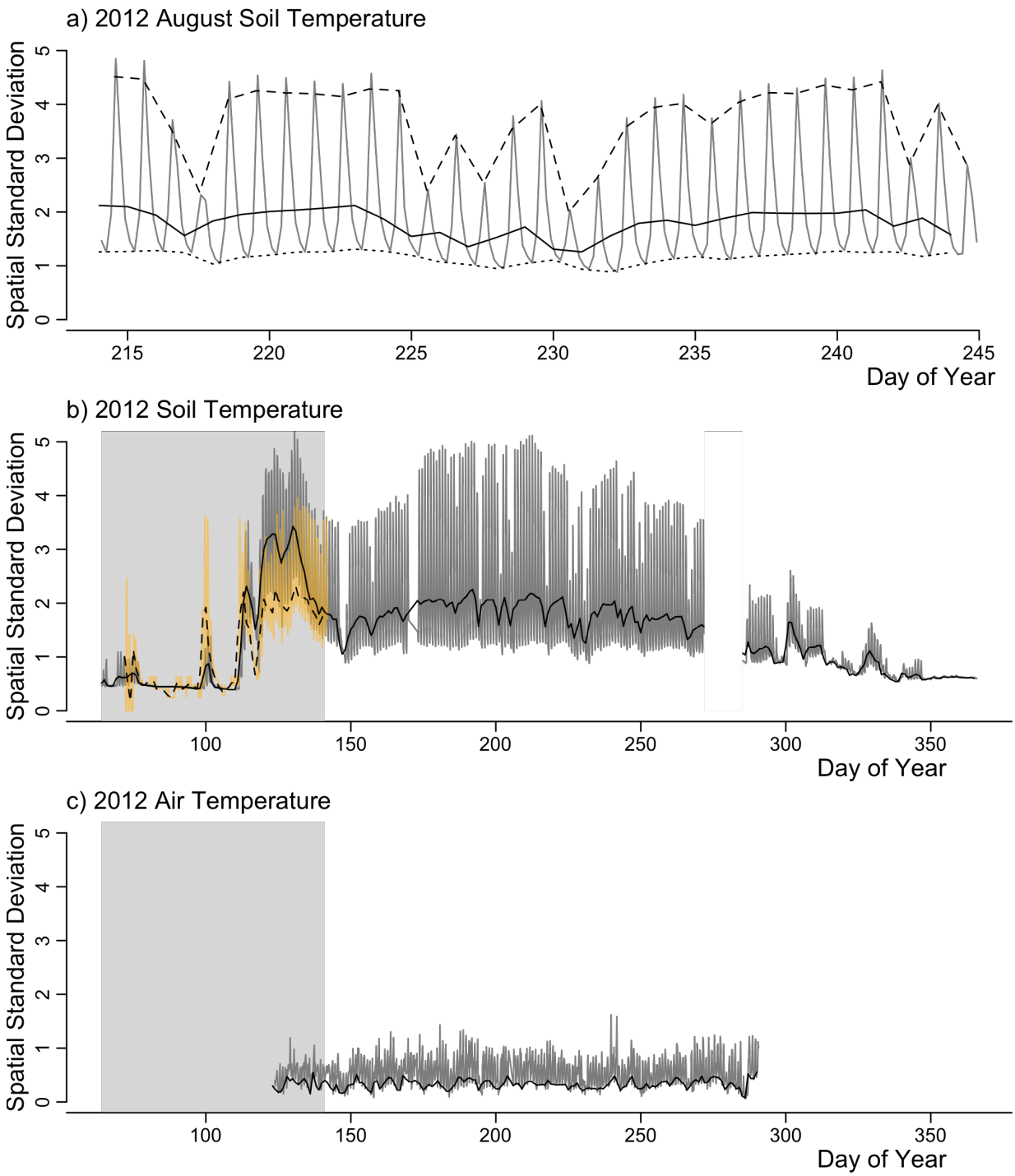


Figure 2.2: Timeseries of temperature heterogeneity at SEKI site during 2012. (a) August soil temperature heterogeneity every 4 hours is shown (gray), with heterogeneity in the daily min (dotted), mean (solid black), and max (dash). (b) Heterogeneity is shown every 4 hours throughout the entire growing season. During the snowmelt period (gray shade), heterogeneity differs when calculated amongst all locations (gray line) or amongst snow-free locations (yellow). Heterogeneity in the daily mean is calculated amongst all locations (black solid line) and amongst snow-free locations (dashed line). The gap in soil temperature data between day of year 170–174 and 272–285 is due to data retrieval. (c) Air temperature spatial heterogeneity every 4 hours at 2m height is shown, with heterogeneity in the daily mean air temperature (black). Note the difference in temporal scales between (a) and (b-c).

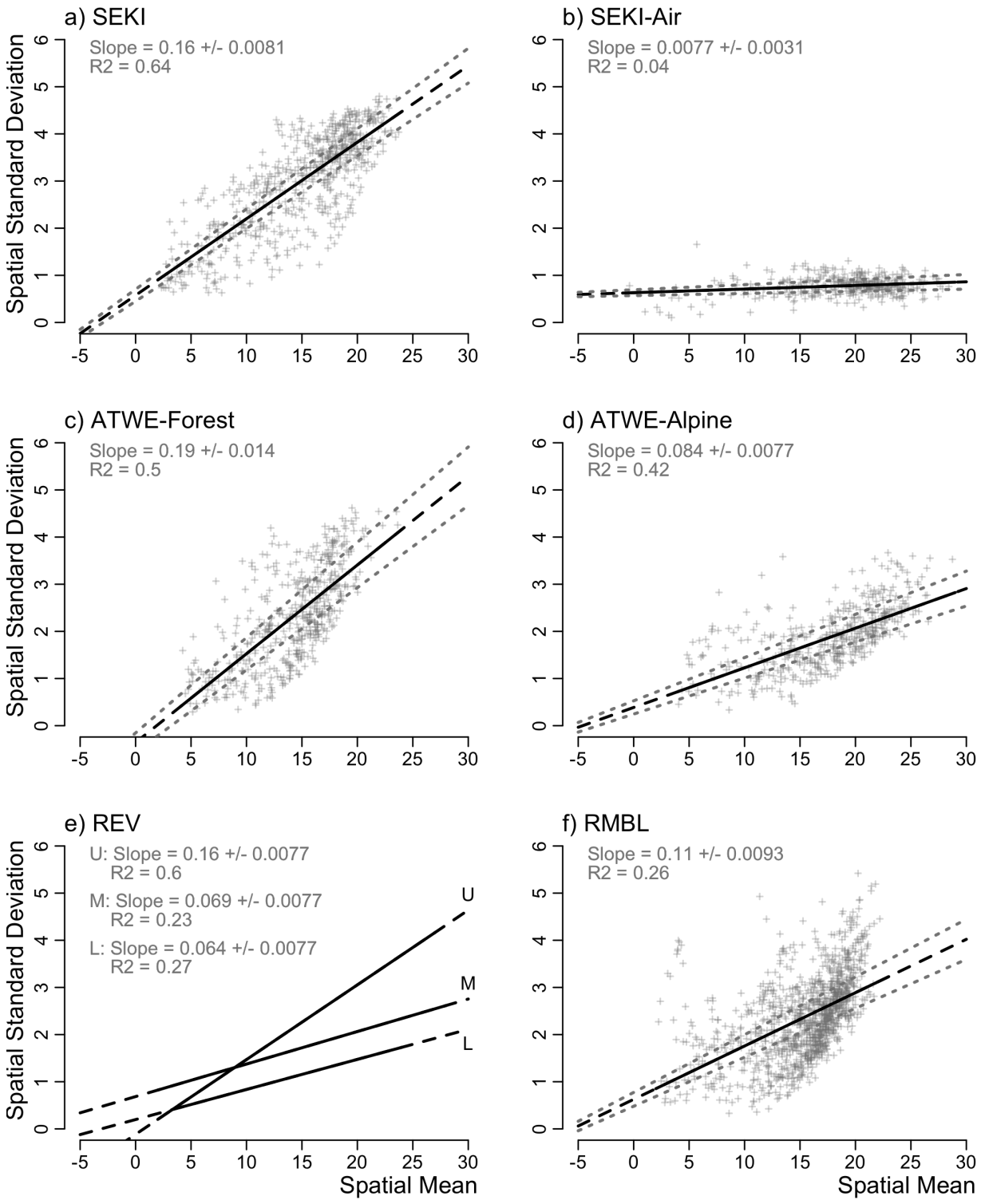


Figure 2.3: Spatial heterogeneity versus spatial mean for daily maximum soil temperature at different mountainous sites. Each point represents a day within sufficient snow-free and error-free locations (Table 2.1). Solid black line is the slope within the data range and the dashed black line is the slope outside the data range. The dotted gray lines are the slope's 95% confidence interval (CI). The slope ± 95% CI is also reported in each panel.

to 125 g C/m^2 respectively), a trend largely driven by increasing herbaceous forbs cover as elevation decreases. However, the above ground shrub biomass is mixed across sites: 13, 5, and 36 g C/m^2, for U, M, and L, respectively. The canopy structure of U with patchy sun/shade patterns from the taller shrubs and little herbaceous cover may be more similar to the forested sites (A-Forest and SEKI) than the M and L sites.

2.3.3 Aggregated monthly temperature values show similar trends to daily values

Across all months of the growing season, heterogeneity in the average monthly maximum daily temperature is higher in warmer months similar to that seen in the daily maximum temperature values (Figure 2.4a). As in the daily minimum temperature, no relationship is observed in the average

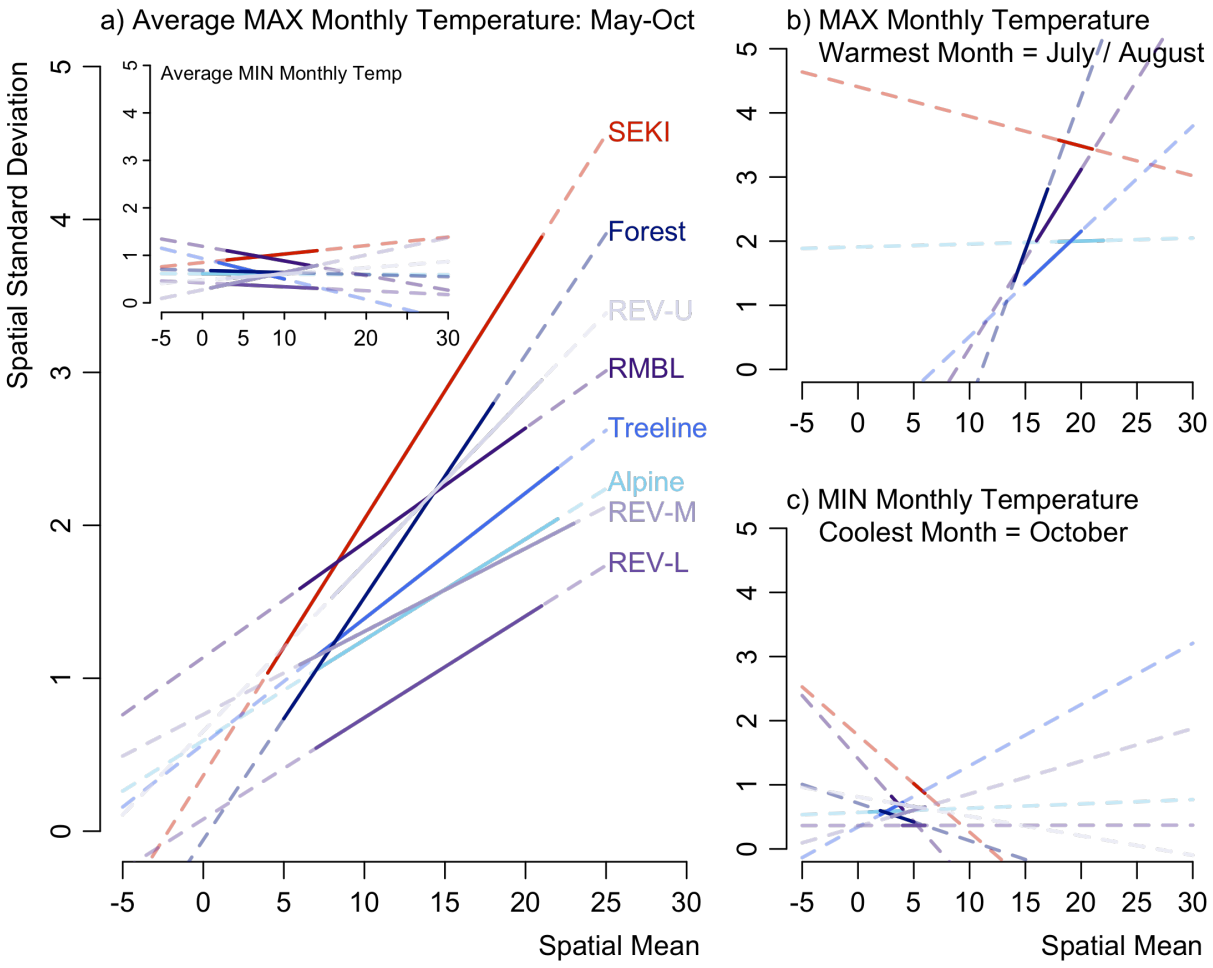


Figure 2.4: Average monthly minimum and maximum soil temperatures for all montane sites: (a) Max and min (inset) for all months and all years; (b) Max monthly temp for warmest growing season month (July for RMBL; Aug for SEKI and ATWE; REV sites have too few years of data.) for all years; (c) Min monthly temp for coolest growing season month (October) for all years. The estimated slope is represented by solid lines over the range of observations and by dashed lines for extrapolations beyond the observational range. The latter is included so that slopes can be easily compared across all analyses on the same axes.

monthly minimum daily temperature (inset). We observe inconsistent relationships when comparing average monthly values of the warmest and coolest months over multiple years (2.4b & 2.4c), which is likely due to the low sample size. For example, in the SEKI site, the monthly trend is quite different than the daily trend for the warmest month of July, while in August, which is nearly as warm, the monthly trend is suggestive of the underlying daily trend (Figure 2.5). At the SEKI site, despite representing the general daily trend, the monthly values of July and August do not capture the full range of heterogeneity occurring at the daily level within the month.

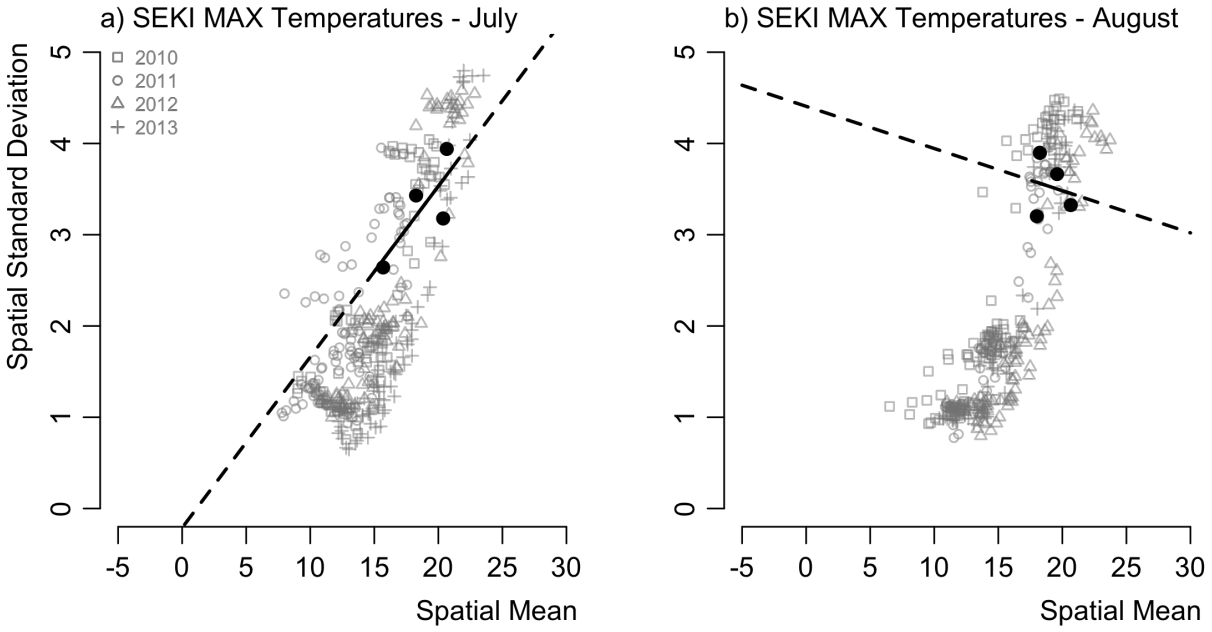


Figure 2.5: Maximum daily temperatures (gray symbols) and average maximum monthly temperature (solid black circles) for July and August for all years at SEKI. Slope estimated from average maximum monthly temperature over data range in solid black and beyond in dashed black line (we extend the slopes for easier comparison). The squares, circles, triangles, and cross symbols indicated a daily value from 2010, 2011, 2012, and 2013, respectively.

2.3.4 Bioclimatic variables have mixed heterogeneity characteristics

At the REV shrub-dominated sites, heterogeneity of snowmelt date is higher when the average snowmelt data is later, while the alpine and forested ATWE sites have higher heterogeneity with earlier snowmelt (Figure 2.6c). The SEKI site is the only site in which soil degree days show a positive relationship between heterogeneity and the spatial mean (2.6b). Amongst the study sites, mean growing season soil temperatures show inconsistent heterogeneity relationships to the spatial mean (2.6a). These mixed results again may be due to limited data at several of the study sites. However, the heterogeneity observed in the annual value is less than that observed in most monthly values.

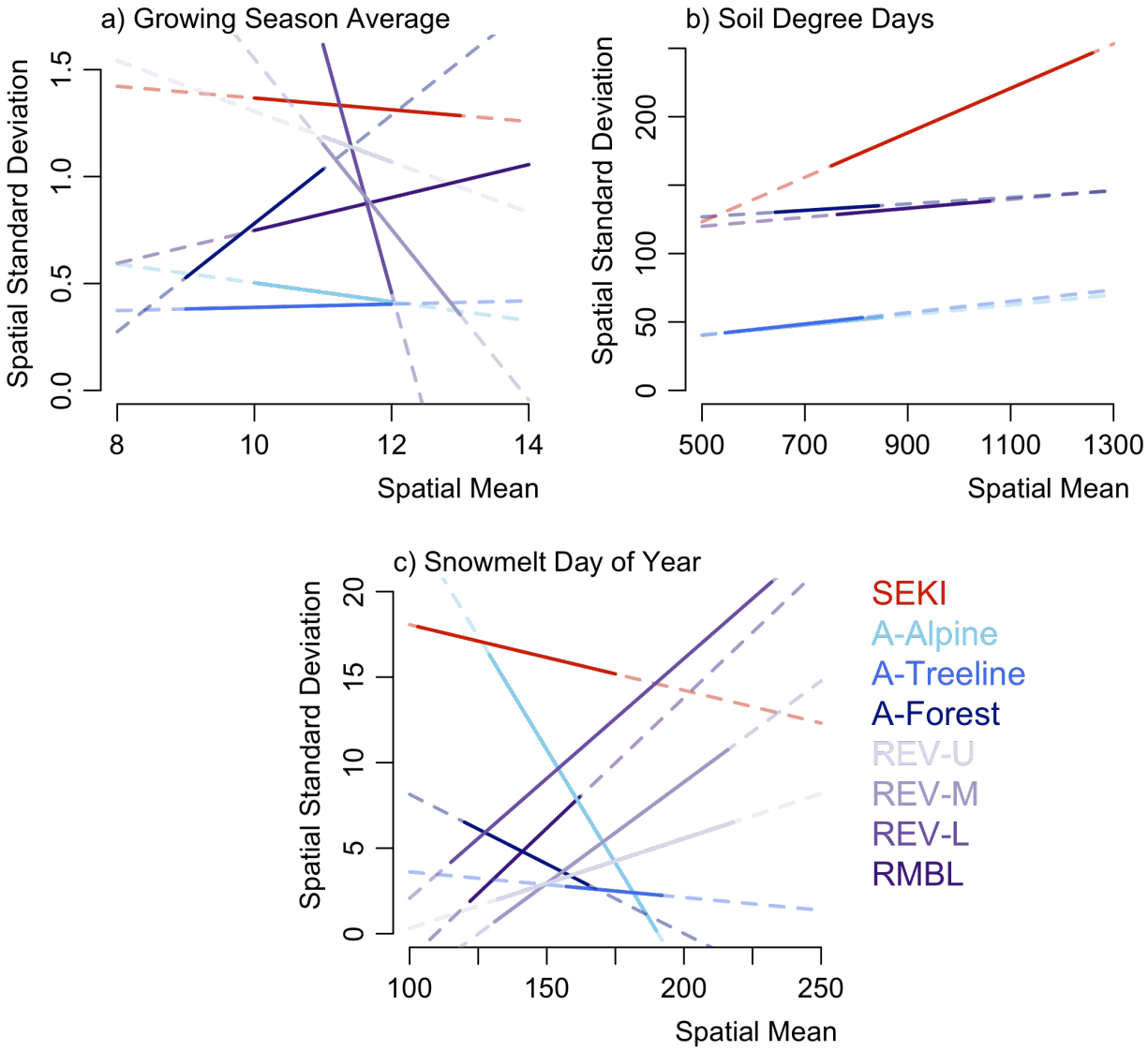


Figure 2.6: Spatial mean versus spatial heterogeneity for a) growing season average and bioclimatic metrics, b) soil degree days and c) snowmelt date for the mountainous sites. Slope estimated from average maximum monthly temperature over data range in solid lines and beyond in dashed (we extend the slopes for easier comparison).

2.4 Discussion

Our goal in this analysis is to characterize heterogeneity temperature patterns across complex mountainous environments. In addition, we ask whether aggregated temporal metrics adequately represents observed temporal dynamics and if heterogeneity in soil temperatures is similar to typically measured air temperature observations. We summarize our results comparing heterogeneity to average conditions in Figure 2.7.

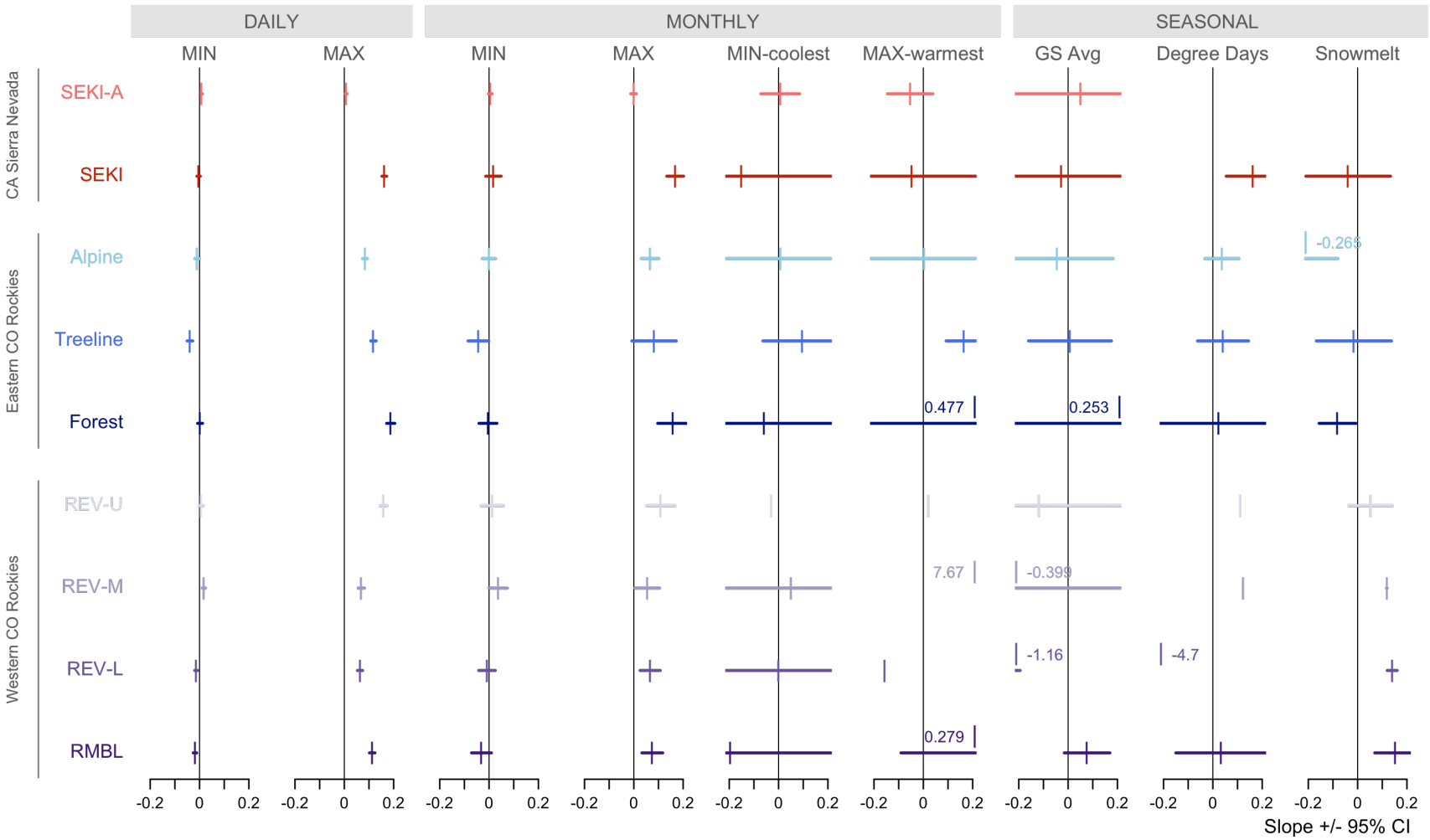


Figure 2.7: The estimated slope for spatial heterogeneity – spatial mean relationship is indicated with the vertical bar and the 95% confidence interval (CI) is reported with the horizontal bar. If the slope CI is outside the range of -0.2 to 0.2, the value is given.

2.4.1 Temporal patterns in soil temperature heterogeneity

At all of our sites, we observed a wide range of heterogeneity in soil temperature throughout the daily cycle and throughout the growing season. The maximum heterogeneity, occurring at the daily maximum temperature, is quite large up to 20°C at 5cm depth at the SEKI site across 95% of the landscape, which corresponds to 30-50°C of air temperature heterogeneity at the very near surface (< 5cm). This is a large range of conditions when compared to the projected average increase of 1.9°C and 4.0°C (1.0–2.9°C and 2.9–5.0°C, 5th – 95th quartiles) for 2050 and 2085 in daily maximum air temperatures during a May–October growing seasons at the SEKI location (Appendix B.2). The consistent daily minimum temperatures observed at our SEKI site (~5.6°C for 95% of the landscape) (Figure 2.2a–b) is commensurate with the projected average increase of 1.7°C and 3.6°C (1.1–2.6°C and 2.5–4.7°C, 5th – 95th quartiles) for 2050 and 2085 in daily maximum air temperatures.

From a plant's perspective near the surface, differences in heterogeneity are likely to have important consequences during the following time periods: (1) the period when snow covers the entire landscape, (2) the period of patchy snowmelt, and (3) the period of when the landscape is completely snow-free. The period of complete snow cover is uninteresting from a heterogeneity perspective because (1) there is no heterogeneity in soil and near surface temperatures because the snow insulates the surface keeping temperatures hovering near 0°C and (2) most near surface plants are either dormant or unable to grow / germinate when covered with snow. Heterogeneity calculated from all locations during the period of patchy snowmelt is misleading because most snow-covered plants are inactive before snowmelt in their immediate vicinity. Patchy snowmelt artificially inflates the heterogeneity in maximum temperature until all locations are melted out as the daily maximum temperature under snow is ~0°C (Figure 2.2b). Once all locations in the plot are snow-free, heterogeneity becomes an unbiased representation of the variability of conditions experienced by the near surface plants. Thus, we only calculate heterogeneity for snow-free days. To capture the important effects of variable snowmelt, heterogeneity in snowmelt date itself should be calculated.

After snow melts, greater heterogeneity occurs on warmer days. We observed this positive relationship at all study sites although with varying strengths (slopes from 0.06 to 0.18, Figure 2.7). On the other hand, the heterogeneity in daily minimum temperatures is relatively constant throughout the growing season and is quite small (*e.g.,* ~5°C across 95% of the SEKI site) compared to daily maximum. How these differences in daily minimum and maximum temperature heterogeneity matter for plant species is dependent on the corresponding average condition. If the average minimum temperature is hovering around the frost tolerance of a species, then even a little heterogeneity in minimum temperatures can mean survival for an individual in more suitable locations. Similarly, if the average maximum condition is above the heat stress tolerance of a species, the large range of heterogeneous conditions can provide refugia if individuals of a heat-sensitive species are present in those buffered locations.

2.4.2 Influences on temporal patterns in fine-scale heterogeneity

The strength of the relationship between heterogeneity and the average conditions for daily maximum soil temperatures varies amongst the mountainous sites (Figure 2.3). Our results are consistent with other studies that find canopy complexity affects soil temperature patterns [Hungerford and Babbitt 1987, Van Pelt and Franklin 2000]. The subalpine semi-open forested sites (SEKI & A-Forest) have similarly complex canopies and similar heterogeneity relationships, which are in turn stronger (more positive) than the alpine meadow site (A-Alpine). The subalpine meadow (RMBL), whose canopy reaches 80cm tall is much more complex than the alpine meadow's 15-25cm canopy, has a stronger relationship between heterogeneity and the average conditions than the alpine

site. Along the elevational gradient in subalpine shrubland (REV), less dense shrub yields more heterogeneity change (larger slope). As the shrub cover becomes denser, it is possible that the near-surface conditions become more similar and heterogeneity drops.

Other factors influencing fine-scale soil temperature heterogeneity include fine-scale topography and soil moisture, as well as coarse-scale topography and weather patterns [Geiger *et al.* 2009]. We observed reductions in both the heterogeneity and mean values during the mid-summer that we hypothesize are due to cloudy / stormy weather conditions. We were surprised by the significant heterogeneity observed in the alpine meadow. Fine-scale topography may influence heterogeneity more in this alpine system than in the forests due to higher winds, a significant mechanism for surface heat removal, at the alpine site. The alpine canopy is likely contributing to further wind blocking, and thus contributing to the heterogeneity of soil temperature through topographic mechanisms in addition to radiation patterning.

The monthly differences in heterogeneity that we observed are likely a combination of soil moisture, radiation input, and coarse-scale weather. We observe less heterogeneity in the cooler months of May and October than the warmer months of July and August. Soil moisture influences soil temperature heterogeneity least when it is wet everywhere, as it is early in the growing season (May). A wet location in shade is more similar to a wet condition in the sun than a dry condition in the sun because the energy input into the system can be removed via evaporative cooling (latent heat). When soil moisture is patchy and or similarly dry across the landscape, soil moisture contributes to soil temperature heterogeneity. Interestingly, in our years with late snowmelt at the SEKI site, heterogeneity and spatial mean are high right after snowmelt. Either an extremely quick soil moisture draw down occurs (quickly eliminating the buffering effect of soil moisture) or perhaps direct radiation input trumps the soil moisture buffering effects. One could assess the potential influence of soil moisture by comparing heterogeneity in wet and dry periods of the growing season.

Direct radiation changes throughout the growing season, with the largest input into the system occurring in July and August when heterogeneity is the greatest. This makes sense as more energy entering the system can enhance sun/shade differences. Topographic position of the locations on the landscape also interact with direct radiation by changing the interception angle which further alters intensity of the energy input. Finally, coarse scale weather can influence fine-scale heterogeneity. In October especially, cold air masses from storms are routinely moving through the mountain terrain, counteracting temperature differences due to direct radiation.

2.4.3 Temporal aggregation masks daily heterogeneity magnitude and dynamics

Because of the diurnal patterns in heterogeneity, the daily average represents less heterogeneity than observed in the maximum temperatures and more heterogeneity than observed in the minimum temperatures. Thus, as for absolute temperature values, the heterogeneity in the daily minimum and maximum values can be more biologically significant, especially when conditions are close to physiological thresholds relevant to frost occurrence and heat stress.

Similarly because of differing day-to-day weather conditions, heterogeneity in average monthly daily maximum temperatures are not representative of widely varying daily maximum heterogeneity. If high temperatures are important to physiological plant functions [Kolb and Robberecht 1996, Moyes *et al.* 2015] that in turn influence species persistence, this omission is problematic because the extreme events are not represented. However, the relationship between the heterogeneity and spatial mean of monthly values across all growing season months (Figure 2.4a) is similar to that of the daily values (Figure 2.3). This result suggests that we can use monthly values as a proxy for daily

characteristics, although more investigation is warranted. Because we observed little variability in daily minimum temperature values throughout the growing season, the average monthly minimum temperature heterogeneity is representative of daily minimum temperature heterogeneity.

2.4.4 Heterogeneity in air temperature differs from near surface heterogeneity

Heterogeneity characteristics of air temperature measured at the standard 2m height are quite different than the soil characteristics at the SEKI site. We do not observe high levels of heterogeneity in maximum daily air temperature, similar to other findings [Chen and Franklin 1997]. However, unlike previous work [Chen and Franklin 1997], we do not observe increasing heterogeneity with warmer conditions. While we did expect air temperature at 2m height to be different than that at the near surface primarily due to air mixing, we did not expect such comparatively low and consistent heterogeneity throughout the growing season. We may have observed more air temperature heterogeneity if the study extent had included coarse scale topographic features, like steep stream drainages with cold air pooling and/or protection from prevailing wind, which may be decoupled from other portions of the landscape. The spatial mean of air temperature does track the spatial mean of the soil temperature (Figure 5.2 in the conclusion chapter). However, the disparity in heterogeneity characteristics underscores previous work [Chen *et al.* 1999] suggesting that the coarse-scale 2m air temperatures, often used to characterize a species niche in projection models, do not represent the conditions experienced by near surface plants, as well as near surface animals [Ashcroft *et al.* 2008, Franklin 2010, de Frenne *et al.* 2013].

2.5 Conclusions

Our results suggest that significant fine-scale heterogeneity in soil temperature occurs in mountainous ecosystems. Aggregated or bioclimatic metrics are not adequate to capture the full range of heterogeneity observed, especially maximum temperature values that may indicate stressful conditions. Air temperature as commonly measured at 2m also does not capture heterogeneity in the near-surface conditions that many organisms experience. Thus, ecological tools that utilize aggregated metrics or 2m air temperature are likely misrepresenting the influence of fine-scale spatiotemporal temperatures on the organisms living at the very near surface (< 5cm).

2.6 Acknowledgements

We thank Jennifer A. Dunne for sharing her REV data, Andrew B. Moyes for soil and near surface profile models, field location logistical support staff, and the many field assistants who helped gather these datasets. Thanks also to Maya Hayden, Adam B. Smith, and Margaret S. Torn for comments on early drafts. The ATWE project was supported by US Department of Energy Office of Science (BER); the RMBL project was supported by National Science Foundation; the SEKI project was supported by US Department of Energy Office of Science (BER), Berkeley Atmospheric Science Center, National Park Service (NPS) George Melendez Wright Climate Change Fellowship, and the NPS California Cooperative Ecosystem Unit.

2.7 References

Ashcroft, M.B., Chisholm, L.A. & French, K.O. (2009). Climate change at the landscape scale: predicting fine-grained spatial heterogeneity in warming and potential refugia for vegetation. *Global Change Biology*, **15**, 656–667.

Bond-Lamberty, B., Wang, C. & Gower, S.T. (2005). Spatiotemporal measurement and modeling of stand-level boreal forest soil temperatures. *Agricultural and Forest Meteorology*, **131**, 27–40.

Castanha, C., Torn, M.S., Germino, M.J., Weibel, B. & Kueppers, L.M. (2013). Conifer seedling recruitment across a gradient from forest to alpine tundra: effects of species, provenance, and site. *Plant Ecology & Diversity*, **6**, 307–318.

Chen, J.Q. & Franklin, J.F. (1997). Growing season microclimate variability within an old-growth Douglas-fir forest. *Climate Research*, **8**, 21–34.

Chen, J.Q., Saunders, S.C., Crow, T.R., Naiman, R.J., Brosofske, K.D., Mroz, G.D., Brookshire, B.L. & Franklin, J.F. (1999). Microclimate in forest ecosystem and landscape ecology - Variations in local climate can be used to monitor and compare the effects of different management regimes. *Bioscience*, **49**, 288–297.

Clark, J.S., Bell, D.M., Hersh, M.H., Kwit, M.C., Moran, E., Salk, C., Stine, A., Valle, D. & Zhu, K. (2011). Individual-scale variation, species-scale differences: inference needed to understand diversity. *Ecology Letters*, **14**, 1273–1287.

Daly, C., Taylor, G.H., Gibson, W.P., Parzybok, T.W., Johnson, G.L. & Pasteris, P.A. (2000). High-quality spatial climate data sets for the United States and beyond. *Transactions of the Asae*, **43**, 1957–1962.

De Frenne, P., Rodríguez-Sánchez, F., Coomes, D.A., Baeten, L., Verstraeten, G., Vellend, M., Bernhardt-Roemermann, M., Brown, C.D., Brunet, J., Cornelis, J., Decocq, G.M., Dierschke, H., Eriksson, O., Gilliam, F.S., Hedl, R., Heinken, T., Hermy, M., Hommel, P., Jenkins, M.A., Kelly, D.L., Kirby, K.J., Mitchell, F.J.G., Naaf, T., Newman, M., Peterken, G., Petřík, P., Schultz, J., Sonnier, G., Van Calster, H., Waller, D.M., Walther, G.-R., White, P.S., Woods, K.D., Wulf, M., Graae, B.J. & Verheyen, K. (2013). Microclimate moderates plant responses to macroclimate warming. *Proceedings of the National Academy of Sciences*, **110**, 18561–18565.

Dobrowski, S.Z. (2011). A climatic basis for microrefugia: the influence of terrain on climate. *Global Change Biology*, **17**, 1022–1035.

Dunne, J.A., Harte, J. & Taylor, K.J. (2003). Subalpine meadow flowering phenology responses to climate change: integrating experimental and gradient methods. *Ecological Monographs*, **73**, 69–86.

Famiglietti, J.S., Ryu, D., Berg, A.A., Rodell, M. & Jackson, T.J. (2008). Field observations of soil moisture variability across scales. *Water Resources Research*, **44**, W01423.

Franklin, J. (2010). *Mapping Species Distributions*. Cambridge University Press.

Geiger, R., Aron, R.H. & Todhunter, P. (2009). *The Climate Near the Ground*. Rowman & Littlefield Publishers, Inc, Plymouth, United Kindom.

Gillingham, P.K., Huntley, B., Kunin, W.E. & Thomas, C.D. (2012). The effect of spatial resolution on projected responses to climate warming. *Diversity and Distributions*, **18**, 990–1000.

Grubb, P.J. (1977). Maintenance of Species-Richness in Plant Communities - Importance of Regeneration Niche. *Biological Reviews of the Cambridge Philosophical Society*, **52**, 107–145.

Harper, J.L. (1977). *Population biology of plants*. Academic Press, London.

Harte, J., Torn, M.S., Chang, F.R. & Feifarek, B. (1995). Global warming and soil microclimate: results from a meadow-warming experiment. *Ecological Applications*, **5**, 132.

Harwood, T.D., Mokany, K. & Paini, D.R. (2014). Microclimate is integral to the modeling of plant responses to macroclimate. *Proceedings of the National Academy of Sciences*, **111**, E1164–E1165.

Hungerford, R.D. & Babbitt, R.E. (1987). Overstory Removal and Residue Treatments Affect Soil Surface, Air, and Soil-Temperature - Implications for Seedling Survival. *USDA Forest Service Intermountain Research Station Research Paper*, 1–19.

Keppel, G. & Wardell-Johnson, G.W. (2012). Refugia: keys to climate change management. *Global Change Biology*, **18**, 2389–2391.

Kolb, P.F. & Robberecht, R. (1996). High temperature and drought stress effects on survival of Pinus ponderosa seedlings. *Tree Physiology*, **16**, 665–672.

Kondrashov, D. & Ghil, M. (2006). Spatio-temporal filling of missing points in geophysical data sets. *Nonlinear Processes in Geophysics*, **13**, 151–159.

Lawler, J.J., Ackerly, D.D., Albano, C.M., Anderson, M.G., DOBROWSKI, S.Z., Gill, J.L., Heller, N.E., Pressey, R.L., Sanderson, E.W. & Weiss, S.B. (2015). The theory behind, and the challenges of, conserving nature's stage in a time of rapid change. *Conservation Biology*, **29**, 618–629.

Li, B. & Rodell, M. (2013). Spatial variability and its scale dependency of observed and modeled soil moisture over different climate regions. *Hydrology and Earth System Sciences*, **17**, 1177–1188.

Moyes, A.B., Castanha, C., Germino, M.J. & Kueppers, L.M. (2012). Warming and the dependence of limber pine (Pinus flexilis) establishment on summer soil moisture within and above its current elevation range. *Oecologia*, **171**, 271–282.

Moyes, A.B., Germino, M.J. & Kueppers, L.M. (2015). Moisture rivals temperature in limiting photosynthesis by trees establishing beyond their cold-edge range limit under ambient and warmed conditions. *New Phytologist*, **207**, 1005–1014.

Oyler, J.W., Ballantyne, A., Jencso, K., Sweet, M. & Running, S.W. (2014). Creating a topoclimatic daily air temperature dataset for the conterminous United States using homogenized station data and remotely sensed land skin temperature. *International Journal of Climatology*, 2258–2279.

Peterson, A.T., Soberón, J., Pearson, R.G., Anderson, R.P., Martínez-Meyer, E., Nakamura, M. & Araújo, M.B. (2011). *Ecological Niches and Geographic Distributions*. Princeton University Press.

Potter, K.A., Arthur Woods, H. & Pincebourde, S. (2013). Microclimatic challenges in global change biology. *Global Change Biology*, **19**, 2932–2939.

R Core Development Team. (2013). R: A language and environment for statistical computing. R Foundation for Statistical Computing, Vienna, Austria. URL http://www.R-project.org/

Reifsnyder, W.E., Furnival, G.M. & Horowitz, J.L. (1972). Spatial and temporal distribution of solar radiation beneath forest canopies. *Agricultural Meteorology*, **9**, 21–37.

Reinhardt, K., Castanha, C., Germino, M.J. & Kueppers, L.M. (2011). Ecophysiological variation in two provenances of Pinus flexilis seedlings across an elevation gradient from forest to alpine. *Tree Physiology*, **31**, 615–625.

Saleska, S.R., Shaw, M.R., Fischer, M.L., Dunne, J.A., Still, C.J., Holman, M.L. & Harte, J. (2002). Plant community composition mediates both large transient decline and predicted long-term recovery of soil carbon under climate warming. *Global Biogeochemical Cycles*, **16**, 4, 1055.

Wolfe , J. N. *et al.* (1949). Microclimates and Macroclimate of Neotoma, A Small Valley in Central Ohio, Publication No. 488. - Department of Botany and Plant Pathology, Ohio State University.

Chapter 3: Untangling influences on tree seedling establishment at fine spatial scales: abiotic and biotic factors explain seedling occupancy patterns

Regeneration is critical to forest persistence. To understand and manage the effects of climate change on forests, we must know what abiotic factors influence the persistence and abundance of tree seedlings and adult individuals. Recent studies suggest that the regeneration niche of tree seedlings differs from that of adults. Empirical plot-scale studies suggest that tree seedlings are responding to abiotic conditions. There is also evidence that forest stand structure affects seedling recruitment via direct and indirect biotic interactions. However, systematic study of both the influence of abiotic (physical) and biotic factors (forest stand structure) on tree seedling occupancy patterns is lacking. Thus, we conducted an observational study of red fir (*Abies magnifica* Andr. Murray) recruitment in California's Sierra Nevada, monitoring seedling persistence over 4 years for both an older and younger seedling group. We measured a suite of abiotic and biotic factors at 225 locations within a 1-hectare study plot and estimated their values on a 1x1m grid using spatial statistics. We identified factors that influence occupancy (seedling presence / absence) as observed at the study period end and compared mortality occurring throughout the study period with predicted probability of seedling presence. We find that (1) abiotic and biotic factors, including snowmelt date, potential evaporation, canopy cover, distance to nearest adult tree, and seed rain density, explain a large portion of red fir seedling occupancy at fine spatial scales; (2) soil factors are more important for younger seedlings; and (3) seedling mortality occurs in areas with higher seedling density as the predicted probability of seedling presence increases, which suggests that as seedlings grow, mortality due to density-dependence may increase. Thus, to promote forest regeneration under a changing climate, we recommend (1) including locations with fine-scale abiotic heterogeneity in conservation efforts and (2) distinguishing between direct and indirect biotic influences so that the role of forest stand structure on fine-scale abiotic heterogeneity can be better understood and incorporated into resource management tools.

3.1 Introduction

Tree seedling establishment is critical to the persistence of forests in their current geographical ranges and especially for movement into new areas. As defined by Grubb [1977], regeneration is composed of several stages, including production of viable seed, dispersal, seed germination, seedling establishment, and juvenile growth. Individuals in each stage have potentially different responses to the same environmental conditions, meaning there are different regeneration niche characteristics. Empirical evidence suggests that younger life history stages may have more limiting physiological tolerances, as tree seedlings and germinants are often more sensitive to radiation, water availability, and soil conditions than older individuals [Battaglia *et al.* 2000, Maher and Germino 2006, Collins and Carson 2004, Johnson *et al.* 2011, Carón *et al.* 2015]. Similarly, recent studies have suggested that juvenile trees have narrower coarse-scale climatic tolerances than adult individuals

This chapter was written in a style for publication with advisors Cari G. Kaufman and Lara M. Kueppers. Thus, I use "we." All Tables and Figures with prefix "C" can be found in Appendix C.

[Lenior *et al.* 2009, McLaughlin and Zavaleta 2012, Bell *et al.* 2013, Dobrowski *et al.* 2015]. Identifying the factors that influence all regeneration stages is necessary to understand where tree species will and will not occur on the landscape [Jackson *et al.* 2009].

Empirical studies suggest that both abiotic (physical environmental) and biotic (intra- and interspecific interactions) factors are important for tree seedling establishment. For example, abiotic factors such as minimum and maximum temperature thresholds kill seedlings through frost and reduced carbon assimilation [Mayr *et al.* 2006, Moyes *et al.* 2015]. Drought stress and soil conditions can also prevent seedling presence in a location [*e.g.,* Gordon 1970, Ustin *et al.* 1984, Ibáñez *et al.* 2007, Moyes *et al.* 2015]. For red fir (*Abies magnifica* Andr. Murray), a conifer species of Western North America, empirical work has suggested the importance of several abiotic factors in successful seedling establishment, including timing and duration of direct radiation exposure, drought stress, exposure to thermal extremes, and access to mineral soil [Gordon 1970, Ustin *et al.* 1984, Chappell and Agee 1996, Barbour *et al.* 1998]. Additionally, Gordon [1970] reported that access to mineral soil is a key factor for younger red and white fir seedlings, suggesting different abiotic requirements amongst the early life stages. These studies, each concluding that a different factor or set of factors primarily explain successful seedling establishment, hint at a complex abiotic regeneration niche.

Biotic interactions also play a role in successful seeding establishment. Intra- and interspecific interactions may influence seedling establishment through direct competition for resources [George and Bazzaz 2014, Carón *et al.* 2015, Kroiss and HilleRisLambers 2015 but see Moles and Westoby 2004], herbivory [George and Bazzaz 2014, Moles and Westoby 2004], and disease [Moles and Westoby 2004, Ibáñez *et al.* 2007]. Plant-to-plant interactions may occur between individuals of similar size, *e.g.,* seedling-to-seedling and seedling-to-understory vegetation, or between seedlings and adult trees. The latter can take the form of a Janzen-Connell effect in which an adult is not directly competing with a seedling for resources but rather is a source of pathogens or herbivores [Janzen 1970, Connell 1971]. Coupled with dispersal patterns, seedling establishment is often most successful at mid-range distance from the adult tree. In forests, another type of seedling-to-adult biotic interaction occurs when the stand structure, composed of adults and larger juveniles, influences fine-scale abiotic conditions that affect seedling establishment [de Frenne *et al.* 2013, Dowbrowski *et al.* 2015]. For example, the sun/shade patterns created on a forest floor have a large effect on both the temperature and moisture regime near the soil surface [Geiger *et al.* 2009, von Arx *et al.* 2013]. Forest stand structure can also affect soil conditions through uneven litter accumulation [Frankland *et al.* 1963, Chambers 2001]. The forest stand structure works in concert with topographic complexity, which can similarly generate fine-scale habitat suitable for seedling establishment [Wolfe *et al.* 1949, Geiger *et al.* 2009].

The combination of both abiotic and biotic factors, together with dispersal limitation, is thought to determine a species' realized niche and observed patterns of presence/absence on the landscape, *i.e.,* occupancy [Soberón 2007, Peterson *et al.* 2011]. We have an understanding of the important abiotic factors on seedling establishment from plot-based research that reveals correlations between abiotic factors and seedling density, growth, or mortality from sampled areas of the landscape. But we are not aware of any studies that directly assess the influence of these factors on continuous landscape patterns of seedling occupancy. In recent studies of patterns of juvenile trees, Dobrowski *et al.* [2015] report that forest stand characteristics explained more of the juvenile spatial pattern than climatic factors. However, like most studies of adult landscape patterns, this study was conducted at coarse-spatial scales (~1-km resolution) [Franklin 2010 but see Gottfried *et al.* 1999, Trivedi *et al.* 2008, Randin *et al.* 2009].

Assessing abiotic and biotic factors that influence occupancy at coarse-spatial scale presents two challenges for understanding seedling establishment. First, it is generally thought an individual responds to the conditions immediately surrounding it [Clark *et al.* 2011, Potter *et al.* 2013, Harwood *et al.* 2014]. Hence, in complex systems such as forests, coarse-scale conditions may not accurately represent the fine-scale conditions that the seedling experiences [von Arx *et al.* 2013, de Frenne *et al.* 2013]. Thus, an analysis untangling the important factors affecting seedling establishment is needed at spatial scales similar to which a seedling experiences its environment, *i.e.,* much less than 1-km resolution [Potter *et al.* 2013]. Secondly, recent coarse-scale studies suggest that characteristics of the forest stand structure (*i.e.,* older juvenile and adult trees) play an important role in the presence/absence of tree seedlings and understory species [de Frenne *et al.* 2013, Dobrowski *et al.* 2015]. It is unclear whether this influence of older trees results from direct biotic interactions, in the traditional sense of resource competition and disease transmission, or an indirect biotic interaction in which the adult trees affect the fine-scale abiotic conditions. The distinction is important in order to understand what mechanisms are controlling seedling establishment, and if abiotic mechanisms are important, to locate favorable fine-scale habitat on the landscape.

Thus, we conducted an observational study in the red fir forest of California's Sierra Nevada to assess the influence of abiotic factors and biotic factors on seedling establishment at fine-spatial scales of 1-m resolution. We chose red fir forest as a study system because red fir seedling establishment is well studied. Additionally, because red fir forest comprises a significant portion of California's forested area, it is important economically for water and timber resources [Fites-Kaufman *et al.* 2007, Laacke 1990]. Specifically we ask the following: (1) What are the relative influences of fine-scale abiotic and biotic factors on seedling occupancy, and (2) are these factors the same for younger and older seedling groups? In the process, we confirm the influence of fine-scale abiotic factors in shaping seedling occupancy with subtle yet important differences between younger and older seedlings, and we begin to tease apart the role of the forest stand structure as a direct and indirect biotic influence.

3.2 Methods

3.2.1 Study site

In 2008-2009, we established a 20x640m study site on the Western slope of the Sierra Nevada in Sequoia National Park, California, USA, at elevation approximately 2,550m (~ 36°36' N, 118°42 W). The site topography varies 25m in elevation with coarse-scale aspects ranging from north to west to south. The semi-open red fir forest is dominated by red fir, with a sparse and patchy understory of primarily perennial herbs and a few stands of Chinquipin (*Chrysolepis sempervirens* Kellogg) that are usually associated with rocky outcrops (Figure C1). Winter snowpack is the primary water source and persists on average from October through May, followed by intermittent, generally mild rainstorms during the summer active growing season. Annual weather conditions varied over the course of the study period. In particular, the 2010 and 2011 growing seasons were unusually wet from large snowpacks and late snowmelt, while 2012 and 2013 were unusually dry with small snowpacks and early melt [CA DWR 2015]. The winter of 2011-2012 was atypical in that snow-free periods occurred, resulting in freezing near-surface ground temperatures; whereas during typical winters, snow insulates the ground and near-surface soil temperatures hover at 0°C.

3.2.2 Environmental measures

We measured a suite of physical environmental characteristics at 225 locations arranged 1.5 to 12m apart to enable estimation of the environmental conditions at any location in the study site. We subsampled 20 areas of the plot with a nested spatial pattern located between a regularly spaced triangular 12m grid (Figure 3.1). In order to capture the range of environmental conditions, we

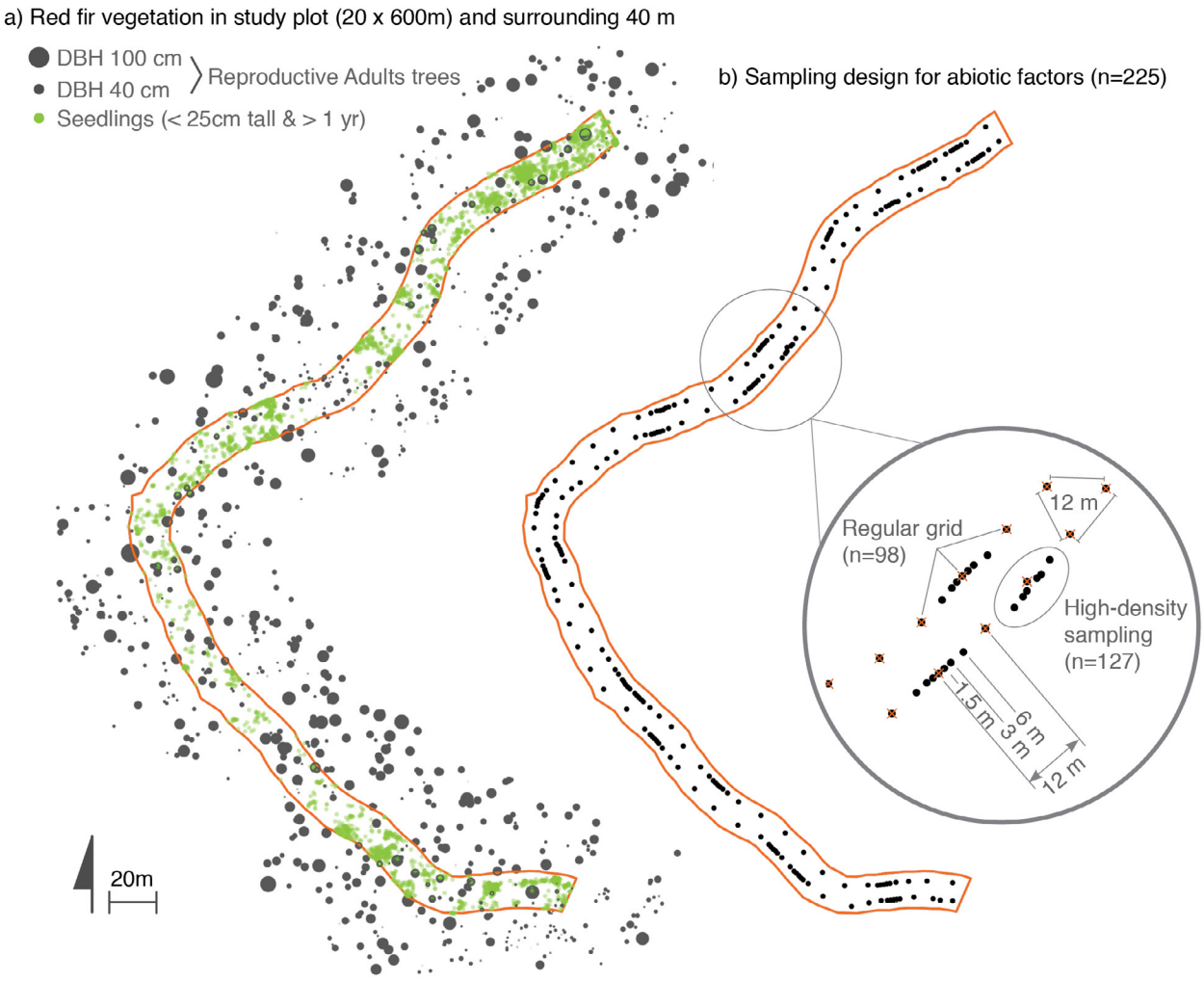


Figure 3.1: Red fir forest study area and sampling scheme. (a) Seedlings (green) are shown within the 640x20m study site (orange border), and adult reproducing trees (dark gray) scaled by diameter at breast height (DBH) are shown both within the study site and in the surrounding 40m area. (b) The sampling scheme is shown, with inset showing the regular spaced 12m grid (black points with orange x) and three examples of the nested subsampling pattern (black points).

subsampled across seedling density and canopy cover gradients. The latter, correlated with incident radiation, has been reported to influence conifer seedling density and mortality [Ustin *et al.* 1984, Gray and Spies 1996]. All measures at each location are within 20cm of a permanently installed soil moisture access tube. We conducted measurements during the 2010-2013 growing seasons, determined annually for the study site as a whole by the first date of spring / summer snowmelt and last date of fall persistent snow cover. In contrast, we define an active season for each location within the study site as the local snow-free period. Table 3.1 summarizes the measurements. It

Table 3.1: Candidate variables and source observations

Source Observation	Observation details*		Variables*	Units*	Variable calculation details*
Soil Temperature	5cm depth (iButton Thermochron DS1921G); every 4 hours, 2010-2013	Abiotic	Snowmelt Date	Julian Day	Avg: first day with max > 5°C
			AS Min Soil Temp	°C	Avg: annual AS mean daily min
			AS Max Soil Temp	°C	Avg: annual AS mean daily max
			Soil Degree Days	°C day	Avg: annual cumulative degree days
Soil Moisture	Volumetric Water Content at 10cm (Delta-T PR2/4); 4-7 campaigns / GS, 2010-2013		Late AUG Soil Moisture	m^3 H_2O / m^3 soil	Avg: latest August observation
			Early JUL Soil Moisture	m^3 H_2O / m^3 soil	Avg: earliest July observation
			GS Mean Soil Moisture	m^3 H_2O / m^3 soil	Avg: GS mean
Soil Profile	Vertical depth of the organic layer (fibric & hemric) and to the mineral layer; 2013		Organic Layer Depth	cm	Avg: 2 samples at each location
			Depth to Mineral	cm	Avg: 2 samples at each location
Surface Cover	Counts of gridcells of each type using a 1x1m frame with 100 10x10cm gridcells; 2013		Big Rock Cover	%	Cells with rocks > 1 cm dia.
			Solid Woody Cover	%	Cells with woody pieces > 1 cm dia.
			Fine Litter/Dirt Cover	%	Cells with dirt, needle litter, small rocks & woody pieces (< 1 cm dia.)
Topography	Terrestrial Laser Scanning (I-Site 4400CR & TopCon CTS-2); 2009		Aspect	°	Based on best fit plane through lowest point in neighbor gridcells
			Slope	°	
Potential Evaporation (PE)	Piche Evaporators located 5-8cm above the ground surface; 4-5 campaigns / GS, 2012-2013		GS Mean PE	g $H_2O/m^2/hr$	Avg: GS mean
			GS Minimum PE	g $H_2O/m^2/hr$	Avg: GS minimum
			GS Maximum PE	g $H_2O/m^2/hr$	Avg: GS maximum
Canopy Cover	Hemispherical Photography (Nikon D60 with Sigma Fisheye 4.5mm f/2.8 lens); 2013		GS Diffuse Rad	$W/m^2/GS$	Modeled[+] GS diffuse Rad
			GS AM Direct Rad	$W/m^2/GS$	Modeled[+] GS direct Rad, 6am-12pm
			GS PM Direct Rad	$W/m^2/GS$	Modeled[+] GS direct Rad, 12-6pm
		Biotic	Canopy Cover	Sky fraction	DCP[++]; sky pixel counts
Reproductive red fir adults	Terrestrial Laser Scanning (I-Site 4400CR & TopCon CTS-2) DBH measurement; 2009 & 2013		Seed Density	$seeds/m^2$	Modeled[+++] seed dispersal
			Nearest Tree	m	Min distance between gridcell and nearest reproducing adult

* AS = Active Season (snow-free period at each observation location); GS = Growing Season (day of first location snowmelt to last location snow accumulation over entire study site); Min = Minimum; Max = Maximum; PE = Potential Evaporation; Rad = Radiation, Avg = average; see Appendix C.1.5 for AS and GS details.

[+] CIMES-Fisheye [Gonsamo *et al.* 2011]; see Appendix C.1.2.7 for parameterization.

[++] DCP = Digital Cover Photography [Macfarlane 2011], see Appendix C.1.2.7 for details.

[+++] following Clark *et al.* 1999; see Appendix C.1.5.3 for parameterization.

should be noted that we developed a custom Piche evaporator to quantify potential evaporation and used terrestrial laser scanning to quantify fine-scale topography. Additional details are described in Appendix C.1.2.

3.2.3 Vegetation measures

Seedlings: In 2008 and 2009, 2,641 red fir seedlings (98.7% of total seedlings in plot) older than 1 year, *i.e.,* seedlings that had germinated in previous summers, and less than 25cm tall were located and tagged (Figure C2a). These seedlings are referred to as Older Seedlings and are greater than 6 years old at the study end in 2013. In 2010, we located and tagged 1,157 an additional seedlings that had germinated in 2009 and survived their first winter (Figure C2b). This 2009 cohort is referred to as Younger Seedlings, and is 4 years old at the study end in 2013. We considered a seedling to be present if it survived the entire study period. If a seedling died during the study period, we considered it an absence and counted it as a mortality event. We used a total station (Topcon CTS-2, Topcon Positioning Systems, Inc., Tokyo, Japan) to map the seedling locations with position errors less than 1cm. During early fall of each growing season from 2010-2013, we re-surveyed the plot, recording each seedling as alive, dead, or missing. Seedlings that were missing are treated as dead for this analysis as we continued to look unsuccessfully in subsequent years. Missing to dead ratios are 48:168, 182:173, 123:399, 79:175 in 2010-2013 respectively.

Reproductive red fir adults: We measured the diameter at breast height (DBH) of all adult trees with DBH greater than 25cm within the plot using standard forestry methods. Trees smaller than 25cm DBH were observed to be non-reproductive. We located and estimated DBH for all reproductive adults both inside the plot and within a 40m border surrounding the plot using terrestrial laser scanning (see Appendix C.1.3 for extraction details). We verified the resulting point cloud data both in UC Davis KeckCAVES 3D immersive environment and corrected remaining issues in the field. Using a linear model between the field-measured and point cloud DBHs (slope = 1.015 ± 0.02 (95% CI), intercept = 7.39 ± 1.53 (95% CI), R^2 = 0.93), we standardized the border tree DBH to match the field-based measurements.

3.2.4 Data processing

To assess seedling occupancy at a spatial scale commensurate with their size, we predicted conditions at each location on a 1x1m spatial grid within the study plot. We assumed a stationary Gaussian process [Cressie 1993] to estimate the conditions for each environmental factor throughout the study period. In other words, we assume the measured values at each time step (*e.g.,* one soil moisture campaign, the soil temperature measures from a particular hour, or the canopy cover) are drawn from an underlying distribution of values. We modeled this distribution using a multivariate normal (MVN):

$$\boldsymbol{Y_s} \sim MVN(\mu, \boldsymbol{\Sigma}), \qquad \text{eqn 3.1}$$

where $\boldsymbol{Y_s}$ is the vector of Y values at the sample locations 1 to s, and μ is the mean value. The s x s covariance matrix $\boldsymbol{\Sigma}$ describes the pairwise relationship between sample locations. We decomposed the covariance $\boldsymbol{\Sigma}$ into a variance parameter $\mathbf{x}\sigma^2$, an autocorrelation matrix $\boldsymbol{K}$, a measurement error parameter τ^2, and an observation-specific error term $\nu^2(\boldsymbol{\theta_s})$ for potential evaporation and surface cover observations, where ν^2 is an observation error parameter and $\boldsymbol{\theta_s}$ is an error observation at each location s:

$$\boldsymbol{\Sigma} = \sigma^2\boldsymbol{K} + \tau^2 + \nu^2(\boldsymbol{\theta_s}). \qquad \text{eqn 3.2}$$

By doing this, we assumed constant variance and error parameters across all locations. In the case of potential evaporation, we estimated each time step jointly to estimate single error parameter additionally across all observation campaigns. Similarly, we estimated all surface cover observations (rock, wood, litter/dirt) jointly to obtain a single measurement error estimation.

We modeled autocorrelation between sample locations with the commonly used exponential function (Zimmerman & Stein 2010):

$$\boldsymbol{K} = e^{-\boldsymbol{d_s}/\rho}, \qquad \text{eqn 3.3}$$

where $\boldsymbol{d_s}$ is an s x s matrix of the pairwise Euclidean distance between all locations, and $\rho > 0$ is a range parameter that determines the distance at which locations no longer have strong influence on one another. By maximizing the log-likelihood, we estimated the model parameters (Table C2). Using these parameter estimates, we then predicted the conditions at each location on the 1x1m grid at each measurement time step. For example, we estimate temperature values on the 1x1m gridded landscape every 4 hours. See Appendix C.1.4 for details.

Each seedling was assigned to a gridcell by finding the nearest gridcell center. Because most factors are spatially autocorrelated with an estimated range parameter greater than 1m (SI-Table 1), the gridcell value with which each seedling is associated is essentially the same value that would be estimated at the seedling location. We chose to conduct the analysis with a gridded landscape because (1) using a regular gridded sample design yields better estimates of heterogeneity on landscapes with autocorrelation (see chapter 1); and (2) all locations with seedling absence will inform the model. All data processing and analysis were performed with R 3.0.2 [R Core Development Team 2013].

3.2.5 Variable generation

From the predicted gridded data, we calculated a series of abiotic and forest stand variables to be considered explanatory in a model of seedling occupancy. We chose these variables based on empirical work by others, common inclusion in models projecting species geographical ranges, and/or ecophysiological understanding. Specific calculation of each variable is described in Table 3.1 and additional details are in Appendix C.1.5. For multi-year observations, we calculated the mean variable over those years to represent an average condition at each location. Of particular note, we modeled Seed Density with modifications to the likelihood methods of Clark *et al.* [1999] (Appendix C.1.5.4). As seed dispersal can be stand- and year-specific due to both fecundity variation and weather conditions, we performed a sensitivity analysis comparing different fecundity and dispersal model parameterizations. Our results are robust to variation in modeled Seed Density.

3.2.6 Model configuration

We examined correlations between variable pairs (Figure C14) and identified 3 groups of highly correlated variables (correlation > 0.7): soil temperature (Soil Degree Days and Active Season (AS) Max Soil Temp), soil moisture (Early JUL and Late AUG Soil Moisture), and soil profile (Organic Layer Depth and Depth to Mineral). Additionally, Canopy Cover was correlated with Growing Season (GS) Diffuse Radiation at 0.99. However, we included only Canopy Cover because it is the direct measurement. From the 3 correlated pairs, we configured all possible combinations of variables forming 8 variable configurations. We report results averaged over all 8 configurations.

For all models described in the following sections, we weighted the presence gridcells so that each seedling would inform the model, *i.e.,* so that gridcells with more than one seedling would "count" proportionally more than gridcells with only one seedling). To avoid the absent gridcells dominating

model fit, we weighted the absent gridcells so that total number of absent gridcells equals the total number of seedling-weighted gridcells [Maggini *et al.* 2006]. Alternatively, we could have sampled absent gridcells with sample size equal to the number of present gridcells. By using all absent, down-weighted gridcells, the entire absent portion of the study site informs the model.

3.2.7 Model selection

We considered five model frameworks to determine the best modeling approach for predicting seedling presence / absence [Hothorn *et al.* 2011]:

- *Spatial*: Seedling occupancy is predicted by x, y location coordinates only*, i.e.* the presences and absences can be explained by spatial autocorrelation.
- *Additive only*: Seedling occupancy is predicted by a Generalized Additive Model with each variable modeled by a p-spline. No variable interactions were included.
- *Interaction only*: Seedling occupancy is predicted by a Classification Tree with maximum base trees with depth of 2-4, *i.e.,* the maximum interactions allowed are 2-, 3-, or 4-way. Note that main effects are inherently included in this model.
- *Additive Spatial*: Combination of the Additive only and Spatial models.
- *Interaction Spatial*: Combination of Interaction only and Spatial models.

We boosted each model, determining the optimal number of boosts using bootstrap validation with 25-folds. The interaction models performed best and are significantly different from the additive models (Figure C15). The addition of spatial autocorrelation to classification tree (Interaction Spatial) did not yield a better fit; thus we chose amongst the Interaction only models. Interaction models with interaction depths of 3 and 4 slightly improved model performance; however for simplicity and interpretability, we chose an interaction depth of 2. This analysis was performed with the R package mboost [Hothorn *et al.* 2015].

3.2.8 Model analysis

For three seedling groups, All, Older, and Younger, we trained boosted classification tree models, with maximum node depth of 2, on 70% of the study plot area using the R package gbm [Ridgeway *et al.* 2015]. We trained models for each of the 8 variable configurations within each seedling group. We specified the binomial distribution for the seedling occupancy data, for which the model uses a logit transformation to yield output in log-odds.

For each variable configuration, we used 10-fold cross-validation to determine the optimal number of boosts [James *et al.* 2013] and extracted the relative importance and marginal effects of the variables [gbm R package: Ridgeway *et al.* 2015]. We reported relative importance and marginal effect for each variable each variable configuration as well as the mean across all variable configurations. We assessed model performance by first predicting seedling occupancy for a test dataset, 30% of the study area, and then comparing these predicted results to observed seedling occupancy [James *et al.* 2013, Hijiams 2012]. We assumed predicted log-odds values greater than 0 (> 0.5 probability of presence) to have a seedling presence. Again, model performance results are averaged over the variable configurations; variables in the 3 variable groups are averaged over 4 models, and all others over all 8 models.

We assessed habitat suitability with a single model configured with Soil Degree Days, Late AUG Soil Moisture, and Depth to Mineral Soil variables from the variable groups. Suitability is a combination of the fitted model values for the training data and the predicted model values for the

test data. We reported suitability as the probability of a seedling presence, which is the log-odds model output transformed to probability. We defined suitable habitat as areas with a probability of seedling presence greater than 50%. Reported mortality events, which do not inform the model, occurred during all 4 years of the study period.

3.3 Results

3.3.1 Both abiotic and biotic forest stand variables explain seedling occupancy at fine-spatial scales

The average percent of correctly predicted seedling occupancy on an independent test set (30% of study area) across variable configurations was above 82% for all seedling groups (Table 3.2). As expected with a large absence to presence ratio, absences are better predicted than presences for all groups. However, presences are well predicted for older seedlings (60%) and slightly less well predicted for younger seedlings (50%). Total abiotic variable relative importance is high for all seedling groups (approx. 75%). Soil variables (soil profile and soil surface cover) influence younger seedlings on par with climatic variables, while climatic variables are more important for older seedlings (see section 3.3.2 below).

Table 3.2: Model performance.

Model performance	Younger seedlings (4 years old)	Older seedlings (> 6 years old)	All Seedlings
Total correct PA predictions*	88.5 ± 0.5	84.6 ± 0.1	82.9 ± 0.1
Presences	50.3 ± 1.0	60.2 ± 0.3	58.6 ± 0.3
Absences	89.5 ± 0.5	86.8 ± 0.2	85.5 ± 0.1
Total abiotic relative importance+	75.3 ± 0.2	74.7 ± 0.2	74.8 ± 0.2
Climate variables	36.0 ± 0.2	43.8 ± 0.2	42.7 ± 0.3
Soil Variable	29.1 ± 0.2	20.8 ± 0.2	21.3 ± 0.2
Topographic variables	10.3 ± 0.3	10.1 ± 0.2	10.7 ± 0.2
Total forest stand (biotic) relative importance+	24.6 ± 0.2	25.3 ± 0.2	25.2 ± 0.2

* Percent correct predictions on independent test set; mean ± 95% confidence interval across 8 variable configurations. Percent of weighted locations with presences = 13.6% and 3.6%, Older and Younger seedlings respectively.

+ Percent relative importance; mean ± 95% confidence interval across 8 variable configurations

Across a variety of variable configurations, no single variable strongly predicts seedling occupancy for Older and Younger Seedlings (Figure 3.2). For both seedling groups, the top variables include both abiotic and forest stand characteristics. Furthermore, the influence of each variable on seedling occupancy is relatively consistent between models with different variable combinations. Although all variables have some influence on seedling occupancy, we primarily focus on variables with relative importance greater than 5%.

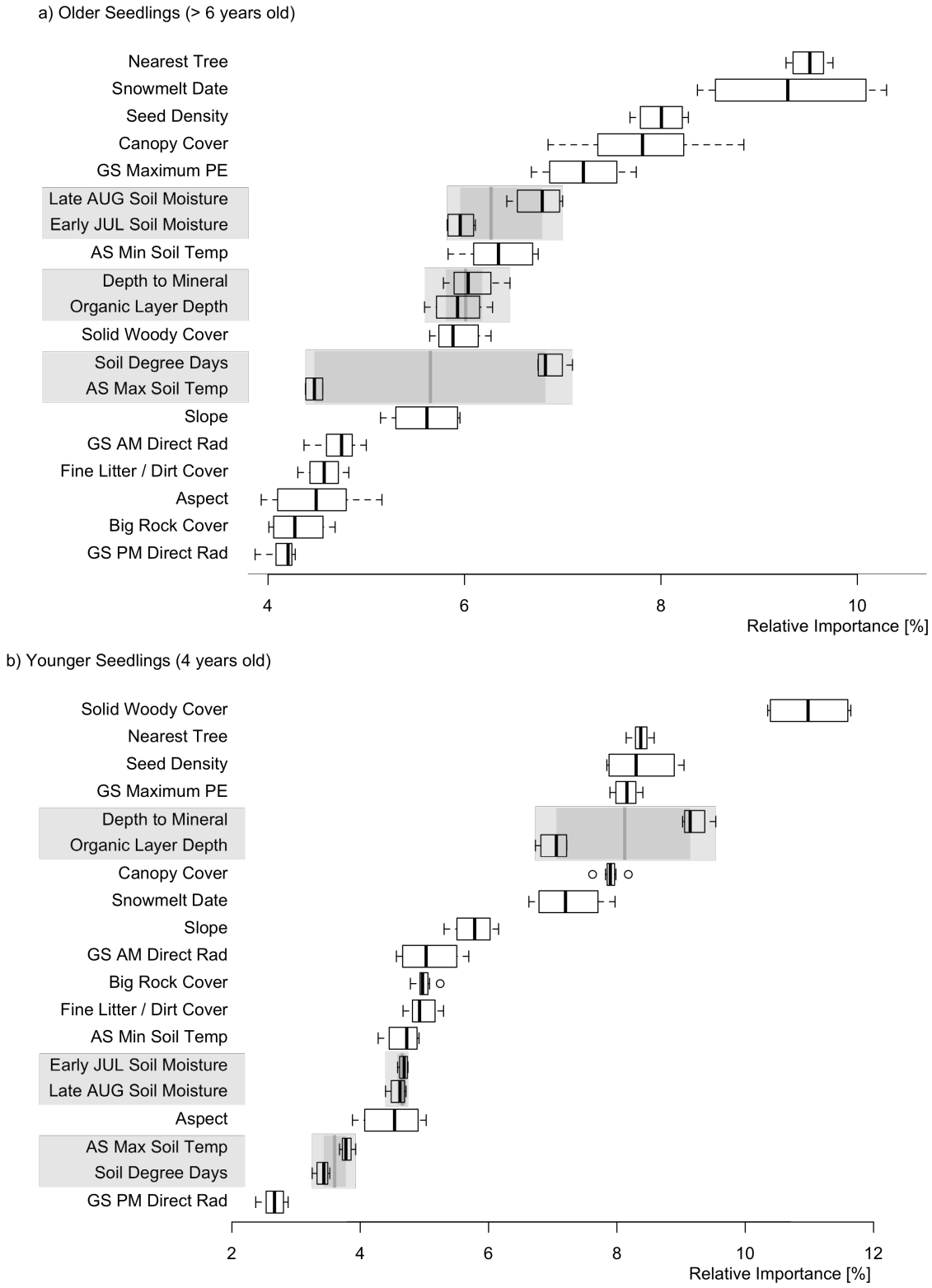


Figure 3.2: Summary of relative metric importance from 8 variable configurations for the (a) Older Seedlings and (b) Younger Seedlings are shown ordered by the median value (solid vertical line). Box edges indicate the 25 and 75 quartile values while the whiskers indicate the entire range. Each variable configuration has one of the variables in the soil temperature, soil moisture, and soil profile groups (gray highlights), but never both at the same time. The grayed box and whisker plots represent the combined relative importance for each variable pair.

While the combined total effect of abiotic factors is more influential in predicting seedling occupancy, forest stand structure also contributes substantial influence (25% relative importance). The three forest stand variables included, Nearest Tree, Canopy Cover, and Seed Density, are consistently top variables. As shown by the marginal effects of Nearest Tree (Figure 3.3), seedlings are more likely to occur at distances farther from the nearest reproducing adult tree, with that probability weakening for the Younger Seedling group at the highest distances. For the Younger Seedlings especially, the shape of the response curve suggests a threshold effect around 5m, which is commensurate with the crown width of adult trees and also with the average minimum distance to an adult tree from any location within the study site (4.3m).

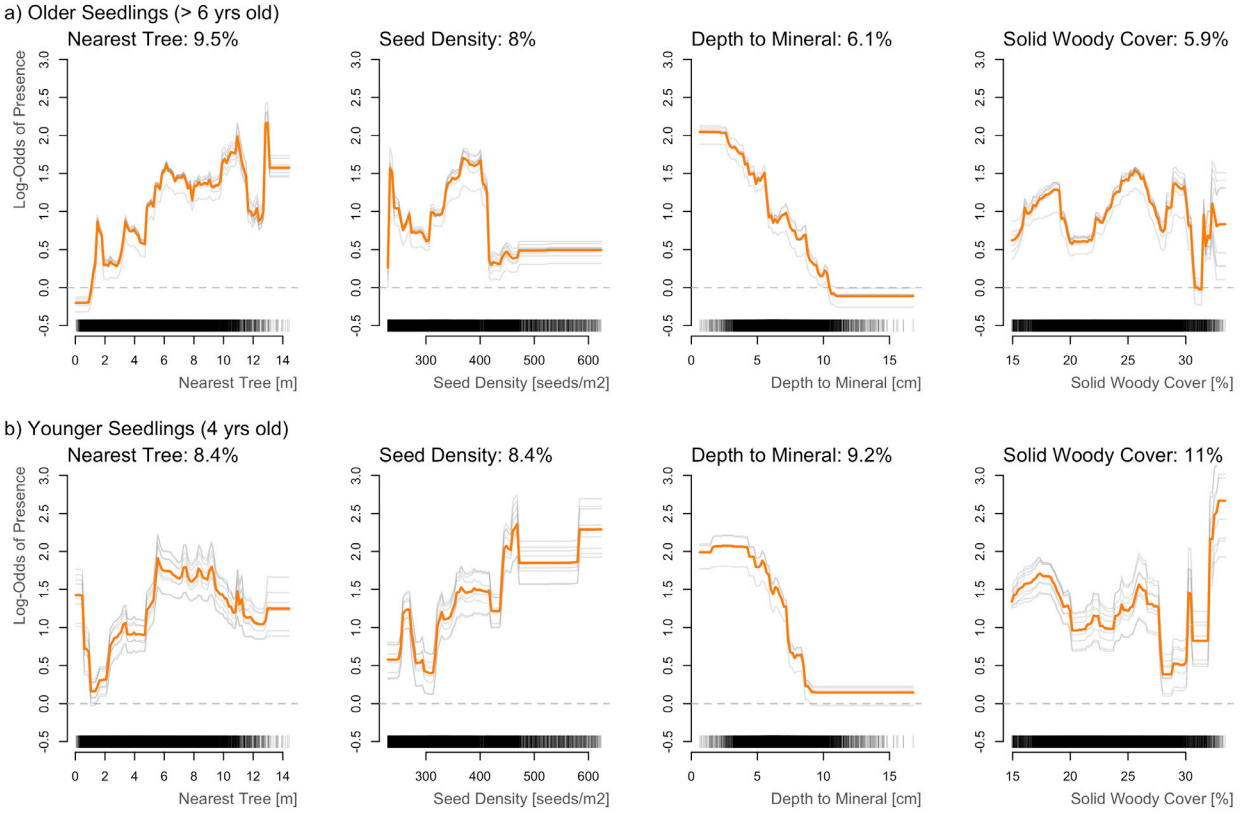


Figure 3.3: Comparison of marginal effects of selected variables between (a) Older Seedlings and (b) Younger Seedling groups. Individual variable combinations are shown in gray and the mean effects are shown in orange (n=8 for Nearest Tree, Seed Density, and Solid Woody Cover; n=4 for Depth to Mineral). The range of values for each variable that occurs in the study site is indicated by the density bars at the bottom, with the P bar indicating values with presences and the A bar values with absences. Highly occurring values are in black and low occurring values are in white. Due to the nature of boosted classification tree models, these effects should be interpreted as loosely describing a trend [Merow *et al.* 2014] and care should be used when assessing responses at values with low representation within the study site. Additional variables have similar marginal effects between the two seedling groups (Figure C16).

Interestingly, seedlings are more likely to occur in areas with higher Canopy Cover, another forest stand variable (Figure C16). While we consider Canopy Cover a forest stand variable, it may be describing the abiotic radiation condition, at least partially (*i.e.,* the diffuse radiation). It is important to note that Nearest Tree does not account for the influence of saplings and immature adults (trees > 25cm tall and less than 30cm DBH), which occur within the study area and were not measured directly in this study. However, Canopy Cover does capture the effects of saplings.

Seed Density, the third forest stand variable, affects both seedling groups (Figure 3.3). For the Older Seedlings, the probability of seedling presence peaks at a mid-range seed density, while for the Younger Seedlings, the probability increases continuously with higher seed density. Younger Seedlings, which are more likely to occur in areas with high seed density, may die as they grow and compete with each other, which leads to the decline in the probability of presence of Older Seedlings at higher Seed Density. The relative importance and marginal effects of Seed Density is robust to its model parameterization (Appendix C.1.5.4).

3.3.2 Soil factors differentiate Younger and Older Seedling abiotic niche characteristics

Several abiotic climatic variables define the regeneration niche for Older Seedlings. The relative importance of these variables depends on the specific combination of variables included in the model. There is a strong tradeoff in relative variable importance between Snowmelt Date and the Soil Temperature group variable (Figure C17). Related variables, GS Maximum PE, Canopy Cover, and AS Min Soil Temp, are not as affected as Snowmelt Date, suggesting that Snowmelt Date may represent the effects of temperature on seedling occupancy. However, it is unclear from this analysis whether the effect of Snowmelt Date is a purely temperature effect or is also coupled to water availability. Snowmelt may operate as a threshold effect, whereby seedlings, on average, are more likely to occur in locations where snowmelt persists until DOY 135 (May 15) (Figure C16).

GS Maximum PE, a variable rarely measured at fine spatial scales, is an important abiotic variable for both seedling groups. Potential evaporation is a strong predictor of Western forest vegetation pattern at coarse spatial scales [Stephenson 1998]. It has more influence on seedling occupancy than the soil moisture variables, which are traditionally used to assess water stress in empirical studies. As expected, seedlings are more likely to occur in areas with lower evaporative demand (Figure C16).

Interestingly, no variables have strongly negative effects on seedling presence (negative log-odds), except Canopy Cover when less than 0.2 (Figure C16), despite the large area of unsuitable habitat predicted (Figure 3.4). The interaction effects, which proved important in model selection, may play a significant role. Unfortunately, these effects are difficult to tease apart in boosted classification tree models [Horton *et al.* 2011], and we leave them for future analyses.

In addition to climatic variables, abiotic soil variables are also important for Younger Seedlings. In fact, Solid Woody Cover is the top variable for Younger Seedlings. Higher probability of occupancy occurs with lower woody cover, as might be expected (Figure 3.3). Another soil variable, Depth to Mineral soil, is also important for Younger Seedlings. A precipitous drop in the probability of seedling presence occurs between 5 and 8 cm (Figure 3.3). Depth to Mineral has a similar, but less important, influence on Older Seedlings. Gordon [1970] reported similar effects on young seedlings, and others studies have suggested the influence of soil conditions on conifer seedling establishment [Grey and Spies 1996].

3.3.3 Mortality rate increases as predicted habitat suitability decreases

There is almost twice as much predicted suitable habitat for Older Seedlings than for Younger Seedlings, 18% and 10%, respectively. However, the spatial pattern of suitability is similar for both seedling groups, where Younger Seedling suitability is generally a subset of Older Seedling suitability except in an area near the southern end of the study area (Figure 3.4). There are very few seedlings in areas predicted to have unsuitable habitat — 2% and 0.5% of predicted unsuitable habitat have presences for Older and Younger seedlings, respectively. Most seedlings in poor habitat seem to be near areas of suitable habitat. Surprisingly, large portions of predicted suitable habitat are not

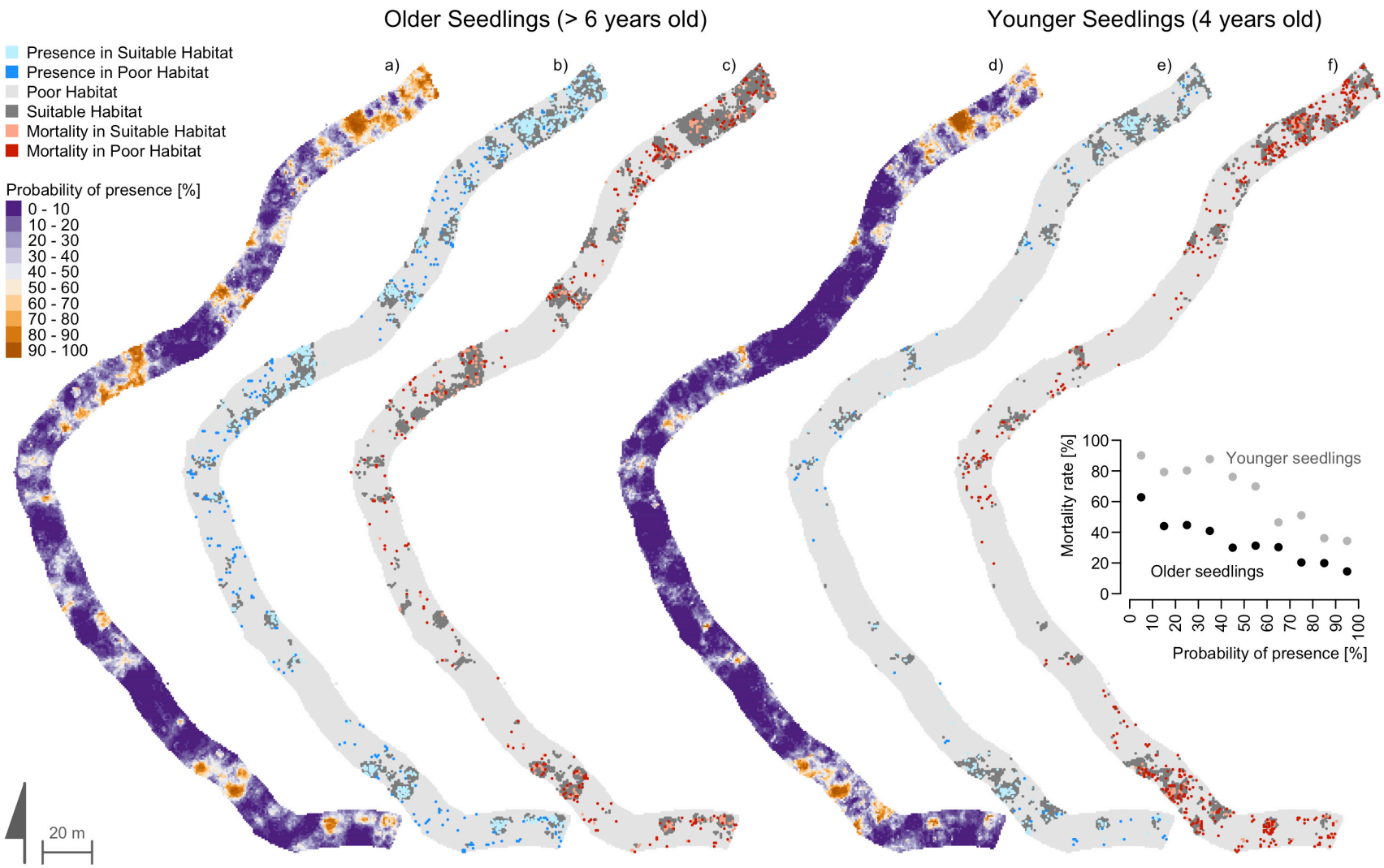


Figure 3.4: Predicted probability of presence, *i.e.,* habitat suitability (a & d), seedling occupancy in predicted suitable and unsuitable habitats (b & c), and mortality in suitability and unsuitable habitats (c & f) are shown for Older (a-c) and Younger Seedlings (d-f). The inset figure shows mortality rates versus suitability for Older Seedlings (black) and Younger Seedlings (gray).

occupied, 67% and 78% for Older and Younger Seedlings, respectively. However, the fraction of unoccupied habitat decreases as suitability increases (Figure 3.5).

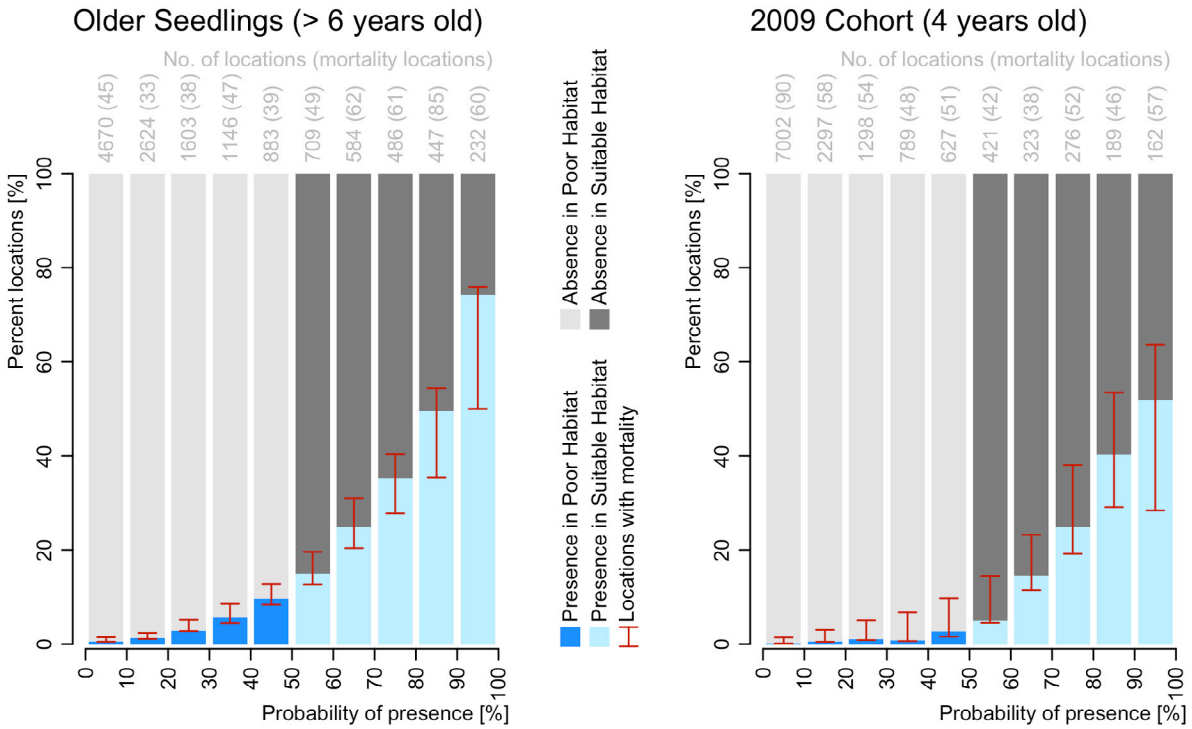


Figure 3.5: Percent of locations with seedling presence (blues) / absences (grays) is presented by predicted suitability (probability of presence) for Older Seedlings (a) and Younger Seedlings (b). Percent of presence and absence locations with mortality events is shown in red. A location is considered present if the seedling survived the entire 4-year study. Thus, mortality events can occur in absent locations if the mortality rate is 100%. Mortality events in present locations indicate mortality rates less than 100%. Total number of locations and number of locations with mortality in each suitability range are shown above the range bar.

As expected with a well-performing occupancy model, per capita mortality rates decrease as predicted suitability increases for both Older and Younger Seedlings (Figure 3.4 inset). Furthermore, mortality rates for Older Seedlings in the least suitable locations are similar to mortality rates for Younger Seedlings in the most suitable locations. This pattern may be due to demographics; surviving older seedlings have survived more environmental conditions or biotic interactions, *i.e.*, the less fit individuals have been weeded out of the Older Seedling group.

Many more Older Seedlings died in areas of predicted suitable habitat than in predicted unsuitable habitat, whereas Younger Seedlings died in approximately even numbers across predicted habitat suitability (Figure 3.6). This pattern suggests that abiotic or biotic factors are affecting seedling occupancy after initial influence of seed density. Furthermore, the effects of abiotic and biotic factors occur strongly within the first 4 years of a seedling's life. Unfortunately, we did not track the Younger Seedlings until they survived their first winter. We would have a stronger case for abiotic factors driving seedling occupancy rather than seed density if we had observed roughly equal numbers of germinants (individuals in their first summer season) across all levels of habitat suitability followed by high rates of mortality in unsuitable habitat, similar to those we did observe.

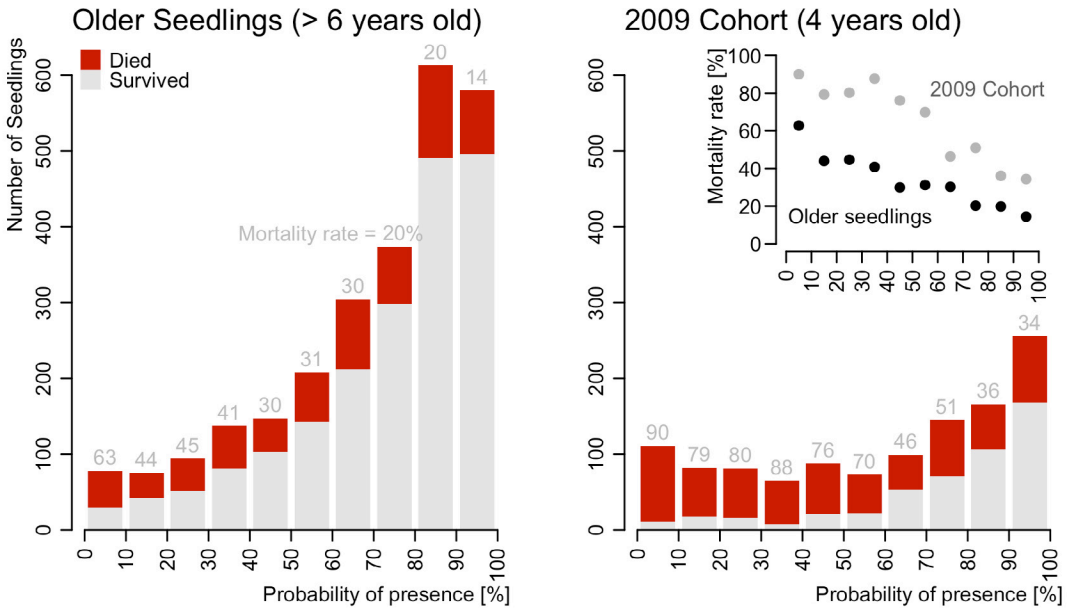


Figure 3.6: Number of living (gray) and dead (red) seedlings are shown for predicted suitability ranges (probability of presence) for Older (a) and Younger (b) Seedling groups. Mortality rates for each suitability range are shown above each bar. The inset figure shows mortality rates versus suitability for Older Seedlings (black) and Younger Seedlings (gray).

3.3.4 Density-dependence influences occupancy patterns as seedlings mature

For Older Seedlings as habitat suitability increases, mortality occurs more frequently in areas near other seedlings than it does in locations with few seedlings (Figure 3.5). This pattern, however, does not hold strongly for Younger Seedlings. A large portion of Young Seedling mortality events occurred in areas with fewer Young Seedlings.

3.4 Discussion

We found that abiotic and biotic fine-scale factors explain seedling occupancy patterns in largely similar ways between seedling groups, with a few notable exceptions. In this section, we discuss the implications of these results for forest regeneration. Additionally, we consider the direct and indirect biotic influence of forest stand structure in maintaining forest regeneration under future climates.

3.4.1 A many faceted fine-scale seedling establishment niche

At fine spatial scales, no one single factor dominates the occupancy of red fir seedlings on the landscape. Seedling occupancy is well explained by abiotic factors describing radiation, water availability, and soil conditions, which are all factors shown to correlate with seedling establishment [Gordon 1970, Ustin *et al.* 1984, Chappell and Agee 1996, Barbour *et al.* 1998] and to be physiologically important [Johnson *et al.* 2011]. If seedlings were not responding to abiotic influences, we would have either expected poor model performance or low relative importance of the abiotic variables compared to the biotic forest stand variables. Due to the heterogeneity of the abiotic factors on the landscape, it is possible that different abiotic factors are limiting at different locations [Greenberg *et al.* 2015]. Additionally, as indicated in our model selection process, specific interactions may be important influences on seedling occupancy. As such, limiting-factor analysis of abiotic and biotic factors and interactions between them warrant attention in future analyses.

Biotic forest structure variables, including seed dispersal, do contribute to seedling occupancy; however, no more so than several other abiotic variables. These results differ from those of Dobrowski *et al.* [2015], who report that stand structure characteristics (stand basal area and stem density) had higher relative importance than climatic variables on the juvenile trees of many species. These results are based on coarse-scale models that cover the geographic range of the tree species. As such, it is not surprising that biotic factors, especially living stem density that the authors used to represent seed source (*i.e.,* seed dispersal), play a strong role in coarse-scale occupancy patterns. In contrast, our results suggest that, in the case of red fir, abiotic climatic and soil conditions play a significant role in structuring seedling occupancy at fine scales. Furthermore, seed dispersal can be thought of as an initial source of landscape pattern upon which abiotic factors shape seedling establishment. An outstanding question remains: how do the fine-scale controls on individuals scale up to the population-level patterns observed at coarse scales [Clark *et al.* 2011]?

We did not include variables in our model that explicitly describe fine-scale biotic interactions, *e.g.,* competition with understory plants, herbivory, and disease, that may additionally influence seedling establishment patterns. However, if such fine-scale biotic interactions were primarily driving seedling occurrence, we would not have been able to explain the seedling occupancy with fine-scale abiotic and forest stand variables, unless these abiotic factors were correlated with disease, herbivory, *etc.* Through our comparison of mortality rates with habitat suitability, we observed that for older seedlings deaths preferentially occurred where other seedlings were present. Thus, density-dependent mortality, a fine-scale biotic effect, may be shaping seedling occupancy after seedlings survive fine-scale abiotic conditions.

We argue that the explanation of seed dispersal patterns primarily driving seedling occupancy is unlikely. While spatial differences in seed quality and annual seed dispersal patterns cannot be entirely ruled out as strong influences without direct measurement at our site, our seed density model suggests that the entire study area receives ample seed input, especially if considered over decadal time scales. We anecdotally observed ubiquitous seed rain during 2008, a mast year that was the source of the younger seedling group. We similarly observed relatively uniform seed densities across the study site in other years. Thus, without seed dispersal as a strong spatial influence, abiotic or biotic mechanisms are likely important drivers of the observed pattern.

3.4.2 Niche differences amongst life history stages

Our results also suggest that abiotic conditions have different effects within the first few years of a seedling's life. Similar to other studies [Gordon 1970, Ustin *et al.* 1984], we found that soil factors are more influential to younger seedling establishment than that of older seedlings. In early years, access to available nutrients and higher water holding capacity in mineral soil (as opposed to organic litter layers) can be critical [Cheplick and Quinn 1987], while thicker organic layers can be beneficial in later establishment phases by reducing soil evaporative loss deeper in the soil horizon [Holland and Coleman 1987]. This underscores how abiotic variables have different relative importance at different life history stages, even within the regeneration niche. As a result, emphasis on adult occupancy in projecting species ranges may be problematic [Jackson *et al.* 2009, McLaughlin and Zavaleta 2012, Dobrowski *et al.* 2015].

Despite the stronger role of soil factors in early establishment years, the suitability of locations for each seedling group is strikingly similar (Figure 3.4). In other words, younger seedlings are largely surviving in the same areas as older seedlings. For abiotic factors with temporal observations (*e.g.,* soil temperature, soil moisture, potential evaporation), we observed similar annual patterns throughout the study. In other words, the relative differences in abiotic conditions between

locations are stable over the study period, and we expect this to be the case historically over longer time periods. The spatial consistency of both seedling establishment and abiotic factors over time supports our claim that abiotic conditions are strongly influencing seedling establishment.

Although similar habitat suitability between the seedling groups suggests that suitable seedling conditions, and presumably seedling occupancy patterns, are more-or-less stationary on time scales of at least 20 years, adult trees occur throughout the study site, including in areas of unsuitable seedling habitat. This disparity in spatial pattern is suggestive of niche differences between seedling and adult life history stages and may indicate that changes in climate have constricted the area suitable for seedling establishment. We emphasis the suggestive nature of this evidence as we do not directly compare seedling and adult niche factors, study the entire species' geographical range, nor conduct the study over time periods long enough to observe climatic shifts. An alternative, but not mutually exclusive, hypothesis is that over longer time-scales the spatial pattern of suitable establishment conditions may change, for example due to natural demographic change in forest stand structure. Fire can also influence seedling regeneration on time scales commensurate with fire return interval [Chappell and Agee 1996, Scholl and Taylor 2006], and burn patterns may rearrange abiotic conditions suitable for seedling establishment [Chappell and Agee 1996]. Additionally, although we observed similar relative patterns in abiotic conditions across the study site each year, episodic events may change marginal locations to good locations for establishment, and vice versa.

3.4.3 Direct and indirect effects of forest stand structure on seedling establishment

Our results indicate that forest stand structure influences seedling establishment. The Nearest Tree variable suggests that a seedling is more likely to be present at distances farther, especially distances greater than 5m, from the nearest reproducing adult. Direct biotic effects via biotic mechanisms as well as indirect biotic effects via abiotic mechanisms can explain this trend. Biotic mechanisms include resource competition (light and water especially) [George and Bazzaz 2014], pathogen avoidance [Janzen 1970], seed herbivory [Connell 1971], and seed dispersal shadows (*e.g.,* wind eddies may form around adult trees influencing how seeds fall from the tree tops [Nuttle and Haefner 2005]). Advanced snowmelt, which occurs early around the base of trees, is a possible abiotic mechanism.

Canopy cover affects seedling occupancy in a way somewhat opposite than Nearest Tree: the more cover the better. We cannot know if this effect is due primarily to reproducing trees — which if coupled with the effect of Nearest Tree would result in a sweet spot, not too close but not too far, from the reproducing trees [Janzen 1970, Connell 1971] — or if the juveniles trees, boulders, or other understory vegetation are additionally contributing the influence of canopy cover. We were surprised at the relatively low importance of the radiation variables compared to Canopy Cover, as radiation timing and duration have been reported to best explain seedling densities [Ustin *et al.* 1984]. This may be due to the moderate correlation between canopy cover and GS Direct AM Rad (Pearson's coefficient of 0.6), which may prevent the model from partitioning variance in the occupancy between these two variables. Alternatively, our direct radiation variables might not differentiate temporal patterns sufficiently to distinguish the effects of, for example, a few intense versus many mild exposure events that have the same total exposure time.

An important question is the extent to which the forest stand structure influences the fine-scale abiotic conditions that affect seedling occupancy patterns. Other authors have reported evidence that forest stand structure mediates coarse-scale climate [Chen *et al.* 1999, Geiger *et al.* 2009, de Frenne *et al.* 2013, von Arx *et al.* 2013]. In this analysis, we do not test for this directly. However, we do have evidence that the near-surface fine-scale conditions differ from coarse-scale conditions. For

example, heterogeneity in our soil temperature measures, which are representative of the near-surface temperatures that the seedlings experience, is greater than heterogeneity in air temperature at 2m height, a standard measure of coarse-scale climate (SI-II). Because direct radiation is largely determined by the sun/shade patterns created by the forest canopy, and these patterns strongly influence surface temperatures [Geiger *et al.* 2009, von Arx *et al.* 2013], it is likely that forest structure does influence the fine-scale abiotic conditions at our study site.

Topography also mediates coarse-scale climate to create fine-scale heterogeneity [Wolfe *et al.* 1949, Chen *et al.* 1999, Geiger *et al.* 2009]. We observed minimal direct effects of topography, in terms of both slope and aspect, at the fine-spatial scales of this study. However, this result does not indicate that slope and aspect are unimportant, but rather that either (1) the influence of slope and aspect in generating fine-scale heterogeneity was directly captured by other fine-scale abiotic variables or (2) slope and aspect have a direct effect at spatial scales greater than 1m [Bello *et al.* 2013, Meynard *et al.* 2013]. There are more areas of suitable habitat on the northern half of the study site, which happens to be northerly facing at coarser spatial scales, than the southern half of the site, which is southerly facing at coarse spatial scales (Figure 3.4). We plan future analyses to better understand the influence of both abiotic and biotic factors at multiple spatial scales.

3.4.4 Implications for managing effects of climate change on forests

Our finding that seedling occupancy is influenced strongly by a complex mix of abiotic conditions supports the idea of conserving "nature's abiotic stage", *i.e.,* areas of high abiotic heterogeneity [Lawler *et al.* 2015]. Areas of high heterogeneity increase the probability that suitable combinations of abiotic conditions will occur at some locations on the landscape. To promote seedling establishment specifically, such conservation efforts need to include areas of high *fine-scale* heterogeneity. Thus, a more detailed understanding of (1) what fine-scale heterogeneity is currently available in forests, especially those in complex mountainous regions (*i.e.,* a characterization of the current stage available to seedlings) and (2) how landscape features, both topographic and vegetative, generate fine-scale abiotic conditions is needed. The former informs our understanding of the magnitude of heterogeneity to seek in conservation efforts, while the latter helps us know in what kind of landscapes to find it.

Because an understanding of how vegetation influences fine-scale abiotic conditions is important to identifying areas of high heterogeneity, we suggest considering indirect biotic interactions via abiotic mechanisms (*e.g.,* the influence of forest stand structure on the heterogeneity of fine-scale conditions) differently than direct biotic interactions. Currently, abiotic conditions that are biologically mediated are often classified as biotic interactions [*e.g.,* Dobrowski *et al.* 2015, Lewlar *et al.* 2015]. However, non-living features like standing dead trees and complex topography can create fine-scale heterogeneity. If an individual is responding to an abiotic condition, then the source of that condition, living or not, should not be differentiated.

The lack of distinction between direct and indirect biotic interactions is particularly problematic for modeling tools, like climate envelope and dynamic forest gap models, which are used to project current and future forest distributions. In assuming that coarse-scale climate-based projections of adult tree populations incorporate the effects of fine-scale conditions, several untested and questionable assumptions are made in these types of models. First, it is unclear what fine-scale conditions may be generated from a given coarse-scale condition for a particular forest structure. This is in part because it is unknown how certain features of forest stand structure create fine-scale conditions. Furthermore, we do not know if the stand-generated fine-scale conditions will be consistent over a range of coarse-scale conditions. The complexity of forests, especially those in the

topographically complex mountainous regions, is likely to cause non-linear relationships between coarse- and fine-scale conditions. Non-linear relationships may have critical impacts on projecting future species distributions, as existing forests may mediate new climate regimes in unexpected ways. Additionally, for tree species transitioning into new regions without standing forests, the fine-scale conditions for seedling establishment cannot be assumed to exist. For the same coarse-scale condition, a more homogeneous grassland may have much less fine-scale heterogeneity than a heterogeneous forest. While we have illustrated the importance of fine-scale conditions for tree species, similar issues also exist for other species such as herbaceous understory plants.

We are not suggesting that coarse-scale abiotic conditions do not play an important role in species distributions. Rather, we suggest that species persistence may be influenced abiotically at multiple spatial scales [Bello *et al.* 2013, Dobrowski *et al.* 2015]. The importance of fine-scale abiotic conditions on seedling occupancy does not diminish the role of biotic interactions. We argue for the addition of abiotic influences to biotic interactions at fine scales. This is a challenging task because measuring fine-scale abiotic conditions over large spatial extents is still not feasible with current, yet continually improving, sensor technologies. In the meantime, it is necessary to assess how fine-scale conditions scale up to coarse-scale data readily available at over large spatial extents. In addition to studying homogeneous systems [Potter *et al.* 2013], this endeavor should include empirical work over a variety of landscape types from simple to complex (*e.g.,* grasslands, savannah, and montane regions). Additionally, we echo Potter *et al.*'s [2013] call for more down-scaling techniques that estimate fine-scale conditions based on landscape features, including forest structure.

3.5 Conclusions

Our results indicate that the seedling establishment niche for red fir tree seedlings is influenced by both abiotic and biotic factors at the fine-spatial scales of 1m resolution. Abiotic factors, like snowmelt date and potential evaporation, along with biotic factors, like canopy cover and distance to nearest adult tree, shape occupancy patterns that are initially influenced by seed dispersal. As seedlings mature, our findings suggest that density-dependent mortality further affects seedling presence/absence on the landscape. Because biotic forest stand structure variables were amongst the top predictors of seedling occupancy, we suggest distinguishing between direct biotic influences (adult-seedling interactions) and indirect biotic influences that occur when the forest stand structure affects the fine-scale conditions to which seedlings respond. This distinction is important for identification of fine-scale refugia and for projection of tree species geographic ranges under future climates.

3.6 Acknowledgements

The authors thank Erin Conlisk, John Harte, and Adam B. Smith for thoughtful comments on early drafts. Additionally, we offer our gratitude to the many assistants who helped collect the field observations and to the USGS Western Ecological Research Center, Sequoia / Kings Canyon National Park scientists and staff and the Sierra Nevada Research Institute for logistical field support. This project was supported by the US Department of Energy Office of Science (BER), the National Park Service Californian Cooperative Ecosystem Unit, a George Melendez Wright Climate Change Fellowship to DSC, and a Berkeley Atmospheric Sciences Center Fellowship to DSC.

3.7 References

Arx, von, G., Graf Pannatier, E., Thimonier, A. & Rebetez, M. (2013). Microclimate in forests with varying leaf area index and soil moisture: potential implications for seedling establishment in a changing climate. *Journal of Ecology*, **101**, 1201–1213.

Barbour, M.G., Fernau, R.F., Benayas, J., Jurjavcic, N. & Royce, E.B. (1998). Tree regeneration following clearcut logging in red fir forests of California. *Forest Ecology and Management*, **104**, 101–111.

Battaglia, L.L., Fore, S.A. & Sharitz, R.R. (2000). Seedling emergence, survival and size in relation to light and water availability in two bottomland hardwood species. *Journal of Ecology*, **88**, 1041–1050.

Bell, D.M., Bradford, J.B. & Lauenroth, W.K. (2013). Early indicators of change: divergent climate envelopes between tree life stages imply range shifts in the western United States. *Global Ecology and Biogeography*, **23**, 168–180.

Bello, F. de, Lavorel, S., Lavergne, S., Albert, C.H., Boulangeat, I., Mazel, F. & Thuiller, W. (2012). Hierarchical effects of environmental filters on the functional structure of plant communities: a case study in the French Alps. *Ecography*, **36**, 393–402.

Buehlmann, P. and Hothorn, T. 2007. Boosting Algorithms: Regularization, Prediction and Model Fitting (with Discussion). *Statistical Science* **22**, 477-505.

CA DWR (California Department of Water Resources). http://cdec.water.ca.gov/cdecapp/snowapp/swcchart.action. Accessed Oct 25, 2015.

Carón, M.M., De Frenne, P., Brunet, J., Chabrerie, O., Cousins, S.A.O., Decocq, G., Diekmann, M., Graae, B.J., Heinken, T., Kolb, A., Lenoir, J., Naaf, T., Plue, J., Selvi, F., Wulf, M. & Verheyen, K. (2015). Divergent regeneration responses of two closely related tree species to direct abiotic and indirect biotic effects of climate change. *Forest Ecology and Management*, **342**, 21–29.

Chambers, J.C. (2001). Pinus monophylla establishment in an expanding Pinus-Juniperus woodland: Environmental conditions, facilitation and interacting factors. *Journal of Vegetation Science*, **12**, 27–40.

Chappell, C.B. & Agee, J.K. (1996). Fire severity and tree seedling establishment in Abies magnifica forests, southern Cascades, Oregon. *Ecological Applications*, **6**, 628–640.

Chen, J.Q., Saunders, S.C., Crow, T.R., Naiman, R.J., Brosofske, K.D., Mroz, G.D., Brookshire, B.L. & Franklin, J.F. (1999). Microclimate in forest ecosystem and landscape ecology - Variations in local climate can be used to monitor and compare the effects of different management regimes. *Bioscience*, **49**, 288–297.

Cheplick, G.P. & Quinn, J.A. (1987). The Role of Seed Depth, Litter, and Fire in the Seedling Establishment of Amphicarpic Peanutgrass (Amphicarpum-Purshii). *Oecologia*, **73**, 459–464.

Clark, J.S., Bell, D.M., Hersh, M.H., Kwit, M.C., Moran, E., Salk, C., Stine, A., Valle, D. & Zhu, K. (2011). Individual-scale variation, species-scale differences: inference needed to understand diversity. *Ecology Letters*, **14**, 1273–1287.

Clark, J.S., Silman, M., Kern, R., Macklin, E. & HilleRisLambers, J. (1999). Seed dispersal near and far: Patterns across temperate and tropical forests. *Ecology*, **80**, 1475–1494.

Collins, R.J. & Carson, W.P. (2004). The effects of environment and life stage on Quercus abundance in the eastern deciduous forest, USA: are sapling densities most responsive to environmental gradients? *Forest Ecology and Management*, **201**, 241–258.

Connell, J.H. (1971). On the role of natural enemies in preventing competitive exclusion in some marine animals and in rain forest trees. *Dynamics of Populations* (eds P.J. den Boer & G. GR). Proceedingss of the Advanced Study Institute in Dynamics of Numbers in Populations, Ossterbeck. Centre for Agricultural Publishing and Documentation, Wageningen.

Cressie, N.A.C. (1993). *Statistics for spatial data*. Wiley-Interscience.

De Frenne, P., Rodríguez-Sánchez, F., Coomes, D.A., Baeten, L., Verstraeten, G., Vellend, M., Bernhardt-Roemermann, M., Brown, C.D., Brunet, J., Cornelis, J., Decocq, G.M., Dierschke, H., Eriksson, O., Gilliam, F.S., Hedl, R., Heinken, T., Hermy, M., Hommel, P., Jenkins, M.A., Kelly, D.L., Kirby, K.J., Mitchell, F.J.G., Naaf, T., Newman, M., Peterken, G., Petřík, P., Schultz, J., Sonnier, G., Van Calster, H., Waller, D.M., Walther, G.-R., White, P.S., Woods, K.D., Wulf, M., Graae, B.J. & Verheyen, K. (2013). Microclimate moderates plant responses to macroclimate warming. *Proceedings of the National Academy of Sciences*, **110**, 18561–18565.

Dobrowski, S.Z., Swanson, A.K., Abatzoglou, J.T., Holden, Z.A., Safford, H.D., Schwartz, M.K. & Gavin, D.G. (2015). Forest structure and species traits mediate projected recruitment declines in western US tree species. *Global Ecology and Biogeography*, **24**, 917–927.

Fites-Kaufman, J. A., Rundel, P., Stephenson, N., and Weixelman, D.A., (2007). Montane and Subalpine Vegetation of the Sierra Nevada and Cascade Ranges. In *Terrestrial Vegetation of California 3rd edition*. (eds. M. G. Barbour, T. Keller-Wolf, and A. A. Schoenherr). University of California Press, 456-501.

Frankland, J.C., Ovington, J.D. & Macrae, C. (1963). Spatial and Seasonal-Variations in Soil, Litter and Ground Vegetation in Some Lake District Woodlands. *Journal of Ecology*, **51**, 97–112.

Franklin, J. (2010). *Mapping Species Distributions*. Cambridge University Press.

Geiger, R., Aron, R.H. & Todhunter, P. (2009). *The Climate Near the Ground*. Rowman & Littlefield Publishers, Inc, Plymouth, United Kindom.

George, L. O. and Bazzaz, F. A. (2014).The Herbaceous Layer as a Filter Determining Spatial Pattern in Forest Tree Regeneration. *The Herbaceous Layer in Forests of Eastern North America* (ed. F Gilliam). Oxford University Press, 340-355.

Gonsamo A.,Walter, J-M.N., and Pellikka, P. (2011). CIMES: A package of programs for determining canopy geometry and solar radiation regimes through hemispherical photographs. *Computers and Electronics in Agriculture* **79**, 207-215.

Gordon, D. T. 1970. Natural regeneration of white and red fir ... influence of several factors, PSW–58. USDA Forest Service.

Gottfried, M., Pauli, H., Reiter, K. & Grabherr, G. (2010). A Fine-Scaled Predictive Model for Changes in Species Distribution Patterns of High Mountain Plants Induced by Climate Warming. *Diversity and Distributions*, **5**, 241–251.

Gray, A.N. & Spies, T.A. (1996). Gap size, within-gap position and canopy structure effects on conifer seedling establishment. *Journal of Ecology*, **84**, 635–645.

Greenberg, J.A., Santos, M.J., Dobrowski, S.Z., Vanderbilt, V.C. & Ustin, S.L. (2015). Quantifying Environmental Limiting Factors on Tree Cover Using Geospatial Data (M. Hanewinkel, Ed.). *PLoS ONE*, **10**, e0114648–15.

Grubb, P.J. (1977). Maintenance of Species-Richness in Plant Communities - Importance of Regeneration Niche. *Biological Reviews of the Cambridge Philosophical Society*, **52**, 107–145.

Harwood, T.D., Mokany, K. & Paini, D.R. (2014). Microclimate is integral to the modeling of plant responses to macroclimate *Proceedings of the National Academy of Sciences*, **111**, E1164–E1165.

Hijmans, R.J. (2012). Cross-validation of species distribution models: removing spatial sorting bias and calibration with a null model. *Ecology*, **93**, 679–688.

Holland, E.A. & Coleman, D.C. (1987). Litter Placement Effects on Microbial and Organic-Matter Dynamics in an Agroecosystem. *Ecology*, **68**, 425–433.

Hothorn, T. Buehlmann, P., Kneib, T., Schmid, M., and Hofner, B. (2015). mboost: Model-Based Boosting, R package version R package version 2.4-2, http://CRAN.R-project.org/package=mboost.

Hothorn, T., Buehlmann, P., Kneib, T., Schmid. M., and Hofner, B. (2010). Model-based Boosting 2.0. *Journal of Machine Learning Research* **11**, 2109-2113.

Hothorn, T., Mueller, J., Schroeder, B., Kneib, T. & Brandl, R. (2011). Decomposing environmental, spatial, and spatiotemporal components of species distributions. *Ecological Monographs*, **81**, 329–347.

Hothorn, T. et al. 2015. mboost: Model-Based Boosting, R package version R package version 2.4-2, http://CRAN.R-project.org/package=mboost.

Ibáñez, I., Clark, J.S., LaDeau, S. & Hille Ris Lambers, J. (2007). Exploiting temporal variability to understand tree recruitment response to climate change. *Ecological Monographs*, **77**, 163–177.

Jackson, S.T., Betancourt, J.L., Booth, R.K. & Gray, S.T. (2009). Ecology and the ratchet of events: Climate variability, niche dimensions, and species distributions. *Proceedings of the National Academy of Sciences*, **106**, 19685–19692.

James, G., Witten, D., Hastie, T. & Tibshirani, R. (2013). *An Introduction to Statistical Learning*. Springer Science & Business Media, New York, NY.

Janzen, D.H. (1970). Herbivores and the Number of Tree Species in Tropical Forests. *American Naturalist*, **104**, 501–528.

Johnson, D.M., McCulloh, A., and Reinhardt, K. (2011). The Earliest Stages of Tree Growth: Development, Physiology and Impacts of Microclimate. *Size- and Age-Related Changes in Tree Structure and Function* (eds. F. C. Meinzer, B. Lachenbruch, and T. E. Dawson). Springer Science & Business Media, 65-87.

Kroiss, S.J. & HilleRisLambers, J. (2015). Recruitment limitation of long-lived conifers: implications for climate change responses. *Ecology*, **96**, 1286–1297.

Laacke, R. J. (1990). Abies magnifica A. Murr. California red fir. *Silvics of North America. Volume 1. Conifers* (R. M. Burns and B. H. Honkala, technical coordinators). US Department of Agriculture.

Lawler, J.J., Ackerly, D.D., Albano, C.M., Anderson, M.G., Dobrowski, S.Z., Gill, J.L., Heller, N.E., Pressey, R.L., Sanderson, E.W. & Weiss, S.B. (2015). The theory behind, and the challenges of, conserving nature's stage in a time of rapid change. *Conservation Biology*, **29**, 618–629.

Lenoir, J., Gégout, J-C., Pierrat, J-C., Bontemps, J-D. & Dhôte, J-F. (2009). Differences between tree species seedling and adult altitudinal distribution in mountain forests during the recent warm period (1986-2006). *Ecography*, **32**, 765–777.

Macfarlane, C. (2011). Agricultural and Forest Meteorology. *Agricultural and Forest Meteorology*, **151**, 833–840.

Maggini, R., Lehmann, A., Zimmermann, N.E. & Guisan, A. (2006). Improving generalized regression analysis for the spatial prediction of forest communities. *Journal of Biogeography*, **33**, 1729–1749.

Maher, E.L. & Germino, M.J. (2006). Microsite differentiation among conifer species during seedling establishment at alpine treeline. *Ecoscience*, **13**, 334–341.

Mayr, S., Hacke, U., Schmid, P., Schwienbacher, F. & Gruber, A. (2006). Frost drought in conifers at the alpine timberline: Xylem dysfunction and adaptations. *Ecology*, **87**, 3175–3185.

Mclaughlin, B.C. & Zavaleta, E.S. (2012). Predicting species responses to climate change: demography and climate microrefugia in California valley oak (Quercus lobata). *Global Change Biology*, **18**, 2301–2312.

Meinzer, F.C., Lachenbruch, B. & Dawson, T.E. (2011). *Size- and Age-Related Changes in Tree Structure and Function* (eds. F.C. Meinzer, B. Lachenbruch & T.E. Dawson). Springer Science & Business Media, Dordrecht.

Merow, C., Smith, M.J., Edwards, T.C., Jr, Guisan, A., McMahon, S.M., Normand, S., Thuiller, W., Wüest, R.O., Zimmermann, N.E. & Elith, J. (2014). What do we gain from simplicity versus complexity in species distribution models? *Ecography*, **37**, 1267–1281.

Meynard, C.N., Lavergne, S., Boulangeat, I., Garraud, L., Van Es, J., Mouquet, N. & Thuiller, W. (2013). Disentangling the drivers of metacommunity structure across spatial scales (L.N. Gillman, Ed.). *Journal of Biogeography*, **40**, 1560–1571.

Moles, A.T. & Westoby, M. (2004). What do seedlings die from and what are the implications for evolution of seed size? *Oikos*, **106**, 193–199.

Moyes, A.B., Germino, M.J. & Kueppers, L.M. (2015). Moisture rivals temperature in limiting photosynthesis by trees establishing beyond their cold-edge range limit under ambient and warmed conditions. *New Phytologist*, **207**, 1005–1014.

Nuttle, T. & Haefner, J.W. (2005). Seed Dispersal in Heterogeneous Environments: Bridging the Gap between Mechanistic Dispersal and Forest Dynamics Models. *The American Naturalist*, **165**, 336–349.

Peterson, A.T., Soberón, J., Pearson, R.G., Anderson, R.P., Martínez-Meyer, E., Nakamura, M. & Araújo, M.B. (2011). *Ecological Niches and Geographic Distributions*. Princeton University Press.

Potter, K.A., Arthur Woods, H. & Pincebourde, S. (2013). Microclimatic challenges in global change biology. *Global Change Biology*, **19**, 2932–2939.

R Core Development Team. (2013). R: A language and environment for statistical computing. R Foundation for Statistical Computing, Vienna, Austria. URL http://www.R-project.org/

Randin, C.F., Engler, R., Normand, S., Zappa, M., Zimmermann, N.E., Pearman, P.B., Vittoz, P., Thuiller, W. & Guisan, A. (2009). Climate change and plant distribution: local models predict high-elevation persistence. *Global Change Biology*, **15**, 1557–1569.

Ridgeway, G. with contributions from others. (2015). gbm: Generalized Boosted Regression Models. R package version 2.1.1. http://CRAN.R-project.org/package=gbm

Scholl, A.E. & Taylor, A.H. (2006). Regeneration patterns in old-growth red fir–western white pine forests in the northern Sierra Nevada, Lake Tahoe, USA. *Forest Ecology and Management*, **235**, 143–154.

Soberón, J. (2007). Grinnellian and Eltonian niches and geographic distributions of species. *Ecology Letters*, **10**, 1115–1123.

Stephenson, N.L. (1998). Actual evapotranspiration and deficit: biologically meaningful correlates of vegetation distribution across spatial scales. *Journal of Biogeography*, **25**, 855–870.

Trivedi, M.R., Berry, P.M., Morecroft, M.D. & Dawson, T.P. (2008). Spatial scale affects bioclimate model projections of climate change impacts on mountain plants. *Global Change Biology*, **14**, 1089–1103.

Ustin, S.L., Woodward, R.A., Barbour, M.G. & Hatfield, J.L. (1984). Relationships Between Sunfleck Dynamics and Red Fir Seedling Distribution. *Ecology*, **65**, 1420–1428.

Wolfe , J. N. *et al.* (1949). Microclimates and Macroclimate of Neotoma, A Small Valley in Central Ohio, Publication No. 488. Department of Botany and Plant Pathology, Ohio State University.

Zimmerman, D.L. & Stein, M.L. (2010). Classical Geostatistic Methods. *Handbook of Spatial Statistics* (eds A. Gelfand, P. Diggle, M. Fuentes & P. Guttorp). CRC Press.

Chapter 4: 01100110 01101111 01110010 01100101 01110011 01110100 [forest]

> "How do we tease apart separate storable information bytes out of the flow of events or landscapes?" – Bowker [2008, pg. 135]

As my ecological research in the red fir forests of California's Sierra Nevada progressed over the period of 7 summers, I grew more and more uneasy. I was trying to understand this living system by a series of representations: charts, diagrams, photographs, graphs. The fundamental process: collect quantifiable bits and reconfigure them into a representation of the system. After I scanned my 1-hectare study site with a terrestrial laser scanner and viewed the resulting point cloud data on my computer screen (Figure 4.1), I realized I was turning this complex collection of organisms interacting with their analog environment into discretized 0s and 1s. But if the forest could explain itself [Kohn 2013], would it speak binary? Would it represent itself with a collection of small information bits?

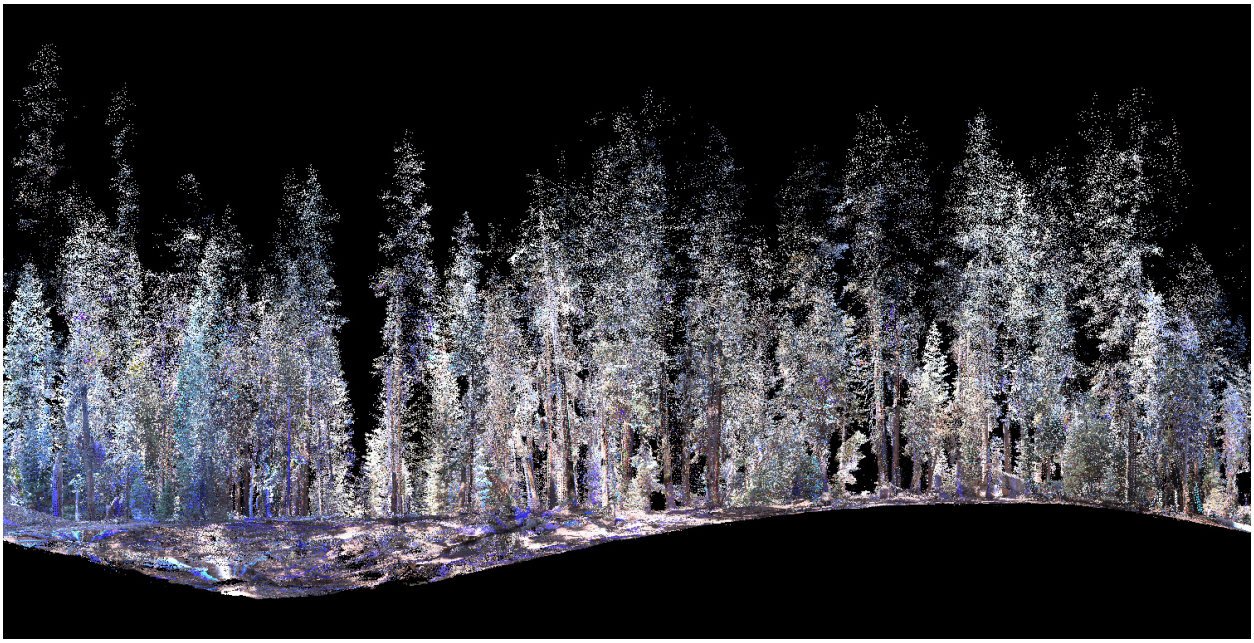


Figure 4.1: The digital forest is a point cloud representation of red fir study site, located in California's Sierra Nevada.

Scientists have long used representations to great effect. In particular visual representations hold an elevated status. Many science technology studies (STS) scholars have described this core methodology, highlighting its benefits and also its epistemological risks, both often stemming from technological advances. In the burgeoning era of big data and associated digital technologies, my use of such a technology, terrestrial laser scanning with its 2D and 3D visualizations of point cloud data, offers a unique opportunity to explore how new practices of visual representation affect ecological

study.[1] In this chapter, I compare a representation of my forest study as a collection of points to established ecological representations, describing how the use of laser scanning technologies intensifies research logistics compared to more established field-based methodologies. Then, I assess the scientific opportunities that using such technologies afford, in my case by fostering a conceptual model of the forest that is more malleable than commonly used representations. Leveraging STS critiques of representations, especially visual representations enabled by technology, I examine the potential risks of this new type of visual representation. Through this self-examination, I aim to offer a framework for ecologists to harness the opportunities of new visual technologies responsibly.

4.1 Background: The many ways to (scientifically) represent a forest

4.1.1 Latour's cascades of immutable mobiles; Bowker's classification; Haraway's partial perspectives; and Barad's agential realism

Fundamentally, the majority of representation in scientific practice relies on collecting what Latour [1990] calls "immutable mobiles", the "things" a scientist goes and comes back with to convince others of a particular argument. My ecological research, like many other studies, is focused on collecting quantifiable bits of the forest. My scientific goal was to understand what combination of environmental conditions influence tree seedling establishment, *i.e.,* what light levels, soil moisture, nutrient levels, all the things a seedling needs to survive, allow for seedlings to grow well. To study this question, I collected a lot of information about the seedlings themselves and the physical environment around them, and I did so in a quantitative manner (Figure 4.2). To be effective pieces of evidence according to Latour, these quantifiable bits or "data" must be immutable, mobile, flat, scalable, reproducible, recombinable, superimposable, integrable with written text, and mergeable with geometry (*i.e.,* made 2D) [1990, pg. 44-46]. Many of these characteristics are important so that the collector can organize the data into a simplified representation of the observed phenomenon.

Latour [1990] calls this organization a "cascade of cascades" in which the scientist makes sense of a phenomenon. Latour is referring to a series or hierarchy of reduction processes that combine the data into a smaller set of knowable entities. Classification [Bowker 2008, Bowker and Starr 2000] and/or standardization [Scott 1998, Edwards 2010] play an important role in these reductions. In Latour's data requirements, classification and standardization are especially important to make the data scalable, recombinable, and superimposable, *i.e.,* these practices make data comparable to other data or existing data.

Haraway [1991] cautions that these reductions of the studied entity, especially those enabled by technologies, are partial perspectives. With the extension of their senses however, scientists are easily seduced into a practice that regards technologically-enabled perspectives as complete and objective. What Haraway calls a "god-trick" allows scientists and users of scientific information, *i.e.,* the rest of human society, to "transcend … all limits and responsibility" [1991, pg. 190]. But by understanding

[1] I take an atypical approach relative to STS and other social science traditions. I reflect on my own ecological research practices. While this approach is undoubtedly subjective, so is that of another researcher studying my practice. Through this auto-ethnographical [Holbrook 2006, Brown 2006] and interactive-researcher introspection [Ellis 1991] approach, I hope to (1) illuminate insights not accessible to an outside researcher and (2) exemplify a practice of self-reflection that I will eventually argue may benefit the field of ecology and possibly humanity's relationship with our surrounding environs. I also follow Geertz's [1973] notion of "thick description," in which I attempt to provide a detailed account of my ecological practice so that the reader can better assess my claims regarding scientific visualization practices.

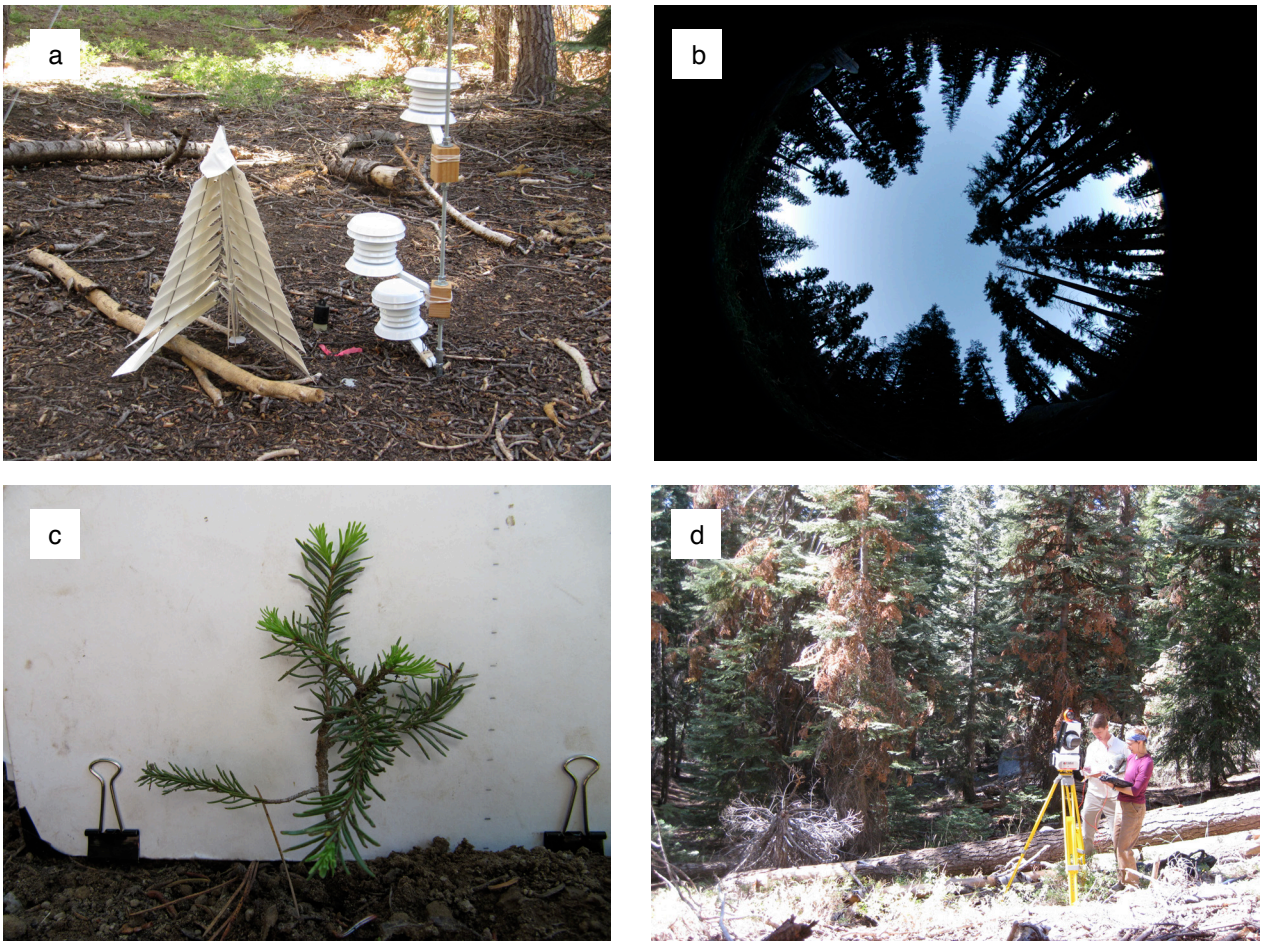


Figure 4.2: A sample of the type of information that I collected in my ecological study. (a) One of 225 sample locations within the 640x20m study site: manually deployed piche evaporator under triangular radiation shield measuring potential evaporation; soil moisture access tube (black cap) used to manually measure soil moisture; automated sensors in cylindrical radiation shields measuring the vertical air temperature and relative humidity profile; automated sensors (marked by silver tag just below pink flagging) buried 5cm below the surface measuring soil temperature every four hours. (b) I took hemispherical "fisheye" photographs of the forest canopy at those same 225 locations. (c) I manually collected tens of thousands of measurements on thousands of tree seedlings. (d) I scanned my study site with a terrestrial laser scanner (colleagues are configuring a scan with the I-Site 4400 scanner and hand-held controller tablet).

that all representations are partial and by seeking many of them, scientists can recognize the limits to a particular perspective defined in part by the technology utilized and seek to fill those gaps.

Barad [2003] extends Haraway's framework through her concept of agential realism in which phenomena are understood in local contexts that are particular to the observed, observer, and the apparatuses used in the act of observing. As illustrated by the uncertainty principle[2], the observer and observed are both essential to create understanding through "intra-actions" that are additionally constrained by any apparatus used. With this framework, Barad questions critiques of representations that focus on whether they adequately capture an external truth (traditional realist epistemologies) or how they are shaped by cultural forces (social constructionist epistemologies). Instead, with agential realism, Barad embeds representations within a dynamic performative

[2] Uncertainty principle is a mathematical inequality that limits the knowledge of pairs of physical properties, for example the position and momentum of a particle.

understanding of the world that comes into being through the emergent "intra-actions" of the observed, observer, and the apparatus employed.[3] Because this understanding is not predefined by an exterior truth or societal norms, scientific knowledge practice becomes more objective and open to reconfiguration with new perspectives.

4.1.2 Visual representation in scientific practice

> "A new visual culture redefines both what it is to see, and what there is to see."
> – Latour [1990, pg. 30]

Understanding of cognitive processes supports Latour's claim that visualizations are an important form of representation. First, visual communication often results in very fast cognition [Baird *et al.* 1993]. Compared to verbal descriptions of a visual concept, visual representations can be better understood because the concept is already constructed [Miller & Burton 1994]. Another benefit of visual communication is that visual understanding is an innate process [Hewes 1978 as cited by Seels 1994]. Human physiology is literally hard-wired for visual input: 75% of information entering the brain is from the eyes, and the optical nerve comprises 38% of the fibers entering or leaving the central nervous system [Hansen 1987 as cited by Barry 1994]. Visual understanding is our primary form of learning as children [Hartin 1994, Marthewson 1999]. Feldman [1976 as cited by Hartin 1994] suggests that we have to unlearn many of our childhood learning skills in order to transition to a language based communication system.

Additionally, complex concepts can often be concisely communicated through visualizations as opposed to lengthy language descriptions [Braden 1994, Mathewson 1999]. This is so because visualizations can display an entire concept at once [Messaris 1997], where as language-based communication is linear and piecemeal, *i.e.,* each word piece is arranged one after another. Its holistic, non-linear representation makes visualization a multi-dimensional form of communication [Frascara 2001]. Tufte [2006] notes that representing concepts over multiple scales is an important reason why visualization of complex concepts is successful.

Finally, visual representations are powerful because they provide evidence [Moser 1996, Brown 1996, Messaris 1997] or an experience of reality [Barry 1994]. Latour also notes the evidential qualities of visual representation:

> What is so important in the images and in the inscriptions scientists and engineers are busy obtaining, drawing, inspecting, calculating, and discussing? It is, first of all, the unique advantage they give in the rhetorical or polemical situation. "You doubt what I say? I'll show you." And, without moving more than a few inches, I unfold in front of your eyes figures, diagrams, plates, texts, silhouettes, and then and there present things that are far away and with which some sort of two-way connection has now been established. I do not think the importance of this simple mechanism can be overestimated. [Latour 1990, pg. 35-36]

Pierce [1998] incorporates the ideas of evidential representation in his framework of signs: icon, index, and symbol. An icon is a representation of an object or action that still bears resemblance to the referent although it may be stylized; an index is a representation that is directly mapped to the

[3] I use Barad's term "intra-actions" or the relationships between the observed, observer, and apparatus that become defined as an understanding of a phenomenon emerges. Because these relationships are not pre-defined and develop *within* the phenomenon's description, Barad makes a distinction from "interaction," which would describe relationships *between* pre-defined entities [Barad 2003].

referent; and a symbol is an abstract representation of the referent that almost always requires cultural convention for understanding. Kohn [2013] considers Pierce's semiotic triad in the context of forest ecology, extending the concepts of icons and indices to nonhuman species and noting that indices, with direct ties to referents, can map to both the past and future. By pointing to the future, indices may create anticipation and expectation.

Scientific visualization is being redefined continuously by ongoing technological development. An iconic example is the optical instruments that make the small large (microscopes) and the distant near (telescopes). Techniques that expand the human "eye" take a vast array of forms, from scanning electron microscopes, DNA sequencing processes, and neutrino detectors to radio telescopes, satellite imagery, and general circulation models. These technologies allow us to bring the tiny, the distant, the large, the fast, the slow into human perspectives and also into forms that scientists can manipulate. While new types of visual representations often involve technologies that expand human senses, they are not required. I define new visual representations as a collection of "immutable mobiles" that are primarily understood through our visual senses and require training outside established practices to produce the representation and/or engage with it.

While certainly enabling insights into the world and improving many aspects of the human condition, the ability to see beyond our natural senses has also been critiqued. For example, Haraway [1991] posits that these technologies, as generated from industrial-military complex, evoke a practice of observer dominance over the observed. The observed become flattened things, similar to Latour's ideal immutable mobiles, that the observer can manipulate and recombine to her desire. In the process, responsibility towards the observed is lost. Instead, the technologies offer a partial perspective. Similarly, Barad [2003] suggests that failure to recognize the "intra-actions" that these technologies enable blinds the observer to full understanding because the observer is unaware of what she may not be observing. Myers [2014] describes scientific practices in which technological metaphor shapes both the types of discoveries that are made and the group of scientists that are making them. Finally, Vertesi [2014] warns that technologies can inscribe perspectives that become so engrained within a scientific practice that they become *the* way to see the observed rather than *a* way to understand it.

It is in this scientific practice of visual representation, strongly shaped by technological capabilities, that I explore my use of new technologies, terrestrial laser scanning and associated 2D and 3D visualization technologies, in my ecological study of forest regeneration. How is it the same as established scientific visual representation practices and how does it differ? I first describe my use of hemispherical photography, an established technical methodology, which I use as a simplified and abstracted visual representation of my forest study site. My goal in doing so is to further illustrate how STS scholars interpret the role of representation, especially visual representation, and to provide an example to which I will compare a new digital visualization of the forest.

4.1.3 An example of established scientific representation: hemispherical photography

In my ecological study, I used hemispherical photography to quantify the direct and indirect radiation entering the forest, *i.e.,* the patterns of sun and shade. In this example, I trace this established technical methodology from field collection to analysis. To take the hemispherical photographs, I first consulted the literature to understand the best practices for this technique (Figure 4.3). To obtain the recommended photographic characteristics, I took the photographs in diffuse light — on a completely cloudy day, before dawn, or after dusk — constantly monitoring the histogram to adjust the exposure length. At the end of a week hiking to and from my field site (3 miles each way) in complete darkness so that I could shoot ~25 photos before dawn and about ~10

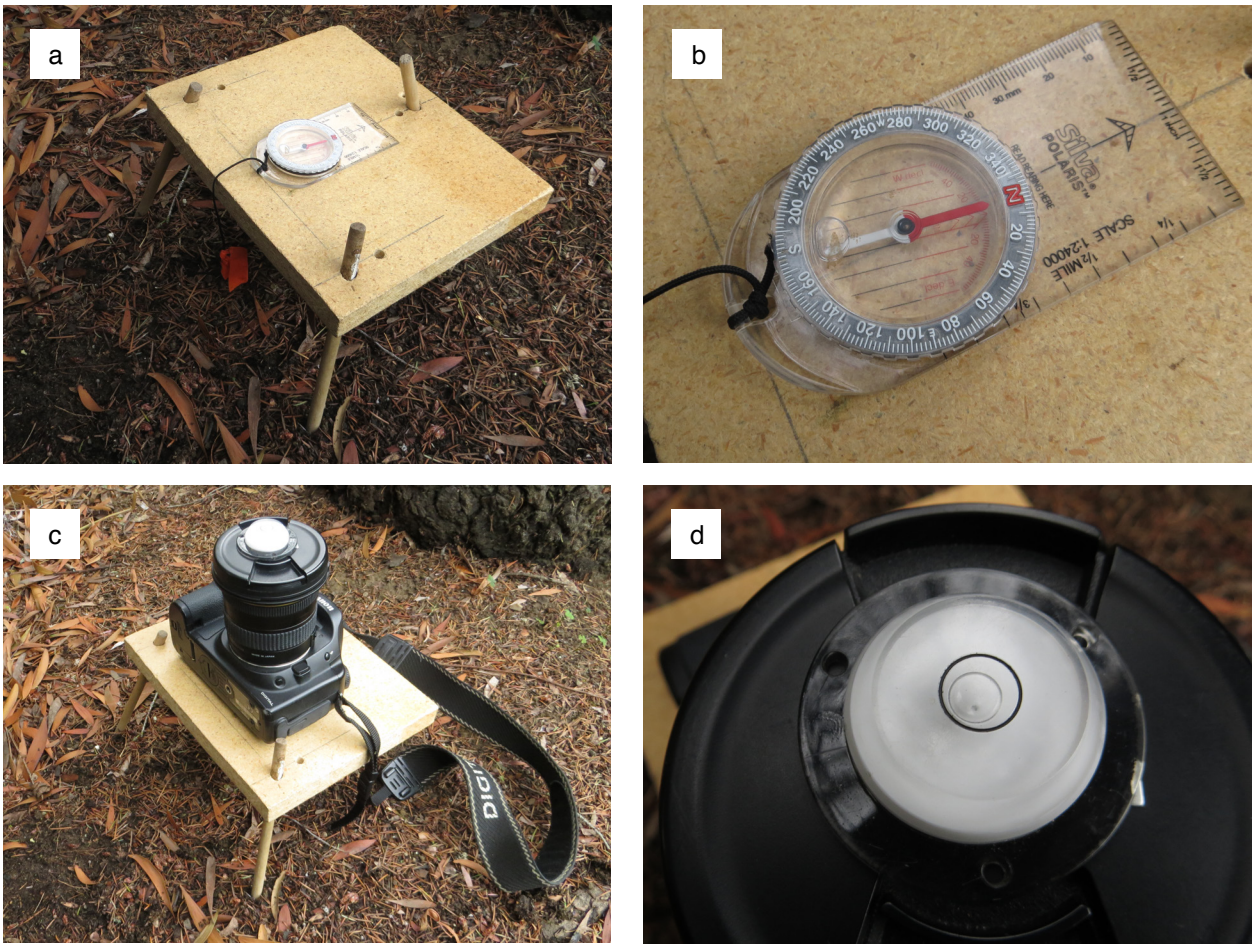


Figure 4.3: Best practices for hemispherical photography of forest canopies: I acquired the suitable equipment, a circular fisheye lens that was compatible with a high-end digital camera (camera and lens pictured are not the actual camera and lens used but are representative). In the field, I used a homemade tripod with adjustable legs and bubble level to make the camera lens level at each location on the uneven forest terrain (c-d). Using a compass, I oriented the camera so that the top of the photograph would point north (a-b). Because the camera exposure affects the quality of photograph, I aimed for a certain characteristic distribution of pixel values in the blue channel..

photos after dusk, I had collected the raw data, hemispherical photographs (Figure 4.4a) at all 225 measurement locations.

But is this data really raw? According to many STS scholars, there is no such thing as raw data. The choices that I made in taking the hemispherical photos, the measurement locations, the type of lens, leveling the photo, the exposure length might be different for another researcher. The pixel values created by the exposure length combined with the atmospheric conditions at the time of the photo are not even exactly repeatable for me. Thus, these data are theory-laden, *i.e.,* they are based on existing knowledge and expectations [Brine and Poovey 2013, Myers & Dumit 2013, Vertesi 2014], prior to collection.

After acquiring the photographs in the field, my assistant and I processed the photos using a new automated tool that changes the color photo to black (vegetation) and white (sky) (Figure 4.4c). Through this software tool, we classified the digital representation into a simpler, flatter representation that can be recombined or "reshuffled" [Latour 1990]. By assigning each pixel value

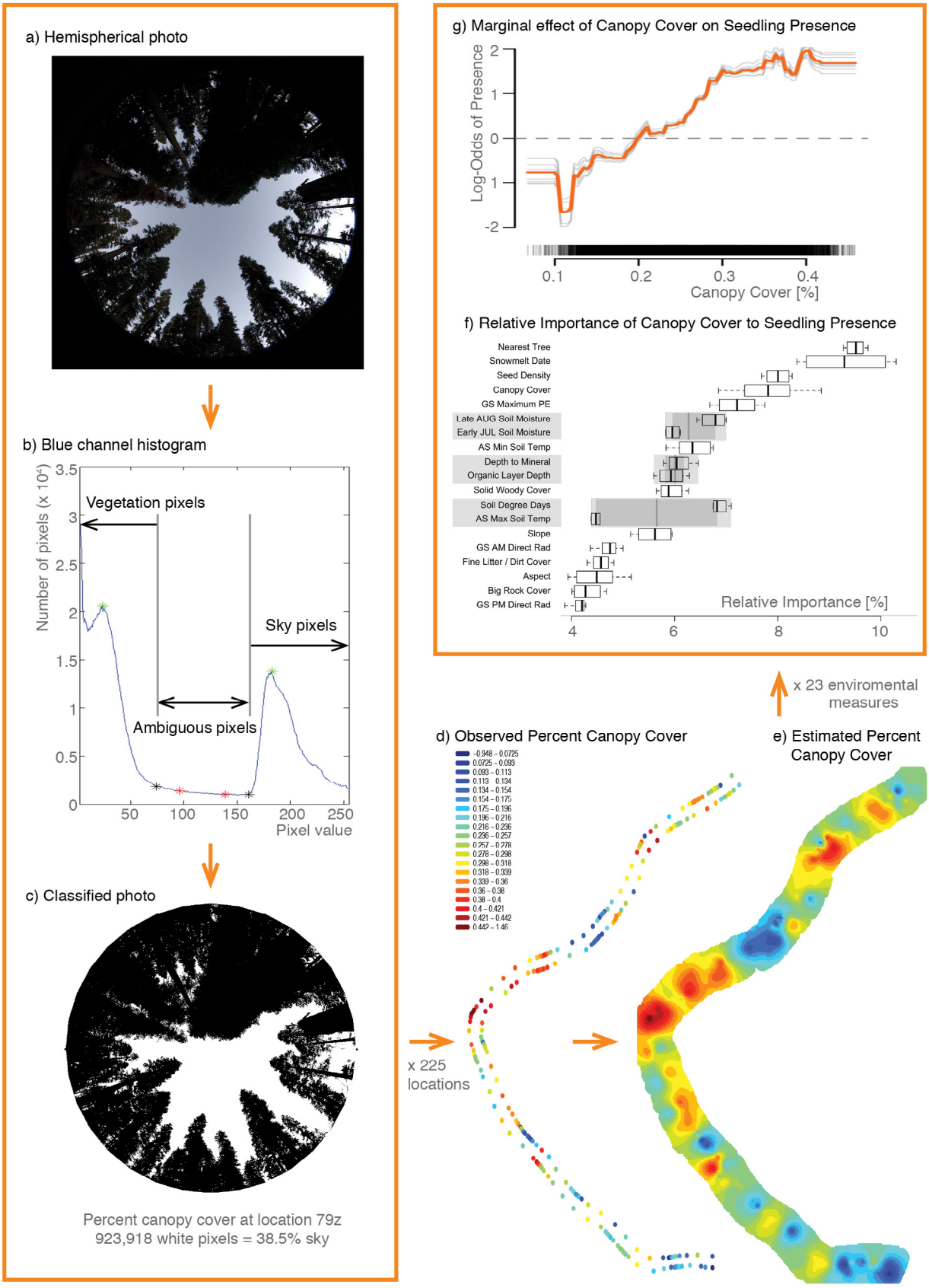


Figure 4.4 See caption on next page.

Figure 4.4 (previous page): A trace of the use of hemispherical photography in explaining tree seedling presence absence. Starting in the upper left and following the orange arrows: (a) Hemispherical photograph at location 79z; (b) Histogram of pixel values in blue channel of digital photograph, automatically divided into sky (white) and vegetation (black) pixels with DCP software;[4] (c) Classified sky and vegetation pixels mapped onto the original photograph; (d) The canopy openness (fraction of pixels that are sky) at all 225 locations within the study site as calculated by the process illustrated in a-c; (e) Canopy openness values modeled at every location on a 1x1m grid with in the study site using spatial statistics; (f) The relative influence of canopy cover and 22 other theory-laden environmental variables influencing the presence and absence of tree seedlings on the landscape;[5] (g) The marginal effects of canopy cover on the probability[6] of a tree seedling occurring at a given canopy openness value.

either black or white, we could then sum each color, *i.e.,* reshuffle the image, to learn how much of the forest canopy was open to sky or blocked by trees. Via this process, we quantified the percent canopy cover at the location of the hemispherical photo.

However, this classification process is difficult for areas in the photograph that transition from tree to sky. Light refracts around the tree needles, making the edges of the tree canopy fuzzy in the photograph. Their pixel values are not clearly vegetation or clearly sky, but rather an intermediate ambiguous value. The automated software separates these borderline values based on a series of rules (Figure 4.4b) that were once subjective decisions made by the scientist.[7] Throughout the acquisition of the hemispherical photos, we strived to standardize the information. However, by explicitly removing the scientist from the equation, we made the product of this process, the black and white photo, in theory more comparable to other photos processed in the same way. This process of standardization reduces the role of the individual experts and centralizes the expertise in the software to create a more objective representation [Porter 1996, Scott 1998].

Bowker [2008] would argue otherwise. When classifying things that are difficult to classify, he describes a process of representing singularities in time and space. In the hemispherical photo example, each processed photograph represents a unique location captured at a unique time. Bowker postulates that these singularities yield a skewed representation of the actual system because when put into model frameworks these unique quantifications present the illusion of a dynamic system. But they are actually just repeated singularities rather than changing conditions. My ultimate goal with this hemispherical data is to incorporate it into such a modeled representation of the forest system, but a few more "cascades," *i.e.* processing steps, remain.

Ideally when creating a model of a complex system, one would have a data value at every location. In ecology, this is no exception, and as in other scientific fields, it is impossible. Obtaining a representative sample is required but is unsatisfactory in some cases. Thus, scientists use modeled data as the basis of other models, instead of direct observations [Edwards 2010]. I did just that. For percent canopy cover and the other environment measures that I collected at 225 locations in the study plot, I estimated the measurement value at every location on a 1x1m grid (Figure 4.4d & 4.4e). Edwards [2010] describes this estimation practice as used in atmospheric circulation models and an

[4] Ambiguous pixels are eventually divided into sky and vegetation pixels by software as well.

[5] Relative importance values are reported for 8 different model configurations in the form of box and whisker plots (dashed whiskers show full range of values, box ends show 25 and 75 quartiles, and vertical line shows median value). See Chapter 3 for full details.

[6] Probability is reported in log-odds: values greater than zero contribute to a seedling presence, while those less than zero contribute to a seedling absence. See Chapter 3 for full details.

[7] Interestingly, because this was new software, we compared photos processed by the software to manually processed photos to establish how the automated process compares to the established manual process. In a way we had to vet the new software against a more subjective classification.

extreme version applied in weather forecasts. In the latter, "data" input into forecast models are the output of the previous modeled forecast, updated where needed to match observed values. Once

standardized on the 1x1m grid within my study site, I ultimately combined the estimated values of percent canopy cover with other metrics into a model describing the presence and absence of tree seedlings within the study site. The percent canopy cover values along with the rest of the model components are reduced further as the cascade grows. I describe the full model through multiple abstract visual representations (Figure 4.4f–g).

4.1.4 The forest as a cascades of quantified bits

By tracing the hemispherical photograph data from field collection to model incorporation, a series of different forest representations are revealed (Figure 4.4). What do these standard scientific representations [Latour 1990] of the forest have in common? They are composed of quantified bits, organized such that the viewer "sees" the forest "as" in particular way [Vertesi 2014]. The original hemispherical photo (Figure 4.4a) is composed of reflected light from the sky and vegetation collected on a gridded array of red, green, and blue sensors. The orientation is straight up so that the viewer sees the forest as a collection of tall trees that block part of the sky. A special lens is used so that the entire 180° view is captured in the image. To most viewers who have prior knowledge of forest, the photograph, an indexical representation [Pierce 1998, Kohn 2013], is clearly a representation of the forest with directed focus upward toward the sky.

The forest, however, is completely abstracted in the histogram of blue channel pixel values (Figure 4.4b). Nonetheless, it is still a valid, symbolic [Pierce 1998, Kohn 2013] representation of the forest; the quantified standardized bits have just been reshuffled to illustrate the pixel groups that are sky, vegetation, and ambiguous. There is much more information about these 3 pixel groups in the graphical representation than, for example, a written transcription of each pixel value.[8] The viewer can easily see that most of the pixels are grouped in either the sky or vegetation groups. From the histogram, the viewer gains understanding of how the pixels are classified to generate the black and white photo (Figure 4.4c). This simplified photograph, another indexical representation of the forest, is organized to remove the ambiguity from the original color photo to yield a disambiguous vegetation / sky representation. This image processing procedure is similar to Vertesi's description of how NASA scientists process photographic images from Mars so that certain soil features can be identified. Both inscribe a particular perspective so that other viewers can observe the phenomenon as I (or the NASA scientists) want them to see it [Vertesi 2014].

In the representation of observed canopy cover values across the study site (Figure 4.4d), Latour's cascade of cascades is beginning to really take shape. The entire process of classifying, standardizing, and reorganizing the quantified bits of light in the photo into a canopy cover value is now itself a quantified bit. The graphical representation is again a symbolic one, in need of interpretation for the viewer to understand that it represents a portion of forest. In fact, it is in the flattening of the forest that viewer can quickly gain an understanding of the canopy cover patterns [Latour 1990]. In this visualization, the areas not quantified are easily noticed next to those that are. The estimated values on the 1x1m grid (Figure 4.4e) suggest a more complete picture. However, it is important to remember that this visualization based on modeled estimates is also a level in the cascade. Instead of reducing data through more commonly-used methods of combination like summation and

[8] For example: The center pixel has a blue channel value of 145. The pixel on its right has a value of 145 also. Continuing to the right again, the pixel value equals 146….

averaging, quantified bits are added via another form of representation, the estimation model [Edwards 2010].

Yet another level of abstraction occurs when I combined the canopy cover data with other environmental data, all with their own classifications, standardizations, and reorganizations, into the overarching model framework, in which I attempt to represent the forest through correlations of the environmental data with seedling presences. Explanations of this specific understanding of the forest rely heavily on visualizations of the modeled representation in highly abstract tables and graphics (Figures 4.4f-g), which are still organizations of quantified bits like the original hemispherical photos. Haraway [1991] would ascribe this understanding as partial noting the particular perspective granted by the technologies involved, while Barad [2003] would suggest this understanding as a phenomenon that rose from the "intra-action" of myself, the forest, and the particular technologies that I employed. Using this description of how visual representations are commonly utilized in scientific practice, I aim to illustrate similarities and differences between it and a new ecological representation obtained with terrestrial laser scanning technologies and visualized with 2 and 3D analysis platforms.

4.2 Creating a digital forest

4.2.1 Data collection in the field

To create a digital representation of my forested study site, I used laser-scanning technology, specifically the I-Site 4400 [Maptek / KRJA Systems Ltd, Lakewood, CO, USA] that functions as follows. The scanner fires a low intensity laser, which hits a solid object and bounces back to the instrument where a sensor detects it. The time it takes for the laser to return to the instrument is converted to a distance. The I-Site 4400 repeats this process one million times, each in a slightly different known direction, radiating outward from the instrument in a donut shaped volume, 40° above and below the horizon and 360° around. From the known direction and distance to a solid object in that direction, XYZ coordinates are calculated. I scanned the forest with a point resolution of 0.216°, which yields a distance of 37cm between the closest points at a distance of 100m (most objects were less than 50m from the scanner). To capture my entire forest study site, I conducted 87 scans that I then merged together. The resulting dataset is a collection of points in 3D space called a point cloud. In addition to the coordinate information, the scanner collected the intensity of the return laser as well as red, green, blue (RGB) color information from a simultaneously collected photograph. It is important to know these limitations of the technology: (1) only an object's surface is captured, not any information about the inside of an object, and (2) an object will not be captured by the scanner if another object is between it and the scanner.

The process of data collection and processing using the terrestrial laser scanner is generally similar to established forms of scientific practice, as exemplified earlier by hemispherical photography. The initial process of acquiring equipment and organizing logistics follows the same basic steps but they are more involved[9] (Appendix D). The scanning process required three people completing physically demanding fieldwork despite the highly technical nature of the methodology. Additionally, the process of data collection was full of subjective decisions often made in critical moments. For example, after the first half day of scanning, I realized that we could not complete our objectives without reassessing our procedure. Thus, in the middle of the stressful 3-day data collection

[9] The increased effort is reflective of the monetary value of the methodologies: several thousands dollars for hemispherical photography and several hundred thousand dollars for laser scanning.

campaign, we reduced the number of planned scans so that we would only capture partial scans of the trees outside of the primary study site; we reduced our in-field power consumption and adjusted our re-charging strategy to include a mid-day recharge[10]; and we extended our data collection to before and after daylight hours.

Scanning in the dark (lasers do not require visible light to function) makes for an odd juxtaposition with how the point cloud is visualized – tiny points of light within a sea of black. Additionally during each scan, we were careful to walk around the scanner, always staying behind the laser aperture, or we huddled beneath the scanner tripod outside of the scanner range. We sought a human-free representation of the forest even though, like most ecological data collection processes, humans are an integral component of creating the representation [Barad 2003]. It is the blatant, active avoidance of detection that stands out in this situation.

The data collection process was also heavily influenced by money constraints, time constraints, learning curves, and surprise challenges. Because of equipment costs, I had only 3 days to scan my study site. My choice of scanner was largely in part because a colleague with prior experience using that specific scanner was available to advise me during the data collection. I almost was not able to scan my site because a critical piece of equipment was not delivered with the scanner. Surprisingly I acquired one despite the remote location with limited phone service and tight time schedule. Additionally, the scanning activities overlapped with lively celebrations of the seasonal forest staff. I prepared the equipment, *i.e.,* recharged our batteries, next to the beer fridge. It's important to note the messy reality of data collection. Science does not happen in pristine circumstances; it happens amongst everyday life. As such, successful collections require a little bit of luck.

These aspects of data collection are all characteristics of established scientific representation practices; however with highly technical equipment, the required resources, skills, and challenges become enhanced. In other words, the more subjectively theory-laden the data becomes. This finding is not new and supports Edwards' [2010] description of it with general circulation models. Additionally, the messy, subjective, manual work is often forgotten in clean, polished scientific representations based on highly technical methodologies [Latour 1999, Coopmans 2014]. I posit that when the digital forest is viewed, few viewers think about how the point cloud was collected.

4.2.2 Data analysis with 2D and 3D platforms

While field collection of the laser scanning data is an extreme example of similar issues found in established ecological methods, important differences are found in the analysis of the point cloud. Before looking at specific new capabilities and risks, I first (1) describe the visualization platforms and (2) compare my digital forest to closely related visualization practices.

One of the visualization platforms that I used is I-Site Studio (Figure 4.5), software developed by the scanning manufacture to work seamlessly with the files generated by the scanner. It is essentially Computer Aided Design (CAD) software that renders points instead of traditionally rendered surfaces in 3D, although the representation is displayed in 2D on a computer screen. The functionality is otherwise similar. A key functionality of I-Site Studio is that it automatically aligns multiple scans in conjunction with scanner locations and start direction data. If an I-Site scanner is used, one must initially use I-Site Studio software in order to convert the I-Site data files into a globally usable ascii file with XYZ coordinate information.

[10] The mid-day recharge involved an extra 6-mile, 2000' elevation gain/loss during the already physically demanding 20 hour-day.

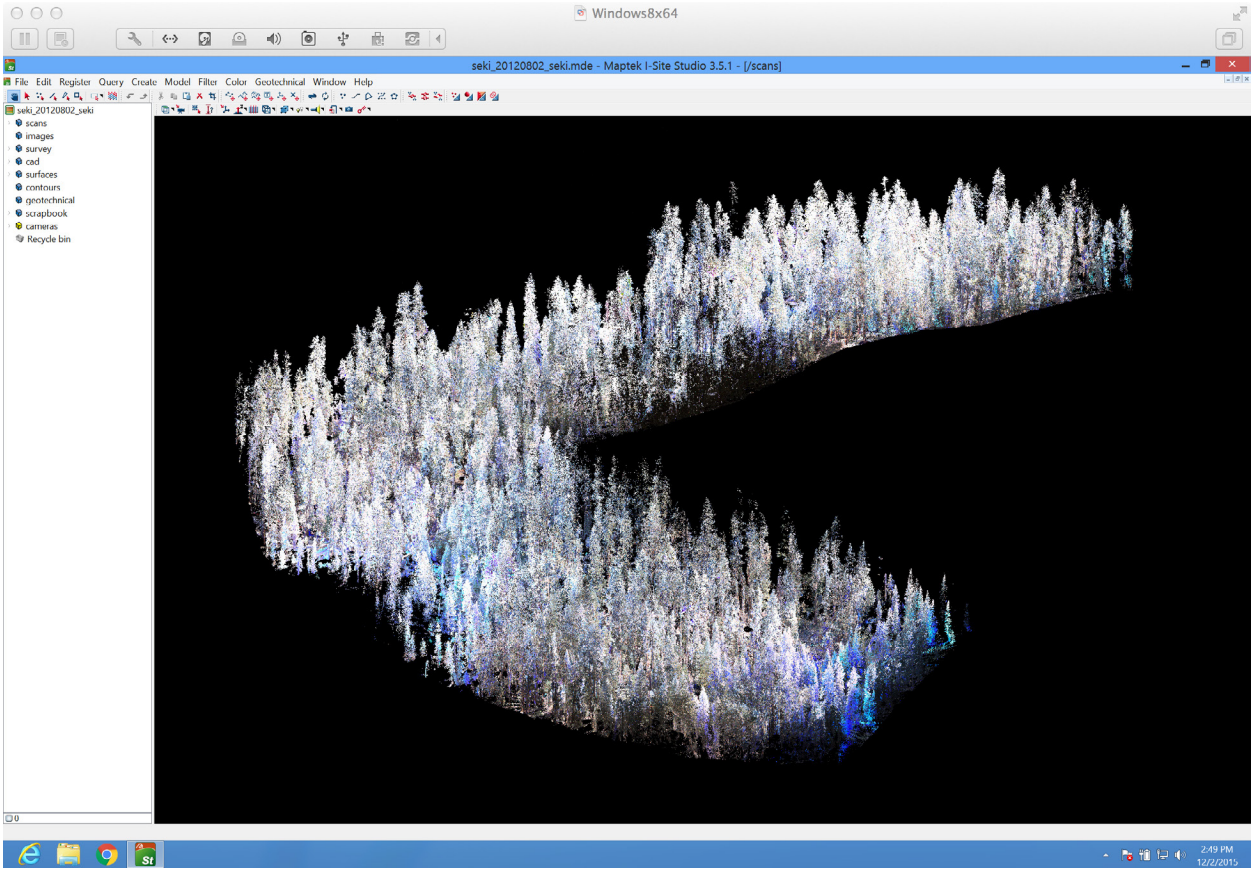


Figure 4.5: In I-Site Studio, the user can zoom in and out, rotate the point cloud, add points, select points manually or via selection rules, modify groups of points (*e.g.,* delete points, move point position, change point color), model lines or surfaces, *etc.* Other datasets, like my surveyed geo-referenced tree seedling location data, can be imported to analyze with the scanned data.

The other visualization platform that I used is the UC Davis KeckCAVES 3D immersive environment for visualizing and analyzing various forms of 3D data (Figure 4.6). I used LIDARViewer, a freeware developed for visualizing point cloud data in the Computer Aided Visualization Environment (CAVE) and other virtual platforms [Kreylos *et al.* 2008]. The CAVE is housed in the Geography Department at UC Davis and is primarily used for geological applications, although microbiological researchers and artists have also used the CAVE [UC Davis KeckCAVES, Myers and Dumit 2011]. While point clouds are becoming more common in ecological study, especially airborne laser scanning [Dassot *et al.* 2011], this is the first project, of which I am aware, to use a CAVE to visualize and analyze point cloud data for ecological application.

Representation of the forest in both the 2D and 3D platforms share characteristics with other highly technical representations. For example, 3D models of protein structure (Figure 4.7c) have revolutionized the study of cell function [Myers 2014]. By bringing microscopic proteins into human view, giving it the depth of 3D, and allowing multiple viewing perspectives, biological engineers have made new insights. At the opposite scale, satellite imagery brings the gigantic into human view, allowing the entire planet to be seen in one view and then inspected in detail. Google Earth (Figure 4.7a–b) is an example rooted in visual portion of the electromagnetic spectrum; however, many other types of similar remote-sensing based representations are possible, such as the Normalized

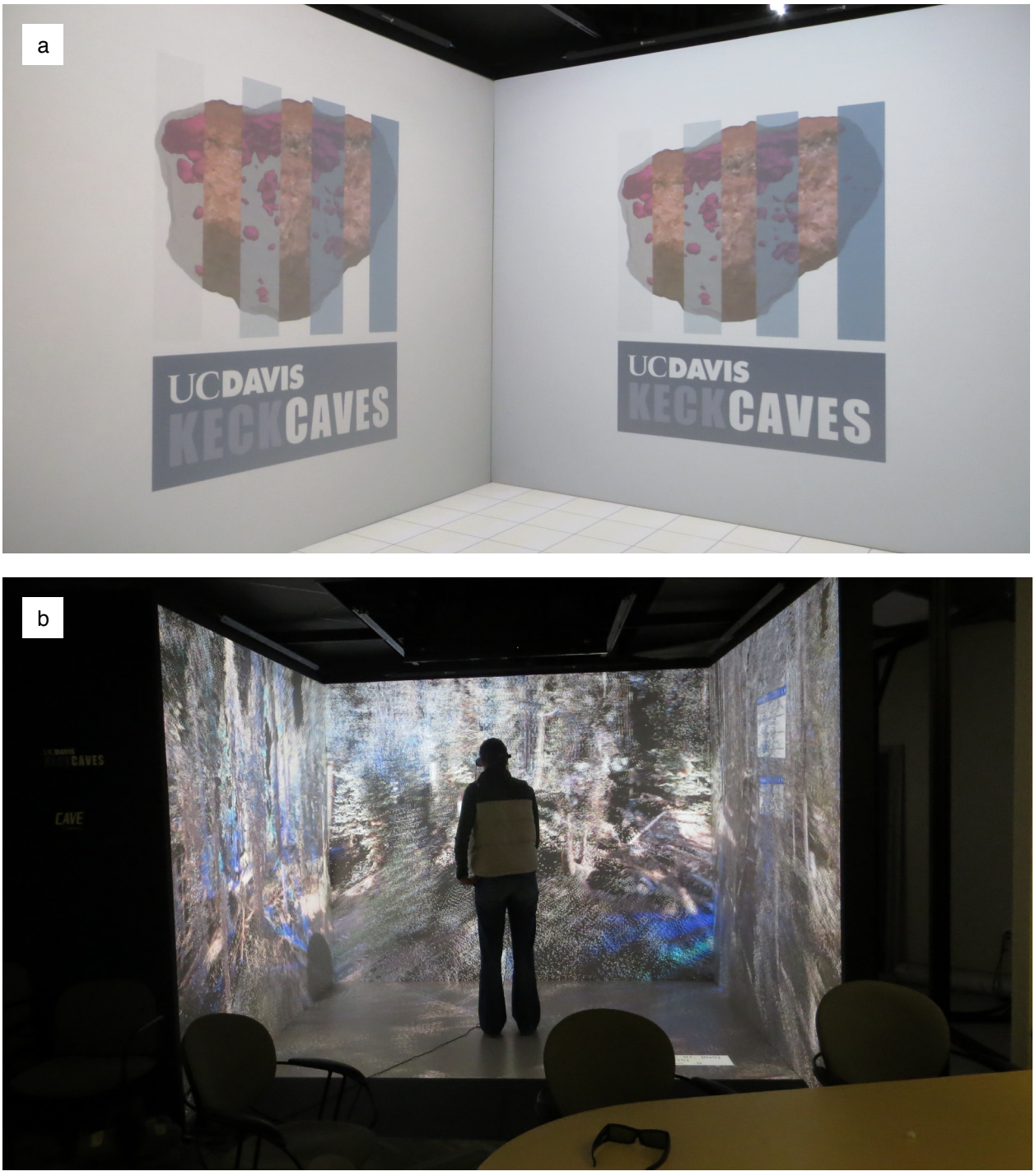


Figure 4.6: The KeckCAVES is an immersive 3D environment, *i.e.,* it is virtual reality. The space is roughly a 2.5m x 2.5m x 2m volume with projection walls on three sides and the floor, upon which stereographic imagery is projected. While wearing 3D glasses, the user(s) experience seamless imagery in which they are embedded. For the main user, who wears a head-tracking device, the images remain fixed while she moves within the image. For other users, the images move with their movement. A hand held controller is used to manipulate the imagery. The user can zoom in and out and rotate the image in any direction. For point cloud data, settings can be adjusted to increase the point size, alter the lighting source, and compress the data in a direction (*i.e.,* the data can be squashed). Additionally, using a spherical selector tool, the size of which determined by the user, points can be selected and exported as a group.

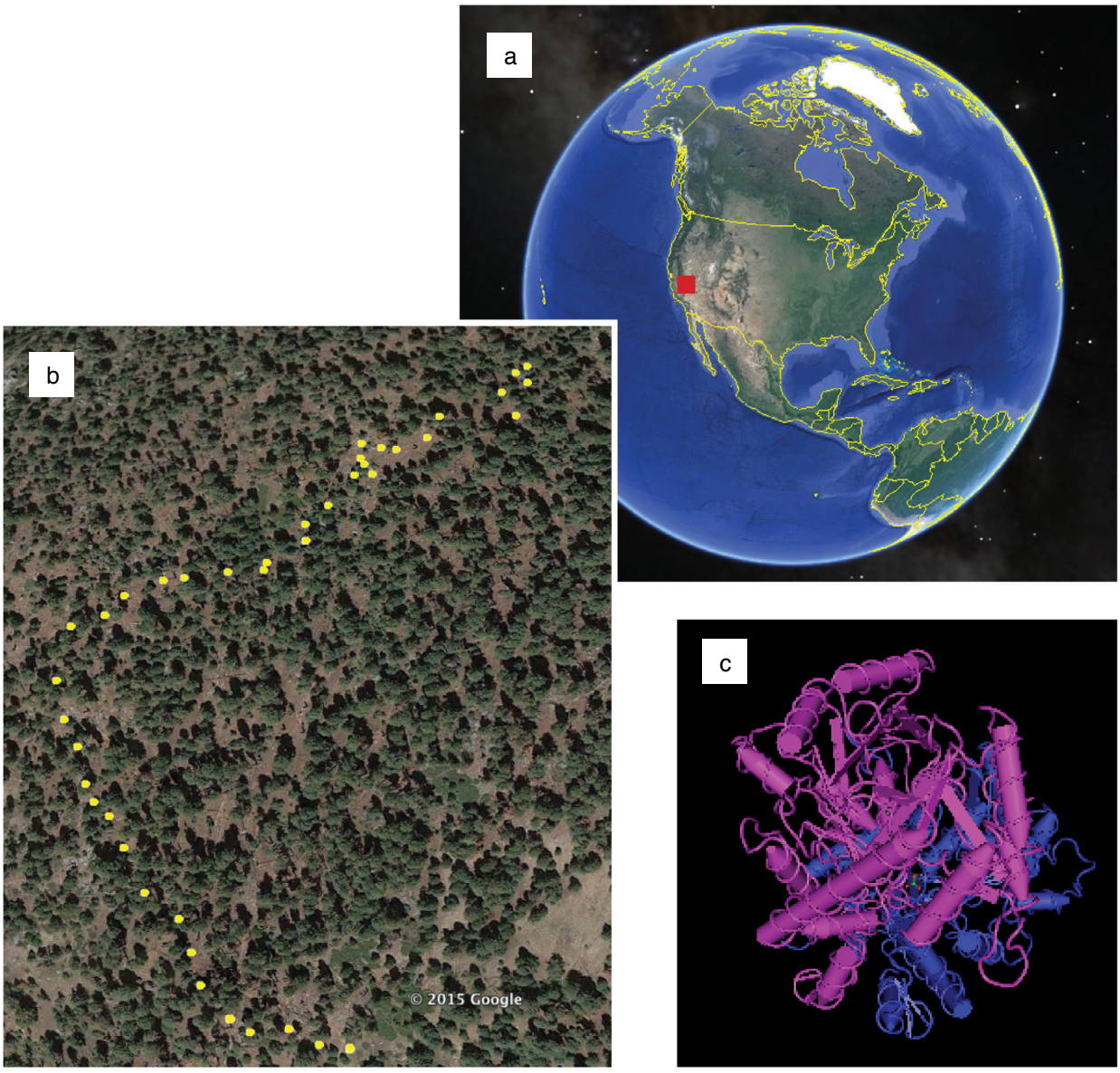


Figure 4.7: Comparison of technologies similar to point cloud data that extend human vision: (a-b) Google Earth satellite imagery provides a perspective of the forested study site location (red square) relative to the whole planet and in closer detail. Yellow points are GPS locations along the length of the study site (600m). (c) 3D models of proteins enable human views and manipulation of the microscopic [National Center for Biotechnical Information].

Difference Vegetation Index that uses the photosynthetically active radiation and near-infrared spectral bands to indicate the amount of living plant biomass.

The digital forest viewed in either 2D or 3D combines aspects of both example technologies. The point cloud visualization is composed of the observed data, although theory laden, like the satellite imagery; it is not a stylized modeled representation like the 3D protein models. The digital forest and satellite imagery is more indexical which conveys more authenticity as evidence [Messaris 1997]. Although satellite imagery such as Google Earth hints at the 3D reality of its represented earth surface, its relatively flat compared to 3D protein models and the digital forest. Furthermore, the detail captured by satellite imagery is good but limited to human scale, 1m for the highest resolution,

and the viewing angle is always looking down from above the surface. Perhaps, one of the most novel aspects of the digital forest is that it merges the spatial scaling range and multiple viewing angle possibilities of the protein model and the remote sensing representations. The viewer breaks free of the within forest perspective of typical forest experience (Video 1[11] and Video 2[12]). She is able to see the forest as a whole from a bird's eye view all the way down to subhuman perspectives, passing through the normal human scale. And she is able to take these relative perspectives from any view. This is unprecedented for a representation of a natural system that is based on observations. In the next section, I expand on how these new perspectives of a forest system may lead to new scientific insight.

4.3 New understandings of the forest

4.3.1 Multiple spatial scales from any perspective

The digital forest can be explored at any spatial scale from any perspective (Video 2). As the video begins, the view is beyond the human allowing for the entire forest study site to be seen simultaneously. This broad-scale view can be taken from any perspective—from above, the side, or below. The ability to visually isolate the forest study site in an external representation is also an unusual perspective. Researchers can internally reconstruct specific portions of the forest, but isolation of the complete or partial study site in traditional representations like photography or satellite imagery is difficult and uncommon. Zooming into the digital forest, the viewer can experience it at normal human and smaller scales. Myers and Dumit [2013] hypothesize that limitless scaling capability and degrees of freedom give researchers space for creativity.

In my ecological study, I used the unique perspectives afforded by the digital representation to extract the location and size of the reproducing trees[13], which I ultimately used to assess the influence of forest stand structure characteristics[14] on tree seedling presence and absence. Common acquisition of this type of data would entail geo-referencing each tree individually and measuring its circumference with a tape measure[15]. Given time and resource constraints in collecting measurements during the summer field season, I could not have collected this information over the necessary area surrounding the study site.[16] Instead, I developed a method to extract the location and size of each adult tree that begins with selectively viewing only a portion of the forest—a 0.5m thick

[11] Video 1: A Walk in the Forest (see additional materials as well as https://vimeo.com/148433829). Video from my red fir forest study site as I walk through about 30m of the plot. The down tree with white bark can be seen in Video 2 (1:00-1:16).

[12] Video 2: Many Scales and Perspectives (see additional materials as well as https://vimeo.com/148433827). Screen shot of the digital forest as seen in I-Site Studio Software. In the first portion of the video, the digital forest is isolated from its surroundings with a scale beyond human. The forest can be observed from any perspective. As I zoom into the point cloud, details of the trees, boulders, and forest surface can be seen.

[13] Adult trees greater than 30cm diameter at breast height (DBH).

[14] Examples of forest stand structure characteristics are seed density, the sum at a particular location of seeds produced and dispersed from each nearby tree, and distance to nearest adult tree.

[15] Diameter at breast height (DBH) is calculated from measuring tree circumference at 1.375m.

[16] Red fir seed can be dispersed up to 40m from the tree, thus I needed to know the locations and sizes of all adult trees in a boarder area surrounding the study site. This border area needs to be at least 30m wide to accurately assess seed density.

slice of points centered at 1.375m from the soil surface.[17] I then viewed these points from a top down perspective, from which I could see the trunks of the trees represented by circles and arcs (Figure 4.8b). I measured the diameter at breast height (DBH) of these point trunks by fitting a circle to the points, and I used the center of the circle as the location of the tree (Figure 4.8a). Through creative use of the novel perspectives available in the digital forest, I was able to acquire information that was unavailable to me using established methods.

To vet this method of locating and sizing the trees, I located and measured a subset of the trees with established methods in the actual forest. The correlation between measures from the two techniques was good ($R^2 = 0.93$). However, I could not use data extracted from the point cloud without further assessment because I could not distinguish living and dead trees from the slice of DBH points. I also could not make this distinction when viewing the full point cloud in 2D with I-Site Studio.

The unique viewing perspective enabled by the KeckCAVES allowed me to rapidly distinguish between the two (Video 3[18]). Using the KeckCAVES immersive environment, I inspected the forest scaled so that the tallest trees were ~50cm tall. Additionally, I oriented the forest so that the trees were coming out of one of the vertical walls, *i.e.,* I was looking straight out in front of me but down into the forest. From this perspective, I could easily determine which trees were obviously dead (broken snags or no foliage). To do so, I often moved around the data so that I could create new views. My experience supports Myers & Dumit's observation of geologist working in the CAVE and a biologist using microscopic videos: "By changing their relationship with the object, they keep opening up new views" [2013, pg. 251]. With this view from above, I was able to coordinate the trees in the point cloud with a map of the DBH slice. The ease in which I was able to orient myself between the point cloud and the map was enabled by rescaling the point cloud and viewing it from a similar vantage point as it was represented in the map (Figure 4.8c–d). Tracking position within the actual forest relative to a map is much more difficult and uncertain. Not only did the CAVE enable me to obtain the necessary perspectives to distinguish between living and dead trees, it also enabled me to record that information in an efficient way.

In addition to promoting creativity, new scales and perspectives enable a holistic seeing of the forest. Alpers [1958 as quoted in Latour 1990] suggests that to really see and understand an entity, it must first be seen as a whole. Then parts are distinguished so that each and every detail can be examined in turn. The digital forest enables such deliberate investigation. The entire forest study site can be viewed as a whole. Each part, the trees, boulders, soil surface, down logs, *etc.* can be distinguished and then examined in detail. Traditional representations do not allow this holistic process of visually knowing. In addition to a more comprehensive understanding of the physical structure of the forest, new understandings of complex forest dynamics may be possible when other data, like temperature or elevation, are overlaid on the point cloud. In future work, I anticipate using this holistic yet detailed view to generate new hypothesis about how to link coarse-scale characteristics, like adult

[17] To model the forest surface in I-Site Studio, I selected the lowest point on a 1x1m grid. I used I-Site Studio algorithms to model a surface from these lowest points. Automated and manual post-processing is required.

[18] Video 3: DBH Color Slice (see additional materials as well as https://vimeo.com/148433826). Video of the digital forest in the UC Davis KeckCAVES in which I distinguished between alive and dead adult trees. The 0.5m-thick slice of points at diameter at breast height (DBH) are colored yellow, with points included for models of individual tree colored orange. Magenta numbers identify specific trees and a 5x5m reference grid installed in the actual forest is marked with cyan points. In the first portion of the video filmed with 3D glasses, the flickering light is an artifact of the video. In the second portion of the video, the image is double as it is seen without 3D glasses. In both cases, I am immersed in the data as evidenced by the projection on myself.

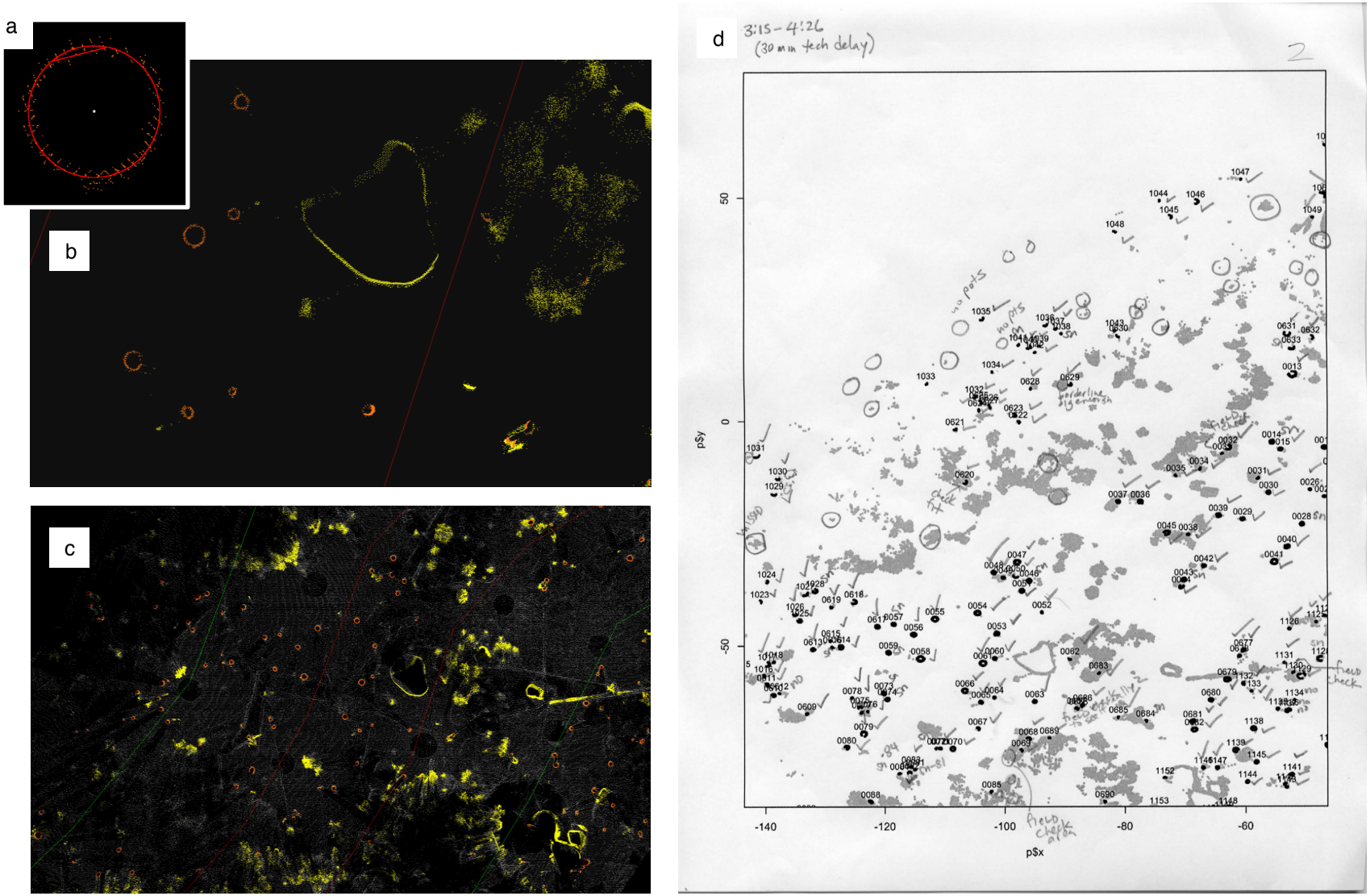


Figure 4.8: Measuring and locating adult tree in the digital forest: a) Modeled tree diameter at breast height (DBH, solid red circle) with tree location indicated by white in the center of the circle, b) Top-down view of the DBH band in colored yellow with point included in models of individual trees colored in orange, c) top down view of DBH band over larger extent commensurate with d) 2D maps of DBH band used for noting alive and dead trees in the KeckCAVES (Video 3).

tree density or macro-scale topography, to fine-scale processes, like the persistence and growth of an individual tree seedling.

4.3.2 Lively interactions with the forest

New perspectives, both viewpoint and spatial scale, enabled me to have new types of interactions with my forest study site. The interactions I had with the forest when extracting the location and size of the adult trees are a good example. This interactive process includes a series of experiences: actual forest → point cloud in 2D → point cloud in 3D → actual forest → point cloud in 2D. I first scanned the forest while actually in it. Then, I extracted the location and size information in 2D as described in the previous section. I used the 3D perspectives of the KeckCAVES to distinguish obviously dead trees from living trees. However, I needed to return to the field to verify ambiguously represented trees and to look for trees whose trunks at DBH height were not captured in the point cloud. The former is possible when adult trees have branches at DBH height or when an adult tree is obscured by juvenile trees' foliage. The latter occurred at the edges of the point cloud where scanning density was thin and/or the tree trunks at DBH were occluded by other forest features. Indeed, I found several trees in the field that I had not been able to identify in the DBH slice (Figure 4.8d). I was able to mentally combine 2D maps of the DBH slice with tree patterns in the field to estimate the missing tree locations. With these field-based estimates, I returned to the 2D I-Site Studio to map their XYZ coordinate locations in the geo-referenced data. It was these series of new interactions, one leading to the other, that enabled me to fully assess the adult forest stand structure.

I utilized a similarly iterative approach when developing the appropriate color choice for extracting fine-scale topography. In the point cloud, automated extraction of the forest floor is not yet possible. Thus, I attempted to manually extract the points representing the soil surface, downed logs, and boulders. The original plan involved creating a model of the forest floor based on the lowest points in a 2m grid. Then, all points within 25cm of this modeled surface were extracted from the point cloud. I call these extracted points topo data. Viewing these topo data in the KeckCAVE, I manually selected the surface points using a 3D spherical selector (Figure 4.9a and Video 4[19]). I positioned the topo data at eye height so that I could distinguish surface points from near surface points that represent seedlings, understory vegetation, or downed branches. I then painted the surface points by holding the selector tool underneath the forest surface and running the edge of the selector tool just over the surface points. The fundamentals of this strategy worked well, but it was difficult to distinguish surface from near-surface points especially if the near-surface points density was sparse, which is common for seedlings and understory herbs. Thus, I used employed color to help me tease apart these two types of points. I began to play. In an iterative process, I tried a color scheme, tested it, readjusted, and tried it again. Eventually I found a scheme that worked. I divided up the study site into a series of sections. For each section, I colored the points in a gradient from red to white to blue as their elevation increased (Figure 4.9b).

In both cases, the digital form of the data along with its 2D and 3D representations allowed a responsitvity, in which I as a researcher evolved with the data processing. Myers and Dumit [2011]

[19] Video 4: Topo Painting (see additional materials as well as https://vimeo.com/148434642). Video of the digital forest in the UC Davis KeckCAVES in which I demonstrate extraction of the fine-scale topography using a spherical selector tool. The near-surface points are colored by their distance from a horizontal plane. By positioning the surface at eye-level, I can select the surface points with the selector from underneath the surface.

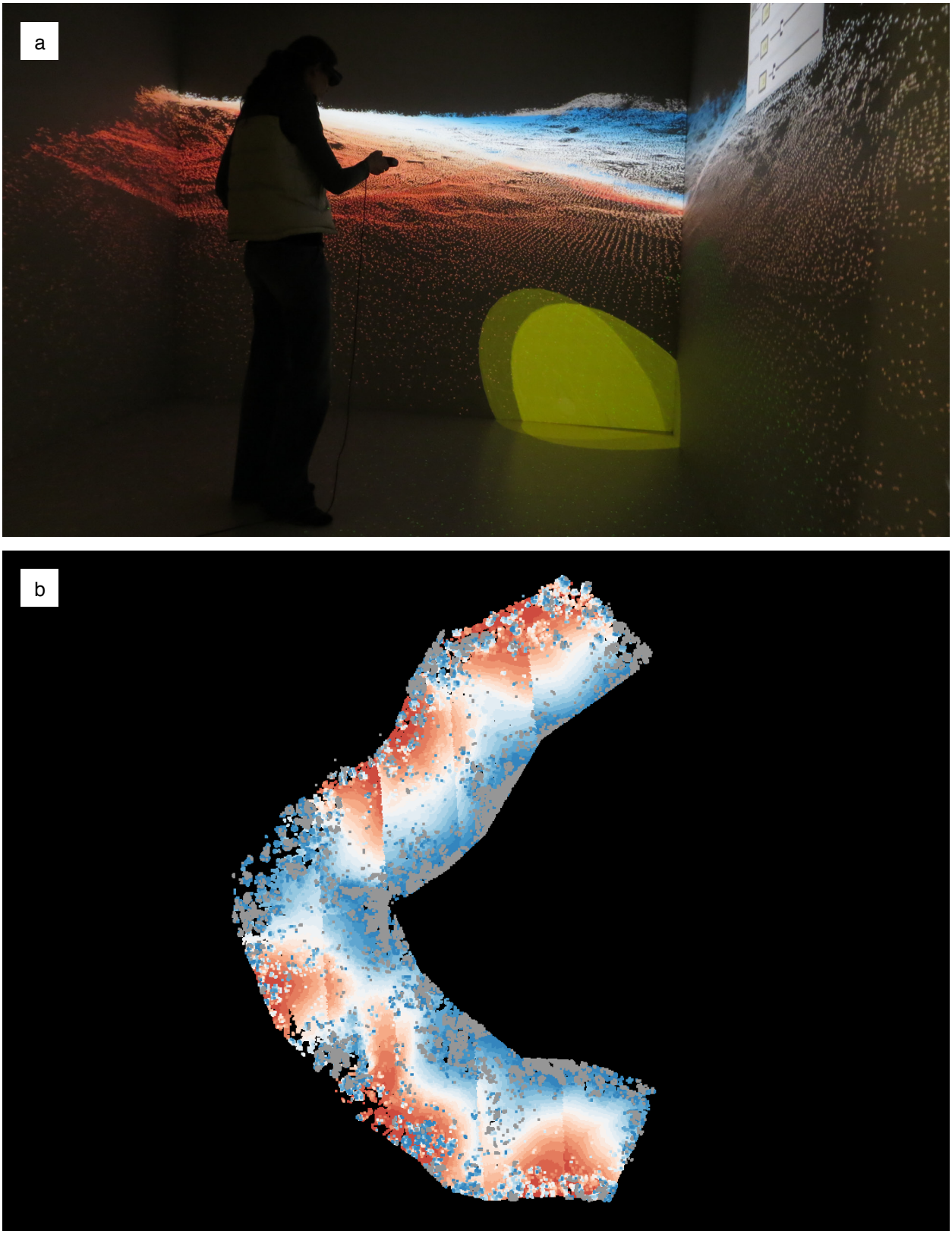


Figure 4.9: Extracting fine-scale topography in the 3D immersive KeckCAVES: (a) Selecting points with spherical selector (yellow circle). Image is double as seen without 3D glasses and (b) Color scheme.

describe this co-evolution as a fundamental aspect of the benefits of interactive representations by observing a geologist working in the KeckCAVES:

> As the geologist reaches out and hesitates, not knowing yet what or where or how to measure, we observe both her subjectivity and the objectivity of the phenomena wavering. The scientist is no longer the architect or choreographer in this experiment. There is no well-mapped experimental method: experimenter, instrument, data, and phenomena are all in the making. The result is that there are no clear-cut subjects of objects, until the final proof is rendered. In this geologist's hesitation, therefore, everything is at stake: the experiment, the instruments, the data, the phenomena, her lived perceptions, and her status as a scientist. [2013, pg. 247]

This responsivity and co-evolution of scientist and understanding provides opportunities for the new understandings:

> Similarly for CAVES researchers, the shock of swimming in a 3D environment is the "liveness" — the tangibility and multidimensionality — of the structures that had been so reduced in previous publications. They too are working with data whose scales and spaces and temporal dimensions are not easy to parse. They are faced with a slew of shifting questions: Where to look? How to look? What to look at? What counts as an interesting phenomenon? What might be an artifact?
>
> One particular phrase gets repeated over and over by those working in the CAVES and watching time-lapse footage. It goes like this: "I'm looking for something interesting." This "looking" is an example of the middle voice. Normally, the things we are interested in finding are already known ahead of time, before we go out looking. But here the subject of the sentence works to "locate" or "discover" something they don't already know about, something worth further exploration. This thing will be one that piques the scientist's interest, and in fact, changes what is interesting for them. As one researcher put it: "I'm still at the stage where I'm deciding where I'm looking at what thing." There's a marvelous disorientation in the syntax of this statement. For us, this dizziness demonstrates the openness of inquiry in the CAVES. [2013, pg. 254]

My development of the methodologies to locate and size the adult trees, as well as extract the fine-scale topography, supports Myers and Dumit's description of uncertainty leading to new understandings, albeit new methodological understandings in my case.

I also experienced uncertainty when using the digital forest in the KeckCAVES to check alignment between my surveyed seedling data and the point cloud. My initial attempts to use seedlings relative positions to adult trees failed because the surveyed tree point was a single survey point at the tree base that did not indicate the orientation of the tree. I was stumped. It wasn't until I returned to the actual forest that I was able to develop a new plan to assess alignment. While walking through my study site, I realized that I could map distinct features, such as unique boulders and logs that were near seedlings, onto my 2D maps of the seedling locations (Figure 4.10). I could then use this positional information to vet the alignment of the digital points in the KeckCAVES. The interesting finding here that extends Myers and Dumit is that I needed the liveliness of both the digital and the actual forest for creative thinking.

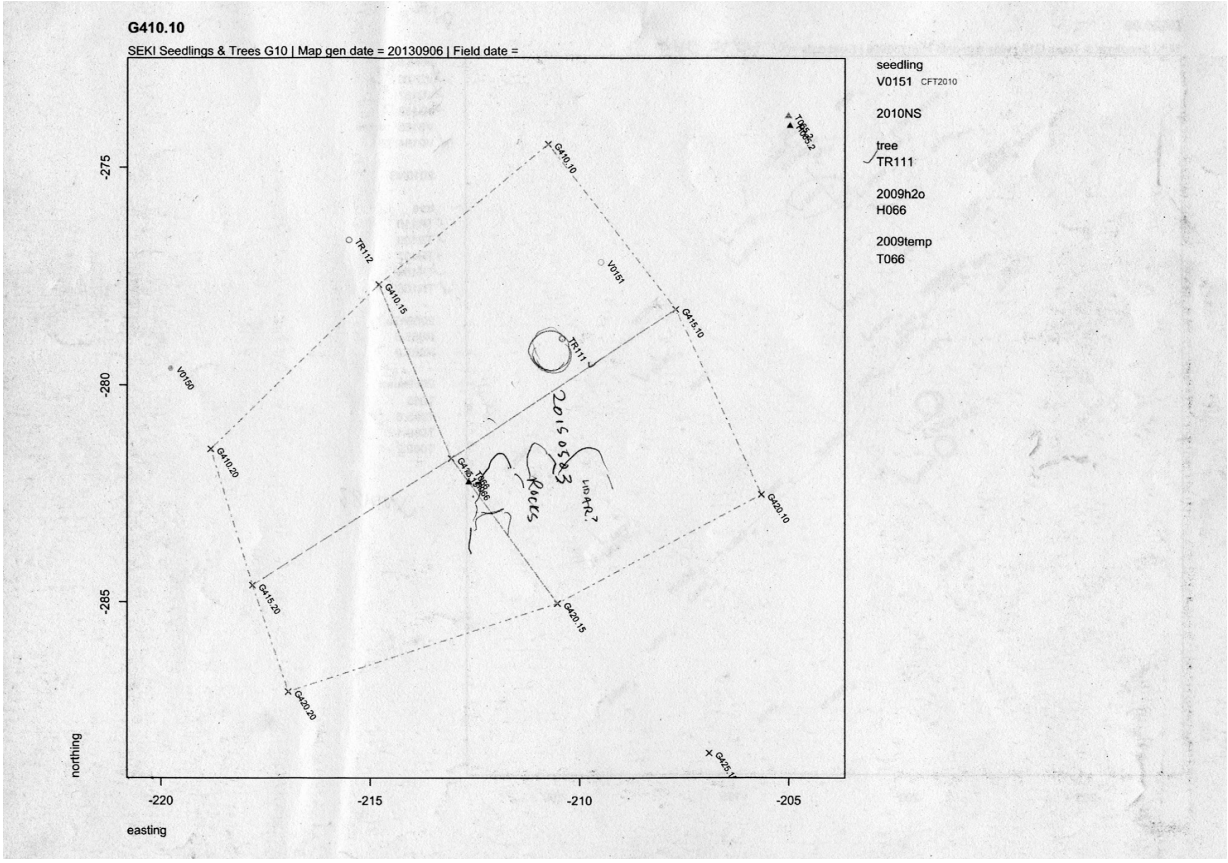


Figure 4.10: Mapping of unique forest features on to 2D seedling maps for assessing alignment in the 3D immersive KeckCAVES: Tree diameter and rock cluster drawn near sensor locations (T086 & H086) and plot marker (G415.15).

In addition to feeling a sense of exciting ambiguity while developing methodology, I feel a sense of unknown potential discovery of forest dynamics through new visualizations the physical environment of the forest, *i.e.,* mapping soil and air temperatures, moisture availability and demand, and soil profiles onto the physical forest itself. I anticipate that such visualizations will lead to hypothesis that I cannot generate by other established representations. Developing ways to dynamically display environmental information on the point cloud is especially exciting to me. My interest is indeed piqued although I don't know exactly where exploration of these new visualizations will take me as a researcher or how they might enable new understandings of forest phenomena. No doubt that the real-time interactions coupled with the scaling possibilities and new perspectives will be essential components of this co-evolution.

4.3.3 Relearning to see the forest

New spatial scales and perspectives and new interactions lead to new ways of seeing. At first, one might think that because the point cloud is an evidential representation of the forest, interpreting it and engaging with it would be straightforward. It is in some ways, especially compared to highly abstracted representations such as graphical figures (Figure 4.4f–g). But in other ways it isn't straightforward and requires the viewer to re-learn how to engage with the forest. This is likely true for any viewer, regardless of whether she had experienced the actual forest being represented, because as I will explain I had to change how I utilized visual references. However in my case, my

intimate knowledge of the actual forest heightens the differences that I perceive between the actual forest and the digital representation.

A striking example of this contrast occurred during my first visit to the KeckCAVE. It was incredible to be inside this hauntingly beautiful landscape, as I knew it albeit in a different form. A short time into the experience, I realized that while I was seeing the forest as represented by a collection of bright points that formed tree trunks and foliage, boulders, down logs, and the rough forest floor in the darkness, I was mentally overlaying my memories of specific locations in full resolution and color on to the point cloud. In this way, I seemed to be merging these two sets of cognitive imagery. I still typically visualize the forest based on my experiences in the actual forest, but I can also now visualize it as a point cloud. I built the capacity to hold this dual representation over time. An important tool in doing so was re-learning how to navigate in the digital forest. While in the actual forest, I look into the near distance to locate myself when disoriented. Initially in the digital forest, I could not look into the distance to find references because (1) the points become indistinguishable from one another (Figure 4.11) and (2) I have not yet formed new references in the digital representation. Thus, I would zoom completely out of the study site and acquire a top down view. Based on my experiences with the actual forest[20], I identified the location to which I wanted to go and zoomed back in. Through this new form of navigation, I built new memories of the forest in the digital form.

Color also played an important role in my new understanding of the forest. During my initial interactions with the digital forest in both 2D and 3D, the points were colored from a photograph simultaneously taken with the laser scan (Video 5[21]). Thus, many aspects of the forest are colored realistically.[22] However, to complete most of my analyses, I needed to use color to help me focus on specific portions of the forest. To extract tree location and size, I colored all points not in the DBH slice a light gray and the DBH slice yellow (Video 3). As I located and sized each tree, I changed the points belonging to the particular tree orange so that I could track which trees I had already processed. The difference in color allowed me to see the forest in a particular way that was useful to my analyses and not possible in the actual forest. I also used color in the fine-scale topography extraction to distinguish surface and near-surface points. These examples illustrate a form of inscription that not only allows me, the scientist, to understand the forest in a particular way but also others to view the forest in the way that I am seeing it. Vertesi highlights the inscription benefit of digital media in her discussion of scientists studying Martian soil with visual imagery: "'drawing as' not only reveals new aspects of a visual dataset but also produces a 'seeing as' experience for other viewers" [2014, pg. 29]. As Vertesi suggests, I am "not passive, but rather actively compose the image into something meaningful through image-process practices" [2014, pg. 24].

What I did not expect in learning to see the forest in new ways was the embodied effects of working the CAVE. I did not anticipate the cognitive load of the CAVE itself. It was mentally exhausting

[20] I believe part of my spatial understanding of the forest came from mapping the seedlings and reference markers in 2D. I already had a conceptual framework of the relative locations of certain parts of the forest based on a top-down perspective.

[21] Video 5: In the Digital Forest (see additional materials as well as https://vimeo.com/148433828). Video of the digital forest in the UC Davis KeckCAVES in which the point cloud is colored by the photograph taken simultaneously with the laser scans. The background sound is from the 5 computers and 4 projectors that generate the imagery.

[22] Because scans were made during the day, the exposure of the photograph could not compensate the full range of light and dark patterns beneath the forest canopy. Thus, some atypical coloration occurs. This is most apparent in areas of overexposure that are recorded as white-yellow and sometimes blue. The under exposed areas of the forest are colored dark blues and browns which are not readily visible against the black background.

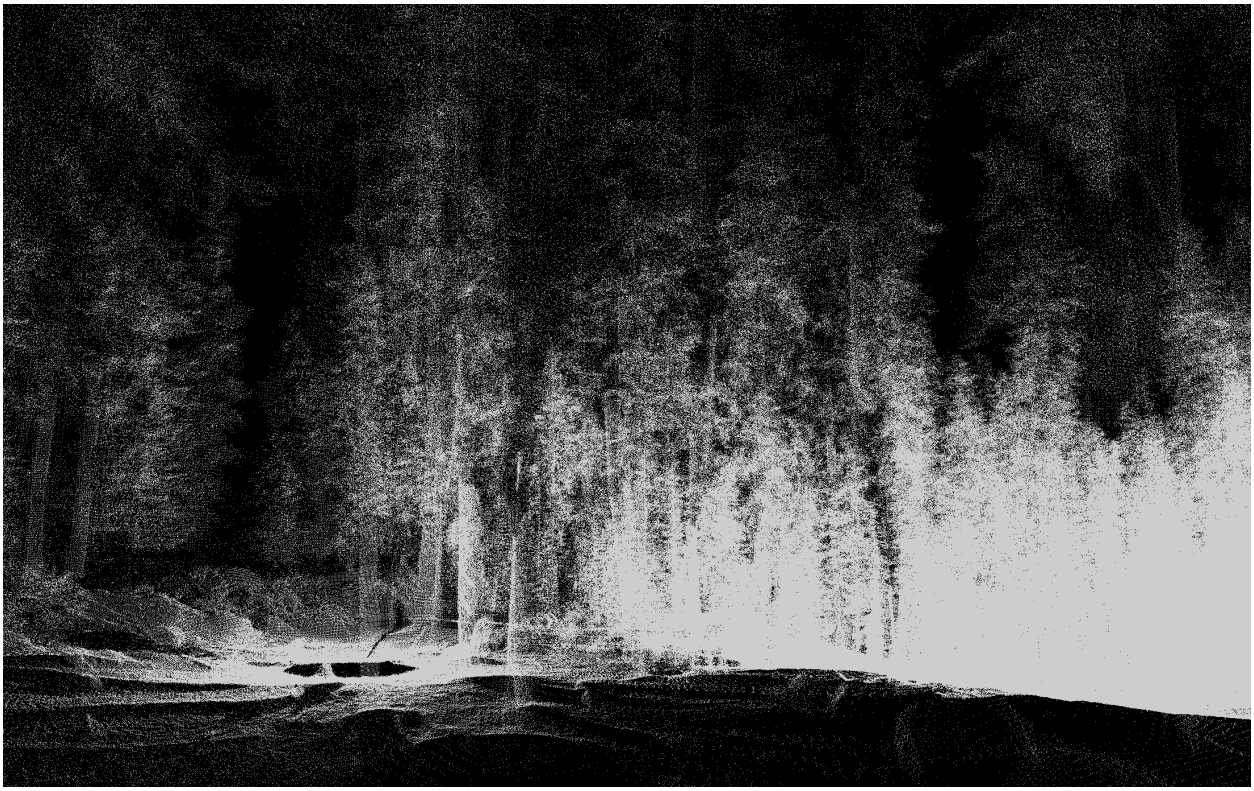


Figure 4.11: Digital forest as view in 2D I-Site Studio software. Points are indistinguishable from one another in the distance, especially when colored the same color.

learning to navigate the forest as a set of points. This was especially true during my mistaken first attempt to recolor the bulk of the forest a neutral color. I chose a light gray that made the forest too intensely bright. Additionally, I colored points of interest cyan and magenta, but in the sea of gray I was squinting to find them. I eventually added additional points in specific patterns so that the color had some density to stand out against the gray background. In addition to eye-strain due to mis-colorations, it was initially tiring to look through the points to see something in the distance or my notebook when recording notes. Also, due to equipment quirks, I learned to adjust to an image that would jump in and out of 3D.[23] Working in the CAVE was physically taxing as well. The CAVE is kept quite cool to provide an adequate environment for the 5 computers that run it; the constant whir of the computers is ever present; and unlike working in the actual forest, I stood in the same position for hours. Thus, it has taken time for my body and my cognitive systems to be able to engage meaningfully with the digital forest, a place that is both familiar and foreign.

Now that I have some skill in working with the digital forest and inscribing particular views to facilitate understanding, do I approach my ecological studies differently? The answer is yes. What's similar is that I can use the point cloud like other methodological tools to extract quantitative information, Latour's immutable mobiles, from the forest system. What's different is that through that process of interacting with these data, I have built a new conceptual model of the forest that is more malleable than most traditional ecological tools. The point cloud is not a quantitative entity

[23] Some pairs of the 3D glasses are twitchy and jump back and forth between the correct 3D view and disjointed stereo imagery.

itself. Instead it is a model of the forest that can be quantified, which counters Latour's contention that reduction from nature is necessary:

> Scientists start seeing something once they stop looking at nature and look exclusively and obsessively at prints and flat inscriptions. In the debates around perception, what is always forgotten is this simple drift from watching confusing three-dimensional objects, to inspecting two-dimensional images which have been "made less confusing." [1990, pg. 29]

The point cloud is a simpler nature that retains its 3D complexity. In exploration of it, new creative uses lie in wait to be discovered [Myers & Dumit 2013]. As an addition to the actual forest, my research opportunities, or field of view so to speak, have broadened because the digital forest offers new inscriptions possibilities (color, enhancement, scale, perspectives) that are not available in the forest itself or via other established ecological tools.

4.3.4 A high-resolution structural index

I claim that with approximately 87 million point locations, my digital forest is ecological big data. The point cloud has orders of magnitude more spatial resolution than typical ecological studies, in which spatial coverage over a similar study are might consist of tens of locations. An example is the difference between satellite-derived digital elevation maps (DEMs) and fine-scale topography from the point cloud. Visually the difference is stunning and even more so when we compare the occurrence frequency of elevation and aspects on the landscape between the two spatial scales (Figure 4.12 and 4.13). The topographical information at one scale is not more valid than the other, but with the fine-scale data enabled by the point cloud we gain new insights. For example, fine scale slope and aspect compared to other environmental factors (like canopy cover, soil moisture, and snowmelt date) does not influence tree seedlings in my study site. This finding is contrary to long-standing observations that topographic factors especially aspect, influence patterns of species on the landscape [Geiger *et al.* 2009]. The new data enabled by the point cloud have allowed me to hypothesize that the influence of topographic factors are scale specific.

In addition, to new ecological understandings, the point cloud's fine-scale resolution purports more credence to an argument in three ways. First, the power already granted to data is multiplied by the shear number of data [Leonelli 2014]. Latour [1990] too acknowledges that the organization of larger amounts of immutable mobiles yields persuasive power. Whether we are correct in allowing the amount of evidence alone to sway our options is another question that I address briefly in the section 4.4.2 below. Secondly, the mass of data must be arranged in evermore sophisticated and dramatic ways to convince the scientific audience: "It is precisely because the dissenter can always escape and try out another interpretation, that so much energy and time is devoted by scientists to 'corner' him and surround him with ever more dramatic visual effects" [Latour 1990, pg. 41-42]. The digital forest serves this purpose well with its immense array of data point shining against the black background. Videos of the data are especially convincing that the project is highly advanced. Again whether this influence is well founded is debatable. One thing is certain; it can capture an audience's attention. Finally, the digital forest is different than other forms of big data, such as tweets or sub-minute stock market trading data, in that it is an indexical representation. According to Pierce's semiotic scheme, indexical representations that have direct association with the represented object, hold special influence [Messaris 1997]. For example, we see reality in a photograph or a cell phone video. The evidence is unquestioned. Like a photograph, we see the forest in the point cloud.

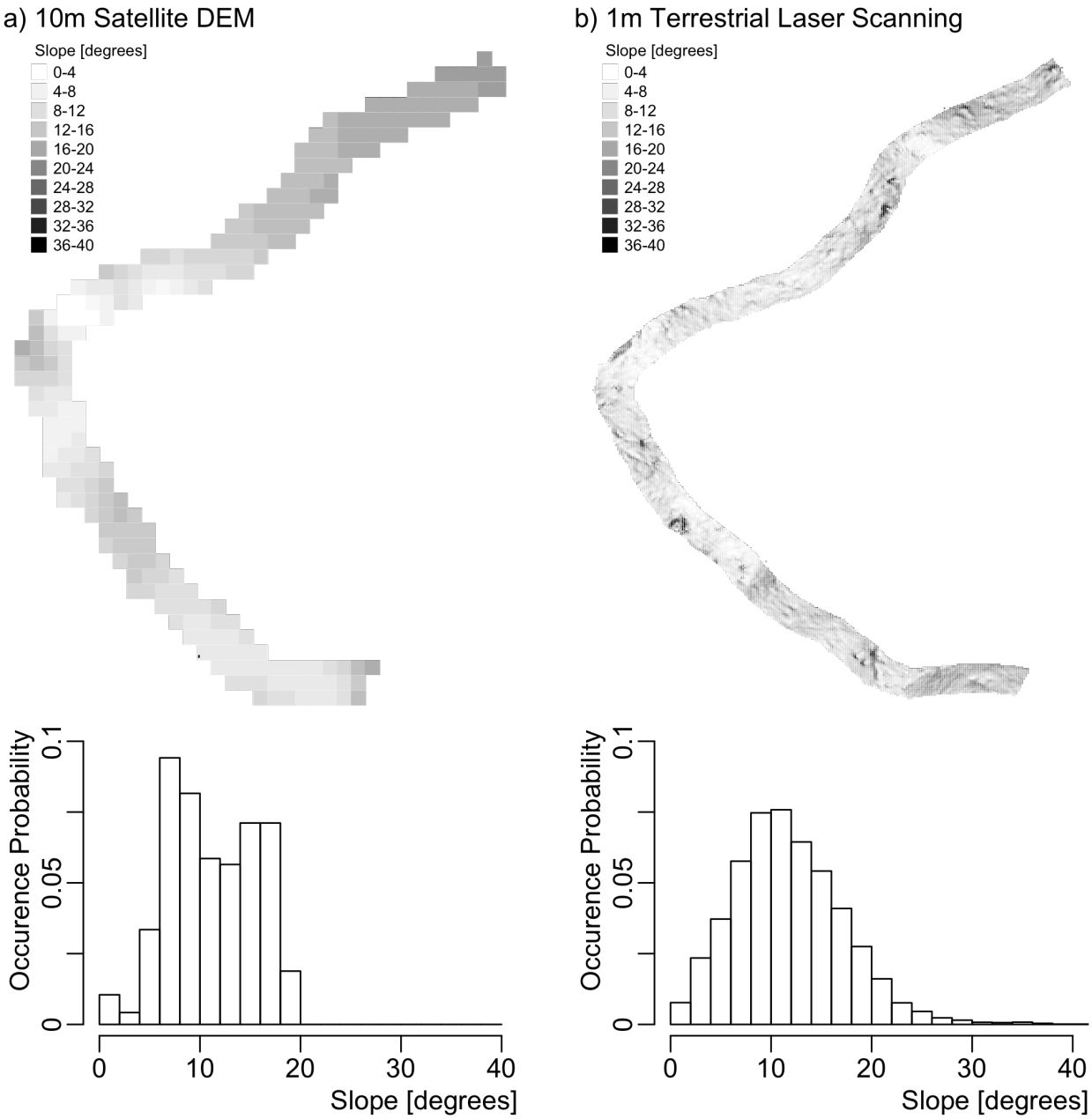


Figure 4.12: Spatial pattern and histograms for topographic slope that was generated from (a) 10m satellite-based (remote sensing) Digital Elevation Map (DEM) and (b) 1-m point cloud data.

Two characteristics of the digital forest make it an uncommon indexical representation. First, it is a structural index rather than visual only. Whereas a photograph implies structure, the digital forest is structure, although both can only be visually interpreted[24]. The structural representation acts as a foundation upon which multiple color references can be overlaid. While other forms of scientific structural representation exist (*e.g.,* ball and stick models in chemistry), few indexical ones do. A second unique characteristic of the digital forest is that the indexical representation is scale dependent. Arguably all representations are scale dependent. For example, satellite photographs of

[24] As opposed to a physical model.

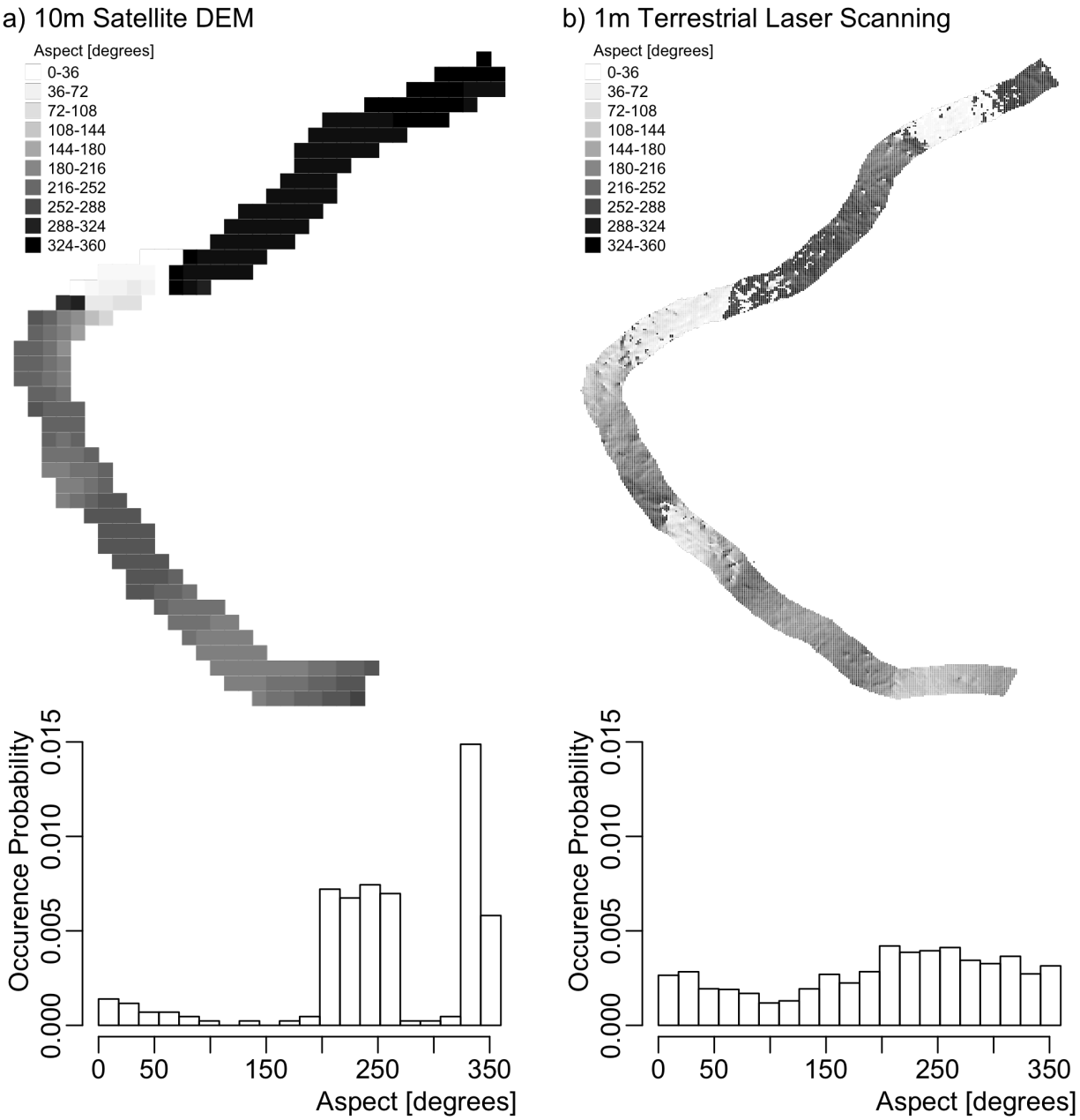


Figure 4.13: Spatial pattern and histograms for topographic aspect that was generated from (a) 10m satellite-based (remote sensing) Digital Elevation Map (DEM) and (b) 1-m point cloud data.

the forest will not have high enough resolution to distinguish individual tree seedlings. The difference here is that the user, choosing the scale and perspective, actively engages with the indexicality. If zoomed in too close, the density of the points becomes too sparse to render the feature recognizable. Additionally without color reference or without movement, distinction between objects can become blurred. These characteristics expand the concept of Pierce's index, literally and figuratively, challenging what scientists accept as credible evidence.

In addition to eliciting attention and credence from scientific audiences, the digital forest is a data form that arguably allows easier access for non-specialists. The indexical nature of the data, which is

afforded by the fine-spatial resolution, connects to existing representations of forests that most people have through personal or cultural experiences. The potential usefulness for non-scientific audiences is worth exploring.

4.4 Looking between the points

4.4.1 A god-trick

With the ability to interact with the forest from any perspective and at any scale in the digital forest, I assumed omnipotent control over it. I could slice the forest into pieces, view it from above, and color it as I desire. I have brought the forest within my technical toolkit. It is at my disposal. This reconfiguration is in sharp contrast with an experience of the actual forest, where I am at the mercy of the uneven terrain, bitter cold mornings, fixed limited view from the forest floor, daylight hours, and mosquito attacks. Haraway describes the dangers of this omnipotent god-trick as false, alluring one into believing that such perspective is the best and whole truth.

> Vision in this technological feast becomes unregulated gluttony; all perspective gives way to infinitely mobile vision, which no longer seems just mythically about the god-trick of seeing everything from nowhere, but to have put the myth into ordinary practice. And like the god-trick, this eye fucks the world to make techno-monsters. [1991, pg. 189]

She argues that instead many partial perspectives are necessary to fully understand the entity under investigation and one's relation to it: "objectivity turns out to be about particular and specific embodiment, and definitely not about the false vision promising transcendence of all limits and responsibility. The moral is simple: only partial perspective promises objective vision" [Haraway 1991, pg. 190].

Latour also warns against the types of manipulation available in the digital forest. He argues it is in part what gives scientists and engineers their authority:

> This trivial change of scale seems innocuous enough, but it is the cause of most of the "superiority" of scientists and engineers: no one else deals only with phenomena that can be dominated with the eyes and held by hands, no matter when and where they come from or what their original size. [Latour 1990, pg. 44-46]

Do I feel domination over the forest system through this work? No, precisely for the reasons mentioned above from my experience working in the forest.[25] Following Haraway's argument, I have several partial perspectives from which to build an understanding of the forest. So then, what is to worry?

Bringing entire ecosystems, such as a forest, inside our technological toolkits to be manipulated at will becomes routine with technologies like terrestrial laser scanning and immersive 3D environments. This is particularly troublesome for two reasons. First, as the technologies and data

[25] You, the reader may question whether this response is because I have read Haraway and Barad, but I don't think so. Fieldwork at the site is always contingent on workable conditions—I have had enough of my plans go awry due to things beyond my control (*e.g.,* uncooperative weather, downed trees burying sensors, bears disrupting measurements) to know that I would never dominate my interactions with the forest. What the digital forest did offer initially was a security blanket of sorts. I thought that by capturing a 3D representation of the forest, I would be able to easily return to rectify measurement inconsistencies. However, as I worked with the data this assumption turned out not to be straightforward as I describe in the following section.

become more common, scientists (and the public) will have access to these omnipotent capabilities without necessarily acquiring the experience of the actual place while collecting it and/or conducting additional field-based research. The partial perspectives that I gained through required activities of collecting the data may have to be voluntarily sought by others. This is unlikely given today's scientific practice in which second-hand data usage is rarely re-examined by the user.

This second-hand data usage with representations like the digital forest also troubles Barad's agential realism epistemology, in which understanding emerges from "intra-actions" between the observed, observer, and observing apparatus. The specific context of the "intra-action" defines the observed and the observer:

> … an agential cut effects a local separability of different "component parts" of the phenomenon, one of which ("the cause") expresses itself in effecting and marking the other ("the effect"). In a scientific context this process is known as a "measurement." … Whether it is thought of as a "measurement," or as part of the universe making itself intelligible to another part in its ongoing differentiating intelligibility and materialization, is a matter of preference. Either way, what is important about causal intra-actions is the fact that marks are left on bodies. Objectivity means being accountable to marks on bodies. [Barad 2003, pg. 824]

When interacting with the digital forest, especially without partaking in the field collection, the emergent understanding is no longer defined from "intra-actions" between the observer and the actual forest. The scientist is "marking" the point cloud (*e.g.,* new perspectives, inscribed color) and the point cloud is marking the scientist (*e.g.,* new digital memories of the forest, mental and physical impacts). Where as my intra-actions with the digital forest are additionally grounded in the data collection and intimate experience with the actual forest, it is very unlikely that the second-hand observer is marked by the actual forest via the digital representation. Thus, the actual forest looses its agency in the Barad sense.

The risk is that human control over natural systems is reinforced in a new form that is extremely visceral and in which the actual forest does not affect the scientist directly. Working with the digital forest, especially in the 3D immersive environment, imparts a feeling of total control over the forest system, which at some level must seep into our consciousness, especially if unchallenged. Bowker suggests "as the representation becomes internally more manipulable, it becomes externally more apparently real" [Bowker 2008, pg. 153].

Secondly, human culture is at a unique, and many argue critical, point in our species relationship with the natural world because we are influencing the environment in ways beyond natural processes [*e.g.,* Vitousek *et al.* 1997]. While our impact is substantial, we are not in control of its implications. To reinforce the idea of control over the natural world, we imply a false level of understanding of the system dynamics that may hinder responsible action [Haraway 1991]. In addition, limitless perspective and manipulation promotes further separation between human culture and the natural world. Feminist scholars argue against such separation as empathy for others may be a key component for the compassion and will to stem environmental insults [*e.g.,* Haraway 2008, Rose 2011].

4.4.2 An incomplete model

The fine-scale resolution of the scanning technology creates a much more spatially continuous representation of the forest than commonly found in ecological studies. The resolution is fine enough that we can see specific elements within the forest (Video 5). The realistic indexical imagery

imparts the sense that the digital forest is an exact copy of the actual forest, similar to photographic imagery that with the correct exposure, *etc*, is a visually exact 2D replication of reality.[26] It is an enhanced representation as its indexicality lies in the 3D structure, upon which realistic color can be overlaid[27]. I found myself, especially initially, considering the digital forest as a backup copy to which I could turn to resolve issues with field-based measures. However, the 3D structure is not an exact copy, it is a theory-laden modeled representation of the actual forest. My first realization of the inaccuracies occurred after my initial intense week of post-processing. The scanning technology only records surfaces, and therefore the forest floor creates a surface under which is nothing. I noticed that one area of the study site had a second surface hovering below the main surface. Also during the process of extracting adult tree locations and sizes, it was apparent that scans were misaligned because arcs in the DBH slice were offset from each other. The misalignment resulted from human error and manual (human) adjustments were necessary to correctly align the scans. The remaining alignment error is small (< 10cm) but it is still present.

In addition to human-based inconsistencies, these data have important inherent omissions. First, it is a discrete representation. Thus, the points are a still sample of the surfaces present in the landscape. The point density is such that small, airy forest features, like tree seedlings, are not captured in the digital forest. Secondly, because the laser-based technology only captures surface features, we have no information on the inside of the tree trunks or rocks. Because the laser cannot penetrate the forest floor, the important underground structures like roots are completely omitted. Even if we had better scan coverage we could never completely eliminate occlusions. Thus, it is impossible in a complex landscape like the forest to capture every surface. Thirdly, the digital forest is a single representation in time. None of the forest fauna is represented. No change in the forest structure itself is captured. For my study the unchanging representation of the forest stand has implications. During the winter of 2011-2012, an ice storm severely damaged the forest, toppling many juvenile trees, breaking off many adult tree tops, and downing several large adult trees. This event, in addition to background rates of tree mortality and fall, has significantly changed the forest stand structure over the course of my study period (2009-2013). These changes affect sun/shade (radiation) patterns, rain fall interception, litter accumulation, all important factors affecting seedling survival and growth. However, the changes are not observable in the digital forest. Finally, the photographic coloring of the forest is distorted. Some areas are overexposed and appear ghostly white-yellow-blue, while other underexposed areas are dark brown-green-black. The underexposed dark colors do not contrast with the black background of the 2D and 3D platforms and are essentially invisible. It was not until I started recoloring the points to highlight specific features that I discovered almost a third of the points. I had not seen them until I colored them so that they contrasted with the dark background.

Bowker articulates the challenges of classifying biological and ecological entities [2008]. Things that are difficult to describe, things that do not break up into natural units, and things that have no easy boundaries or are theoretically ill-defined often get left out because they cannot be quantified. The discrete nature of the digital forest at first glance suggests solutions to these classification challenges. We've already broken up this complex entity into quantifiable immutable mobiles! However, the points are still difficult to describe (*e.g.,* is that one-year old seedling a white or red fir?), do not break

[26] I am thinking of photographic imagery as follows. A viewer is looking out of a window with her gaze in a fixed direction. Photographic equipment could capture an identical visual representation of whatever is viewable through the window so that disregarding depth information the viewer would be presented with the same visual input.

[27] As noted earlier, the color can be changed, which can challenge the realistic representation but not remove the underlying quantitative structural mapping to the actual forest.

up in to natural units (*e.g.,* is that 25cm tall tree a seedling or sapling?), and definitely do not have easily defined boundaries (*e.g.,* should the study site include the meadow or go around it?). Simple classification of the points into tree, shrub, rock, log, surface remains a challenge both technically[28] and manually, especially with insufficient point density.

Once things are not included, they "get ignored, and so receive an ever-decreasing amount of attention" [Bowker 2008, pg. 141]. The digital forest is so enticing because with so much data it is easy to forget that the representation is incomplete. The risk is that these incomplete representations become self-reinforcing:

> … a set of data structures and information retrieval models are set up so that a particular, skewed view of the world can be easily presented. With these structures and models in place, it is easier to get funding and support for research that reproduces this view — your work will be understood more easily, you can make good use of material from cognate areas, and so forth. Thus the world that is explored scientifically becomes more and more closely tied to the world that can be represented by one's theories and in one's databases: and this world is ever more readily recognized as the real world. [Bowker 2008, pg. 151-152]

Once a representation is firmly established, the missing elements are even more likely to not be considered. In the case of the digital forest, the absence of time is a key missing element. More dynamic theoretical frameworks have only recently superseded the concept of ecological equilibrium. It is especially important to incorporate dynamic elements in representations of long-lived forests, the poster children of ecosystems in equilibrium, especially in light of the many temporally dependent environmental threats (*e.g.,* climate change) facing human and other species.

4.4.3 Influence of inscription

Inscription is one of a scientist's most important tools. By creating a representation that highlights particular features or phenomena in a representation, the scientist allows others to see as she does [Vertesi 2014]. For example in the digital forest, I used color to draw attention to the DBH slice as well as indicate which trees were modeled. Even a more basic choice of color scheme influences how another viewer experiences the digital forest, as some points are essentially invisible in photographic color. The point cloud itself is also a type of inscription when compared to other forms of representations such as photography or my 2D sketched maps (Figure 4.10). Several risks arise when a particular inscription becomes engrained in scientific practice.

Vertesi notes the pervasiveness of inscription through Galileo's drawings of the moon, arguing that his particular type of rendering "influenced future viewings, depictions, and theoretical understandings of the moon, blinding viewers to other aspects" [2014, pg. 21]. Representations can become so pervasive that a viewer no longer "sees as" but rather only "sees." Vertesi states further:

> Representation in scientific practice is therefore not a question of creating an ever more true or singular image of an object. Instead, we should note how practical work with images shuts down other ways of seeing in order to focus on one aspect, one set of salient relationships. It is the role of the analyst to identify each image's inscribed and implied aspect, to note the representational choices that produce and reproduce that aspect, and to remind us that it could always be seen otherwise. [2014, pg. 31]

[28] Object classification in point cloud data is at the cutting edge of research. For example, Brodu and Lague (2012) develop methods for identifying vegetation from other surface features.

Vertesi is in effect calling for Haraway's multiple partial perspectives and lays the responsibility of understanding the perspective on the analyst as both inscriber and viewer. Similar to Bowker's claim that entities that are hard to classify are more likely ignored, Latour warns that the uncollected, in Vertesi's language the un-inscribed, are forgotten [Latour 1990]. Thus, Vertesi's call for awareness of other views is critical to inclusion of the many entities and characteristics of a phenomenon.

Myers [2014] also warns of a potential risk of an inscribed perspective in her description of the advantages of machine metaphor as a rendering of protein structures. In her observations of biological engineers, she notes that

> … molecular machines are no longer animating figures that enable the scientist to take a leap across the divide between the visible and the invisible; with atomic-resolution molecular vision, molecular machines have been forged as fact and become unremarkable things-in-themselves. … By naturalizing and literalizing machines in the bodies of organisms and asserting the neutrality of visualization techniques, practitioners risk giving the impression that they are merely unveiling the underlying machinery of life. [Myers 2014, pg. 168]

In other words, the machine metaphor is itself the discovery. Other ways of knowing the proteins are no longer possible. Haraway also makes no distinction between the technological and organic [1991a]. The leap from metaphor as a tool to metaphor as the discovery may not even be necessary. Thus, we must be on guard not to privilege one perspective to the exclusion of others.

I anticipate a similar risk with my digital forest, as it is representative of other big data that is increasing growing in popularity in ecology and the biological sciences [Hampton *et al.* 2013, Leonelli 2014]. Big data proponents claim that because big data captures an entire phenomenon (1) it removes the need for theory and models, rather correlation is sufficient; (2) there is no longer a sampling bias; (3) messy, but complete, data yield truthful insights; and 4) context is not necessary to interpret statistical results or data visualizations [Leonelli 2014, Kitchin 2014]. Critiques of these claims as applied in the environmental sciences are just starting to emerge [Leonelli 2014]. Through my work with the digital forest, I add the following.

My digital forest, like other big data such as remote sensing and distributed sensor networks, is inherently discretized. As this trend towards big data continues, we risk replacing the continuous natural world with these datasets that by their very nature imply that if we just measure each individual piece of the environment, we can reconstruct it through modeling frameworks to gain understanding. I am not arguing that this practice is uninformative. Indeed, our ability to break the environment apart and reform it in simpler models has yielded important ecological understanding. My concern is that it may become the predominant, if not only, acceptable way to scientifically understand ecological phenomena. As such the discretized framework of ecological systems may become the discovery itself. I am not convinced that high-resolution spatiotemporal data, *i.e.,* big data, is sufficient to build a well-rounded set of partial perspectives from which we may gain a richer conceptualization of the natural world.

4.4.4 Limits to time and participation

I described earlier how the logistical requirements to collecting the digital forest point cloud are intensified compared to other established field-based methods that I employed. In the field, more humans were required, costs limited the time available, and equipment management was more complex. Similar intensification of logistical details occurs during analyses. An I-Site Studio month-long license is included in the rental cost of the scanner; otherwise a regular license is on the order

of $20K/year.[29] I spent an intensive week on initial processing after the data collection in 2009 on a colleague's high-end computer during the evening and night while he wasn't using it. I then spent 2 years working with UC Berkeley and Maptek lawyers trying to construct the education software use agreement before the company president cut through the red tape.

The primary Maptek customer use of I-Site scanner and software was originally mining, and it is now gaining popularity with road construction [Maptek, personal communication]. Thus, many forestry applications are not straightforward, and several software functions do not work well because of the complex forest structure[30]. I-Site Studio has developed rapidly during the time that I have used it. This is due, in part, to the continual advance in computing capability of personal computers. Unlike some equipment used in ecology,[31] Maptek kept its software up to date with current computer technology. However, it still wasn't until 2013, four years after I collected the data, that I was able to reasonably interact with my entire point cloud on a common computer (although it still needed to be higher end).

The additional effort in both time and money has paid off with access to new types of data and understanding. However, it is worthwhile noting the not insignificant amount of time lost to logistical details. In my case, analysis was delayed due to these challenges. It is impossible to know whether being able to spend more time on analysis during the data collection process would have led to different or better outcomes. But I did lose the opportunity, and it is a tradeoff worth consideration.

Perhaps a bigger issue than resource tradeoffs within the research itself and time is the potential ethical issue of access to highly technical methodologies. With the current costs of terrestrial laser scanning, it is typically only available to those with large funding sources, often at a select number of institutions. Once at an institution, enabling widespread access to it is challenging.[32] The cost of the I-Site Studio software, which was necessary to transfer my data into a form that was usable with freeware, prevented me from utilizing my digital data for several years. I only regained access once the manufacture created a free educational license. In addition to the costs, the required technical skills also cull the potential user pool. In my case, my digital forest required proficient use of surveying technology, 3D CAD software, Unix command line programming, and R programming. The leap for me was relatively easy because I already had experience with each of these or similar technologies. However, out of all my methodological approaches, many of them technically based, working with the digital forest still congers the most anxiety because of the technological complexity and the potential failure modes. To potential users that have little to no technical expertise, these requirements might be a strong deterrent. Myers [2014] reports that the machine metaphor and technical methods that dominate research of proteins shape the community of researches studying their biological function: "mechinic renderings not only constitute molecular visions; they also

[29] 2009-2010 dollars and prices

[30] For example, later versions of the software can automatically correct misaligned scans. This works quite well for scans with overlapping more-or-less planar surfaces. It failed when trying to merge scans with overlapping cylinders (*i.e.,* tree trunks). Additionally, tree canopies do not merge well at all because they are differentially porous from different scanning locations.

[31] For example, I still have a late 1990s laptop running Windows XP so that I can continue to use a sensor that I purchased in 2008. Until 2015, I was also using this PC to run the commonly used radiation modeling software.

[32] As part of a team that acquired a laser scanner donation, it was difficult to find a party on campus willing to take legal and financial responsibility for such an expensive piece of equipment. Once we found those willing to do so, it was difficult to negotiate a rental policy that yielded financial access to students while assuring that the equipment integrity would be maintained.

reconfigure entire research programs, and, crucially they inform 'who is recruited to do the work' of modeling life-as-machine" [2014, pg. 162]. Given that technological methodologies are already privileged[33] [Bowker 2008], continued technological advancement may limit the partial perspectives that we collectively generate as a scientific community.

4.5 A responsible digital ecology

Along with other STS and Feminist scholars, I applaud and encourage the continued development of technological scientific representations, such as my digital forest, as the potential for new understanding is high. The ability to scale and view the forest from any perspective, interact with the forest in real-time, create new conceptualizations, and work with an indexical representation have opened new possibilities within my own ecological research. However, also with fellow scholars, I urge the ecological research community to use these technologies responsibly. The risks too are high. Through technologies like terrestrial laser scanning and 2D and 3D viewing platforms, we incorporate natural systems into our technical toolkits. We must be wary that we do not adopt omnipotent control over these systems, see them as complete representations, or a single correct way to investigate an ecological phenomenon. Furthermore, we must be wary of the potential exclusion of participants in ecological research by privileging highly technical and cost-prohibitive methods.

Haraway and Barad provide paths for balancing these risks and rewards. Haraway [1991] argues that knowledge practice be situated, meaning that one is aware of her relationship to the studied object and the choices that led to that particular perspective. By acknowledging the partial view, one can take responsibility for that view through an understanding of power dynamics, technological advantages and disadvantages, and other potential perspectives. Barad [2003] suggests agential realism as a framework for acknowledging partial perspectives. She posits that the combination of the observer, the observed, and the instrument creates meaning and understanding. The scientist is in a partnership rather than in complete objective control. Through agential realism the scientist actively acknowledges the partial perspective enabled by the technology in use and by the observed.

For ecology in particular, recognizing the observed as a research partner is especially important as the observed themselves are living beings or integral to the processes being observed. Humans are intimately connected to these other lives by complex relationships through interactions with the physical world. Ecology is the study of these relationships and interactions, much of which is motivated by understanding our own survival amidst the environmental impacts that we humans are increasingly making. What is our ethical responsibility as scholars towards these other beings with which our lives are intertwined? Western anthropology and similar social sciences have faced similar questions in the study of other human cultures. The response has been to break down perceptions of otherness and train scholars to include these other humans as willing and sometimes active participants in the research itself. Learning from Barad and Haraway (her later works included [*e.g.,* Haraway 2008]), ecologists can also utilize other works by scholars such as Rose [2011] and Woelfle-Erskine and Cole [2015], who question perceived differences with other species and suggest reconfigurations with our earthly co-inhabitants.

[33] Bowker [2008, pg 146]: "they (scientists) are more likely to get funding for using exotic, expensive tools"

Also key to acknowledging the partial perspectives enabled by our technological tools is experience in the actual system with as little technical mediation as possible. It was my intimate knowledge of the forest gained through thousands of hours spent at my study site that enabled me to understand what was captured with the laser scanning technology and what was not, as well as how this digital representation afforded me a new conceptualization of the forest. While my intimate relationship was necessary for this critical analysis, thousands of hours are likely not required for *a* grounding in the actual forest. But without such grounding, perception of the forest based primarily on the digital representation would likely be completely different. A colleague recently said to me in so many words: "Big data is the future of ecology." And further suggested that ecologists in the future probably would not need to go to the field. Visualization of the forest with digital data has the potential to alienate us from the actual forest in a way that is troubling. As this type of visual representation becomes more available, ecologists will need to grapple with the allure of the ready-made virtual environs that calls the scientist to the desk rather than the forest.

It is naïve to expect users of big data to experience the locations of observations personally or to form intimate relationships with the technologies that captured the observations. For example understanding a satellite and the imaging technologies that produce 10m resolution remote sensing data is unrealistic. And it is physically impossible to experience all the places captured in spatially and temporally extensive remote sensing data collection. Additionally, the many hours that I spent at my forested site may not be possible for ecologists studying extremely remote or dangerous locations. Bowker [2008] suggests an alternative in which the metadata associated with compiling such a dataset capture the situated position. What this might look like is yet to be determined, could take many forms, and is likely to involve some iteration. The measures of successful implementation are also slippery. I have no easy prescriptions, but beginning a conversation amongst ecologists is a successful start. Perhaps as a community, ecologists can strengthen our collective understandings of forests by situating binary perspectives, like my digital forest, amongst others.

4.6 Acknowledgements

I thank Alenda Chang and Meredith Tromble for encouraging me to question my ecological use of new media. I am indebted to Manisha Anantharaman, Anna Kantenbacher, and Cleo Woelfle-Erskine for formative discussions and comments on early drafts. Additional thanks to Cleo for filming interactions with the digital forest at the UC Davis KeckCAVES. My thanks also to Joe Dumit, Mike Oskin, and M. Burak Yikilmaz for introduction to and assistance in the KeckCAVES.

4.7 References

Baird R.N., D. McDonald, R.H. Pittman, and A.T. Turnball 1993. The graphics of communication: Methods, media, and technology, Harcourt Brace College Publishers: City.

Barad, K. 2003. "Posthumanist Performativity: Toward an Understanding of How Matter Comes to Matter." *Signs: Journal of Women in Culture and Society* 28(3): 801–31.

Barry A.M.S. 1994 "Perceptual Aesthetics and Visual Language" in Visual literacy: A spectrum of visual learning, ed. D.M. Moore and F.M. Dwyer, p. 113–132.

Bowker, G. C. 2008. *Memory Practices in the Sciences*. MIT Press (MA).

Bowker, G. C. and S. L. Star. 2000. *Sorting Things Out*. MIT Press.

Braden R.A. 1994. "Visual Verbal Relationships" in Visual literacy: A spectrum of visual learning, ed. D.M. Moore and F.M. Dwyer, p. 193–208.

Brine, K. R. and M. Poovey. 2013. "From Measuring Desire to Quantifying Expectations." Pp. 61–75 in *Raw Data Is an Oxymoron*, *A Late Nineteenth-Century Effort to Marry Economic Theory and Data*. MIT Press.

Brown J.R. 1996. "Illustration and inference" in *Picturing Knowledge: historical & philosophical problems concerning the use of art in science*, ed. B.S. Baigrie, Publisher: City, p. 250–268.

Brown, S. 2007. "Autobiography." Pp. 440–52 in *Handbook of Qualitative Research Methods in Marketing*. Edward Elgar Publishing.

Coopmans, C. 2014. "Visual Analytics as Artful Revelation." Pp. 37–59 in *Representation in Scientific Practice Revisited*. MIT Press.

Dassot, M., T. Constant, and M. Fournier. 2011. "The Use of Terrestrial LiDAR Technology in Forest Science: Application Fields, Benefits and Challenges." *Annals of Forest Science* 68(5): 959–74.

Edwards, P. N. 2010. *A Vast Machine*. MIT Press.

Frascara J. 2001. "Diagramming as a way of thinking ecologically" *Visual Language* 35(2), p. 164–177.

Ellis, C., T. E. Adams, and A. P. Bochner. 2011. "Autoethnography: an Overview." *Historical Social Research* 12(1): article 10.

Geertz, C. 1973. "Thick Description." Pp. 3–30 in *The Interpretation of Cultures*, *Toward an Interpreative Theory of Culture*. Basic Books.

Geiger, R., R. H. Aron, and P. Todhunter. 2009. *The Climate Near the Ground*. Plymouth, United Kindom: Rowman & Littlefield Publishers, Inc.

Hampton, S. E. et al. 2013. "Big Data and the Future of Ecology." *Frontiers in Ecology and the Environment* 11(3): 156–62.

Haraway, D. J. 1991. "Situated Knowledges." Pp. 183–202 in *Simians, Cyborgs, and Women*, *The Science Question in Feminism and the Privelege of Partial Perspective*. Routledge.

Haraway, D. J. 1991a. "Cyborg Manifesto." Pp. 149–182 in *Simians, Cyborgs, and Women*, *The Science Question in Feminism and the Privelege of Partial Perspective*. Routledge.

Haraway, D. J. 2008. *When Species Meet*. U of Minnesota Press.

Hartin J.A. 1994. "Theoretical Foundations of Visual Learning" in Visual literacy: A spectrum of visual learning, ed. D.M. Moore and F.M. Dwyer, p. 5–29.

Holbrook, M. B. 2006. "Consumption Experience, Customer Value, and Subjective Personal Introspection: an Illustrative Photographic Essay." *Journal of Business Research* 59(6): 714–25.

Kitchin, R. 2014. "Big Data, New Epistemologies and Paradigm Shifts." *Big Data & Society* 1(1): 1–12.

Kohn, E. 2013. *How Forests Think*. Univ of California Press.

Kreylos, O., Bawden, G.W., and Kellogg, L.H. (2008). Immersive Visualization and Analysis of LiDAR Data, in: Bebis, G., et al. *ISVC 2008, Part I* LNCS 5358, Springer-Verlag Berlin Heidelberg, pp. 846-855.

Latour, B. 1990. "Drawing Things Together." Pp. 19–68 in *Representation in Scientific Practice*, edited by M. Lynch and S. Woolgar. MIT Press.

Latour, B. 1999 "Circulating Reference" Pp. 24–79. *Pandora's Hope*. Harvard University Press.

Leonelli, S. 2014. "What Difference Does Quantity Make? on the Epistemology of Big Data in Biology." *Big Data & Society* 1(1): 1–11.

Mathewson J.H. 1999. Visual-spatial thinking: an aspect of science overlooked by educators, Science Education 83, p. 33–54.

Messaris P. 1997. Visual Persuasion: the role of images in advertising, Publisher: City.

Miller H.B. and Burton J.K. 1994. "Images and Imagery Theory" in *Visual literacy: A spectrum of visual learning*, ed. D.M. Moore and F.M. Dwyer, p. 65–83.

Moser S. 1996. "Visual Representation in Archaeology: Depicting the missing-link in human origins" in *Picturing Knowledge: historical & philosophical problems concerning the use of art in science*, ed. B.S. Baigrie, Publisher: City, p. 184–214.

Myers, N. 2014. "Rendering Machinic Life." Pp. 153–75 in *Representation in Scientific Practice Revisited*. MIT Press.

Myers, N. and J. Dumit. 2011. "Haptics." Pp. 239–61 in *A Companion to the Anthropology of the Body and Embodiment*, *Haptic Creativity and the Mid-embodiments of Experimental Life*. John Wiley & Sons.

National Center for Biotechnical Information. 2015. 1B8G: 1-aminocyclopropane-1-carboxylate. Synthase. http://www.ncbi.nlm.nih.gov/Structure/mmdb/mmdbsrv.cgi?uid=12342, accessed October 4.

Peirce, C. S. 1998. "What Is a Sign? (1894)." Pp. 4–10 in *The Essential Peirce, Volume 2*, edited by T. P. E. Project. Indiana University Press.

Porter, T. M. 1996. *Trust in Numbers*. Princeton University Press.

Rose, D. B. 2011. "Flying Fox: Kin, Keystone, Kontaminant." *Australian Humanities Review* 50:119–36.Scott, J. C. 1999. *Seeing Like a State*. Yale University Press.

Seels B.A. 1994. "Visual Literacy: The Definition Problem" in Visual literacy: A spectrum of visual learning, ed. D.M. Moore and F.M. Dwyer, p. 97–112.

Tufte E.R. 2006. Beautiful Evidence, Graphics Press LLC: City.

UC Davis KeckCAVES. 2015. http://keckcaves.org, accessed December 10.

Vertesi, J. 2014. "Drawing as: Distinctions and Disambiguation in Digital Images of Mars." Pp. 15–35 in *Representation in Scientific Practice Revisited*. MIT Press.

Vitousek, P. M., H. A. Mooney, J. Lubchenco, and J. M. Melillo. 1997. "Human Domination of Earth's Ecosystems." *Science* 277(5325): 494–99.

Woelfle-Erskine, C. and J. Cole. 2015. "Transfiguring the Anthropocene: Stochastic Reimaginings of Human-Beaver Worlds." *TSQ: Transgender Studies Quarterly* 2(2): 297–316.

Conclusion: Projecting fine-scale heterogeneity in future climates

A primary motivation for my study of fine-scale environmental heterogeneity in mountainous landscapes is to link fine-scale ecological processes (*e.g.,* a tree seedling response to its local abiotic environs) to emergent characteristics at coarse scales over large extents (*e.g.,* the geographic range of a tree species). In the preceding chapters, I describe beginning steps toward this aim. In chapter 1, I recommended appropriate sampling designs for quantifying spatial heterogeneity on landscapes with autocorrelation and gradient patterns. Additionally, I developed an analytical tool to estimate expected sampling errors for existing sampling designs. In chapter 2, using the techniques developed in chapter 1, I characterized how spatial heterogeneity changes over the growing season in four mountainous studies. I show that fine-scale heterogeneity is large compared to project future temperature change and that it is variable in time. In chapter 3, I reported that fine-scale physical environmental (abiotic) factors explain a large portion of tree seedling occupancy patterns and that some abiotic effects may be due to indirect biotic influences of the forest stand structure. And in chapter 4, in light of current big data trends in ecology, I suggested careful use of fine-scale quantitative representations of ecological phenomena, using terrestrial laser scanning as a case study of advantages and risks of visual representation. In this concluding chapter, I consider a path towards incorporating fine-scale environmental conditions in projections of future species persistence. I suggest a series of questions to be addressed, noting current progress. In particular, I present new data on coarse-scale spatial heterogeneity, which I use to hypothesize how temporal patterns in fine-scale environmental conditions may change over large extents. In other words, I link environmental heterogeneity across spatial scales, which I see as a necessary next step towards understanding how change in fine-scale heterogeneity may affect persistence of species. In addition, I discuss the use of within-season heterogeneity dynamics as a proxy for long-term change. Decades are required to understand long-term change, and fine-scale environmental monitoring over larger extents has only really begun in the last 5–10 years. Given imminent environmental threats like climate change, we must develop alternative ways to project change in fine-scale environments in addition to direct observation.

5.1 Fine-scale environmental conditions and species persistence

Change in fine-scale conditions are thought to be important to the persistence or movement of species under future climates [Clark *et al.* 2011, Potter *et al.* 2013, Harwood *et al.* 2014]. As described in chapter 2, the available fine-scale conditions observed at a particular grain (~1-10s m) within a given extent (100s m – 10s km) can be considered as a probability density (PD). This framework is useful for thinking about fine-scale heterogeneity in the context of coarse-scale projection tools. The coarse-scale values used in projection tools should be the mean of the average fine-scale condition within a given coarser-scale grain (Figure 5.1). In future climates, most coarse-scale values across the globe are projected to increase [Meehl *et al.* 2007]. If species are responding to fine-scale environmental conditions, the mean *and* the shape of the PD in future climates will determine

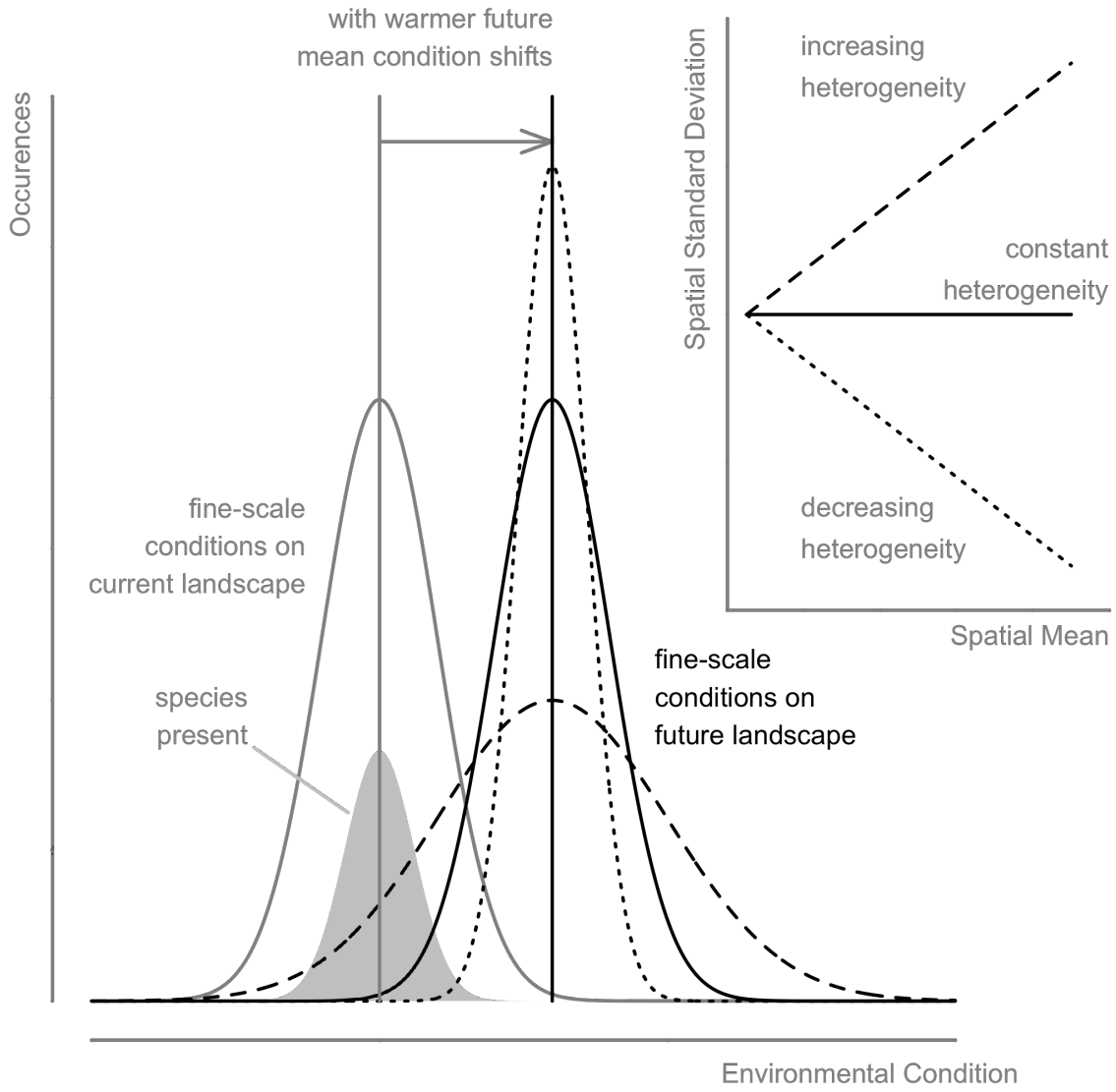


Figure 5.1: Species may or may not persist within a coarse-scale extent depending on how the underlying fine-scale conditions change in a warmer future. Changes in both the mean *and* shape of distribution (probability density) of the available fine-scale conditions matter.

whether a species will persist within that given extent. Current coarse-scale modeling tools inherently assume that the shapes, or the relative differences amongst available fine-scale climates within each coarser-scale grain, remain the same in future climates. Thus, they may be over- or under-projecting species geographic ranges. I have illustrated an idealized case in Figure 5.1, in which the entire range of suitable conditions for a species occurs in the given extent. Over- or under-projections are most likely to occur at the edges of species current ranges that contain marginal conditions for species presence (*i.e.,* PD of species presence would be skewed toward one tail of the currently available fine-scale conditions).

This framework is also useful for thinking about refugia. Where heterogeneity increases with warmer conditions, areas (extents) may retain conditions currently suitable for species, allowing them to persist despite average conditions that are no longer suitable. For refugia, the area of interest can vary from regional scale (10-100s km) to continental scales (> 100s km) that may encompass the

entire species range. Several questions, however, must be addressed to apply this framework to either coarse-scale projection tools or assessments for potential refugia.

- Do fine-scale environmental conditions limit population viability?

  All plant individuals must survive fine-scale environmental conditions, at least at early life stages. It is thought that early life history stages are more vulnerable to both abiotic and biotic stress than other stages because as an individual matures it has access to more resources [Grubb 1977]. Tree seedlings in particular have been found to be sensitive to climatic conditions, especially extreme conditions such as heat, drought, and frost stress [*e.g.,* Kolb and Robberecht 1996, Battaglia *et al.* 2000, Maher and Germino 2006, Collins and Carson 2004, Johnson *et al.* 2011, Carón *et al.* 2015, Moyes *et al.* 2015]. Some tree species also require specific abiotic conditions for seed maturation [Bykova *et al.* 2012]. Additionally, recent work on tree species suggests that juvenile trees have narrower climatic tolerances than adult individuals [Lenior *et al.* 2009, McLaughlin and Zavaleta 2012, Bell *et al.* 2013, Dobrowski *et al.* 2015]. In chapter 3, I show that individual tree seedlings are indeed influenced by fine-scale environmental conditions. However, more work is needed to understand how limiting these influences on early life history stages are compared to influences on other life history stages and/or how these influences on individuals scale up to population dynamics [Clark *et al.* 2011]. I focus here on environmental characteristics, but biotic interactions and dispersal limitations are likely to be important influences on viable populations as well [Soberón 2007, Peterson *et al.* 2011].

- Do individuals respond to abiotic conditions differently at multiple spatial scales?

  Recent work suggests that community vegetation characteristics (*e.g.,* percent cover [Ford *et al.* 2013] and functional traits [Bello *et al.* 2012]) are correlated differently with environmental characteristics quantified at different spatial scales. Climate envelope models, based on correlations between climatic metrics and species occupancy, have different outcomes at different spatial scales [Trivedi *et al.* 2008, Ashcroft *et al.* 2009, Randin *et al.* 2009, Gillingham *et al.* 2012]. While not definitive, these results suggest that environmental factors have differing influence on vegetation at different spatial scales. In chapter 3, I report that several fine-scale environmental conditions influence occupancy patterns of individuals, but not fine-scale slope and aspect. This finding differs from many studies that find aspect, north and south facing slopes in particular, plays a strong role in shaping vegetation patterns on the landscape. I have yet to systematically investigate the scale-dependency of environmental factors at my red fir study site, but at first glance the more northerly facing side of the study site, *i.e.,* coarse-scale aspect, seems to have more tree seedlings than the more southerly facing slope. While I have seen no systematic study of the scale-dependency of environmental conditions on individual plants, the related results described here suggest that environmental influences may differ at multiple spatial scales.

- Can fine-scale environmental influences on one species be generalized to others?

  Understanding the fine-scale environmental influences — not to mention biotic interactions and dispersal limitations — and the scale(s) at which these influences occur for a single species is a large task. It is impractical, if not impossible, to carry out such studies on every plant species, let alone those of other kingdoms. Thus, to be of practical use, we must find characteristic species, use a trait-based approach, or develop new methods to generalize findings from a manageable set of species to others.

- Are fine-scale heterogeneity patterns similar across ecosystems and landscape features?

  In areas of high heterogeneity, a species may currently persist in locations quite different than the average conditions, *i.e.,* in current refugia. In a future location with the same average condition but low heterogeneity, the species would not exist because suitable habitat does not occur in that area. In models based on coarse-scale conditions, which is presumably the spatial mean of the fine-scale conditions, these two scenarios with high and low heterogeneity are indistinguishable. The species occurring in the highly heterogeneous condition would be falsely assumed to be present in the future area of low heterogeneity that did not have suitable fine-scale habitat. Thus, it is important to understand how heterogeneity differs across ecosystem and landscape features. In chapter 2, I begin this work, comparing heterogeneity in temperature across mountainous systems. Surprisingly, I observed high levels of heterogeneity (as measured by standard deviation) in soil temperatures of meadow systems, which seem quite homogenous compared to forest systems. Other studies report differing levels of heterogeneity (as measured by max-min) for air and for soil temperatures between coniferous and broadleaf forests [Chen *et al.* 1999]. More work is needed to assess heterogeneity differences in other influential environmental characteristics, like soil moisture and wind [*e.g.,* Reifsnyder *et al.* 1971, Chen and Franklin 1997, Bond-Lamberty *et al.* 2005, Ford *et al.* 2013]. To assess the potential for heterogeneity change over long time periods (decades), it is important to understand how ecosystem (primarily vegetation) and landscape features influence fine-scale heterogeneity. If vegetation is influential as suggested by some studies [Hungerford and Babbitt 1987, Van Pelt and Franklin 2000, Geiger *et al.* 2009, von Arx *et al.* 2013], projecting fine-scale heterogeneity into the future will be additionally challenging.

- How might coarse-scale values (*i.e.,* the fine-scale spatial mean) change?

  As illustrated in the fine-scale heterogeneity framework (Figure 5.1), shift in the mean of the fine-scale conditions (*i.e.,* the coarse-scale value) also determines whether a species will persist on the landscape. Temporal heterogeneity in coarse-scale climatic conditions has been investigated as extreme weather events are of concern [Meehl *et al.* 2000, Hansen *et al.* 2012, Thornton *et al.* 2014]. However, studies of change in coarse-scale spatial heterogeneity are lacking. Most coarse-scale historical climate sources, based on interpolated weather station data like DAYMET and PRISM, are available at monthly temporal resolution [Thornton *et al.* 1997, Daly *et al.* 2000]. As I demonstrated in chapter 2, monthly average values do not capture the daily dynamics of spatial heterogeneity for fine-scale heterogeneity. Thus, I address this below, with an analysis of the potential change in coarse-scale air temperature using TopoWX, a new climate data source that uses lapse rate and satellite-based skin temperatures for elevational corrections [Olyer *et al.* 2014].

- Are within-season temporal heterogeneity patterns a proxy for long-term temporal change?

  As shown in chapter 2, spatial heterogeneity in maximum daily temperatures increases on warmer days, while minimum daily temperature heterogeneity remain constant over most of the growing season in mountainous landscapes. Within-season or annual change in temperature is driven in large part by changing short-wave energy input into the landscape (*i.e.,* days are longer or shorter). Long-term, climatic change is driven by increases in long-wave (infrared) radiation. In terms of an energy balance approach the two are equivalent (albedo losses with short-wave radiation can be accounted for). However, other factors influence the energy balance at the landscape surface and thus the very near surface. They include heat transfer within the ground (usually negligible on short time scales) as well as latent and sensible heat losses. The latter are intimately tied to vegetation and water dynamics. Macro-scale and regional weather patterns are also factors, as they

influence air mass movements. Vegetation, water dynamics, and weather patterns can change drastically within season. But there may be time periods where these factors are relatively stable. Additionally, the specific influences may be teased apart, for example with modeling approaches. Thus, potential exists for within-season heterogeneity patterns to serve as a roadmap for heterogeneity change in future climates.

It is a daunting agenda, but an important one if we are to develop tools that inform our actions with respect to non-human species and the ecological processes with which we are all intimately intertwined. Because of the immediacy of many environmental threats, we don't have the luxury of waiting decades to observe how fine-scale heterogeneity will change in the future. Thus, I present a thought experiment, in which I consider frameworks for (1) thinking about how fine-scale heterogeneity may change over large extents, which is relevant to identifying potential refugia, and (2) thinking about how fine-scale heterogeneity may change in the future. For the latter, I consider how the drivers of fine-scale heterogeneity may change and what these changes may mean for future fine-scale heterogeneity. I conclude with thoughts on how these hypotheses may affect plant species. Since I focus on spatial heterogeneity throughout the remaining discussion, all further mention of heterogeneity is referring to heterogeneity in space.

5.2 Fine-scale heterogeneity over large extents

In chapter 2, I characterized how fine-scale heterogeneity changes within the growing season over small extents. To assess how fine-scale heterogeneity may change over large extents, I propose coupling our characterization of fine-scale heterogeneity with change in coarse-scale heterogeneity. Because analysis of coarse-scale heterogeneity is lacking as mentioned earlier, I characterized it here using the TopoWX climate source. The TopoWX climate source is comprised of daily minimum and maximum temperatures on a 30 second grid [Oyler *et al.* 2014]. Interpolated values are calculated from observations measured from 1948–2005 at 2m height at weather stations throughout the continental U.S., with altitudinal (based on lapse rates) and satellite surface skin temperature corrections. I used only gridcells occurring in California (Sierra Nevada) and Colorado (Rocky Mountains) between 2,400 and 3,500m elevations, the same elevations as the empirical study sites used in chapter 2. Additionally, I only included days during the growing seasons observed at the empirical sites (May–Oct).

I first used soil and air temperature data from the SEKI study site, located in the Californian Sierra Nevada (see chapter 2 for SEKI study site and data collection details), to verify that our fine-scale heterogeneity characterization of soil temperatures is comparable with the coarse-scale heterogeneity of 2m air temperatures represented in TopoWX. I used the same analysis framework presented in chapter 2. Thus, I assessed change in heterogeneity through time by calculating the slope of the relationship between spatial standard deviation (heterogeneity) and spatial mean (average condition), where points represent days (or other aggregated metric) in the growing season. Similar to the fine-scale analysis in chapter 2, I first calculated the given metric (*e.g.,* daily maximum) for each coarse-scale gridcell, and then calculated the spatial standard deviation and mean across gridcells.

5.2.1 Coarse-scale air temperature is representative of average soil temperatures

At the SEKI site where we measure both soil and air temperatures, the mean fine-scale soil temperature tracks the mean air temperature for hourly observations, daily minimum / maximum, and monthly temperature metrics (Figure 5.2). For hourly and daily observations the relationship is close to 1 with deviations occurring when air temperature drops drastically as shown in panel a. For

monthly aggregated temperatures, the relationship for average monthly minimum temperature is slightly greater than 1, and for average monthly maximum temperature, it is slightly less. For the monthly metrics, air on average is greater than soil by 7.6°C for minimum temperature, while soil is greater than air by 6°C for maximum temperature metrics. The fit as measured by R^2 is the best for these aggregated monthly metrics. These results indicate that air temperature at 2m can be considered a proxy for the mean soil temperature conditions occurring in the same extent. Ideally, the coarse-scale gridcell value in climate sources like TopoWX are representative of the entire gridcell; however, the 2m air temperature observations from which coarse-scale values are interpolated are collected in a single location. Conceptually, one can think about this as if a coarse-scale gridcell (~1km resolution) has a single measurement location within it, but of course not every gridcell has a measurement station. For this analysis, I assume that the coarse-scale gridcell is representative of the entire gridcell.

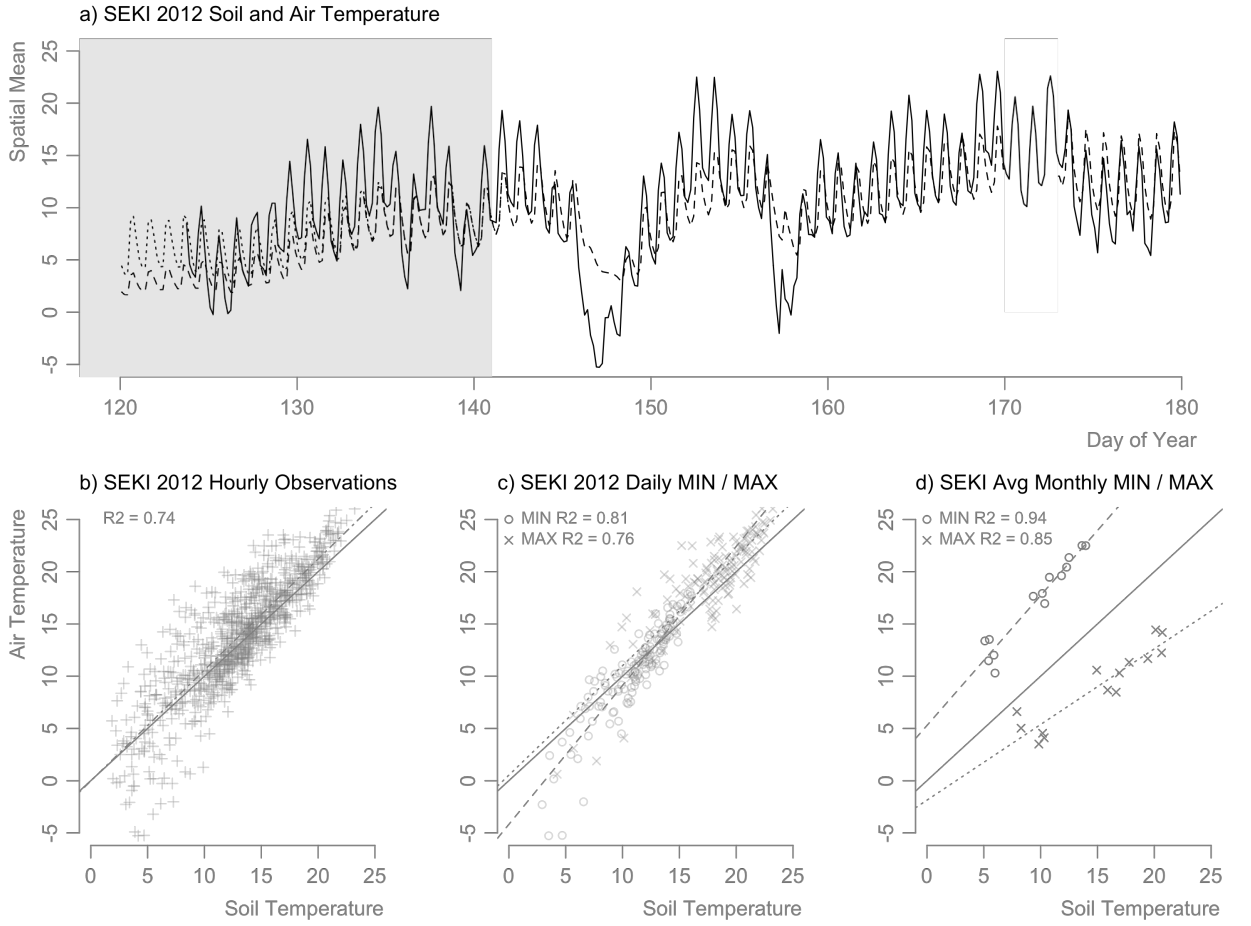


Figure 5.2: The spatial mean of air temperature (21 sensors at 2m height) is compared to that of soil temperature (98 sensors at 5cm depth below the soil surface). Temperatures are reported in °C. Both sets of sensors sample an area of 640x20m (chapter 2). (a) Hourly observations are shown during the heterogeneous snowmelt period (gray shade) and after (no shade). The solid line is air temperature, the dashed line is soil temperature for all sensors, and the dotted line is soil temperatures whose locations are snow-free. Note that both soil temperature time series converge at the end of the snowmelt period when all sensor locations are snow-free. The gap in soil temperature data between day of year 170–174 is due to data retrieval. (b) Correlation between soil and air temperatures for hourly observations for 2012. The 1:1 line is solid and the estimated slope is dot-dash. (c) Correlations between daily minimum (circles) and maximum (x) values for 2012. The 1:1 line is solid and the estimated slopes are dashed for minimum and dotted for maximum values. (d) The average monthly minimum and maximum temperatures for 2011-2013. Symbols and lines are the same as in (c).

5.2.2 Coarse-scale air temperatures have mixed heterogeneity characteristics

The next step in characterizing change in fine-scale heterogeneity over large extents is to assess coarse-scale heterogeneity. Coarse-scale air temperature values show mixed heterogeneity characteristics in California's Sierra Nevada (CA) and the Colorado Rockies (CO), during a typical growing season (May–Oct). In both locations, heterogeneity is large compared to projected change in a single location (Figure 5.3), ~1-3°C and ~1-4°C standard deviation which corresponds to ~4-12°C and ~4-16°C difference over 95% of the landscape, for daily minimum and maximum

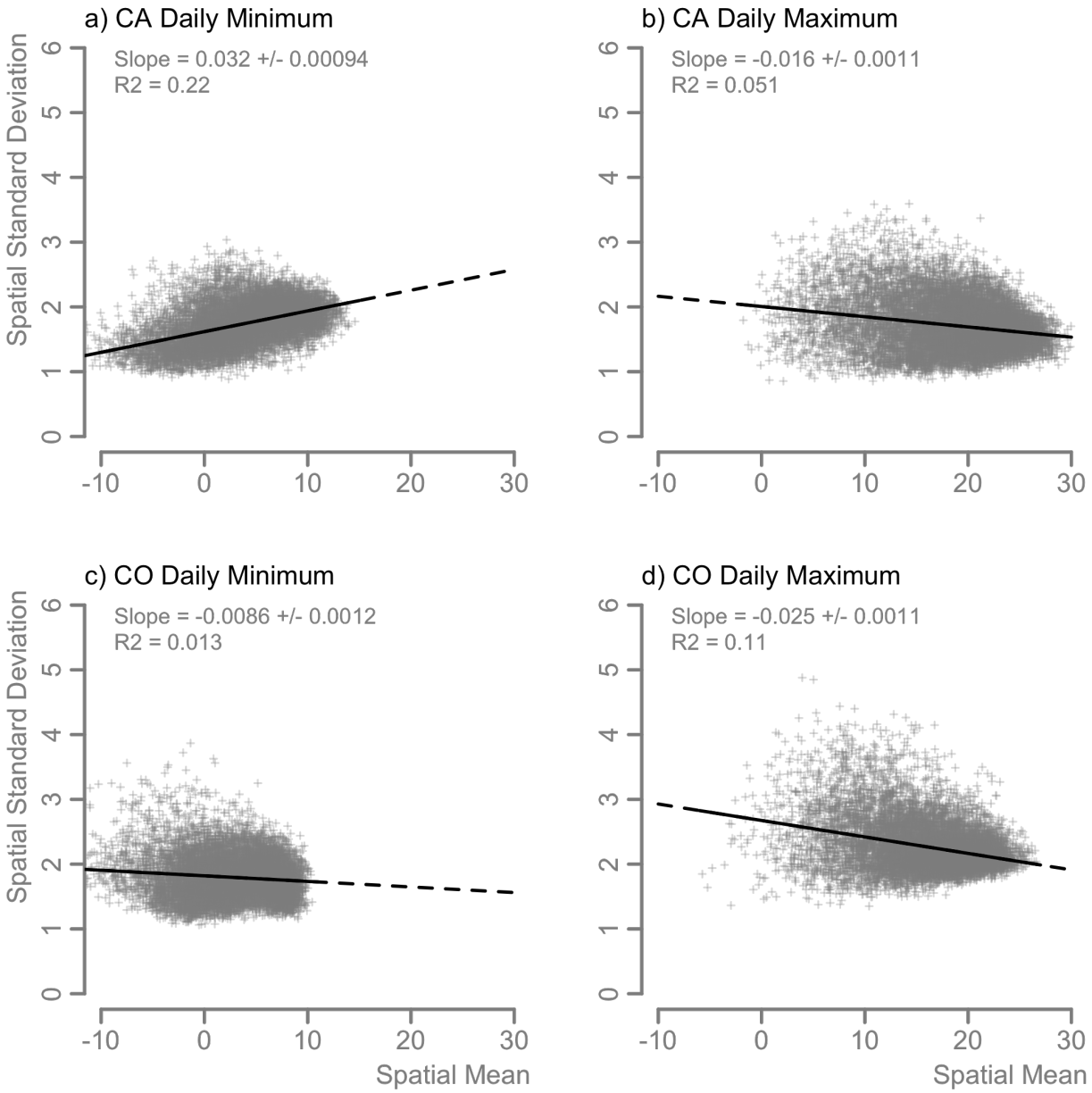


Figure 5.3: Air temperature heterogeneity (spatial standard deviation) versus average conditions (spatial mean) for daily minimum (a & c) and maximum (b & d) temperatures at mountainous elevations in Colorado Rockies, CO (c-d), and Californian Sierra Nevada, CA (a-b), during the typical growing season (May-Oct).

temperatures, respectively. As reported in chapter 2, daily minimum and maximum temperature increases at the SEKI site are projected to be ~4°C in 2085. In addition, the daily minimum heterogeneity is larger than that found at fine-spatial scales, which is expected because the large extent of the coarse scale data covers much more landscape variability than the small extents of the fine-scale studies. Surprisingly, the daily maximum heterogeneity is smaller than that found in the small extents of the fine-scale studies. In CA, heterogeneity in daily minimum temperatures generally increases with warmer conditions; slight decreases are observed for daily maximum at both locations; and it is more-or-less constant for daily minimum in CO. However, these relationships have large variability around the central trend. Whether the coarse-scale patterns are robust or not, they are different than patterns observed at fine-scales (excepting daily minimum temperatures at CO). This result is unsurprising as different mechanisms likely influence heterogeneity at coarse versus fine scales. As in chapter 2, I also characterized monthly aggregated metrics. The results are mixed (Appendix E.1). I continue this thought experiment with daily minimum and maximum values for simplicity.

5.2.3 Influences on coarse-scale heterogeneity

I hypothesize that the coarse scale heterogeneity trends can be explained by elevational and latitudinal differences across the mountain ranges. I use elevation in the following examples but latitudinal influences may be similar. Latitudinal differences may especially be important over larger (*e.g.,* continental) extents. For the example of daily maximum temperatures, let the higher elevations have cool temperatures ~50°F, while lower elevations are warmer at ~70°F during the spring; a difference of 20°F and average of 60°F. During the summer, the higher elevations may warm to ~70°F, while the lower elevations only increase to ~80°F; a difference of 10°F and average of 75°F. Using the difference as a measure of heterogeneity, higher heterogeneity in the spring with a cooler average condition and lower heterogeneity in the summer with warmer average conditions yields a negative relationship between heterogeneity and the average conditions as observed. The same reasoning may also explain the positive trend observed in CA for daily minimum temperatures. In the spring, let the higher elevations have temperatures of ~20°F, and the lower elevations are ~30°F. In the summer, higher elevations may only warm to ~30°F, while lower elevations warm to ~50°F. Thus, daily minimum heterogeneity is lower in the cooler spring and higher in the warmer summer; a positive relationship as observed in CA. The stark difference in daily minimum heterogeneity between CA (slope = 0.04) and CO (slope ≈ 0) is surprising, and it will require more work to untangle. Regional weather patterns are likely to contribute to spatial heterogeneity over larger extents, which may in part explain the large variability around the trends. In contrast, within the small extents of the empirical studies, weather is fairly consistent over the entire study area.

5.2.4 Changes in fine-scale heterogeneity over large extents within the growing season

As demonstrated, air temperature tracks fine-scale soil temperatures. Others have reported that soil temperature tracks very near surface (VNS) air temperature (within 5cm of the surface) [Kolb and Robberecht 1996, Moyes *et al.* 2015]. Thus, as proposed, it is reasonable to consider the coarse-scale air temperature values as the spatial mean of the fine-scale VNS conditions within a coarse-scale gridcell. Furthermore, fine-scale heterogeneity defines the range of conditions around the coarse-scale value. For the rest of the discussion, "coarse-scale" refers to air temperature measured at 2m above the soil surface and "fine-scale" refers to VNS air temperatures.

By overlaying fine-scale heterogeneity on the coarse-scale values, I hypothesize how fine-scale heterogeneity may change within a growing season. I consider daily maximum temperature first. As

reported in chapter 2, I observed less heterogeneity on cooler days than warmer days at fine spatial scales over small extents. Early in the growing season (spring), different elevations / latitudes may differ more in average conditions (coarse-scale values) than in mid-summer for daily maximum temperatures. Evidence for this trend is observed at both CA and CO (Figure 5.3b & d). Thus, the total fine-scale heterogeneity across large extents may actually be quite similar due to the positive relationship for fine-scale conditions over small extents (chapter 2) and the negative relationship for coarse-scale values over large extents (Figure 5.4). This means that over large extents, fine-scale heterogeneity may have no or weakly positive/negative relationships with the average conditions. For daily minimum temperatures, coarse-scale temperatures across different elevations / latitudes may be more similar in the spring than in the summer. I observed evidence of this temporal pattern in CA (Figure 5.3a). Combined with constant fine-scale heterogeneity for minimum temperatures (chapter 2), fine-scale heterogeneity over large extents may increase with warmer average conditions. If coarse-scale heterogeneity for minimum temperatures does not increase with warmer conditions as observed in CO, then the fine-scale heterogeneity may remain constant in warmer conditions.

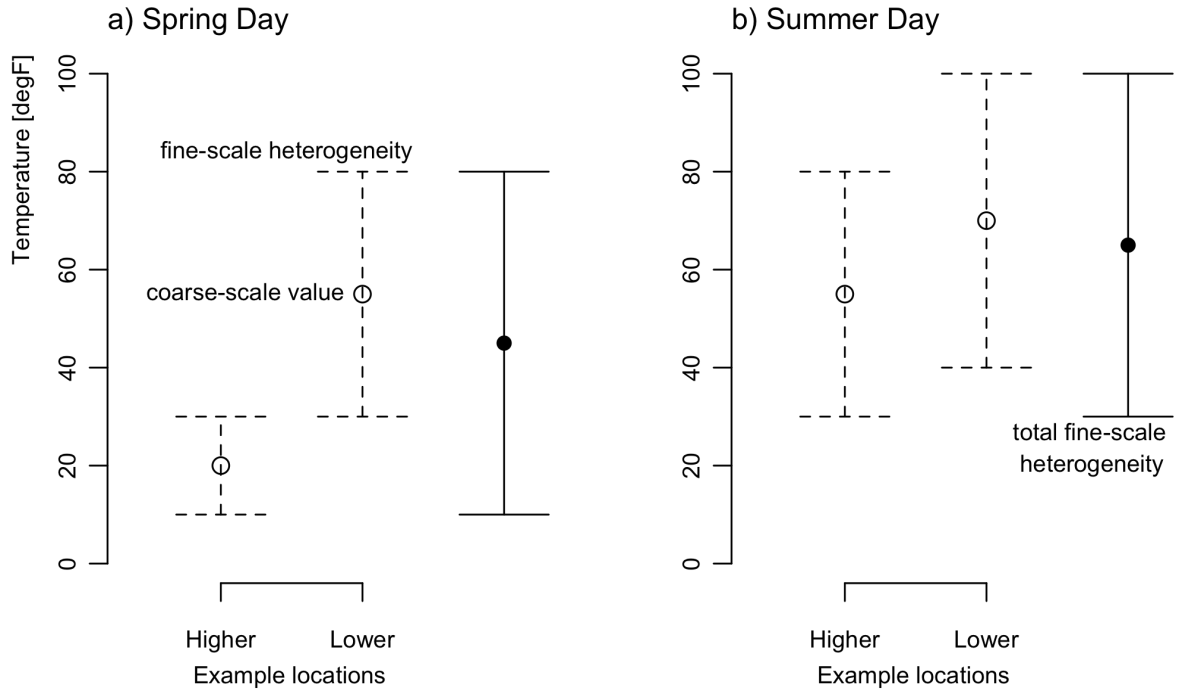


Figure 5.4: Potential fine-scale heterogeneity across large extents from considering coarse temperature values as representative of the average fine-scale conditions. For daily maximum temperatures on a spring day, higher elevations may be cooler with smaller fine-scale heterogeneity than the warmer lower elevations. In the summer, higher elevations will warm and fine-scale heterogeneity increases, while the lower elevations become hot with even larger fine-scale heterogeneity. However, total fine-scale heterogeneity on both days may be similar, which would result in no or weakly positive/negative relationships between fine-scale heterogeneity and the average fine-scale condition across large extents.

5.3. Implications of fine-scale climate heterogeneity in a warmer future

In chapter 2, I characterized the temporal patterns of fine-scale heterogeneity within a growing season over small extents. In the previous section, I reported temporal patterns of coarse-scale heterogeneity within a growing season over large extents and hypothesized that of fine-scale heterogeneity. Using these results as a guide, I next assess how climate change may impact fine- and

coarse-scale heterogeneity through the mechanisms that likely influence it (Table 5.1). I consider each factor as a main effect, *i.e.,* all other factors are held constant. Interaction effects are likely possible, but I do not consider them here for simplicity. Though I interpret the influence of vegetation change through its effects on energy input (increased IR), water dynamics, and topography, these are not interaction effects (*i.e.,* I don't consider the combined interaction effect, for example, of vegetation and water dynamics).

Table 5.1: Climate change impacts on fine-scale and coarse-scale temperature heterogeneity in mountainous landscapes. Arrows indicate that change may be able to be estimated; dashes indicate no change; and question marks indicate uncertain outcomes without further modeling efforts.

Extent	Influence	Minimum Temperature	Maximum Temperature
Effects on fine-scales over small extents	Increased IR*	—	↑
	Vegetation change	— via IR ? via moisture & topography	↑↓ via IR ? via moisture & topography
	Moisture	?	?
	Topography	—	—
Effects on coarse-scales over large extents	Weather patterns	↑?	↑?
	Elevation	↓	↓
	Latitude	↓	↓

* IR = Infrared radiation

5.3.1 Drivers of long-term change in fine-scale heterogeneity over small extents

Future climate change is driven fundamentally by an increase in long-wave infrared radiation (IR). Energy input into a landscape is fundamentally the same whether it is long-wave IR or short-wave visible radiation. Thus, there are many days within the growing season that have an analog day. I calculated analog days using differences in short-wave radiation incident at the top of the vegetation canopy. Long-wave energy input from the atmosphere and albedo losses (short-wave energy reflected) can be calculated to adjust energy input analogs for specific landscapes and time periods. In other words, there is another day within the growing season that has an equivalent amount of energy entering the landscape. As an example, I calculated the energy input analogs for Fresno, CA, the location nearest my SEKI study, for an example year of 1990 with an albedo correction of 0.2 (Figure 5.5). Most days with an energy input analog occur in the spring and fall, and a large number are less than 10 days apart. The number of summer days without an energy input analog depends on the radiative increase, ~27, 41, 51, and 71 days for RCP2.6, 4.5, 6.0, and 8.5, which have radiative forcings in W/m^2 as indicated in the scenario name (Appendix E). Generally, more radiative energy input given similar sky conditions (clear or cloudy) increases the average temperatures. And warmer average temperatures lead to increased fine-scale heterogeneity. Thus, increased IR due to climate change is likely to increase VNS maximum temperatures. As I observed no change in minimum temperatures within a growing season, I do not expect increased IR to affect VNS minimum temperature heterogeneity.

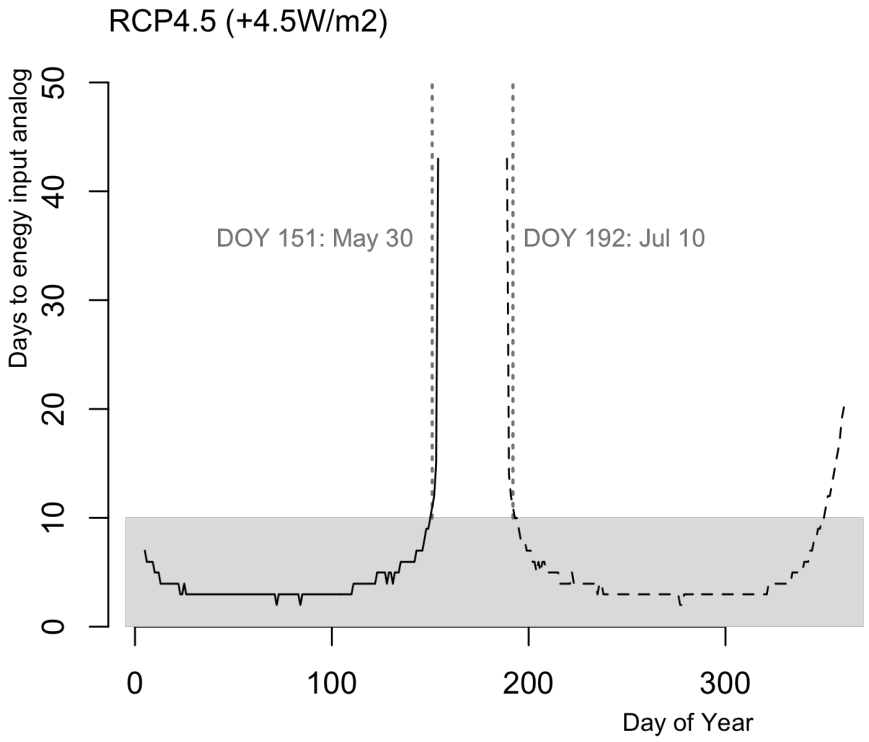


Figure 5.5: The number of days to an energy input analog for each day of year (Julian date) is shown for an energy difference of 4.5 W/m² (RCP4.5). Days forward to the analog are the solid line, and days backward are dashed. Analog days within 10 days (gray shade) are likely to have similar vegetative and soil moisture conditions. Data shown is an illustrative example from radiation observations at Fresno, CA, in 1990 with an albedo adjustment of 0.2.

Vegetation may increase or decrease fine-scale VNS heterogeneity in maximum daily temperature. My observations in chapter 2 support previous work suggesting the important influence of canopy complexity on fine-scale heterogeneity through sun/shade patterns [Hungerford and Babbitt 1987, Van Pelt and Franklin 2000, Geiger *et al.* 2009, von Arx *et al.* 2013]. Thus, change in canopy structure is likely to change heterogeneity characteristics via energy input. For example, increasing mortality of adult trees have been linked to a warmer climate in the Western U.S. [van Mantgem *et al.* 2009]. A slow thinning in canopy density could either increase or decrease fine-scale heterogeneity, the former if a very dense canopy becomes more patchy and the latter if a patchy canopy becomes more uniformly open. Long-term transitions between systems can also have different effects. For example, a transition from alpine meadow to forest, according to my findings in chapter 2, would increase fine-scale heterogeneity. Rapid change is also possible via fire, especially with intense fires that remove entire canopies. The post-canopy vegetation community may or may not increase fine-scale heterogeneity, depending on the initial heterogeneity. Pest outbreaks, such as recent pine bark beetle mortality events [Raffa *et al.* 2008], likely also affect fine-scale heterogeneity. Standing dead biomass influences fine-scale heterogeneity via sun/shade patterns, although by how much compared to a living canopy has not been empirically assessed for temperature (although it has been for snow hydrology). In addition, how long a dead canopy will remain standing or how long until it is replaced is uncertain.

All of the examples given thus far may also change the albedo of the system, which determines the amount of short-wave energy that enters the landscape and that is reflected. Amongst the mountainous sites examined in chapter 2, the forest, with more-or-less constant albedo during the

growing season, can be compared to the montane meadow, with changing albedo throughout the growing season. At the beginning of each growing season, the herbaceous forbs in the montane meadow grow anew from belowground storage tissue and then senesce at the end of the season, *i.e.,* the landscape changes from bare soil to leafy green vegetation cover to brown dried up plant matter. Both systems have similar heterogeneity characteristics: increasing heterogeneity with warmer average conditions. This relationship is less steep for the montane meadow, which may be due to changing albedo or other characteristics like the particular pattern of sun/shade or canopy height. No matter what the cause, the effect seems secondary to increasing energy input. Thus, the effects on VNS heterogeneity in maximum temperatures due to change in albedo is likely a secondary effect throughout the season compared to the daily increases in short-wave radiation.

I expect vegetation influences VNS heterogeneity in minimum temperatures indirectly through IR losses at night. Consider a semi-open forest canopy for example. IR losses are greater in open patches than below the canopy, resulting in cooler temperatures in the open areas. Thus, it is possible that the vegetation canopy complexity plays a primary role in generating VNS heterogeneity in temperature minimums. In chapter 2, I report similar levels of heterogeneity in daily minimum temperatures across mountainous sites, despite difference in canopy cover. Thus, I hypothesize that changing vegetation will have little effect on VNS heterogeneity in minimum daily temperatures.

I have focused above on the vegetative effects on VNS temperatures, primarily through canopy influences on radiative input to the surface. Vegetation can also influence heterogeneity through water dynamics and topography, although the mechanisms are much more complex. Thus, it is difficult to assess how vegetation will affect VNS temperatures through these mechanisms. Untangling them will likely require exploration via modeling.

Moisture in the soil and air may have differing effects on fine-scale VNS heterogeneity. Moisture in the soil acts both as a heat sink, requiring more energy input for temperature to increase, and as an energy output, carrying heat away from the soil surface through evaporation. When the landscape is evenly wet or dry, I hypothesize that soil moisture does not contribute much to VNS heterogeneity. However, when soil moisture is unevenly wet and dry, it is likely to differentiate locations in their ability to absorb and release energy input. Because soil moisture differences can occur at fine-spatial scales [Urban *et al.* 2000], uneven soil moisture conditions likely contribute to increased VNS temperature heterogeneity. In future analyses, I will assess the influence of soil moisture on fine-scale heterogeneity at several of the mountainous sites included in chapter 2.

Humidity, moisture in the air, can also influence temperature heterogeneity via the moisture gradient that, along with temperature itself, determines evaporative loss. Humidity's effects are likely secondary to soil moisture because of rapid air mixing, which leads to smaller spatial differences in humidity. The effect of climate change on soil moisture and humidity spatial patterns is extremely complex as they are influenced by precipitation events, soil properties, vegetation transpiration, mass air movements, and energy input. Thus, although likely to influence fine-scale VNS heterogeneity in both maximum and minimum temperatures, it is difficult to mechanistically project a particular directional change. Modeling efforts are likely required to better understand the role of hydrological dynamics on VNS temperature heterogeneity.

Topography is not likely to change in a warmer future. Thus I expect no change in fine-scale heterogeneity due to topography, which influences radiative input, hydrological dynamics, mass air movements, and fine-scale boundary layer properties (*i.e.,* VNS air mixing that due to wind and thermal expansion affects both sensible and evaporative heat loss). Vegetation canopy patterns (*i.e.,* structure) can enhance the topographic effects of mass air movement and boundary layer properties.

Therefore, vegetation change may affect VNS temperature heterogeneity via these topographic influences. I consider such change as part of the uncertain influence of vegetation in Table 5.1.

5.3.2 Drivers of long-term change in coarse-scale heterogeneity over large extents

So far I have considered change in fine-scale heterogeneity over small extents. Recalling Figure 5.4, fine-scale heterogeneity over large extents can be hypothesized by coupling coarse-scale heterogeneity temporal change with fine-scale change. In section 5.2.4, I proposed weather patterns, elevation, and latitude as likely drivers for change in coarse-scale heterogeneity over large extents. Now, I consider how coarse-scale heterogeneity may be influenced in future climates via these three drivers (Table 5.1).

Local weather events are expected to become more intense in the future, both droughts and storms. I speculate that as these events are more extreme, maximum and minimum temperatures may become more disparate across large extents causing overall increases in the magnitude of coarse-scale heterogeneity both in minimum and maximum temperature.

In general, high latitudes, especially in the northern hemisphere, are expected to warm more than low latitudes [Meehl *et al.* 2007]. Additionally, minimum temperatures are expected to increase more than maximum temperatures everywhere [Meehl *et al.* 2007]. Both empirical and modeling studies suggest that mountainous regions have warmed and will warm more than lower elevations [Rangwala and Miller 2012]. However, evidence for elevation-dependent warming is mixed. Studies that do report an elevational dependency find more warming at higher elevations with larger increases in minimum than maximum temperatures [Rangwala and Miller 2012, Pepin *et al.* 2015, but see Oyler *et al.* 2015]. It's worth noting that these findings are based on seasonal and annual average temperatures, which I found to not adequately represent daily values (chapter 2).

5.4 Potential futures for species in mountainous landscapes

What might these shifts in fine- and coarse-scale heterogeneity mean for persistence of species in mountainous landscapes? I consider implications via two approaches: (1) how change in fine-scale heterogeneity over small extents may influence future projections as made with coarse-scale tools, and (2) how fine-scale heterogeneity may change over large extents in the future.

Coarse-scale modeling tools like species distribution models inherently assume that the fine-scale conditions within each coarse-scale grain are constant. While additional study will be needed to assess the influence of vegetation and moisture dynamics on fine-scale heterogeneity in future climates, I hypothesized the effects due to future increases in IR. I expect heterogeneity in minimum temperatures to remain constant but to increase for maximum temperatures. If these expectations hold given further study on vegetation and moisture effects, then coarse-scale projections of species that are influenced by cold extremes may not be biased, and the coarse-scale modeling assumption is valid. However, the assumption may be incorrect for maximum temperatures. Species with individuals that are influenced by warm temperature extremes may persist in areas where they are projected to go locally extinct.

To estimate future fine-scale heterogeneity over large extents, I again use my hypotheses based on future increases in IR only and combine fine-scale heterogeneity with coarse-scale heterogeneity as in section 5.2.4. Increasing fine-scale and decreasing coarse-scale heterogeneity results in little to no change in fine-scale heterogeneity of maximum temperature. This result is similar to the within-season example in Figure 5.5. However, decreasing coarse-scale heterogeneity coupled with constant

fine-scale heterogeneity may lead to decreased fine-scale heterogeneity for minimum temperatures over large extents. Again these future patterns of fine-scale heterogeneity are conditional on further study of vegetation and moisture effects.

For refugia this is not the worst news. Constant heterogeneity in maximum temperatures means that the potential for heterogeneity is not reduced. For a given species, the occurrence of refugia will depend on (1) its environmental niche compared to the available conditions, *i.e.,* in Figure 5.1, the position of species presence relative to the current available conditions (*e.g.,* centered or at one of the tails of the PD), (2) the amount of current heterogeneity, *i.e.,* the width of the PD of current available conditions, and (3) the shift in the mean of the fine-scale conditions PD. If the overlap between current and future fine-scale conditions includes the species presence, then refugia will exist. This is more likely the case for species that occur in the warm tail of currently available conditions. For minimum temperatures, increases in the average conditions (*i.e.,* a shift in the mean) may offset decreases in heterogeneity. Thus, cold temperature stress may be easier to avoid for species. However, this thought experiment based on spatial heterogeneity does not account for changes in temporal dynamics, which can also affect tree seedling persistence. Events like frost may become more frequent due to earlier snowmelt, which exposes vegetation to spring weather whose variability may increase in future climates.

While I have explored potential effects of future fine-scale heterogeneity on species in this thought experiment, much uncertainty remains. Where do we go from here? I see two important directions. First, we should continue to characterize fine-scale environmental conditions in both space and time across key representative ecosystems and landscapes. Fine-scale environmental conditions are likely influencing organisms and ecological processes, as evidenced by my finding that tree seedling occupancy patterns can be explained in large part by physical environmental factors (chapter 3). Because fine-scale environs matter, heterogeneity in them is an important descriptor of the influences affecting species persistence on landscapes. Characterization tools such as the appropriate sampling design (chapter 1) and frameworks for comparing temporal patterns (chapter 2) are necessary to describe the available environs. As these fine-scale patterns are incorporated into research endeavors, existing statistical frameworks will be advanced [*e.g.,* Clarke *et al.* 2013], enabling a better understanding of the influence of fine-scale heterogeneity on organisms and ecological processes.

Secondly, mechanistic understandings of what types of landscape features contribute to fine-scale heterogeneity should be a priority. Such understanding will facilitate projections of fine-scale heterogeneity under future climates based on knowlege of how the drivers of heterogeneity change. With projections of future fine-scale environmental heterogeneity, we can target conservation efforts towards areas of high heterogeneity and maximize the potential for refugia [Lawler *et al.* 2015]. In addition, we can improve coarse-scale projections of future species geographical ranges or at least our interpretation of them. It will be important to tie mechanistic understandings of fine-scale heterogeneity to coarse-scale landscape features or phenomena so that fine-scale heterogeneity may be assessed over large spatial and temporal extents. Innovative new technologies that let us cross multiple scales, like terrestrial laser scanning, are likely key tools for this work. As these tools that capture large quantities of fine-scale data become common and enable new representations of the natural world (chapter 4), I encourage the ecological community to acknowledge what is gained, as well as, what might be lost so that we employ these new practices responsibly.

5.5 References

Arx, von, G., Graf Pannatier, E., Thimonier, A. & Rebetez, M. (2013). Microclimate in forests with varying leaf area index and soil moisture: potential implications for seedling establishment in a changing climate. *Journal of Ecology*, **101**, 1201–1213.

Ashcroft, M.B., Chisholm, L.A. & French, K.O. (2009). Climate change at the landscape scale: predicting fine-grained spatial heterogeneity in warming and potential refugia for vegetation. *Global Change Biology*, **15**, 656–667.

Battaglia, L.L., Fore, S.A. & Sharitz, R.R. (2000). Seedling emergence, survival and size in relation to light and water availability in two bottomland hardwood species. *Journal of Ecology*, **88**, 1041–1050.

Bell, D.M., Bradford, J.B. & Lauenroth, W.K. (2013). Early indicators of change: divergent climate envelopes between tree life stages imply range shifts in the western United States. *Global Ecology and Biogeography*, **23**, 168–180.

Bello, F. de, Lavorel, S., Lavergne, S., Albert, C.H., Boulangeat, I., Mazel, F. & Thuiller, W. (2012). Hierarchical effects of environmental filters on the functional structure of plant communities: a case study in the French Alps. *Ecography*, **36**, 393–402.

Bykova, O., Chuine, I., Morin, X. & Higgins, S.I. (2012). Temperature dependence of the reproduction niche and its relevance for plant species distributions. *Journal of Biogeography*, **39**, 2191–2200.

Caron, M.M., De Frenne, P., Brunet, J., Chabrerie, O., Cousins, S.A.O., Decocq, G., Diekmann, M., Graae, B.J., Heinken, T., Kolb, A., Lenoir, J., Naaf, T., Plue, J., Selvi, F., Wulf, M. & Verheyen, K. (2015). Divergent regeneration responses of two closely related tree species to direct abiotic and indirect biotic effects of climate change. *Forest Ecology and Management*, **342**, 21–29.

Chen, J.Q., Saunders, S.C., Crow, T.R., Naiman, R.J., Brosofske, K.D., Mroz, G.D., Brookshire, B.L. & Franklin, J.F. (1999). Microclimate in forest ecosystem and landscape ecology - Variations in local climate can be used to monitor and compare the effects of different management regimes. *Bioscience*, **49**, 288–297.

Clark, J.S., Melillo, J., Mohan, J. & Salk, C. (2013). The seasonal timing of warming that controls onset of the growing season. *Global Change Biology*, **20**, 1136–1145.

Clark, J.S., Bell, D.M., Hersh, M.H., Kwit, M.C., Moran, E., Salk, C., Stine, A., Valle, D. & Zhu, K. (2011). Individual-scale variation, species-scale differences: inference needed to understand diversity. *Ecology Letters*, **14**, 1273–1287.

Collins, R.J. & Carson, W.P. (2004). The effects of environment and life stage on Quercus abundance in the eastern deciduous forest, USA: are sapling densities most responsive to environmental gradients? *Forest Ecology and Management*, **201**, 241–258.

Daly, C., Taylor, G.H., Gibson, W.P., Parzybok, T.W., Johnson, G.L. & Pasteris, P.A. (2000). High-quality spatial climate data sets for the United States and beyond. *Transactions of the Asae*, **43**, 1957–1962.

Dobrowski, S.Z., Swanson, A.K., Abatzoglou, J.T., Holden, Z.A., Safford, H.D., Schwartz, M.K. & Gavin, D.G. (2015). Forest structure and species traits mediate projected recruitment declines in western US tree species. *Global Ecology and Biogeography*, **24**, 917–927.

Ford, K.R., Ettinger, A.K., Lundquist, J.D., Raleigh, M.S. & Hille Ris Lambers, J. (2013). Spatial Heterogeneity in Ecologically Important Climate Variables at Coarse and Fine Scales in a High-Snow Mountain Landscape (F. de Bello, Ed.). *PLoS ONE*, **8**, e65008.

Geiger, R., Aron, R.H. & Todhunter, P. (2009). *The Climate Near the Ground*. Rowman & Littlefield Publishers, Inc, Plymouth, United Kindom.

Gillingham, P.K., Huntley, B., Kunin, W.E. & Thomas, C.D. (2012). The effect of spatial resolution on projected responses to climate warming. *Diversity and Distributions*, **18**, 990–1000.

Grubb, P.J. (1977). Maintenance of Species-Richness in Plant Communities - Importance of Regeneration Niche. *Biological Reviews of the Cambridge Philosophical Society*, **52**, 107–145.

Hansen, J., Sato, M. & Ruedy, R. (2012). Perception of climate change. *Proceedings of the National Academy of Sciences,* **109**, E2416–E2423.

Harwood, T.D., Mokany, K. & Paini, D.R. (2014). Microclimate is integral to the modeling of plant responses to macroclimate. *Proceedings of the National Academy of Sciences*, **111**, E1164–E1165.

Hungerford, R.D. & Babbitt, R.E. (1987). Overstory Removal and Residue Treatments Affect Soil Surface, Air, and Soil-Temperature - Implications for Seedling Survival. *USDA Forest Service Intermountain Research Station Research Paper*, 1–19.

Johnson, D.M., McCulloh, A. & Reinhardt, K. (2011). The Earliest Stages of Tree Growth: Development, Physiology and Impacts of Microclimate. *Size- and Age-Related Changes in Tree Structure and Function* (eds F.C. Meinzer, B. Lachenbruch & T.E. Dawson), pp. 65–87. Springer Science & Business Media, Dordrecht.

Kolb, P.F. & Robberecht, R. (1996). High temperature and drought stress effects on survival of Pinus ponderosa seedlings. *Tree Physiology*, **16**, 665–672.

Lawler, J.J., Ackerly, D.D., Albano, C.M., Anderson, M.G., Dobrowski, S.Z., Gill, J.L., Heller, N.E., Pressey, R.L., Sanderson, E.W. & Weiss, S.B. (2015). The theory behind, and the challenges of, conserving nature's stage in a time of rapid change. *Conservation Biology*, **29**, 618–629.

Lenoir, J., Gégout, J.-C., Pierrat, J.-C., Bontemps, J.-D. & Dhôte, J.-F. (2009). Differences between tree species seedling and adult altitudinal distribution in mountain forests during the recent warm period (1986-2006). *Ecography*, **32**, 765–777.

Maher, E.L. & Germino, M.J. (2006). Microsite differentiation among conifer species during seedling establishment at alpine treeline. *Ecoscience*, **13**, 334–341.

Mclaughlin, B.C. & Zavaleta, E.S. (2012). Predicting species responses to climate change: demography and climate microrefugia in California valley oak (Quercus lobata). *Global Change Biology*, **18**, 2301–2312.

Meehl, G.A., Karl, T., Easterling, D.R., Changnon, S., Pielke, R., Changnon, D., Evans, J., Groisman, P.Y., Knutson, T.R., Kunkel, K.E., Mearns, L.O., Parmesan, C., Pulwarty, R., Root, T., Sylves, R.T., Whetton, P. & Zwiers, F. (2000). An introduction to trends in extreme weather and climate events: Observations, socioeconomic impacts, terrestrial ecological impacts, and model projections. *Bulletin of the American Meteorological Society*, **81**, 413–416.

Meehl, G.A., Stocker, T.F., Collins, W.D., Friedlingstein, P., Gaye, A.T., Gregory, J.M., Kitoh, A., Knutti, R., Murphy, J.M., Noda, A., Raper, S.C.B., Watterson, I.G., Weaver, A.J. & Zhao, Z.C. (2007). Global Climate Projections. In: Climate Change 2007: The Physical Science Basis. Contribution of Working Group I to the Fourth Assessment Report of the Intergovernmental Panel on Climate Change [Solomon, S.,D. Qin, M. Manning, Z. Chen, M. Marquis, K.B. Averyt, M. Tignor and H.L. Miller (eds.)]. Cambridge University Press, Cambridge, United Kingdom and New York, NY, USA.

Moyes, A.B., Germino, M.J. & Kueppers, L.M. (2015). Moisture rivals temperature in limiting photosynthesis by trees establishing beyond their cold-edge range limit under ambient and

warmed conditions. *New Phytologist*, **207**, 1005–1014.

Oyler, J.W., Ballantyne, A., Jencso, K., Sweet, M. & Running, S.W. (2014). Creating a topoclimatic daily air temperature dataset for the conterminous United States using homogenized station data and remotely sensed land skin temperature. *International Journal of Climatology*, 2258–2279.

Oyler, J.W., Dobrowski, S.Z., Ballantyne, A.P., Klene, A.E. & Running, S.W. (2015). Artificial amplification of warming trends across the mountains of the western United States. *Geographic Research Letters*, **42**, 153–161.

Pepin, N., Bradley, R.S., Diaz, H.F., Baraer, M., Caceres, E.B., Forsythe, N., Fowler, H., Greenwood, G., Hashmi, M.Z., Liu, X.D., Miller, J.R., Ning, L., Ohmura, A., Palazzi, E., Rangwala, I., Schöner, W., Severskiy, I., Shahgedanova, M., Wang, M.B., Williamson, S.N. & Yang, D.Q. (2015). Elevation-dependent warming in mountain regions of the world. *Nature Climate Change*, **5**, 424–430.

Peterson, A.T., Soberón, J., Pearson, R.G., Anderson, R.P., Martínez-Meyer, E., Nakamura, M. & Araújo, M.B. (2011). *Ecological Niches and Geographic Distributions (MPB-49)*. Princeton University Press.

Potter, K.A., Arthur Woods, H. & Pincebourde, S. (2013). Microclimatic challenges in global change biology. *Global Change Biology*, **19**, 2932–2939.

Raffa, K.F., Aukema, B.H., Bentz, B.J., Carroll, A.L., Hicke, J.A., Turner, M.G. & Romme, W.H. (2008). Cross-scale Drivers of Natural Disturbances Prone to Anthropogenic Amplification: The Dynamics of Bark Beetle Eruptions. *Bioscience*, **58**, 501–19.

Randin, C.F., Engler, R., Normand, S., Zappa, M., Zimmermann, N.E., Pearman, P.B., Vittoz, P., Thuiller, W. & Guisan, A. (2009). Climate change and plant distribution: local models predict high-elevation persistence. *Global Change Biology*, **15**, 1557–1569.

Rangwala, I. & Miller, J.R. (2012). Climate change in mountains: a review of elevation-dependent warming and its possible causes. *Climatic Change*, **114**, 527–547.

Soberón, J. (2007). Grinnellian and Eltonian niches and geographic distributions of species. *Ecology Letters*, **10**, 1115–1123.

Thornton, P.E., Running, S.W. & White, M.A. (1997). Generating surfaces of daily meteorological variables over large regions of complex terrain. *Journal of Hydrology*, **190**, 214–251.

Thornton, P.K., Ericksen, P.J., Herrero, M. & Challinor, A.J. (2014). Climate variability and vulnerability to climate change: a review. *Global Change Biology*, **20**, 3313–3328.

Trivedi, M.R., Berry, P.M., Morecroft, M.D. & Dawson, T.P. (2008). Spatial scale affects bioclimate model projections of climate change impacts on mountain plants. *Global Change Biology*, **14**, 1089–1103.

Urban, D.L., Miller, C., Halpin, P.N. & Stephenson, N.L. (2000). Forest gradient response in Sierran landscapes: the physical template. *Landscape Ecology*, **15**, 603–620.

Van Pelt, R. & Franklin, J.F. (2000). Influence of canopy structure on the understory environment in tall, old-growth, conifer forests. *Canadian Journal of Forest Research-Revue Canadienne De Recherche Forestiere*, **30**, 1231–1245.

Appendix A: Supplemental information for Chapter 1

A.1 Analytical derivation of the expected value of complete variance

We model the environmental characteristic Y for a given period of time as a multivariate normal: $\boldsymbol{Y_N} \sim MVN(\boldsymbol{\mu_N}, \sigma^2 \boldsymbol{K})$, where $\boldsymbol{Y_N}$ is the vector of Y values at all locations N, $\boldsymbol{\mu_N}$ is the vector of means at all locations N, σ^2 is the variance, and $\boldsymbol{K}$ is the autocorrelation matrix. In this model, we assume that (1) there is a gradient modeled in the mean; (2) the correlation matrix is a function of the distances between points only and that the relationships between points separated by the same distance are constant across the spatial extent; and (3) the variance is constant over the spatial extent. We model Y with a multivariate normal distribution for conceptual ease; however, this derivation holds with any distribution. We are restricted to working with variance in this approach as there is no analytical solution for standard deviation.

The mean of all gridcell locations, $\bar{Y}_N$, and complete variance, V_N, can be computed via standard empirical formulas:

$$V_N = \frac{1}{N}\sum_{i=1}^{N}(Y_i - \bar{Y}_N)^2 \text{ and } \bar{Y}_N = \frac{1}{N}\sum_{i=1}^{N} Y_i.$$

We can write these expressions in matrix notation as follows. First, we devolve the mean at all locations N in to a matrix $\boldsymbol{X_N}$ of intercepts of 1, x-coordinates, and y-coordinates for each location N, and a vector of coefficients $\boldsymbol{\beta}$ for each:

$$\boldsymbol{\mu_N} = \boldsymbol{X_N}\boldsymbol{\beta} = \begin{bmatrix} 1 & x_1 & y_1 \\ \vdots & \vdots & \vdots \\ 1 & x_N & y_N \end{bmatrix} \begin{bmatrix} \beta_o \\ \beta_x \\ \beta_y \end{bmatrix}.$$

In practice, $\boldsymbol{X_N}$ can be any independent variable that predicts mean at all locations N. We use spatial location in this analysis to generate spatial gradients; thus, this spatial formation of $\boldsymbol{\mu_N}$. The complete mean and variance written in matrix notation is

$$\bar{Y}_N = \frac{1}{N}\boldsymbol{J_N}\boldsymbol{Y_N} \text{ and } V_N = \frac{1}{N}(\boldsymbol{Y_N} - \bar{Y}_N)^T(\boldsymbol{Y_N} - \bar{Y}_N),$$

where $\boldsymbol{J_N}$ is a N x N matrix of 1s.

Substituting $\bar{Y}_N$ into V_N, and then rearranging:

$$V_N = \frac{1}{N}\left(\boldsymbol{Y_N} - \frac{1}{N}\boldsymbol{J_N}\boldsymbol{Y_N}\right)^T\left(\boldsymbol{Y_N} - \frac{1}{N}\boldsymbol{J_N}\boldsymbol{Y_N}\right);$$

$$V_N = \frac{1}{N}\boldsymbol{Y_N^T}\left(\boldsymbol{I_N} - \frac{1}{N}\boldsymbol{J_N}\right)^T\left(\boldsymbol{I_N} - \frac{1}{N}\boldsymbol{J_N}\right)\boldsymbol{Y_N}, \text{ where } \boldsymbol{I_N} = \begin{bmatrix} 1 & & 0 \\ & \ddots & \\ 0 & & 1 \end{bmatrix} \text{ and } \boldsymbol{J_N} = \begin{bmatrix} 1 & \dots & 1 \\ \vdots & \ddots & \vdots \\ 1 & \dots & 1 \end{bmatrix}.$$

We let

$$\boldsymbol{L_N} = \left(\boldsymbol{I_N} - \frac{1}{N}\boldsymbol{J_N}\right) = \begin{bmatrix} 1-\frac{1}{N} & & -\frac{1}{N} \\ & \ddots & \\ -\frac{1}{N} & & 1-\frac{1}{N} \end{bmatrix}, \text{ and}$$

$$V_N = \frac{1}{N}\boldsymbol{Y_N^T L_N^T L_N Y_N}.$$

$\boldsymbol{L_N}$ is symmetric, thus $\boldsymbol{L_N^T L_N = L_N^2}$. $\boldsymbol{L_N}$ is also an idempotent matrix with the property that it equals its square so $\boldsymbol{L_N^2 = L_N}$, and

$$V_N = \frac{1}{N}\boldsymbol{Y_N}^T\boldsymbol{L_N Y_N}.$$

V_N is a quadratic form, for which the expected value is analytically derived [Mathai and Provost 1992]:

$$\mathrm{E}[V_N] = \frac{1}{N}\mathrm{E}\left[\boldsymbol{Y_N}^T\boldsymbol{L_N Y_N}\right] = \frac{1}{N}\left(tr\{\boldsymbol{L_N}\sigma^2\boldsymbol{K}\} + \boldsymbol{\mu_N^T L_N \mu_N}\right).$$

Thus, the expected value for the complete variance is

$$\mathrm{E}[V_N] = \frac{1}{N}\left[\sigma^2 tr\left\{\left(\boldsymbol{I_N} - \frac{1}{N}\boldsymbol{J_N}\right)\boldsymbol{K}\right\} + \boldsymbol{\mu_N^T}\left(\boldsymbol{I_N} - \frac{1}{N}\boldsymbol{J_N}\right)\boldsymbol{\mu_N}\right].$$

A.1.1 Analytical derivation of the expected value of the sample variance

When a sample design is employed, a matrix $\boldsymbol{H}$ with dimensions s x N can be defined that samples a portion of locations s of all N locations. For example, consider a line divided into 5 locations, *i.e.,* $N = 5$. The $\boldsymbol{H}$ matrix that samples the second and third locations is a 2 x 5 matrix,

$$\boldsymbol{H} = \begin{bmatrix} 0 & 1 & 0 & 0 & 0 \\ 0 & 0 & 1 & 0 & 0 \end{bmatrix},$$

so that when $\boldsymbol{H}$ is multiplied by $\boldsymbol{Y_N}$, the vector of Y values at all N locations, only the second and third locations remain. The vector of sample locations $\boldsymbol{Y_s}$ is then

$$Y_{\boldsymbol{s}} = \boldsymbol{HY_N} \sim MVN(\boldsymbol{H\mu_N}, \sigma^2\boldsymbol{HKH}^T),$$

where $\boldsymbol{H\mu_N}$ is the vector of means for all sample locations s, and $\boldsymbol{HKH}^T$ is the matrix of pairwise Euclidean distances between all sample locations s. Carrying $\boldsymbol{H\mu_N}$ and $\boldsymbol{HKH}^T$ through the derivation for the expected value of the complete variance yields the expected value of the sample variance $\mathrm{E}[\widehat{V_s}]$:

$$E\left[\widehat{V_s}\right] = \frac{1}{s-1}\left[\sigma^2 tr\left\{\left(\boldsymbol{I_s} - \frac{1}{s}\boldsymbol{J_s}\right)\boldsymbol{HKH}^T\right\} + \boldsymbol{\mu_N^T H}^T\left(\boldsymbol{I_s} - \frac{1}{s}\boldsymbol{J_s}\right)\boldsymbol{H\mu_N}\right],$$

where $\boldsymbol{I_s}$ is the identity matrix of dimension s x s, and $\boldsymbol{J_s}$ is a s x s matrix of 1s.

A.1.2 Expected values when there is no gradient

When there is no gradient, the mean is the same for all locations. $\boldsymbol{\mu_N}$ is then a N x 1 vector of the same mean value:

$$\boldsymbol{\mu_N} = \begin{bmatrix} \mu \\ \vdots \\ \mu \end{bmatrix} = \mu\begin{bmatrix} 1 \\ \vdots \\ 1 \end{bmatrix}.$$

Thus, the second term of the expected value of the complete variance becomes

$$\boldsymbol{\mu_N^T L_N \mu_N} = \mu \begin{bmatrix} 1 & \cdots & 1 \end{bmatrix} \boldsymbol{L_N} \begin{bmatrix} 1 \\ \vdots \\ 1 \end{bmatrix} \mu = \mu^2 \begin{bmatrix} 1 & \cdots & 1 \end{bmatrix} \boldsymbol{L_N} \begin{bmatrix} 1 \\ \vdots \\ 1 \end{bmatrix}.$$

This term is zero because of the unique property of the $\boldsymbol{L_N} = \left(\boldsymbol{I_N} - \frac{1}{N}\boldsymbol{J_N}\right)$ matrix. We illustrate this for the case of N = 3:

$$\mu^2 \begin{bmatrix} 1 & 1 & 1 \end{bmatrix} \begin{bmatrix} \frac{2}{3} & \frac{-1}{3} & \frac{-1}{3} \\ \frac{-1}{3} & \frac{2}{3} & \frac{-1}{3} \\ \frac{-1}{3} & \frac{-1}{3} & \frac{2}{3} \end{bmatrix} \begin{bmatrix} 1 \\ 1 \\ 1 \end{bmatrix} = \mu^2 \begin{bmatrix} 0 & 0 & 0 \end{bmatrix} \begin{bmatrix} 1 \\ 1 \\ 1 \end{bmatrix} = 0.$$

Therefore, the expected complete variance and expected sample variance for landscapes with autocorrelation only (*i.e.,* no gradients) are the following:

$$\mathrm{E}\left[\widehat{V_N}\right] = \frac{\sigma^2}{N} tr\left\{\left(\boldsymbol{I_N} - \frac{1}{N}\boldsymbol{J_N}\right)\boldsymbol{K}\right\} \text{ and } \mathrm{E}\left[\widehat{V_s}\right] = \frac{\sigma^2}{s-1} tr\left\{\left(\boldsymbol{I_s} - \frac{1}{s}\boldsymbol{J_s}\right)\boldsymbol{HKH}^T\right\}.$$

Additional reference: Mathai, A.M. & Provost, S.B. (1992) *Quadratic Forms in Random Variables*. M. Dekker, New York.

A.2 Analytical estimates of complete variance of a 1D landscape with varying autocorrelation

We investigated the utility of the analytical derivation to estimating the complete variance using a 1D landscape with varying autocorrelation. First we briefly describe the landscapes and then present a few key results.

A.2.1 Modeling heterogeneity from autocorrelation on a 1D landscape

We divided up a unit line with extent equal 1 into N number of locations. If follows that the grain size equaled the quotient of the extent and number of locations: grain = extent/N. Although, we used 1D space, we will refer to each location as a gridcell of the line. For this exercise, we divided the line into 100 locations or gridcells, resulting in a grain size of 0.01 distance units.

We modeled the environmental characteristic, Y, at each N location on the line with the multivariate normal distribution as described in sections 1.1 and 1.2 of chapter 1: $\boldsymbol{Y_N} \sim MVN(\mu,\sigma^2\boldsymbol{K})$, where μ is the mean across locations and the covariance term is the product of σ^2, a variance parameter, and $\boldsymbol{K}$, an autocorrelation matrix. We used an exponential decay function to model the autocorrelation matrix, parameterized by the range parameter ρ:

$$\boldsymbol{K} = e^{-\boldsymbol{d_N}/\rho},$$

where $\boldsymbol{d_N}$ is a 100x100 matrix of distances between all pairwise locations on the line. Note in this formulation, we did not model gradients on the line.

We varied ρ from 0.001 to 1 distance units or 0.1 to 100 gridcells. With ρ = 0.1 gridcells, Y at each location is essentially independently and identically distributed because neighboring gridcells have essentially zero correlation. At the opposite extreme, with ρ = 100 gridcells, which is equivalent to the extent of the line, each location on the line is influenced by all other locations.

A.2.2 Sampling designs on the 1-D landscape

We investigated a series of structured and random sampling design types: Simple Structured, Clustered Structured, Simple Random, and Clustered Random. We varied the sample size and spacing within types to compare different design configurations. See Figure A6 for a description of this sampling design hierarchy and terminology. We illustrate the designs within the results figures in the following section. For each configuration, we varied the arrangement of sample locations within the extent. For each of these particular designs, we calculated the relative expected sampling error, R_s, as described in equation 1.9 in chapter 1, to evaluate how well the sample variance estimates the complete variance.

A.2.3 Results for a 1-D landscape: autocorrelation can cause significant sampling error

As seen in the ATWE Forest example, landscapes with increasing autocorrelation intensity had larger relative expected sampling error, R_s. However, the import of this effect was different depending on the particular sampling design configuration, a combination of both the sample size and spacing. As an example, we illustrate R_s for a series of Simple Structured designs in Figure A1.

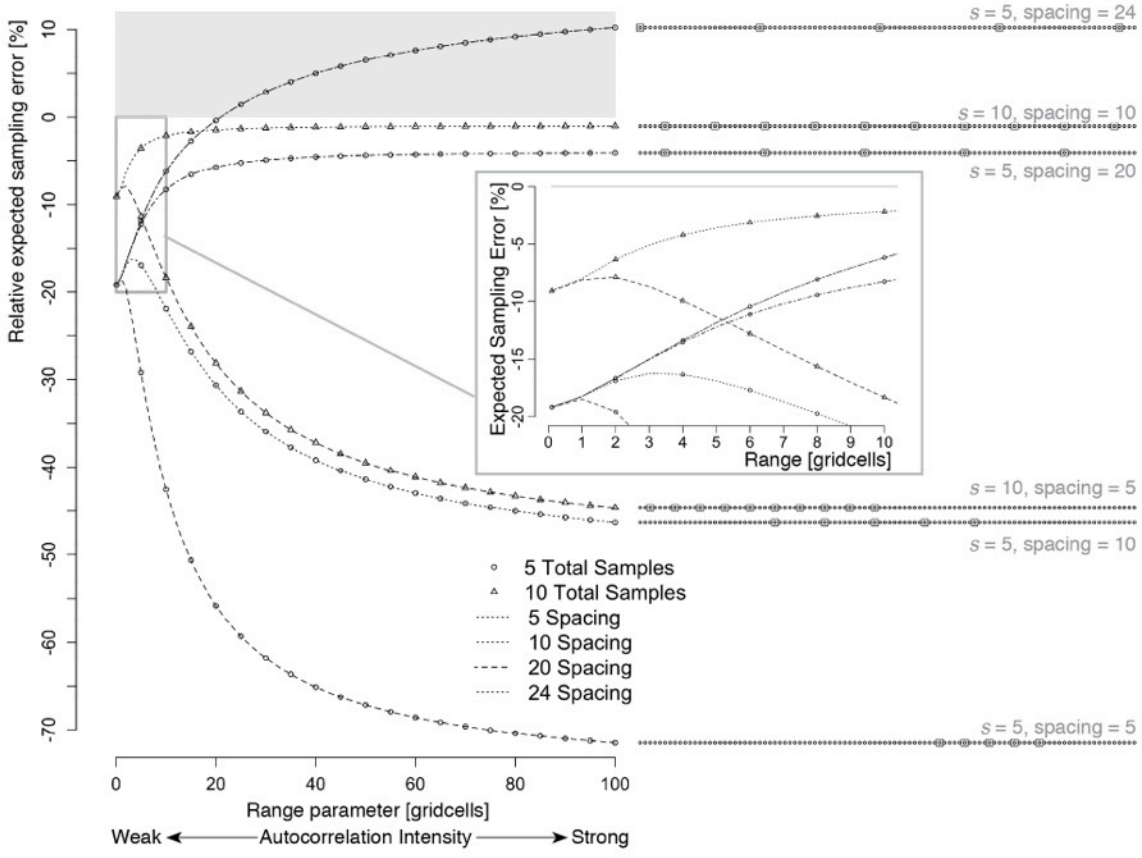


Figure A1: Relative expected sampling error, R_s, for Simple Structured designs on a 1D gridded landscape. The sampling designs are shown to the right and have the sample size, s, and sample spacing indicated. The weak autocorrelation intensity values are enlarged in the inset.

A.2.3.1 Random designs have different relative expected sampling error

As shown in Figure A2, R_s for Simple Structured designs (A2a) are identical regardless of the placement of the design within the extent (relative spatial arrangement of the sample locations is the same). For Simple Random configuration, R_s for each random design is highly variable as the arrangement of the sample locations differs between each design. Some designs over and under-sample certain areas of the line leading to large R_s, while other designs sample the line well and have near-zero sampling.

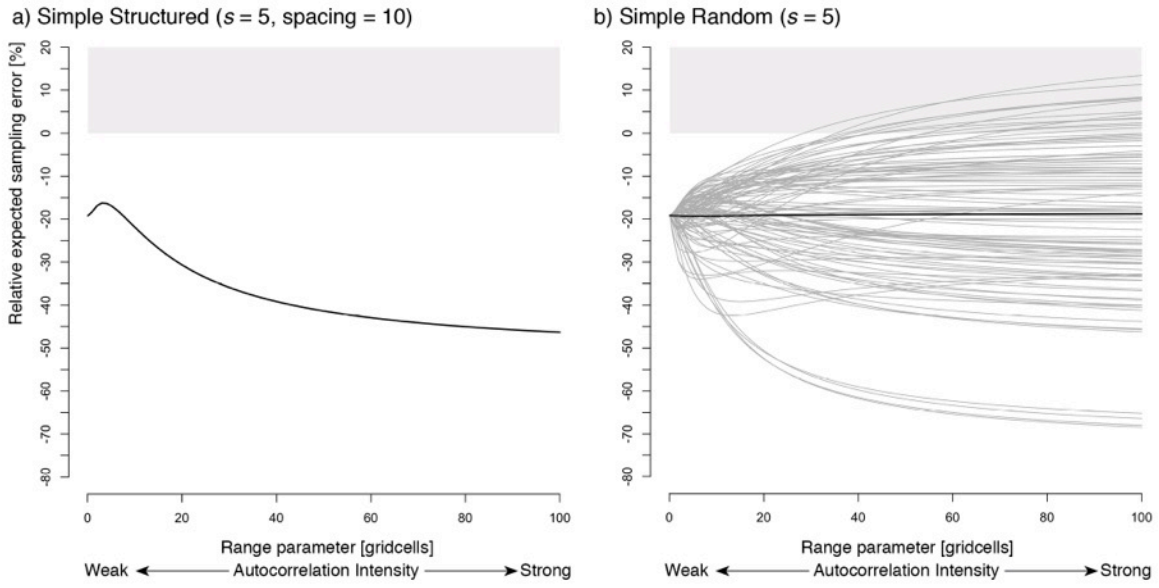


Figure A2: Relative expected sampling error, R_s, for (a) Simple Structured and (b) Simple Random designs on the 1D gridded line. Each design is a represented by a solid gray line, and the average relative expected sampling error across all 100 designs is in solid black. R_s for all Simple Structured designs are the same and therefore cannot be differentiated form the average.

A.2.3.2 Direction of relative expected sampling error is related to sample spacing

As discussed in section 1.3 of chapter 1, sample spacing plays an important role in determining how well the complete variance is estimated by a sample design and whether the sample variance is an over or underestimate. Using the analytical approach on the 1D gridded line, we preliminarily investigated the effect of sample spacing for different sample sizes. As the sample size increases the ideal average spacing must necessarily decrease, approaching 1 gridcell as the sample size nears the total number of gridcells in the extent. For example in Figure A3, the Simple Structured configuration with sample size 5 (A3a) has a larger ideal average spacing of 21, than the Simple Structured configuration with sample size 10 (A3b) with ideal average spacing of 10.

Additionally, the sample size also affects the autocorrelation intensity at which overestimates become possible. Design configurations with larger sample sizes can have overestimates at lower autocorrelation intensities than similar design configurations with smaller sample sizes. In Figure A3 the 10-sample size configuration with spacing 11 (A3b) becomes an overestimate at ~10 gridcells autocorrelation intensity, where as the 5-sample size configuration with spacing 24 (A3a) becomes an overestimate at ~20 gridcells.

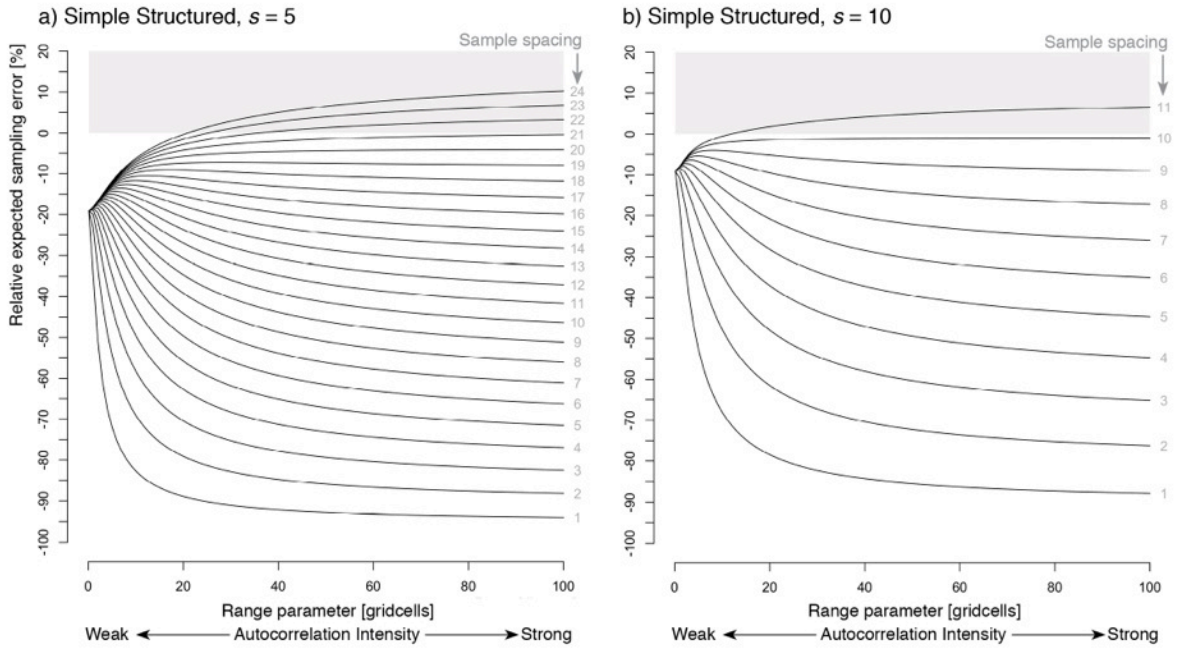


Figure A3: Relative expected sampling error, R_s, for Simple Structured designs with sample size (a) $s = 5$ and (b) $s = 10$ on the 1D gridded line. Each line represents a different sample spacing as indicated on the figure in gray at the end of each line.

A.3 Additional simulation methods

A3.1 Modeling autocorrelation with exponential distance decay

To model autocorrelation in the environmental characteristic, Y, on our simulated 50x50 gridded landscape, we used exponential distance decay, which is a function of the pairwise distance between locations and the range parameter ρ (equation 1.2 in chapter 1). We varied ρ between 0.1 and 100 gridcells. In Figure A4, we show the autocorrelation as a function of the distance between locations for selected values of ρ. When $\rho = 0.1$ gridcells, there is essentially no correlation between locations, and the landscape is in practice a random surface (Figure A5a). At the opposite extreme when $\rho =$ 100 gridcells, each location is influenced by all others on the landscape. If one imagines the Y values pulled from a hat of possibilities described by the multivariate normal model, each Y value is conditional on all the other Y values drawn when ρ is greater than zero. The greater ρ is, the greater the correlation between Y values. Thus, for an autocorrelated landscape, the sample locations cannot be considered independent, which can bias estimates of the complete variance. In Figure A5, we show examples of the 4 main landscape types, including those with autocorrelation in panels c and d. In Table A1 we describe the parameterizations for the landscapes used in each figure in the main and this supplemental text.

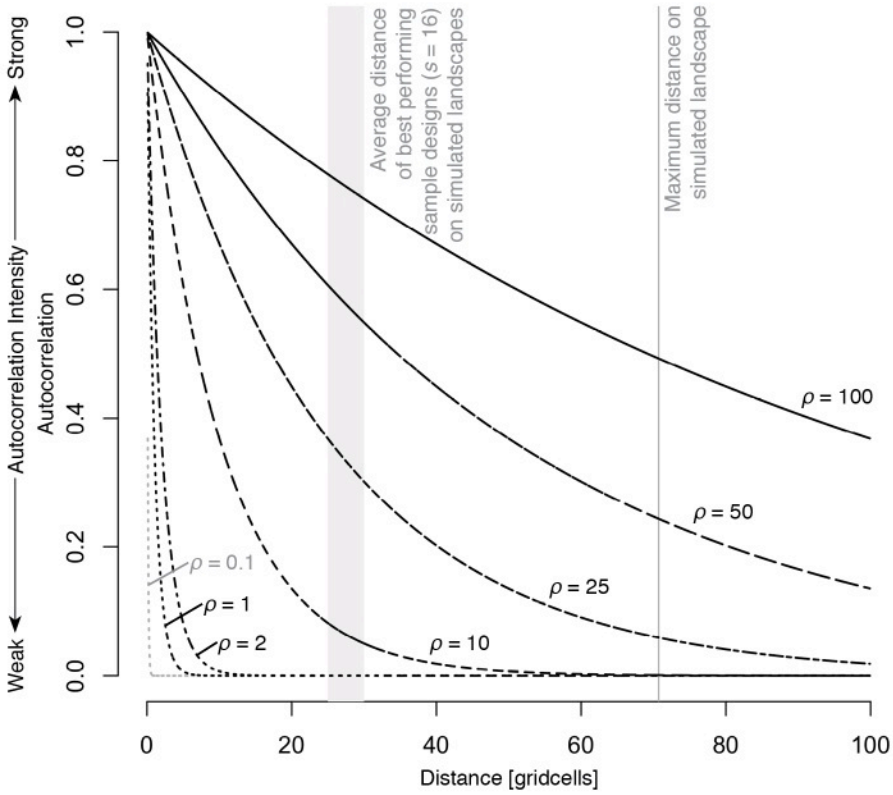


Figure A4: Exponential autocorrelation function as a function of distance for different values of the range parameter ρ. Autocorrelation values near 1 indicate high similarity between locations, while values near zero indicate low similarity between locations.

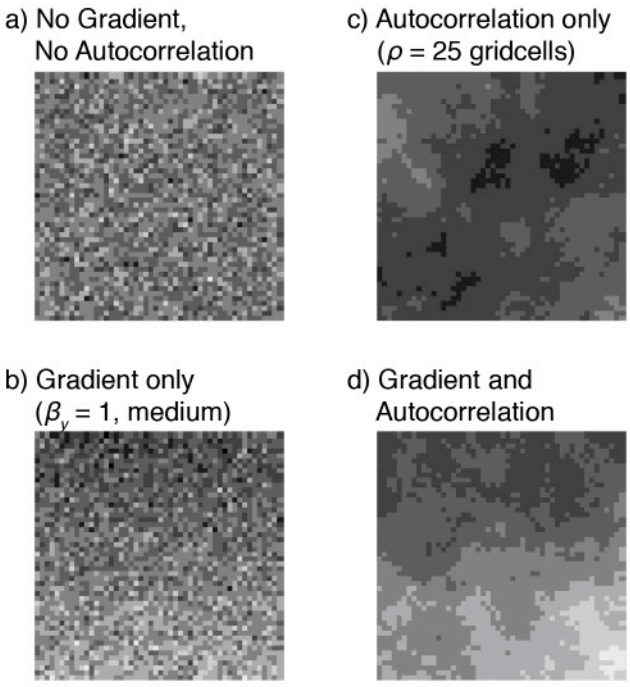


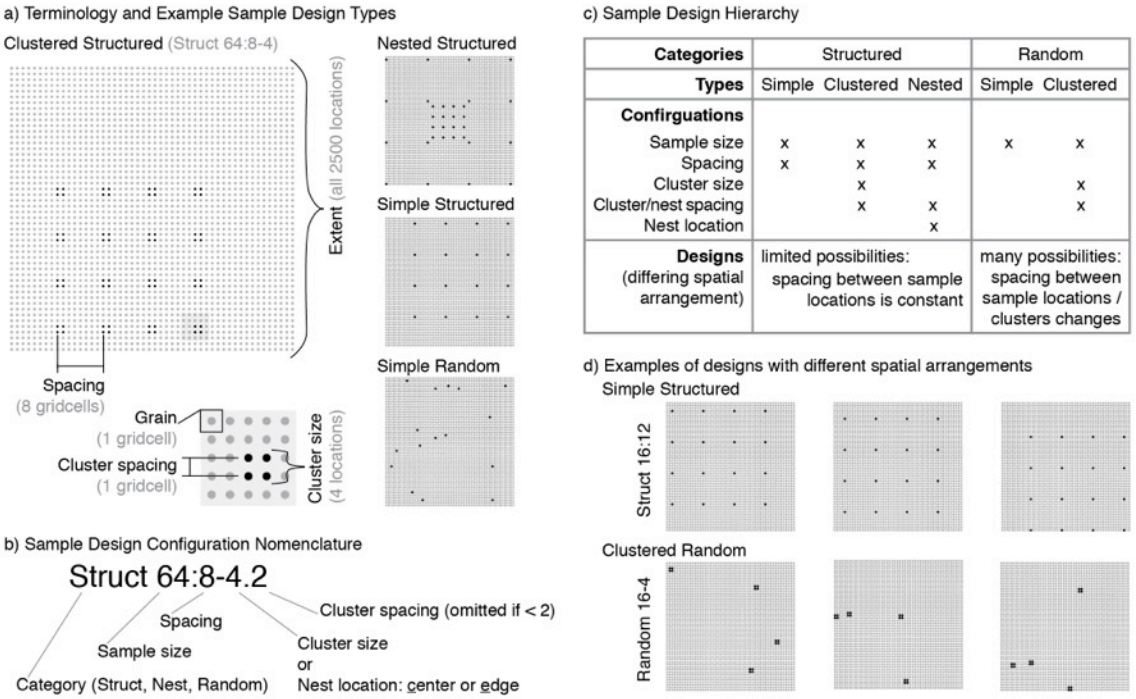
Figure A5: Example landscape types. Row 1 (a and c) has no gradient, while row 2 (b and d) has a medium strength gradient ($\beta_y/\sigma^2 \approx 1$). Column 1 (a and b) has essentially no spatial autocorrelation (ρ=0.1 gridcells), while column 2 (c and d) has medium strength spatial autocorrelation (ρ=25 gridcells).

Table A1: Landscape parameterizations used in chapter 1 figures and figures in this appendix.

Figure	Panel or column	Gradient	Autocorrelation: ρ, range parameter [gridcells]
1.1		Medium gradient: β = (0,0,2)	25
1.2		No gradient: β = (0,0,0) Medium gradient: β = (0,0,2)	0.1, 1-20 by 1
1.3	a	No gradient β = (0,0,0)	0.1, 1-20 by 1, 25-100 by 5
	b	No gradient: β = (0,0,0) Weak gradient: β = (0,0,0.1) Medium gradient: β = (0,0,2) Strong gradient: β = (0,0,10)	0.1, 1-20 by 1, 25-100 by 5
1.4	1	No gradient: β = (0,0,0)	0.1, 1-20 by 1, 25-100 by 5
	2	Medium gradient: β = (0,0,2)	
1.5	a	No gradient: β = (0,0,0)	25
	b	Medium gradient: β = (0,0,2)	
1.6	1	No gradient: β = (0,0,0)	0.1
	2	No gradient: β = (0,0,0)	25
	3	Medium gradient: β = (0,0,2)	25
A1		No gradient: β = (0,0)	0.1, 1-20 by 1, 25-100 by 5
A2		No gradient: β = (0,0)	0.1, 1-20 by 1, 25-100 by 5
A3		No gradient: β = (0,0)	0.1, 1-20 by 1, 25-100 by 5
A5	a	No gradient: β = (0,0)	0
	b	Medium gradient: β = (0,0,2)	0
	c	No gradient: β = (0,0)	25
	d	Medium gradient: β = (0,0,2)	25
A8	a	No gradient: β = (0,0,0)	0.1, 1-20 by 1, 25-100 by 5
	b	Medium gradient: β = (0,0,2)	
A9		No gradient: β = (0,0,0)	0.1, 1-20 by 1, 25-100 by 5
A10		No gradient: β = (0,0,0) Weak gradient: β = (0,0,0.1) Medium gradient: β = (0,0,2) Strong gradient: β = (0,0,10)	0.1, 1-20 by 1, 25-100 by 5
A11	a	No gradient: β = (0,0,0)	25
	b	Medium gradient: β = (0,0,2)	25

A.3.2 Sampling designs

As described in Figure A6, we investigated a series of structured and random design configurations. Each configuration varies in sample size and spacing, cluster size and spacing, and nested location and spacing. In Figure A7, we illustrate all the sampling configurations included in the analyses. In determining the best set of sampling designs to support our results (Figure A7), we ran preliminary analyses on a larger set of sampling designs, particularly structured designs. In these preliminary structured designs, we explored more combinations of sample size and spacing that informed our reported rule of thumb for sample spacing. For example, amongst design configurations with sample size 64 (8x8), sample spacing of 6 (50 / 8 = 6.2 → 6) had the smallest error. Additionally, as expected the appropriately-spaced structured designs with larger sample sizes out performed the appropriately-spaced structured designs with smaller sample sizes.



Categories	Structured			Random	
Types	Simple	Clustered	Nested	Simple	Clustered
Confirguations					
Sample size	x	x	x	x	x
Spacing	x	x	x		
Cluster size		x			x
Cluster/nest spacing		x	x		x
Nest location			x		
Designs (differing spatial arrangement)	limited possibilities: spacing between sample locations is constant			many possibilities: spacing between sample locations / clusters changes	

Figure A6: (a) We illustrate the terminology and give examples of sample design types: Clustered Structured (shown in detail), Simple Structured, Nested Structured, and Simple Random (see panel d for Clustered Random). (b) We outline the nomenclature we use to describe each sample design configuration. (c) We describe the hierarchy of sample design terminology and indicate which configuration parameters are varied for each design type. (d) We give examples of different spatial arrangements for a Simple Structured and Clustered Random configuration.

Recall that within each configuration, the particular placement of the sample design varies. For random configurations, this changes the relatively location of the samples greatly, where as for the structured designs, the relative sample locations remain constant but the entire sample layout shifts within the landscape extent. Only one design per configuration is shown.

Figure A7 (on following pages): Sample design configurations tested within each sample design type: (a) Simple Structured, (b) Clustered Structured, (c) Nested Structured, (d) Simple Random, and (e) Clustered Random. For each configuration, an example design is shown. See Figure A6 for sample design terminology.

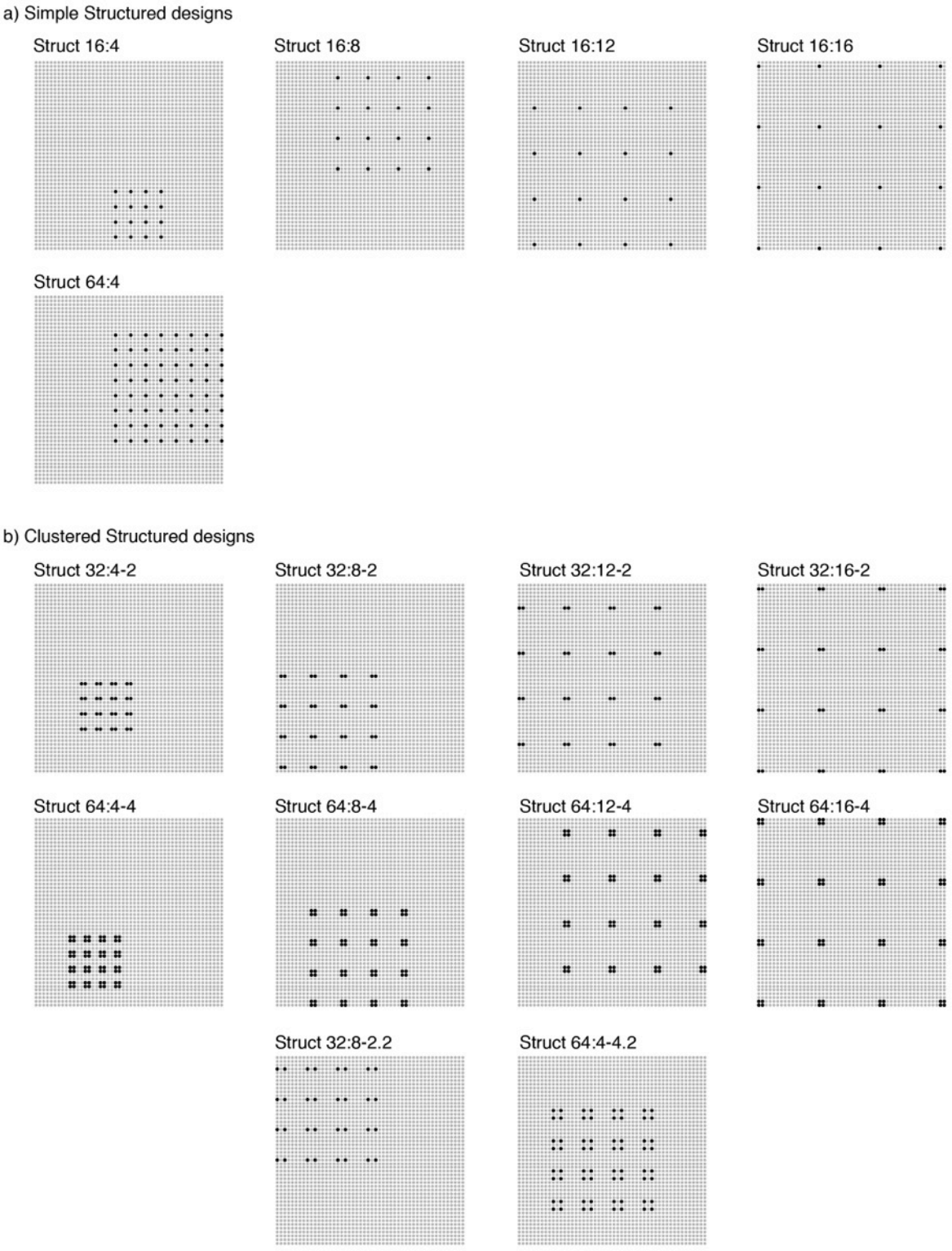


Figure A7: See caption on previous page 131. Figure continued on next page.

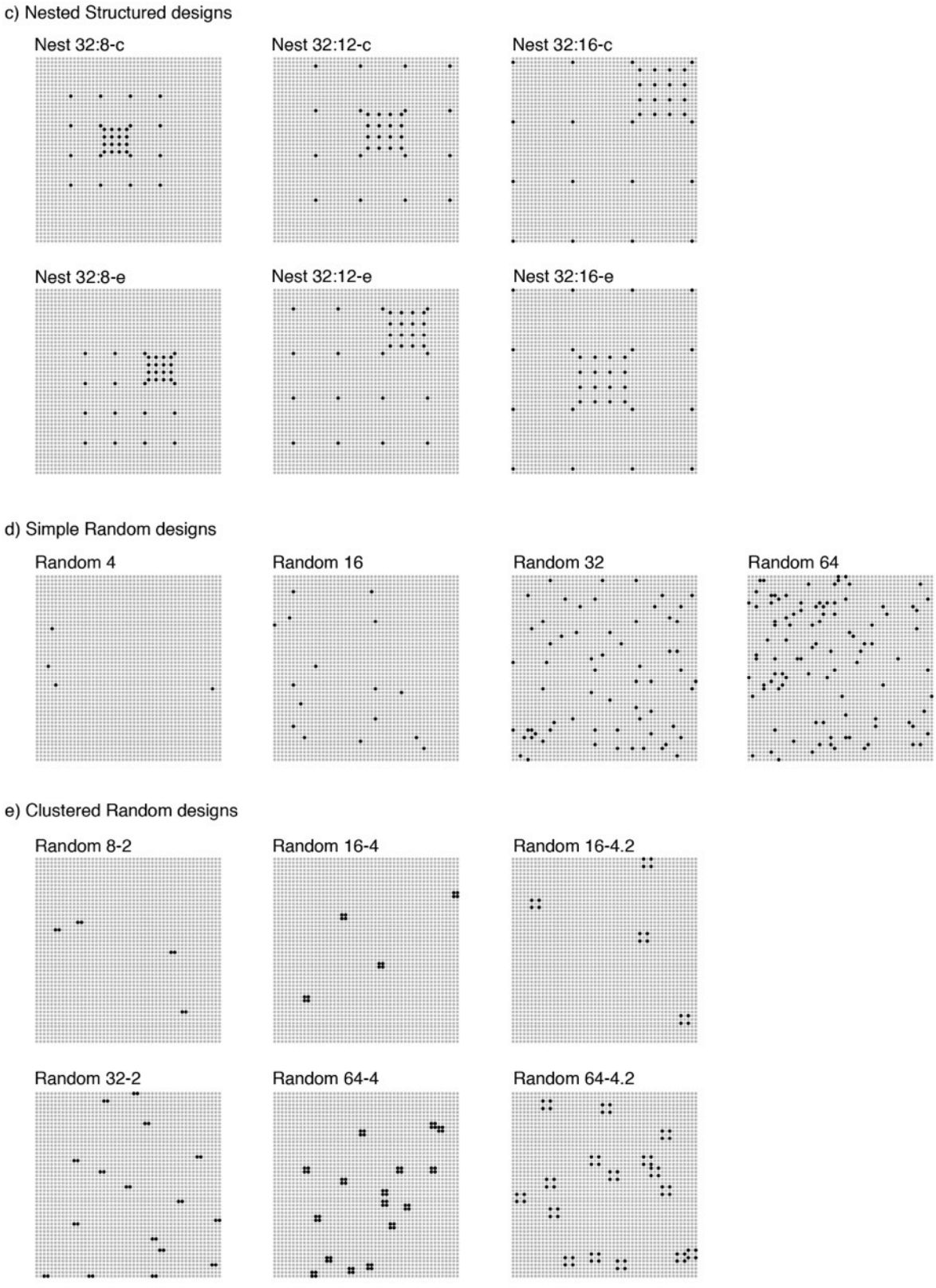


Figure A7 (continued): See caption on previous page 131.

A.4 Additional simulation results

A.4.1 Effects of design variability on average error

As described in Figure A6, within each design configuration there are several to many possible arrangements of the sample locations within the landscape extent. As shown in Figure A8, the average errors within a structured design configuration do not vary greatly. Therefore, for the structured configurations, we randomly selected a single design (*i.e.,* one of the average error lines on Figure A8) to represent the average error for all designs within the configuration. This is not the case however for the random design configurations as we discuss in results section 1.3 and Figure 1.4 in chapter 1.

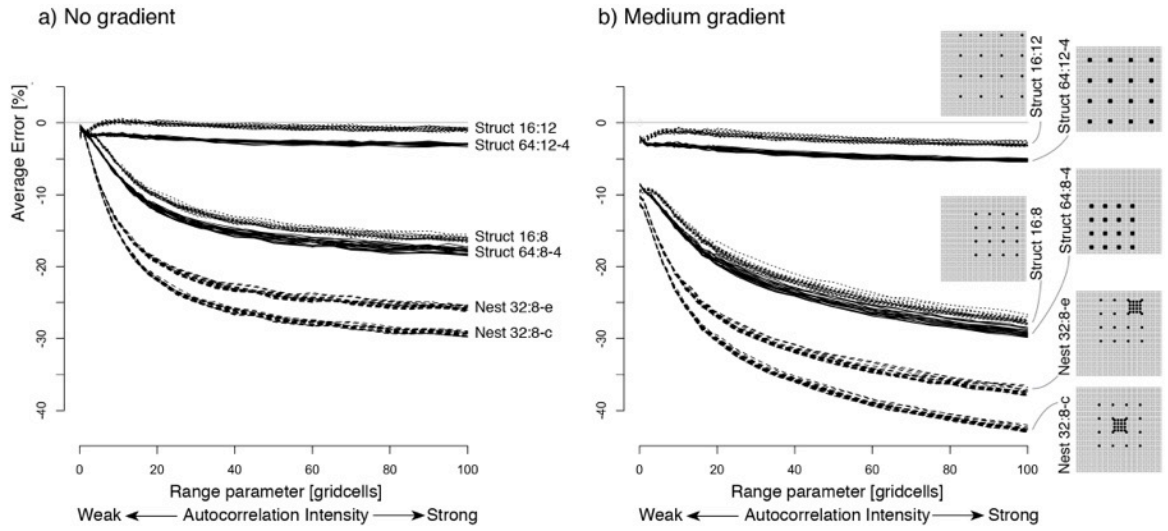


Figure A8: Range of possible average error for structured designs due to design variation, *i.e.,* different spatial arrangement of sample locations. Average error, $\bar{e}_{jk}$, is reported for 20 designs for each of 6 structured design configurations indicated, with each line representing one design. Dotted lines represent designs with sample size 16, dashed lines 32 sample size, and solid lines 64 sample size.

A.4.2 Average error is worse for Clustered or Nested Structured configurations

Many designs employed in ecological studies have clustered groupings and or nested configurations. As shown in Figure A9, most Clustered or Nested Structured design configurations estimate complete standard deviation worse than their Simple Structured analogs, even though the clustered or nested designs have a larger sample size. For example in panel b, when sample locations are added in clusters to our best performing structured configuration Struct 16:12 (solid gray near zero), the resulting configurations Struct 32:12-2 (dashed black) and Struct 64:12-4 (solid black) have larger average error across the majority of autocorrelation intensities (however, when the range is near zero gridcells, the larger sample size yields smaller error). The effect of clusters on average error is much less than nests as seen by comparing panel b to c.

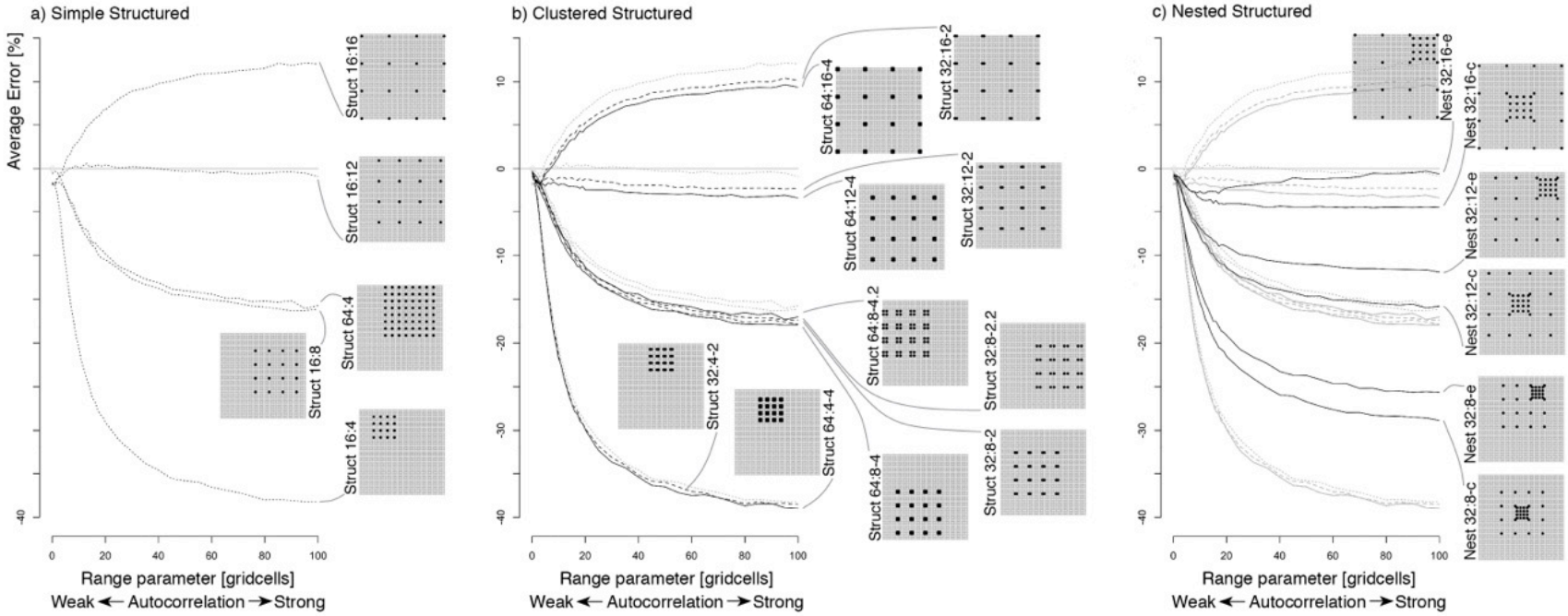


Figure A9: Average error, $\bar{e}_{jk}$, for structured design configurations on landscapes with autocorrelation only. (a), Simple Structured designs are contrasted. (b) Clustered Structured designs are shown in black while the simple designs in panel a are shown in grey for reference. Solid black lines are design configurations with cluster sizes of 4 (64 sample size) and dashed lines are configurations with cluster sizes of 2 (32 sample size). (c) Nested Structured designs are presented in black with the designs in panels a & b repeated in grey. The average error we report here is for the representative design shown.

Interestingly, for design configurations that overestimate the complete standard deviation (positive error values), the addition of sample locations in clusters or nests improves estimates of the complete standard deviation. The improvement is minimal for clusters but can be substantial for nests depending on the relative location of the nest.

Adding sample locations in clusters or nests decreases the average sample spacing. As discussed in results section 2 of chapter 1 and A2.3.2, a sample spacing threshold in part characterizes whether a sample configuration under or overestimates the sampling error. For designs that underestimate sampling error, the sample spacing is smaller than the threshold. Thus, decreasing that spacing by adding clusters or nests worsens the design's estimate of complete standard deviation. On the other hand, for designs that overestimate sampling and have a sample spacing larger than the threshold, decreasing the sample spacing with clusters or nests yields improved estimates. The effect of the nest location is likely related to its effect on average sample spacing as well. When located in the center of the structured layout, the reduction in average sample spacing is greater than when located on the edge of the layout.

A.4.3 Effect of gradients on Clustered or Nested Structured configurations

Gradients have similar effects on Clustered or Nested Structured designs as they do on Simple Structured designs; the magnitude of effect is dependent on the configuration, and stronger gradients have stronger effects. In Figure A10 panel 1, we see that clustered designs that perform consistently well across the range of autocorrelations (b) are less affected by gradients that designs that significantly under or overestimate the complete standard deviation (a and c). For all clustered configurations, gradients worsen performance.

For most Nested Structured designs, gradients generally worsen performance similar to the clustered configurations. The exception, Nest 32:16-e (a), is illustrated in Figure A10 panel 2. While the pattern of the gradient effect is consistent with simple and clustered designs (*i.e.,* the average error increases in absolute value), for some autocorrelation scenarios (range less than 20), Nest 32:16-e performs better on landscapes with a medium gradient.

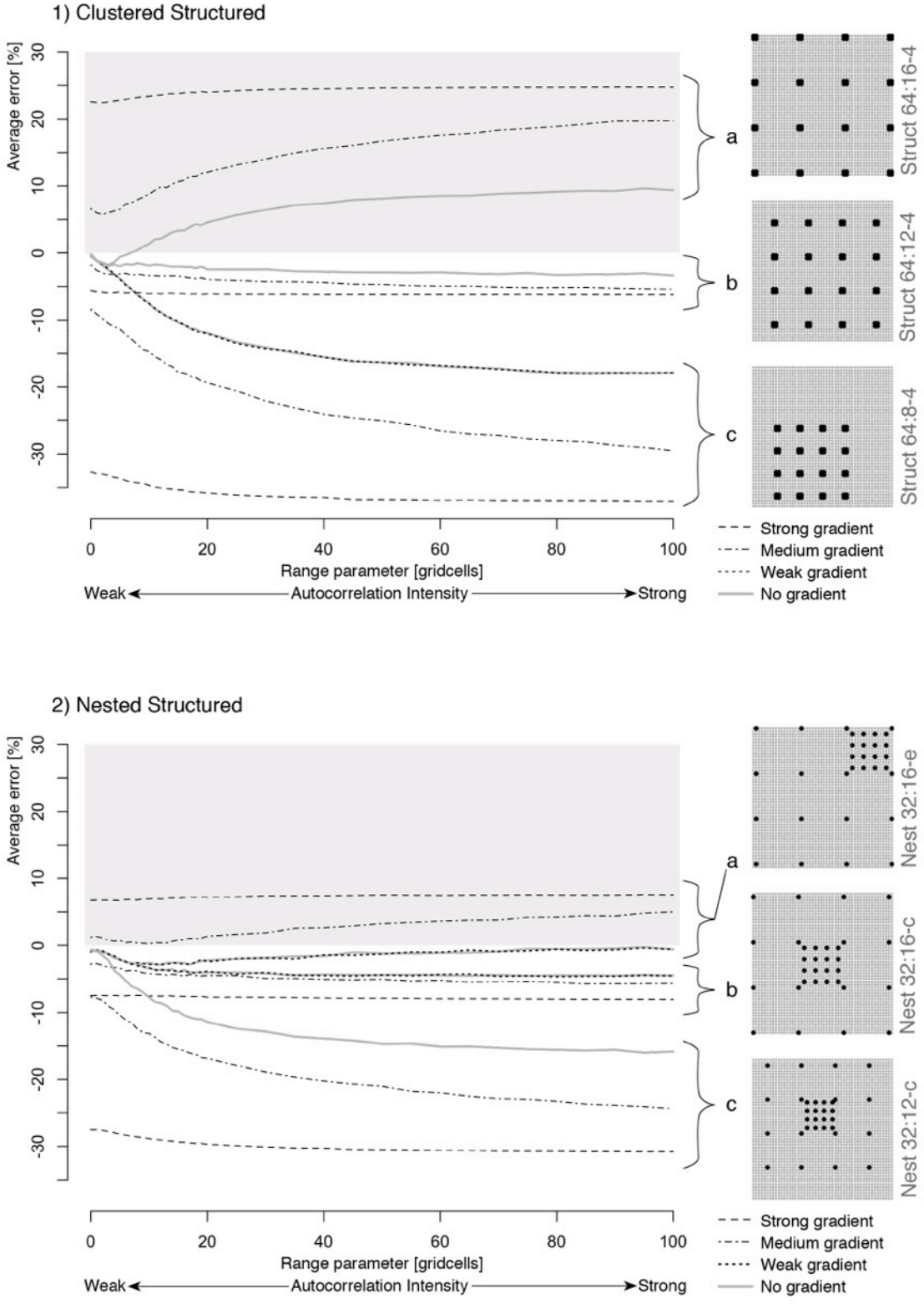


Figure A10: Average error, $\bar{e}_{jk}$, for Clustered (panel 1) and Nested Structured (panel 2) design configurations on landscapes with different gradient strengths.

A.4.4 Spread due to landscape variation is characteristic of configuration not sample spacing

As shown in Figure 1.5 in chapter 1, the average error, $\bar{e}_{jk}$, is correlated with the average sampling distance. We do not see a similarly strong relationship with the spread around $\bar{e}_{jk}$, as measured by the standard deviation of raw sampling error, $e_{jk}^{(i)}$, over the 10,000 simulated landscapes. Instead, as shown in Figure A11, the type of sample configuration appears to determine a more-or-less constant spread. For example, in panel a for landscapes without gradients, the Random 4 configuration has a spread of 35-40%, which is distinct from the spread of Random 16 with a spread of 28-33%. For landscapes with gradients (panel b), the variability in spread increases and a weak correlation with average sampling spacing appears to exist for the random design configurations.

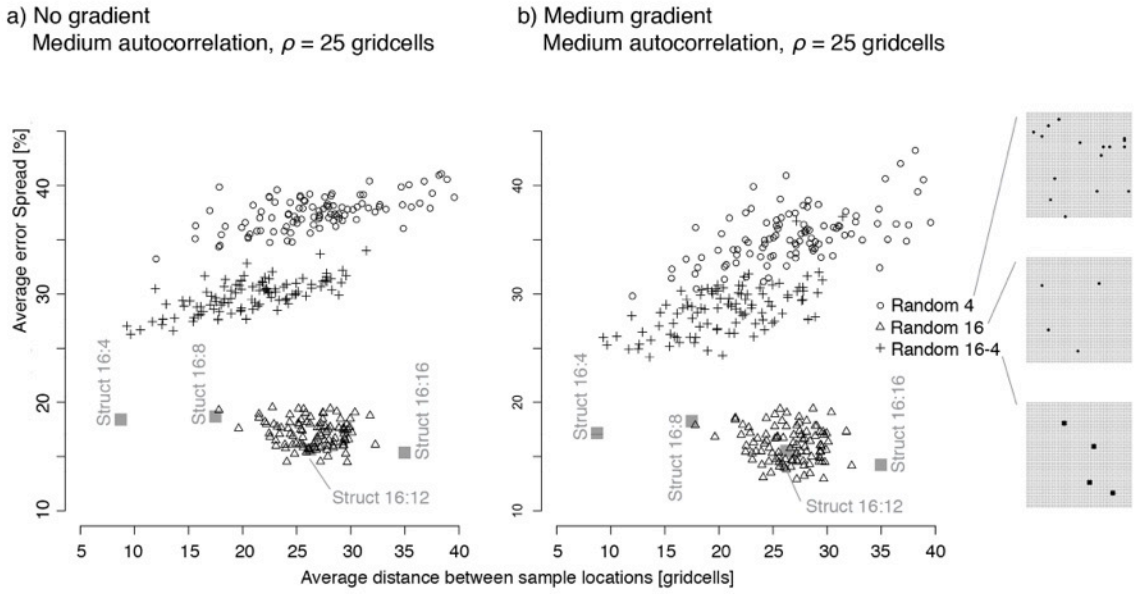


Figure A11: Spread in average error due to landscape variation on the y-axis versus the average distance between sampling locations reported in gridcells on the x-axis. Spread is measured by the standard deviation of sampling error across 10,000 simulated landscapes for each particular design within a design configuration. These designs are the same for which results are reported in Figure 1.4 and Figure 1.5 in chapter 1.

Appendix B: Supplemental information for Chapter 2

B.1 Additional methods

For each study site, we give design schematics, data quality assessment details, and expected error in estimates of heterogeneity due to the sampling design.

B.1.1 Estimating expected sampling error in standard deviation

To account for spatial autocorrelation and spatial gradients that are most likely present in each study, we estimated the sampling error standard deviation following the methods described in chapter 1. For each study, we first gridded the landscapes into gridcells with a grain size commensurate with that used in the study. Then, we simulated measurement values for each gridcell using the model described in the simulation study varying the autocorrelation intensity and gradient strength. Next, we then compared the sample standard deviation calculated from the sample design employed in the study to the complete standard deviation calculated from all gridcells within the extent. We reported the sampling error, which is the percent difference between the sample standard deviation and the complete standard deviation. Negative values indicate that the sample standard deviation underestimated the complete standard deviation and positive values indicate an overestimation. We calculated the average sampling error from the sampling error for 10,000 modeled landscapes with each landscape parameterization as described below. We assessed the average sampling error expected in the SEKI and ATWE studies as described below, as well as the spread around the average. We based our expectations for RMBL and REV based on the conclusions of chapter 1.

We assessed the sampling error for a range of spatial autocorrelation intensities and gradient strengths. We took this approach because for most of our studies we cannot estimate a single autocorrelation intensity or gradient strength. For autocorrelation intensity, we used a exponential decay function to describe how similar one gridcell was to its neighbors. We varied the range parameter from 0.1, indicating no autocorrelation, to 100 gridcells, for which gridcells influence each other up to 100 gridcells away. For SEKI, 100 gridcells is a quarter of the extent in the 600m direction and for ATWE it is equal to or twice the maximum extent dimension. We modeled gradients by multiplying each gridcell's coordinate in the gradient direction by a constant gradient factor. We defined weak, medium, and strong gradients by gradient factor to variance ratios of 0.1, 2, and 10, respectively.

B.1.2 ATWE

The sampling designs employed at ATWE (Figure B1) were chosen to sample a range of canopy cover and surface rockiness at each elevation. Data quality was assured by a series of processing steps. First, an automated cleaning process eliminated any 15-minute measures above and below extreme cutoff levels. We then gap-filled the time series at each elevation separately using Multi-channel Single Spectrum Analysis [Kondrashov and Ghil 2006]. This process uses correlations in space and time to estimate missing values. The gap-filled data was manually inspected to remove erroneous estimates.

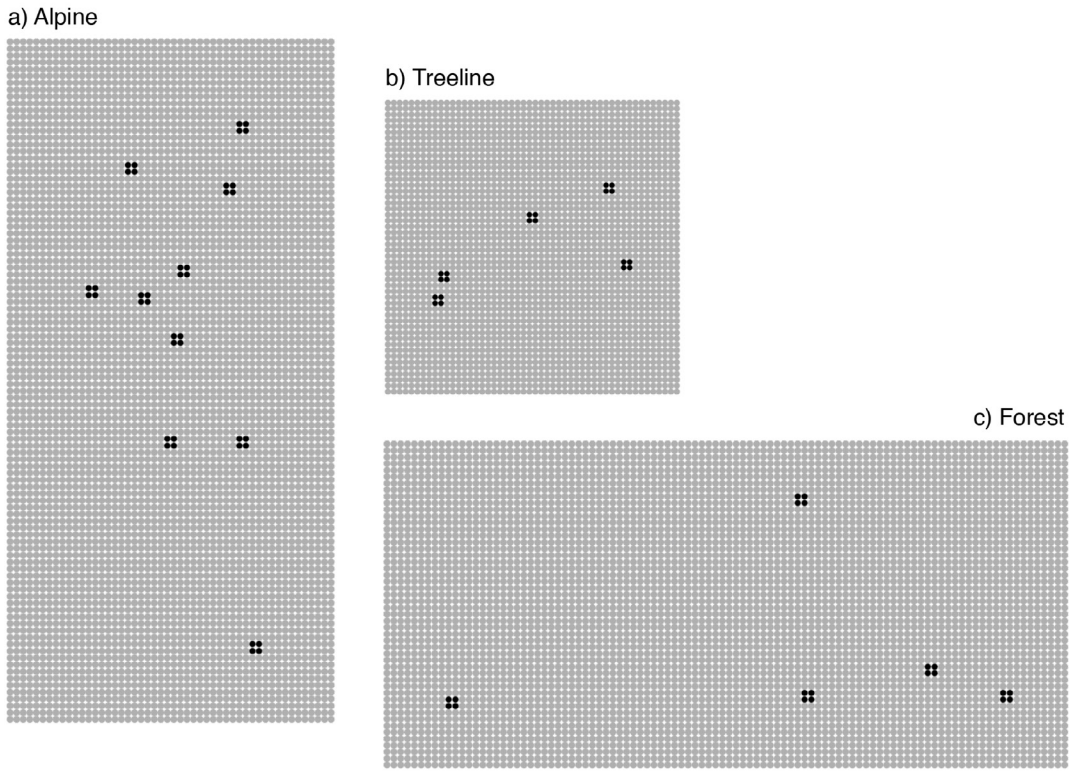


Figure B1: ATWE sampling designs represented as gridded landscapes for the (a), Alpine (b) Treeline, and (c) Forest elevations. The gridcell resolution (grain) is 1m. Four sensors per plot are shown.

For the ATWE study, we compared two sampling possibilities: all 4 sensors per plot and 1 sensor per plot for each elevation. We use a gridded landscape of 50x50 gridcells for the Treeline site and grids of 100x50 for both the Alpine and Forest sites to correspond to each elevation's extents and grains in a 1:1 ratio (*i.e.,* the grain size = 1m). We suspected a medium gradient at Alpine due to elevation; possibly a weak elevational gradient at Treeline; and no gradient at the Forest site. Our spatial autocorrelation expectations also varied at each elevation: at Alpine we expect no to low autocorrelation intensity (0-10 gridcells) due to local topography; at Treeline, we expect low to medium autocorrelation intensity (5-20 gridcells) that corresponds to the patchy krumholtz pattern; at Forest, we expect low to medium autocorrelation intensity (5-20 gridcells) due to patchiness in canopy cover. Nevertheless, we show the average sampling error for the full suite of scenarios in Figure B2. Based on these results, we used 1 sensor/plot sampling design at each elevation because it yielded sampling errors closer to zero in all cases. Most scenarios in the expected autocorrelation ranges underestimated the complete standard deviation, excepting the unlikely strong gradient for the 1 sensor/plot scenario at Forest that has approximately zero sampling error. The spread around the average sampling error is substantial, especially for the Treeline and Forest elevations, each with a total sample of 5 compared to 10 for Alpine in the 1 sensor/plot design. For the surface parameters that we expect, we estimated an average sampling error (5th and 95th quartiles for autocorrelation surfaces less than 21 gridcells for medium gradients) the following at each elevation: Alpine -7 to -10% (-42%, 25%), Treeline -5 to -10% (-59%, 47%), Forest -3 to -5% (-56%, 51%). Thus, the heterogeneity (standard deviation) that we report is on average conservative, *i.e.,* it is likely to be higher than our estimates. For mean-heterogeneity relationships, positive slopes are likely to be more positive and negative slopes more negative.

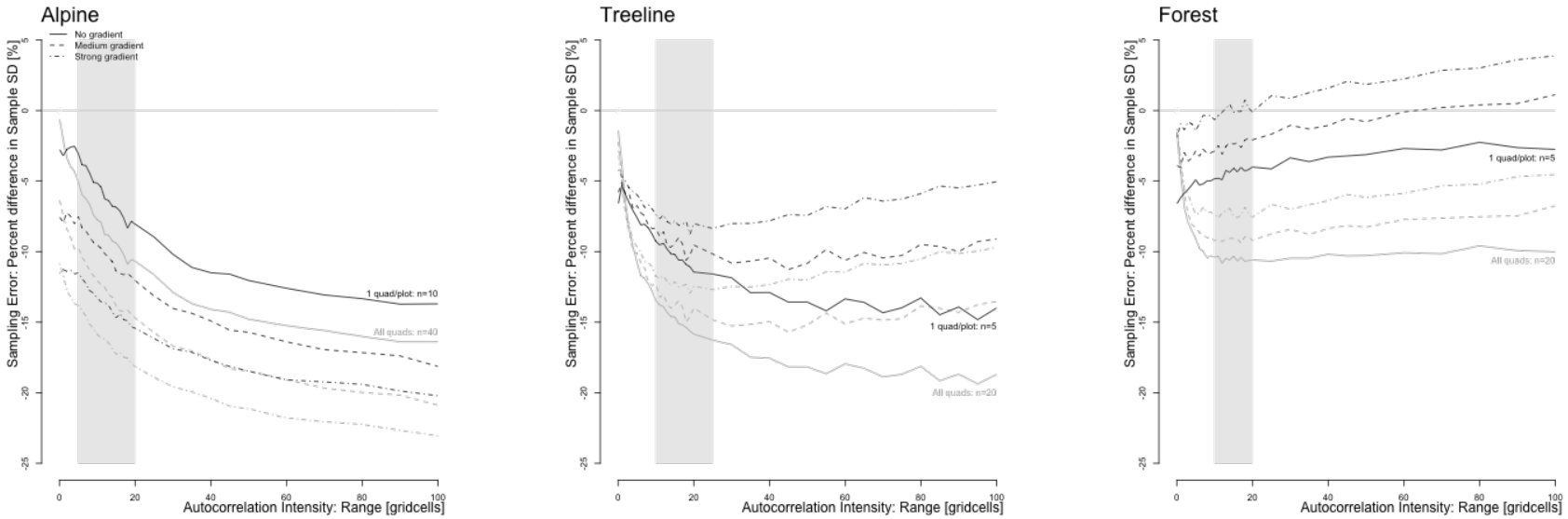


Figure B2: Average sampling error for each ATWE study site calculated from 10,000 surface landscapes for different gradient strength and autocorrelation intensity combinations. Autocorrelation intensity on the x-axis is parameterized by the range parameter. Results for no gradient (solid line), medium gradient (dashed line), and strong gradient (dot-dash line) are shown for 2 sample designs: 4 sensors/plot (gray) and 1 sensors/plot (black). Grayed areas indicate the expected autocorrelation intensity.

B.1.3 RMBL

We used 5 control plots each with 3 sensors in the RMBL study (Figure B3). Data was cleaned manually based on the following criteria. (1) Any value that fell obviously outside of the normal diel pattern was removed. Typically this means a difference of > 7-8 degrees but depends on the pattern observed for each sensor. These points were identified by looking at one year of data together and identifying the points that clearly stood apart from the general series. (2) Values that were boarder-line outside the normal diel pattern were then checked for position in the time series. Time steps that did not occur between their neighbors or at least near their neighboring time steps were considered erroneous. In other words, a more-or-less smooth pattern was expected from the 2-hour data. While it is true that an animal could have caused an unusual value, for this work, we consider this type of event an anomaly. Also, short-lived storms could cause unusual patterns, but ping-pong temperature changes of > 7-8 degrees at 12cm depth over the course of 4 hours is suspect. (3) Drastic changes in the diel range were removed. This type of pattern suggests sensor calibration issues.

The RMBL sampling design is essentially a structured rectangular grid (12x3m spacing) and the sample size (n=15) is approximately 1% of the extent (70x16m) if a grain of 1m is assumed. We expected a strong gradient in the y direction due to elevation and soil water and a no to weak gradient in the x direction due to aspect,. Additionally we expected no to low spatial autocorrlation intensity from topography and vegetation cover. In chapter 1, we found that a structured sample design evenly spaced within the extent yields small negative sampling errors (< 1%). While these results were for a square grid, we expect that they hold as the sampling configuration is similar. Thus we are confident in the heterogeneity itself and mean-heterogeneity relationships reported.

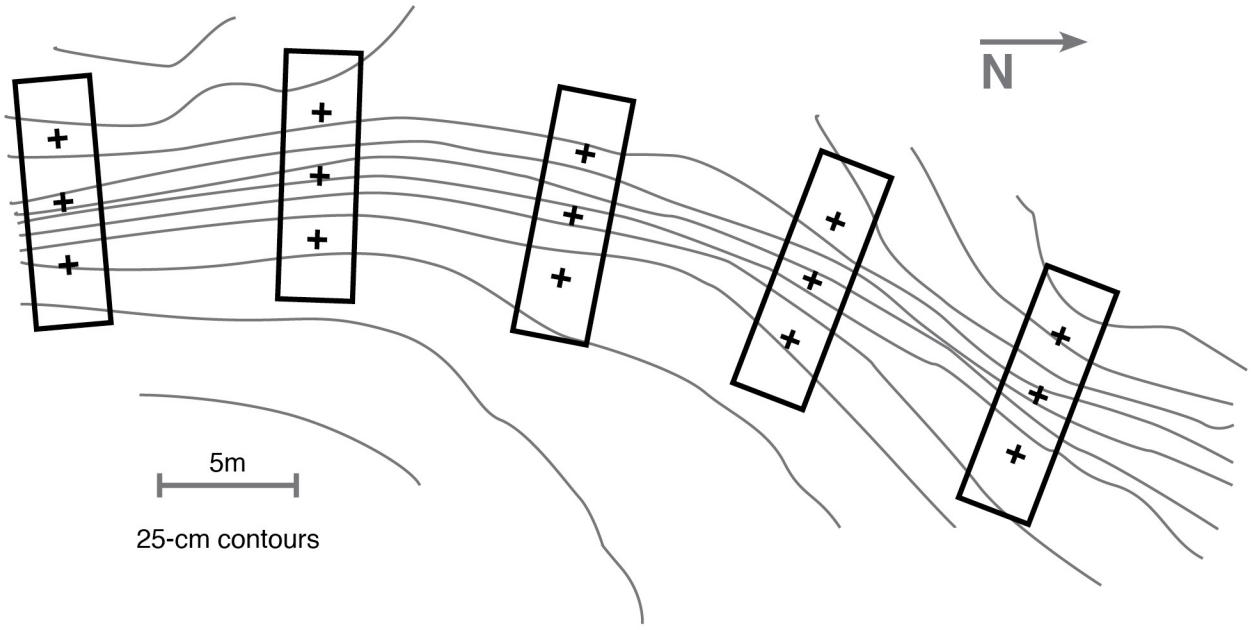


Figure B3: RMBL study design. Figure follows design reported in Dunne *et al.* 2003. Only control plots are shown with sensor locations marked with a cross. Ridgeline is on the western edge of the plots.

B.1.4 REV

The representative study design reported in Dunne et al. 2003 for each L, M, and U site consists of a stratified random sample over an elevational gradient (Figure B4). Without explicit location information, we cannot assess the expected error of the designs employed. However, because of the stratification across the elevational gradient, the sample spacing is relatively even and spread well across the study extent. Additionally, because the samples are arranged across the gradient, we expect relatively small effects of the gradient on the estimated heterogeneity (i.e, relatively small increases in error due to the gradient pattern). While we are unable to confidently report a likely direction of estimation error, we are confident that the sampling design is not an extreme case with large over or underestimation.

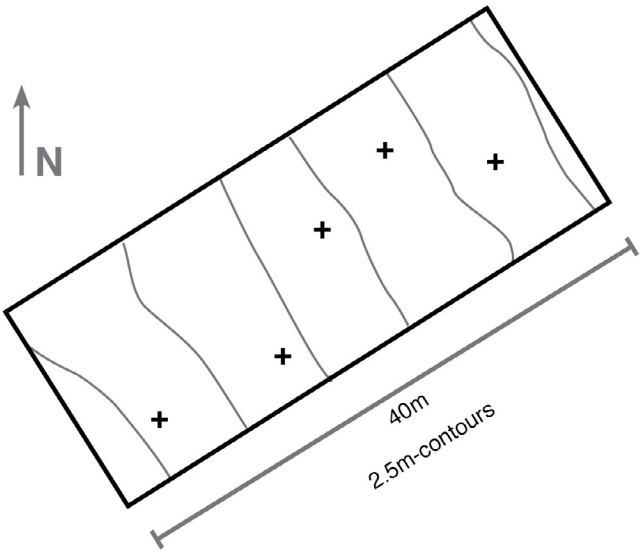


Figure B4: Representative sample design for the REV study. Illustration recreated from Dunne *et al.* 2004 with the author's permission.

B.1.5 SEKI

We assessed data quality at the SEKI manually following the same procedure outlined for the RMBL data. We found no erroneous data points. Additionally, to assess the comparability of the observations between sites, we installed 15 pairs of sensors as close as possible to each other (~1cm apart) across the study site from DOY 154–286 (June 2–Oct 13) in 2014. The mean absolute difference was 0.35°C with standard deviation 0.49°C. These values include several known outliers that occurred with one of the pairs. Despite that the difference is within the sensor specifications (±0.5°C). Some sensor pairs had near-zero differences, while others differed 1-2°C at times that generally corresponded to higher average temperature of the sensor pair. In other words, when temperature differences occurred, they occurred at higher temperatures. This relationship suggests a vertical offset between the sensor pairs. As energy enters the system primarily through incident radiation, the soil surface warms throughout the day. The amount of warming increases throughout the summer. The temperature profile within the soil near the surface can be quite steep so that small differences in vertical position can lead to errors. However, the largest differences that we observed in our sensor pairs (usually in maximum temperatures) are smaller than the smallest maximum temperature heterogeneity differences that we observed at the SEKI study site. Thus we do not expect our results to be affected by any vertical offsets.

We compared two sampling possibilities for the study site: all 225 locations and a triangular grid of 98 evenly spaced (~12m apart) locations (Figure B5). We tested these sampling designs on a 388x14 grid, which corresponds to the study plot dimensions of 640x20m, with grain size 1.5m. There is a

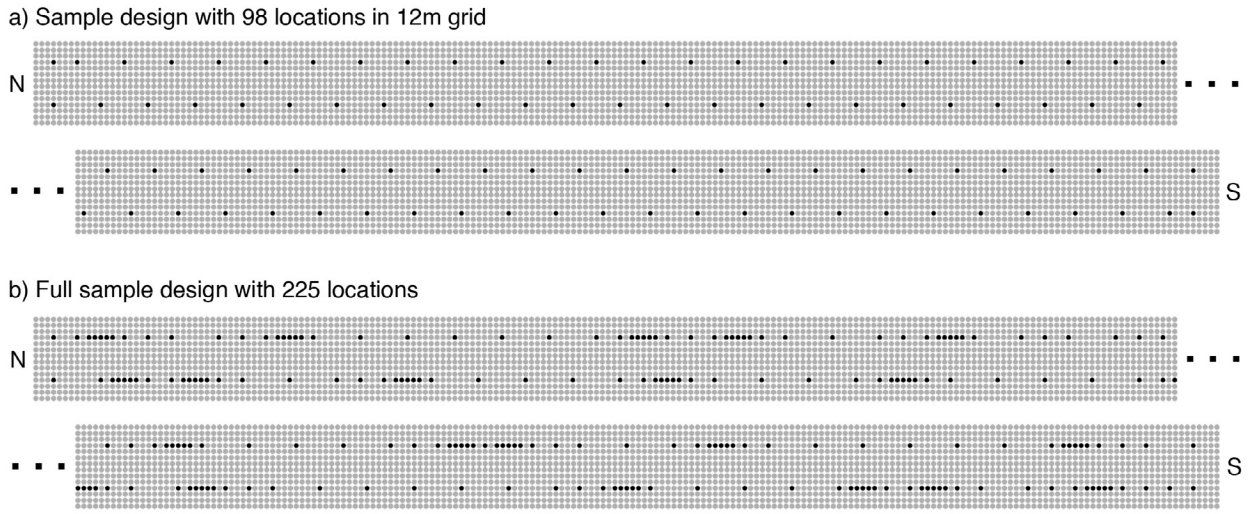


Figure B5: SEKI sampling design represented as a gridded landscape with gridcell resolution 1.5m. Plot is split along 600m length as indicated by the dotted break. The plot is oriented with North (N) on the left and South (S) on the right. (a) The sampling case with 98 locations evenly spaced 12m apart. (b) The full sampling design with 225 sensor locations.

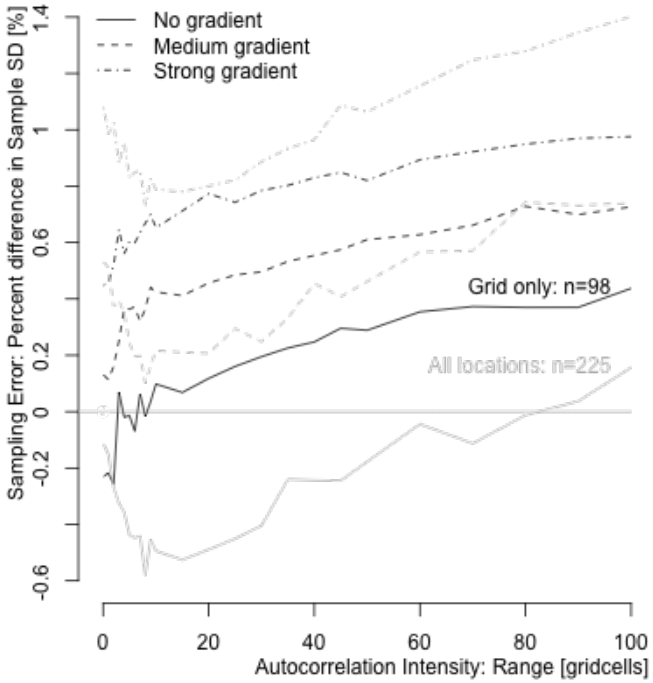


Figure B6: Average sampling error for SEKI sample designs calculated from 10,000 surface realizations for different gradient strength and autocorrelation intensity combinations. Autocorrelation intensity on the x-axis is parameterized by the range parameter. Results for no gradient (solid line), medium gradient (dashed line), and strong gradient (dot-dash line) are shown for 2 sample designs: All 225 locations (gray) and a 98-location triangular grid (black). Grayed areas indicate the suspected autocorrelation intensity.

gradient in the x-direction due to aspect that varies from North to South via West. Thus we included surface types with both a medium and strong gradient in the x-direction. The study's sampling design was originally employed to estimate spatial autocorrelation, thus we have estimates of the spatial autocorrelation, which are between 2-10 gridcells depending on the temperature metric [unpublished data]. As shown in Figure B6, most scenarios overestimated the complete standard deviation; however by very little (< 1.4%). In the estimated range of spatial autocorrelation, average sampling error was from -0.5% to 1%. The spread around the average sampling error was very similar for both sampling designs (-9 and 9%, 5th and 95th quartiles of sampling error for medium gradient averaged for autocorrelation range < 21). Based on these results, we used the sampling design with all 225 locations. Since we expect a gradient, this design results in a sample standard deviation closer to zero for the medium gradient case. While the sampling error is higher for the strong gradient, it is still less than 1%. Therefore, we have confidence in the heterogeneity and the mean-heterogeneity relationships that we report.

B.1.6 Characterizing the probability density of temperature

We conceptualize the soil temperature values on the landscape as a probability density (PDF) with a mean value and the standard deviation as a measure of the width of the distribution. If the density is more-or-less normal, then the mean ± 2 times the standard deviation encompasses the 2.5 to the 97.5% quartiles (Figure B7a). Thus, 4 times the standard deviation is the range of conditions over 95% of the area within the sampled extent. The observations at the SEKI site are typically more-or-less normal (Figure B7b–c). We cannot assess this assumption at the other locations because of the small sample sizes.

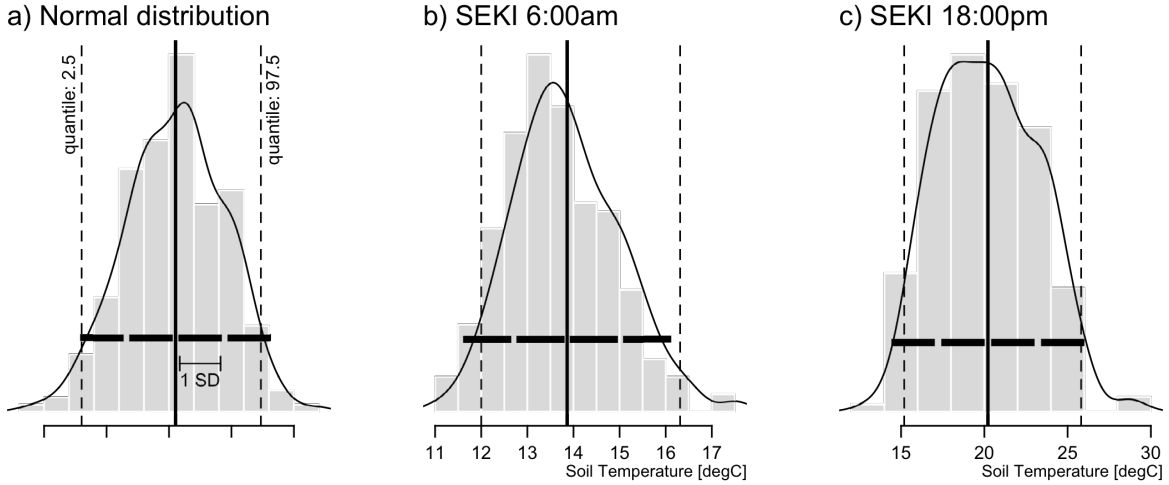


Figure B7: Illustration of 4 times standard deviation (SD) representing the range of temperature values over 95% of the extent. The solid black vertical line is the mean, the dotted lines are the quartiles 2.5 and 97.5; the combined horizontal line is 4 times SD, with each segment equal to 1 SD. Histogram and PDF of (a) 225 draws from a normal distribution; (b) 225 soil temperature values at SEKI on August 1, 2012 at 6:00am; (c) 225 soil temperature values at SEKI on August 1, 2012 at 18:00pm.

B.2 Projected increase in daily minimum and maximum temperatures

We used CCSM4 (ensembles r1i1p1 and r2i1p1) and GFDL (models ESM2G and ESM2M, both with ensemble r1i1p1) CMIP5 historical and projected temperatures [Unidata] to calculate the expected difference in daily minimum and maximum temperatures at the SEKI study site. We used

RCP 8.5 as a worse case emission scenario to project the largest temperature differences. The SEKI site lies within 2 model gridcells. Thus, we averaged the temperature values between these gridcells. We completed the following for both minimum and maximum daily temperatures. First, we calculated the average historical value for each of the models over the years 1976-2005, as well as the average projected values for 2050 with years 2036-2065 and for 2085 with years 2071-2100. Next, we calculated the difference between the projected and historical values for each day of year for each model. Then, we averaged the differences of the 4 models (Figure B8).

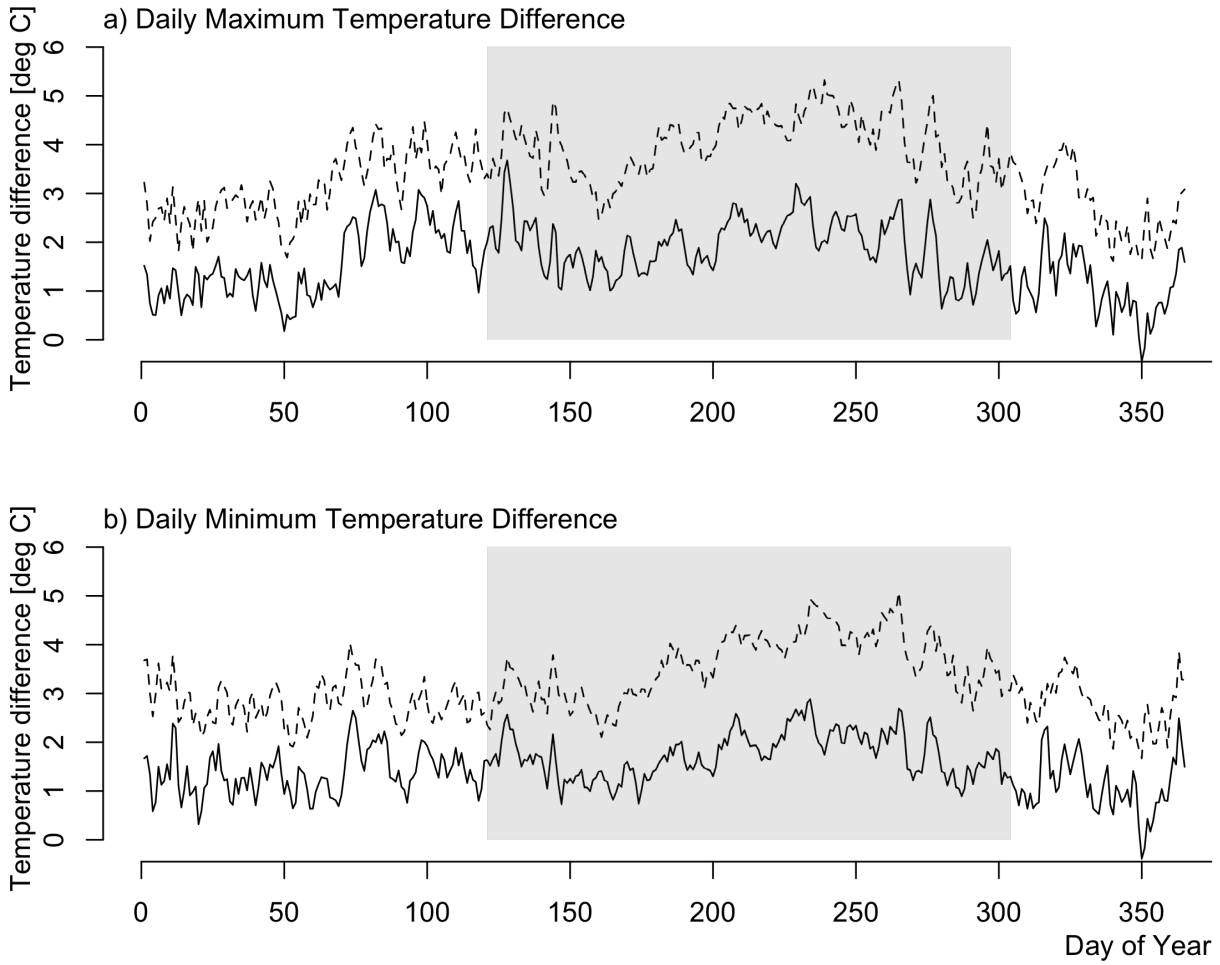


Figure B8: Difference in projected (a) Maximum and (b) Minimum daily temperature values as compared to historical values at the SEKI site. Projections for 2050 are the solid black line and those for 2085 are dashed. The growing season is indicated in gray.

B.3 Additional Results

B.3.1 Minimum daily temperatures: mean – heterogeneity relationship

No relationships are observed between heterogeneity in the average conditions for minimum daily temperatures at any of the mountainous sites (Figure B9).

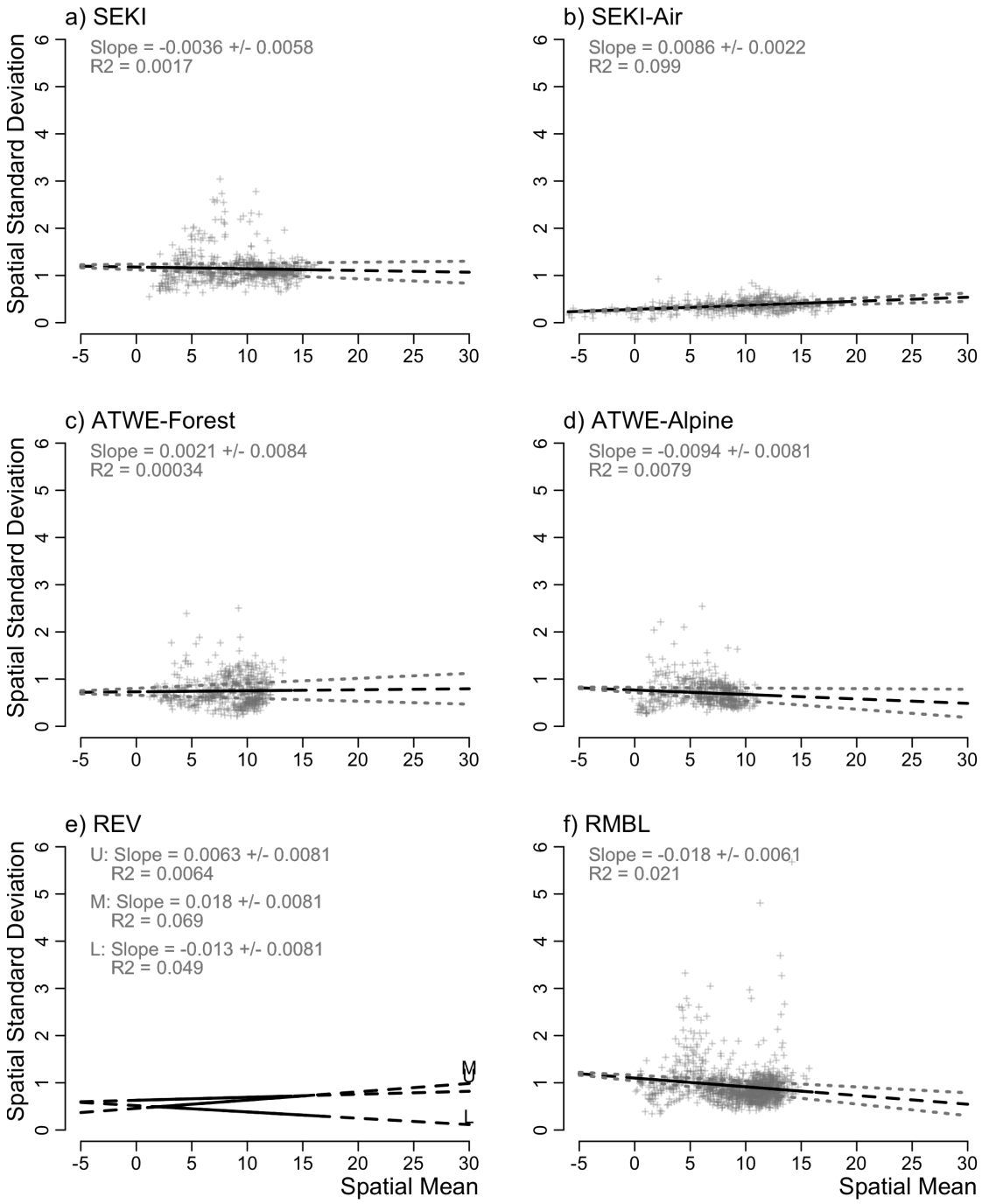


Figure B9: Relationship between heterogeneity (standard deviation) and average conditions (mean) for each mountainous study site.

B.3.2 Soil temperature tracks air temperature at SEKI study site

Soil temperature tracks air temperature at the SEKI study site (Figure B10). See conclusion chapter for additional information (section 5.2.2 and Figure 5.2).

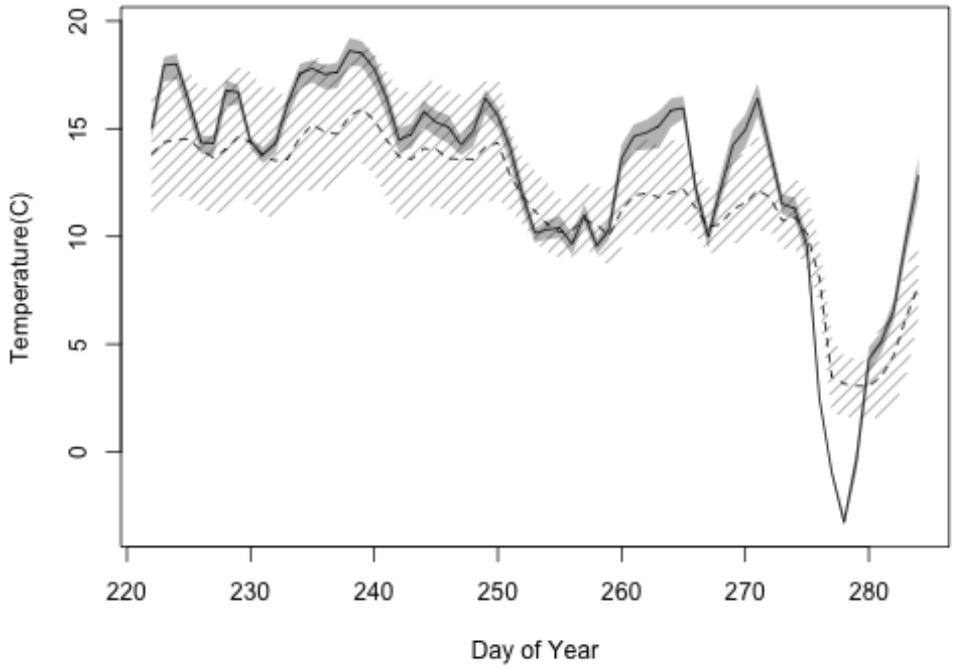


Figure B10: Comparison of 2m air and 5cm deep soil temperature at SEKI: Air temperature mean ± twice the standard deviation (solid gray and black line) and soil temperature mean ± twice the standard deviation (hashed and dashed lines) for Aug–Oct 2011.

B.4 References

Dunne, J.A., Harte, J. & Taylor, K.J. (2003). Subalpine meadow flowering phenology responses to climate change: integrating experimental and gradient methods. *Ecological Monographs*, **73**, 69–86.

Dunne, J.A., Saleska, S.R., Fischer, M.L, & Harte, J. (2004). Integrating experimental and gradient methods in ecological climate change research. *Ecology*, **85**, 904–916.

Kondrashov, D. & Ghil, M. (2006). Spatio-temporal filling of missing points in geophysical data sets. *Nonlinear Processes in Geophysics*, **13**, 151–159.

Unidata (2015). NCSS Grids As Point Data. For historical: http://cida.usgs.gov/thredds/ncss/cmip5_bcca/historical/dataset.html; For future http://cida.usgs.gov/thredds/ncss/cmip5_bcca/future/dataset.html. Accessed November 6, 2015.

Appendix C: Supplemental information for Chapter 3

C.1 Additional methods

C.1.1 Study site

The study site (Figure C1) is located in the red fir forest on the western slope of California's Sierra Nevada. We focused on red fir seedlings (Figure C2), which comprised 98.7% of the total seedlings in study site.



Figure C1: Semi-open red fir forest with sparse herbaceous understory. Study site captures edge of meadow in the background. Photo taken July 27, 2010.



Figure C2: Example of red fir seedlings in (a) Older Seedling and (b) Younger Seedling groups. Marks on background paper are 1cm apart.

C.1.2 Abiotic observations

Soil temperature (100 locations) and moisture observations (50 locations) were made during the 2008–2009 seasons to determine the best sampling design. We calculated semivariograms, despite small sample sizes, with which we determined ~10m to be an independent sampling distance. Thus, we installed a sampling design with 98 sensors arranged 12m apart on a triangular grid design. We arranged the remaining 127 sensors in 17 arrays of varying density in a full factorial of open / shaded and low / high seedling density locations. This type of sampling design is recommended for estimating autocorrelation parameters using likelihood methods [Zhu and Stein 2005].

C.1.2.1 Soil temperature

We measured soil temperature every 4 hours at all 225 sensor locations (iButton Thermochron DS1921G, Dallas Semiconductor, TX, USA) from May 2010 through October 2013. Sensors were attached to stiff metal wire to maintain a constant sensor depth of 5cm. However, some vertical movement did occur mainly due to over-winter freeze thaw cycling but also from litter accumulation. We report results that we corrected for vertical movement as measured prior to removal from soil for data extraction (see section 3.2.4 in chapter 3 and section C.1.4).

C.1.2.2 Soil moisture

We measured the soil moisture profile using time-domain reflectometry (Delta-T PR2/4 with custom access tubes) in 4 to 7 campaigns throughout each growing season at 207 sensor locations. Access tubes were inserted in the fall of 2009 and allowed to set over-winter before measurement acquisition in 2010-2012. Manual data collection occurred over 2-4 rain-free days. We found no

sampling bias due to the sampling time during the day, over the 2-4 day period, or due to manual positioning of the probe in the access tube. We averaged three measures of soil permittivity at depths of 5-cm intervals, ranging from 5 to 35cm below the soil surface and limited by either the access tube depth (40cm) or subsurface obstructions (*e.g.,* large rocks, roots, *etc.*). For this analysis we use the soil moisture observations at 10cm depth because (1) nearly all locations were measured at this depth, (2) 10cm is not as sensitive to light rain events occurring between campaigns, and (3) water availability at this depth is likely a critical resource for younger seedlings. We observed seedlings in their second summer to have roots at least 15cm deep. Each soil moisture observation included in the analysis is the average of three measurements taken at three standardized rotational directions and centered at the 10cm depth. As such, the observation represents soil moisture between depths of 5-15cm.

We calculated volumetric water content (VWC) from soil permittivity using calibration curves generated from gravimetric water content (GWC) and bulk density sampling at 60 locations within the site. Because this is a destructive method, we sampled in 2013 after the observations included in the analysis were collected in 2010-2012. We sampled in May shortly after snowmelt and July during mid-summer to capture the range of wet to dry conditions. At each location we first measured soil moisture at 5cm depth intervals with the Delta-T probe oriented in a consistent direction relative to the soil sample position. Then, we used a soil corer (Soil Sampler HC 21, Oakfield Apparatus, Fond du Lac, WI, USA) to collect samples at 5cm depth intervals at a distance 10cm from the edge of the access tube (one vertical sample extraction per location). We confirmed that removing soil samples did not affect later soil moisture measures so that we could sample at the same locations in both May and September (different orientation from the access tube). We treated each 5cm depth sample (311 total) as independent samples because soil moisture varies with depth.

We kept the samples in airtight bags and at ~5°C between the field collection and laboratory analysis. We weighed the samples before and after freeze-drying them (Lyph Lock 4.5 Model 77500, Labconco, Kansas City, MO, USA), using the difference to calculate the mass of water in the soil sample. We also classified each soil sample as Organic (fibric and hemic layers), Mixed (fine pieces of organic with mineral), and Mineral (sapric layer) to compare calibration curves between each soil type. Samples that spanned multiple litter layers were classified as multiple soil types. We calculated the bulk density of each sample, by dividing the mass of the dry soil sample by the sample volume. The average bulk density across the study site was 969.8 ± 387.1 kg/m^3 (mean ± standard deviation).

Bulk density can be calculated with or without rocks, and guidance for the preferred method to use in calibrating soil moisture measurements is lacking. Thus, we assessed the rock (> 2mm) content of the soil in a subset of the samples (200) to look for potential biases across the study site. We found that the rock fraction varies from 0–0.4 at all depths (Figure C3). Shallower depths are more variable than deeper depths. Excepting the area between locations 80–100 which has no rock-free samples, the rock fraction does not vary systematically across the site, *i.e.,* there are no obvious correlations with aspect (Figure C4). Since there was no systematic bias across locations in rock fraction, we included rocks in the calculation of the bulk density.

Using the GWC and bulk density, ρ_{soil}, we calculate the VWC:

$$VWC = GWC \; x \; \frac{\rho_{soil}}{\rho_{water}} = \frac{M_{water}}{V_{soil} \, x \, \rho_{water}}, \qquad \text{eqn C1}$$

where ρ_{water} is the density of water (0.9999 g/cm^3 at ~5°C), M_{water} is the mass of water in the soil sample, and V_{soil} is the volume of the soil sample including rocks. We calibrated the Delta-T probe using the calculated VWC and its corresponding soil permittivity as measured by the probe in mV.

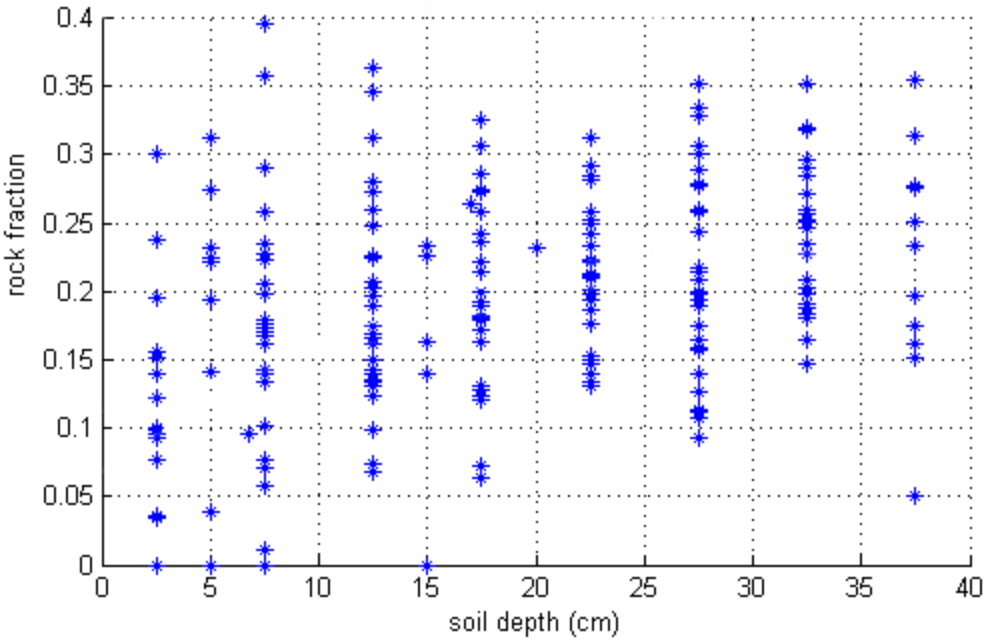


Figure C3: Rock fractions by average depth of the soil sample. Most samples are from 5cm depth intervals (soil depth = 2.5, 7.5, 12.5, 17.5, 22.5, 27.5, 32.5, 37.5cm); however, some samples are 10cm deep centered at soil depth = 5, 15, 20cm.

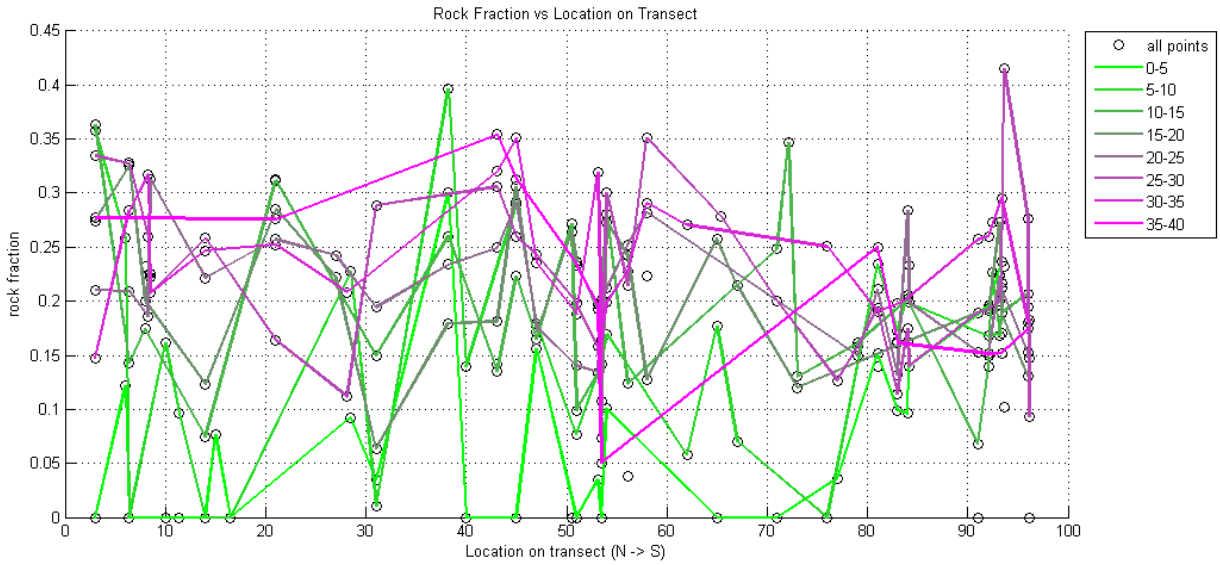


Figure C4: Rock fraction by approximate location along study site. Locations are numbered 1-98 along the 640m length of the study site. Location 1 is at the northern end of the site and 98 at the southern. The different line colors represent samples at the 5cm depth increments. Points without corresponding lines have odd sampling intervals (*e.g.,* 10 cm).

We generated calibration curves following the calibration equations provided by the manufacturer [Delta-T 2004]. The Delta-T probe has 4 sensors positioned such that soil moisture is measured at 10cm depth intervals. Thus, we combined the 5cm soil samples into intervals of 0–10, 10–20, 20–30, and 30–40cm depths. We calculated calibration curves for each soil type individually and for all combinations (Figure C5a). We used the calibration curve generated across all soil types (Figure

C5b) because (1) several of the soil types had small sample sizes, (2) the average curve was a good compromise amongst all soil types, and (3) the error introduced by assigning soil types to each location (via the soil profile information) may be as large as the difference between the specific soil type curves. We converted all soil permittivity measures to VWC using the manufactures conversion equations [Delta-T 2004] with coefficients $a_0 = 1.254$ and $a_1 = 9.336$. At low VWC, this calibration as shown in Figure C5b underestimates the VWC of the organic soils. By using soil moisture at 10cm depth, we avoid this bias since most locations have organic layers less than 5cm deep.

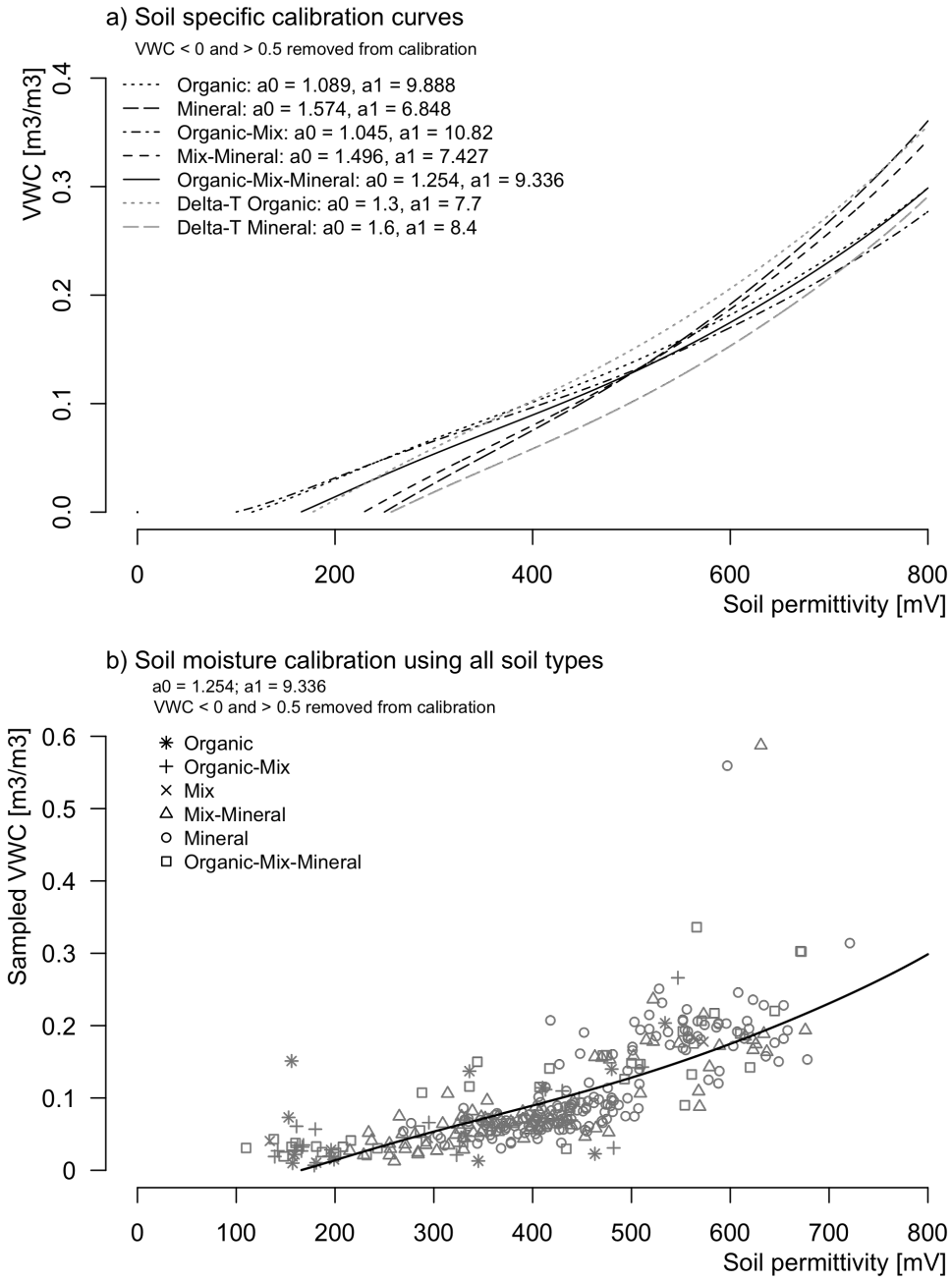


Figure C5: (a) Calibration curves generated for each specific soil type as well as all combinations. (b) Calibration data with curve generated across all soil types and combinations (the Organic-Mix-Mineral curve in panel a).

C.1.2.3 Soil litter profile

We measured vertical soil profile at all 207 soil moisture locations in fall 2013 during removal of the soil moisture access tubes. Using a flat shovel we exposed the soil profile and measured 2 depths: depth of organic material (fibric and hemic layers together) and depth to mineral (sapric) soil (Figure C6). Measures were typically taken on both sides of the soil moisture access tube or at two locations on one side of the access tube if both sides were not accessible (due to rock, log, *etc.*).



Figure C6: Soil profile measurement example: organic layer at the top (~1.5cm thick), followed by the mixed (~3cm thick), and finally mineral soil. For the few sample locations in which the layers were not as clearly defined as this example, we estimated the average depth. Additionally, a small subset of the sample locations had more complex profiles. For example a decaying log occurred below the start of the mineral layer. The distance to the first instance of mineral soil was determined to be the start of the mineral layer.

C.1.2.4 Surface cover

We assessed the surface cover at all 225 locations in the fall of 2013. Using a 1x1m frame with 100 10x10cm gridcells, we counted the number of gridcells whose major composition was one of the following categories: dirt/small litter, big rock (> 1cm), and big wood (>1cm bark or stem pieces).

C.1.2.5 Topography

During the summer of 2009, we scanned the study plot and surrounding area with a terrestrial laser scanner (I-Site 4400CR, Maptek / KRJA Systems Ltd, Lakewood, CO, USA). Individual scans were made at 87 locations that were surveyed with a total station (TopCon CTS-2, Topcon Positioning Systems, Inc., Tokyo, Japan). We aligned and merged the point cloud data (see section C.1.3 for more details), extracted the lowest points on a 1x1m grid, and used automated "despike" to remove erroneous points. Verification was conducted at the UC Davis KeckCAVES 3-D immersive environment by comparing the lowest point selection to the all points within 25cm of a modeled surface (see section C.1.3 for methodology). Because some points were erroneous and thus removed

(due primarily to occlusions during the scanning process), we interpolated elevations for the missing gridcells with the akima package [Akima *et al.* 2013] in R version 3.0.2 [R Development Team 2013]. Slope and aspect measures were calculated at the 1m spatial scale by fitting the best plane through the four neighboring gridcells. The slope is the angle between the horizontal plane to the fitted plane and the aspect is angle between north and the direction of a perpendicular line from the fitted plane. We used R to calculate the slope and aspect values (see Figure 4.12b and 4.13b in chapter 4).

C.1.2.6 Potential Evaporation (PE)

In 2011 and 2012, we measured potential evaporation (PE) at 196 measurement locations in 4 and 5 campaigns respectively, using Piche evaporators with radiation shields (Figure C7). We constructed the evaporators using the Casella Piche Evaporator (HB-3127-02, C.F. Cassella & Co., Ltd., UK) [Stigter and Uiso 1981], which is no longer manufactured, as a reference. We cut 30cm lengths of acrylic tubing (1.28cm (0.5") outer and 0.97cm (0.375") inner diameter) and sealed one end by affixing a solid 1.5cm length piece of acrylic rod with acrylic cement (Weld-on #16, IPS Corporation, Compton, CA, USA). We predrilled the acrylic rod with a 1/8" diameter "hanger hole" so that we could hang the evaporator from the sealed end. We finished the open tube end with a series of steel files so that it was flat and smooth. We designed a "holder" from stiff steel wire and a stainless steel flat washer as shown in Figure C7b–c). We held a 3cm diameter piece of Grade 1 filter paper (1001329, Whatman, GE Healthcare Bio-Sciences, Pittsburg, PA, USA) to the tube's open end with the holder using rubber bands attached to a string that runs through the hanger hole.

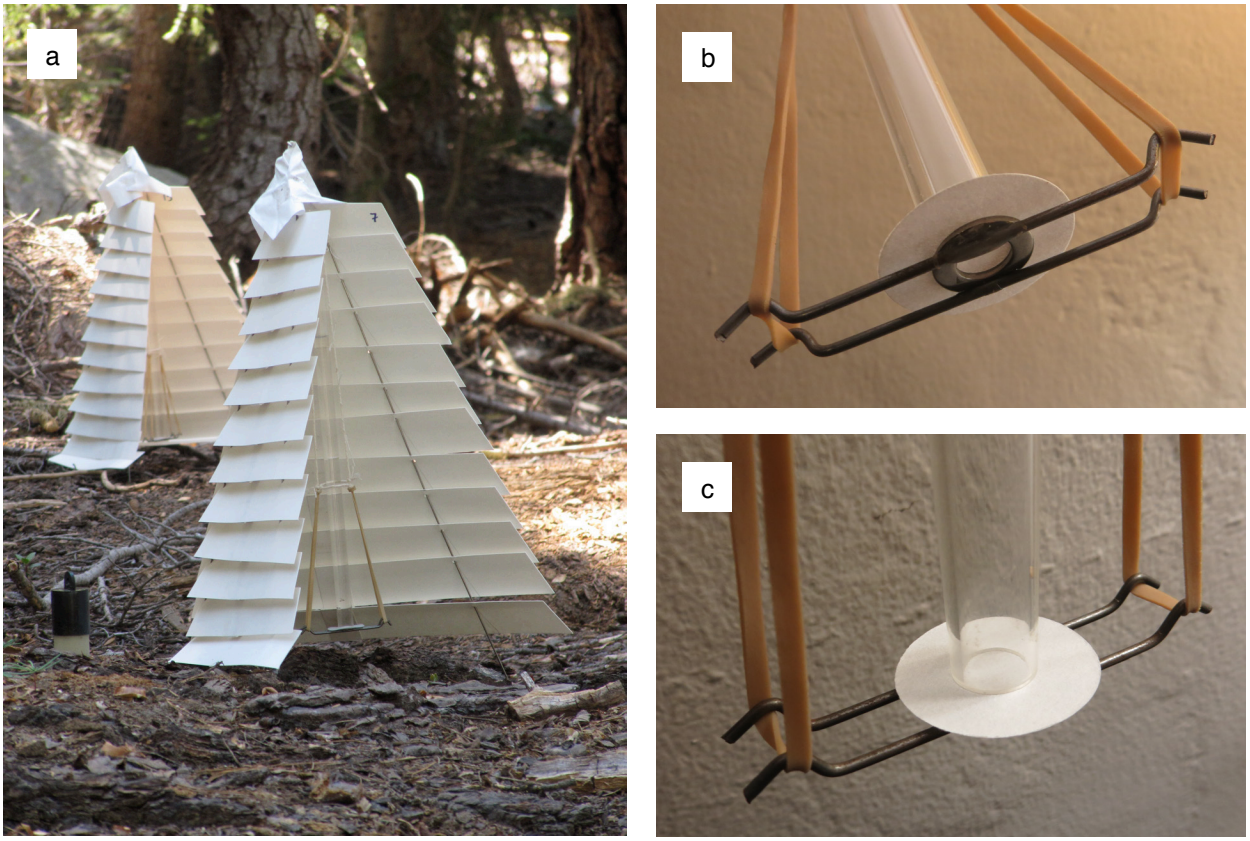


Figure C7: Piche evaporator and radiation shield (a) employed in the field and (b–c) close up of holder mechanism.

We also constructed a 2-sided radiation shield for the evaporator from 3 long white flag markers and slats made of heavy-duty poster board. The slats are held evenly apart by a strip of the poster board bent in a regular pattern. In the field, we installed the shield so that the open side faced north, so that at no time of the day was the evaporator in direct sun. We taped the three flags together (the final closure is done in the field once the evaporator is installed) to form a complete cover at the top of the shield. We secured the shield in the ground by inserting the flag marker ends a few centimeters into the soil. By using the slat design with one completely open side, we reduce effects of air stagnation within the radiation shield.

We validated comparability between the evaporators and amongst variable field conditions using 8 pairs of evaporators, installed in a single radiation shield. The tests were (1) Sensor only: difference between evaporators at same height (within 1cm) over same time period; (2) Sensor + height: differences between evaporators at different heights (2-10cm) over same time period; and (3) Sensor + time of day: differences between evaporators at same height over same length of time offset by an hour. We performed the Sensor only test on 2 different days in 2012, one mid-summer (July 10) and the other early fall (September 14) so that we have 16 replicates for this test. Differences due to the different sensors are minimal (Table C1 and Figure C8). Additional differences due to different height or time of day are negligible. We found no trend in the differences due to position along the study site, average filter paper height from the soil surface, or average flux.

Table C1: Results of Piche evaporator validation testing. Differences two evaporators in the same radiation shield are reported for 16, 8, and 8 pairs, for the three tests. We calculated the relative difference for each pair by dividing the flux difference by the mean flux.

	Units	Sensor only	Sensor + height*	Sensor + time of day
Mean difference ± SD	g $H_2O/m^2/hr$	15.0 ± 13.9	25.2 ± 15.5	18.1 ± 17.5
Difference range	g $H_2O/m^2/hr$	0.4 – 45.3	3.2 – 45.2	1.8 – 52.2
Mean relative difference ± SD	%	3.8 ± 3.9	7.9 ± 4.8	4.1 ± 3.3
Relative difference range	%	0.1 ±14.1	0.9 – 14.5	0.5 – 8.4

* Outlier removed: flux difference = 115.7 g $H_2O/m^2/hr$

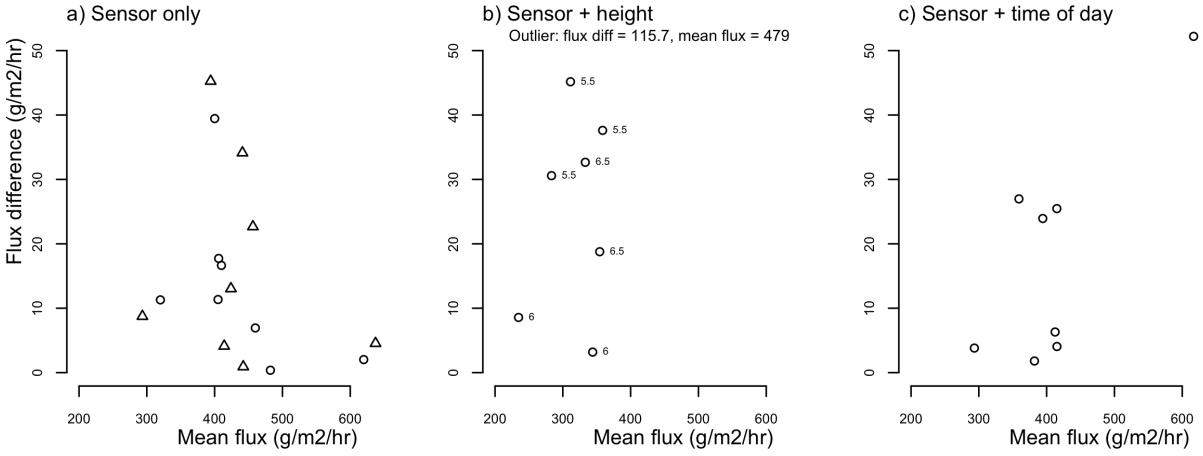


Figure C8: Flux difference versus mean flux for Piche evaporator validation tests: (a) Sensor only: difference between evaporators at same height (within 1cm) over same time period; (2) Sensor + height: differences between evaporators at different heights (2-10cm) over same time period. Differences in height are labeled next to the sensor pair; and (3) Sensor + time of day: differences between evaporators at same height over same length of time offset by an hour.

We conducted PE measurements according to the following protocol. Before heading to the field site, we filled the tube ~80% with deionized water, sealed it with a labeled cap (13mm Stopper, 2047-11600, Bellco Glass, Inc., Vineland, NJ, USA), and record the total mass. At the field site, we installed the radiation shields at 52 locations by 9am. From 9-10am, we installed an evaporator at each location by removing the cap, installed an unused filter paper, and hung the inverted the tube from the radiation shield with a custom metal hanger. We hung the evaporators so that the filter paper was between 4–8cm above the soil surface. We collected the cap in an airtight bag to be able to account for any water adhering to it. We recorded the time of evaporator installation, the distance of the filter paper from the surface, and the position of the setup relative to the permanently installed soil moisture and temperature probes. Evaporator installation was typically completed by 10:30am. Between 4:30 and 5pm, we started removing the evaporators. We chose these installation and removal times because (1) the resulting installed period included the primary portion of the day when the seedlings could be photosynthetically active and (2) they avoid the early morning and late evening when evaporative rates are likely changing quickly. Upon removal of a evaporator, we recorded the time, collected the wet filter paper in the same bag as the cap, installed a new dry cap, and took down the radiation shield. All evaporators were removed typically within an hour. In some cases while capping the evaporator, water wicked out from the evaporator's edge and the cap. We estimated the size of the loss so that we could account for it. These losses were typically less than 0.5% water evaporated during the installation period. Additionally, we made every effort to keep the evaporators upright during transport to minimize water contact with the caps, and thus minimize losses. Back at base camp, we weighed the evaporators, noting the new cap number. We also weighed the bag with the initial cap and wetted filter paper. We calculated the mass of the evaporated water by subtracting the final weight from the intial weight, adjusting for the cap specific weights, and the residual water on the used filter paper. We accounted for estimated water losses when predicting values on the 1x1m grid (see section C.1.4). We calculated the evaporative flux by dividing the mass of evaporated water by the surface area of the filter paper exposed to air (note that portions of the filter paper are covered by the tube, water inside the tube, and the metal holder) and by the total time that the evaporator was installed. We report the flux in g $H_2O/m^2/hr$. For reference, if a location receiving an average annual rainfall of 100cm evaporates all of that water during the daylight hours throughout the year, the actually evaporative flux would be 288 g $H_2O/m^2/hr$. Thus, we expect potential evaporation rates, *i.e.,* rates as if there were an endless supply of water, to be on the order of 100s g $H_2O/m^2/hr$.

We conducted measurement campaigns over four days, measuring 52 locations each day. We kept each measurement group the same over all campaigns and randomly chose the direction of installation / removal along the 640m length of the study site. We chose the four campaign days based on forecasts of similar weather conditions. We chose 5 locations to measure each campaign day so that we could correct for daily variability with a campaign. To correct for daily variability, we calculated the mean flux on each campaign day as well as the mean campaign flux across all days for this set of 5 common locations. Then, we calculated a daily difference between the daily mean flux and campaign mean flux. We adjusted all measurements for a given day by the daily difference (Figure C9).

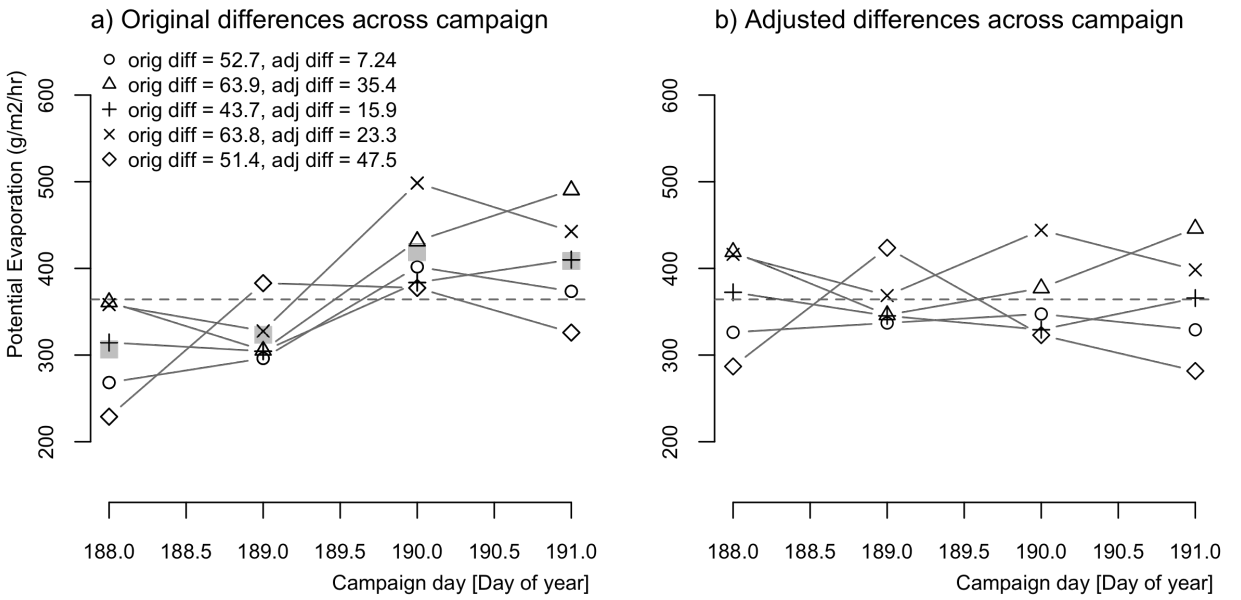


Figure C9: Example of adjustment for daily variability in potential evaporation measure over the 4-day campaign. Data shown is for July 11-14, 2012 campaign. For each location, the (a) original daily flux difference (orig diff) and (b) adjusted daily flux difference (adj diff) from the campaign mean (dashed line) are reported in g $H_2O/m^2/hr$. The original daily mean is shown with gray squares.

C.1.2.7 Canopy Cover and Direct / Diffuse Radiation

In 2012, we photographed the canopy at all 225 measurement locations using a hemispherical lens (Sigma Fisheye 4.5mm f/2.8 EX DC HSM with Nikon D80 DSLR) 10-20cm above the soil surface and in diffuse light (before sunrise, after sunset, and under completely overcast sky). We leveled the camera with an adjustable tripod and oriented it in a known direction (see chapter 4). We adjusted camera exposure levels in the field by monitoring the blue channel histogram to maintain the sky peak between pixel values of 200–255 [MacFarlane 2011].

We thresholded, converted the images to black and white pixels, using Digital Canopy Photography (DCP, version 3.2) [MacFarlane 2011] run in Matlab version R2012a (MathWorks, Natick, MA, USA). We used the following settings: Image type = Fisheye, Threshold Method = Dual binary, Options: Sharpen image, adjust dual threshold, save summary, and save image; Other Settings: N/A; Select Channel = Blue. We chose a single image for each of the 225 locations to use in the analysis based on the narrowness and position of the sky peak in the blue channel histogram. We aimed for the entire peak to be located centrally within pixel values of 200–255.

As DCP is a relatively new automated method for thresholding hemispherical imagery for canopy cover analysis, we compared it with Gap Light Analyzer (GLA) version 2.0 [Frazer *et al.* 1999], a commonly-used manual thresholding tool. Our goals were (1) to assess differences in estimates of canopy openness between the two methods, and (2) to compare sensitivity canopy openness to camera exposure. Canopy openness is the fraction of sky (as opposed to the fraction of vegetation). We based our manual protocol on the methods of Eschtruth and Battles [2008], and used the authors' manual training procedures [Eschtruth, personal communication]. However, we used Photoshop CS6 (Adobe, San Jose, CA, USA) for the image processing instead of GLA itself. We used images from 12 locations for which we had more than 3 images at different exposure levels (43 images total). We processed each image with both thresholding methods and then calculated the

canopy openness using GLA. We found that the DCP method consistently estimated higher canopy openness (mean difference ± standard deviation (SD) = 0.017 ± 0.015, with 2 outliers removed), with average relative difference of 9.5% ± 10% (mean ± SD with 2 outliers removed. We found a slight negative trend in these differences with average canopy openness, when the 2 outliers are excluded, *i.e.,* differences between the methods are less at locations with larger sky fractions (Figure C10). For each location and method, we calculate the average absolute difference between canopy openness. We compared these differences with a paired t-test. We found that the DCP method is less sensitive to variability in exposure (p=0.018). It is worth noting that we did not attempt to separate variability due the different exposure levels from, which is due to variation in manual human processing.

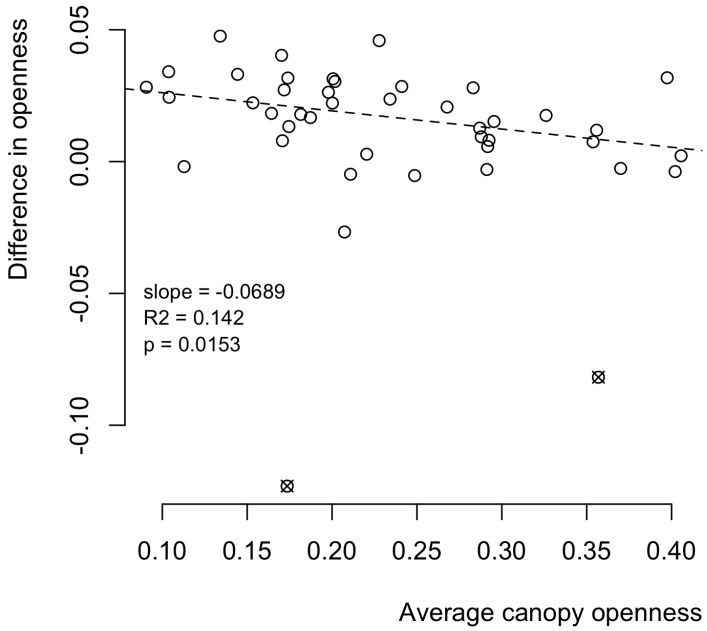


Figure C10: Comparison of canopy openness calculated using images thresholded with automated DCP and manual GLA methods. Difference in canopy openness = DCP – GLA. The slope shown is calculated without the 2 outliers indicated with "x."

Using the DCP thresholded hemispherical photos, we calculated canopy openness and modeled hourly direct and diffuse radiation from May 1 to Oct 31 using CIMES-Fisheye [Gonsamo *et al.* 2011]. To calculate canopy openness (sky fraction) we used the OPENNESS function with parameters: slope = 0, aspect = 0 (all photos were leveled as we sought radiation input to the seedling rather than the input to the soil surface). We calculated the hourly direct and diffuse radiation for each day with the PARHOR function (modified for easier integration with R) using the following parameterization:

- PAR units = 1 (energy)
- Slope = 0
- Aspect = 0
- Altitude = 2.52 (km)
- Latitude = 36.XXXXX
- Longitude = 118.XXXXX
- Time zone = 8
- Condensable water = 5 (mm)
- Haze = 0.15 (particles/cm^3)
- Leaf reflectance in PAR = 0.03 (recommended for needles)
- Leaf transmittance in PAR = 0.03 (recommended for needles)

- Soil reflectance in PAR = 0.33 (recommended value for initiating iteration)
- Mean daily shortwave canopy reflectance = 0.16 (recommended for coniferous forest)
- Number of selected days = total of Julian days below
- Julian days numbers = 120 – 274 in batches of 25
- Full hour or half an hour computation = 0.5 (half an hour)
- Daylight saving time, or summertime = 1 (summertime)
- Estimate ground-reflected radiation? = 0 (no)

We made educated guesses for haze and condensable water based on air quality and summer precipitation patterns for the Western slope of the Sierra Nevada. Because of the small study extent, these values are unlikely to vary from location to location. Thus, the value of the parameter does not affect the relative comparisons that we make between locations within the study site. By estimating the hourly direct and diffuse Photosynthetic Photo Flux Density (PPFD) in the Photosynthetically Active Radiation (PAR) transmitted through the canopy (under a clear-sky), we enabled calculation of the total radiative input to a location during the morning (7–12:30) and afternoon hours (12:30–18:00) over the growing season (see section C.1.4).

C.1.3 Forest stand structure using terrestrial laser scanning

C.1.3.1 Collecting and processing terrestrial laser scanning point cloud data

We scanned the study site at 87 locations in 2009 using a terrestrial laser scanner (I-Site 4400. Maptek / KRJA Systems Ltd, Lakewood, CO, USA). We collected scans at a point resolution of 0.216°, which yields a distance of 37cm between the closest points at a distance of 100m. We scanned at location density so that most objects were less than 50m from the scanner. We located the scanner locations using a total station (Topcon CTS-2, Topcon Positioning Systems, Inc., Tokyo, Japan) and the reference datum established when previously surveying the tree seedlings and sensor locations within the study site. Then, we merged the individual scans with I-Site Studio version 3.5.1 (Maptek / KRJA Systems Ltd, Lakewood, CO, USA). The resulting point cloud is a set of ~87 million points in XYZ space representing approximately 4 hectares of forest (100x700m).

We made additional manual alignment adjustments using overlapping areas of individual scans and distinctive forest features (tree trunks and boulders). We performed the adjustments in a series of groups that were defined by a common total station location (the total station was set up at a known point and 4-14 scanner locations were surveyed from a given set up). Individual adjustments were primarily rotational (most less than 1°; two adjustments were 9 and 18°). A few individual translations in the XY plane were made (all less than 20 cm). Group translation adjustments in the XY plane were then made along the 640m length of the site, which ranged from 15-45cm and one that was 1.4m. Excepting one erroneous height recording in the field, alignment in the Z direction was accurate, which was expected because we surveyed the scanner itself instead of its position on the ground surface.

We adjusted the previously surveyed tree seedlings and sensor locations (TSS) to match the alignment corrections made in the scanned data, since we used the same total station locations for both geo-referencing campaigns. Survey close out errors within each individual total station set up were less than 1cm. Thus, we applied the scanner adjustments to groups of TSS defined by the total station location from which they were located. As some total station locations that were used to survey TSS were not used in the terrestrial laser scanning, we applied estimated adjustments determined as follows. We call the total station locations that were not included in the terrestrial laser scanning seedling-only scans (SOS) and the ones included in both seedling / laser scans (SLS). We calculated the vector between each neighboring SLS. Then, we calculated the distance along that

vector for each SOS located between the neighboring SLS pairs. We translated the SOS seedling group that distance along the vector.

To further assess alignment within the point cloud itself and also between the point cloud and TSS, we used LiDARViewer software in the UC Davis KeckCAVES 3D immersive environment [Kreylos *et al.* 2008]. To assess alignment within the point cloud, we compared total station groups of scans by coloring each group a distinctive color. With the ability to see the point cloud in 3D space, we were able to estimate misalignment distances on the order of 5-15cm by comparing offset points (*e.g.,* on boulders or tree trunks) with the sizes of known objects. To assess alignment between TSS and the point cloud, we identified and mapped distinctive spatial patterns between seedlings, sensor, and plot markers (all in TSS) and landscape features (*e.g.,* down logs, boulders) in the study site. Then we compared the same patterns in the point cloud and TSS data in the KeckCAVES. We found no general pattern discrepancies. In some patterns, we estimated relative distances to be off by 5-15cm. We plan to continue developing new ways to utilize the point cloud and KeckCAVES to assess and adjust the point cloud and TSS data.

C.1.3.2 Measuring forest stand structure characteristics

We used the point cloud data to locate and size the reproducing adults (diameter at breast height (DBH) > 30cm) within the study site and also within a 30m border surrounding the site. First, in I-Site Studio, we modeled the soil surface by finding the lowest point in a 1x1m grid and using the triangular topographic surface modeling algorithm. Then we extracted a 0.5m band of points centered at 1.375m above the modeled surface. When viewed from above, the trees in this DBH band appear as circles or arcs. For each potential tree circle or arc points, we modeled a circle, constrained to the XY plane. We used the modeled circle's diameter as the DBH and its center as the tree's location. We distinguished dead versus living trees in the UC Davis KeckCAVES. In addition, we identified "missing" trees that were not captured via the DBH slice due to occlusions (*e.g.,* if saplings surround an adult tree, their foilage can obscure the adult's trunk). We then returned to the field to (1) verify the tree status (living / dead) and (2) measure the DBH and estimate the position of the missing trees. To verify the modeled DBH estimates, we compared them with DBH

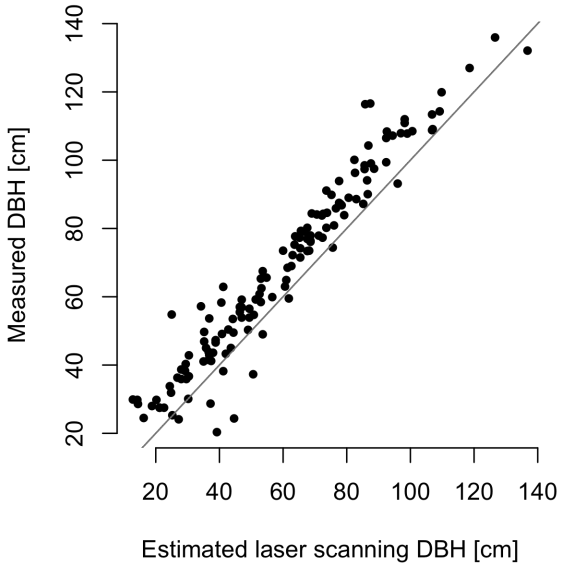


Figure C11: Correlation between measured DBH and estimated DBH from the terrestrial laser scanning point cloud. The 1:1 line is in gray. The relationship is measured DBH = 1.015/cm x estimated DBH + 7.39cm; $R^2 = 0.93$.

measures obtained in the field with standard forestry techniques (*i.e.,* a DBH tape measure at 1.375m). The correlation is high as shown in Figure C11. We applied the relationship to all estimated trees. We used the location of the trees to estimate the Nearest Tree metric by finding the distance between each gridcell and its nearest reproducing tree. We used the size and location to model Seed Density at each gridcell location as described in section C.1.5.2.

C.1.4 Predicting values on the 1x1m grid

For each type of observation, we predicted values for each time step at every gridcell on a 1x1m grid using the method described in section 3.2.4 in chapter 3. For example, we predicted the temperature values on the grid at every 4-hour observation time step, and we predicted the potential evaporation (PE) on the grid for every measurement campaign (Figure C12). For direct and diffuse radiation, we

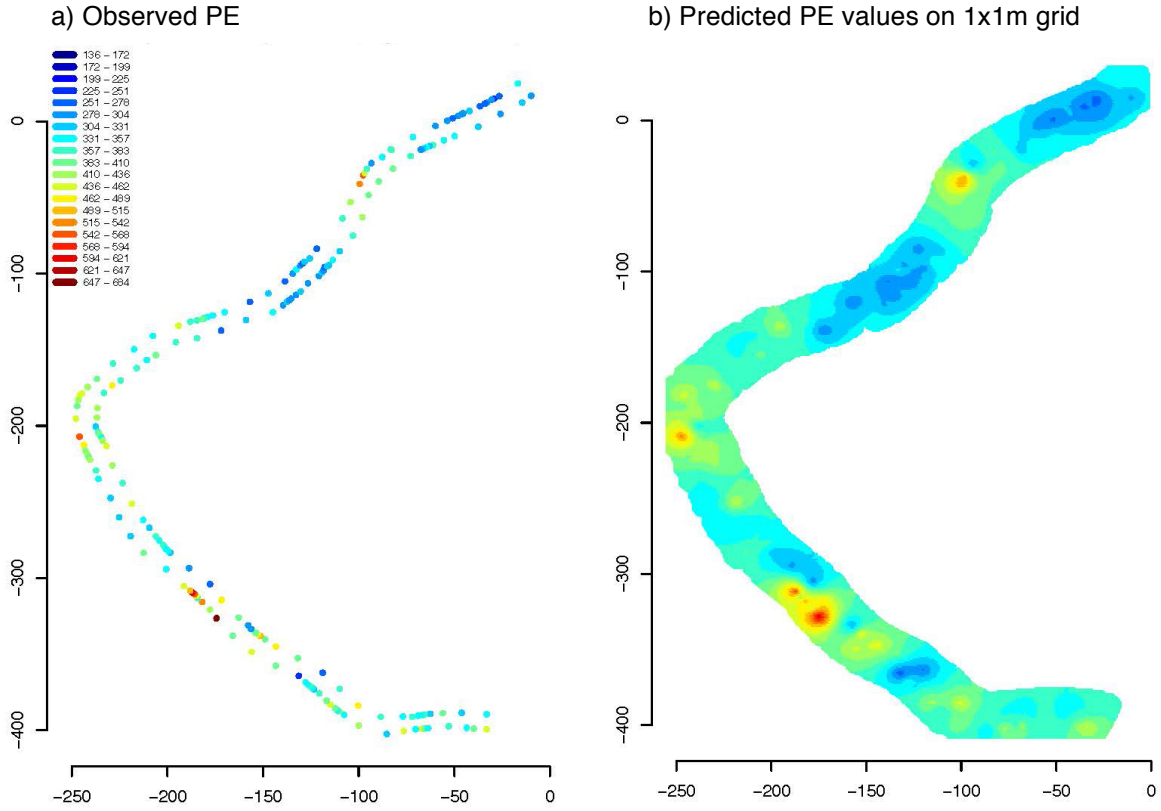


Figure C12: Potential evaporation (a) observations and (b) predicted values on 1x1m grid from the late August 2012 campaign. Values are reported in g $H_2O/m^2/hr$.

modeled the radiation as described in section C1.2.7 at each measurement location and then predicted the hourly values at each gridcell location. In Table C2, we report the mean for the estimated model parameters. For measures with multiple time steps, we include 5th – 95th quartiles in parentheses. We jointly estimated the surface cover measures (Dirt/litter, Solid woody, and Big rock cover) and also the PE campaigns to restrain the measurement error parameter τ to a single value. Additionally for PE, the joint estimation also allowed us to restrain the observation-specific error parameter ν to a single value across measurement campaigns.

The estimated measurement error parameters, τ and ν, for all measurement types were good. For soil temperature, τ is commensurate with the sensor specifications (± 0.5°C). For soil moisture, τ is 10–30% of the observed average values, which is typical for soil moisture measurement. For soil profile (Organic Depth and Depth to Mineral), τ is a reasonable ~1.5cm, commensurate with the variability in defining the surface and layer distinctions in the field. It is 1% or 1 gridcell for the surface cover metrics, which was the lower constraint. While acceptable, this value is likely a little low. For PE, τ is commensurate with the error found during the instrument validation tests (see section C.1.2.6). For Canopy Cover it is a reasonable 0.02 or 5–10% of the measured values. For the hourly radiation estimates (Diffuse / Direct Radiation), τ hovers near the lower bound that we imposed while modeling. We plan to investigate this further in future work. We estimated an observation specific measurement error, ν, to account for any vertical movement of the soil temperature sensors. The mean parameter estimate is reasonable given the small amount of movements observed. For PE, we estimated ν for observed water losses, which were less than 0.5%. As expected, ν was negligible. All autocorrelation range parameter, ρ, estimates are greater than 1.5m, indicating that the 1x1m gridcell value is a good estimate of the conditions at each individual seedling location within that gridcell. Note that we did not use likelihood methods to predict topographic values as they were generated on a 1x1m grid directly.

Table C2: Parameters for predicted abiotic conditions. Units are for μ, σ, τ, and ν, while ρ is in meters. For measures with multiple time steps, the means (5th – 95th quartiles) are reported.

Measure	Units	μ	σ	τ	ν	ρ [m]
Soil Temperature	°C	8.7 (0.5–18.1)	1.9 (0.4–3.9)	0.5 (0.01–1.0)	0.4 (0–1.0)	8.3 (3.5–17.6)
Soil Moisture (10cm)	m^3 H_2O / m^3 soil	0.078 (0.048–0.118)	0.020 (0.008–0.032)	0.015 (0–0.026)	—	10.3 (1.6–23.9)
Organic Depth	cm	3.4	3.4	1.4	—	2.7
Depth to Mineral	cm	6.8	4.1	1.8	—	3.6
Dirt/litter Cover	%	59.4	10.3	1	—	2.3
Solid Woody Cover	%	24.3	12.5		—	2.3
Big Rock Cover	%	2.1	2.8		—	3.6
Potential Evaporation	g H_2O/ m^2/hr	322 (255–386)	70 (69–71)	25	0	13.6 (4.4–26.2)
Canopy Cover	sky fraction	0.26	0.09	0.02	—	14.3
Direct Radiation	W/m^2/ hr	71.9 (0.7–174.2)	86.0 (0.7–149.4)	0.3 (0.01–0.8)	—	7.038 (3.3–17.2)
Diffuse Radiation	W/ m^2/ hr	23.6 (5.2–52.0)	8.4 (1.6–15.7)	0.2 (0.1–0.2)	—	12.8 (11.8–13.8)

C.1.5 Variable generation

We calculated each variable at every location on the 1x1m grid using the predicted values. For aggregated variables, we consider two distinct snow-free periods. The active season (AS) is the period of snow-free time at a specific location, *i.e.,* neighboring gridcells can have different AS due to different snowmelt dates in the spring and snow accumulation dates in the fall. We also defined a growing season (GS) that is the same across all locations but specific to a particular year. It is defined by the snowmelt date of the first location to melt out and the date of the last location to accumulate snow in the fall (see section C.1.5.1). For variables that are generated in multiple years (noted in Table 3.1 in chapter 3), we average the annual values.

C.1.5.1 Snowmelt Date

We designated snow-free days as days with a diel difference greater than 3.5°C. Snowmelt date is the first snow-free day after day of year (DOY or Julian date) 55. We defined the end of the AS by the last snow-free day after DOY 292. These DOY constraints were used to exclude snow-free days that occurred during the winter months. We averaged the snowmelt dates at each gridcell across years 2010–2013.

C.1.5.2 GS Direct / Diffuse Radiation

We used an idealized average GS (May 1–Oct 31) to calculate the direct and diffuse radiation variables. We calculated the cumulative radiation over this period by summing the estimated hourly energy flux. The sum is reported in W/m^2/season.

C.1.5.3 Soil Degree Days

Soil Degree Days is the sum of the positive differences between each day's mean soil temperature and 5°C during the growing season, *i.e.,* if the daily mean is below 5°C it is not included in the sum. We chose base 5°C to represent the cumulative time for seedling growth. We don't expect much growth below temperatures of 5°C. We averaged the Soil Degree Days at each location across years 2010–2013.

C.1.5.4 Seed Density

We modeled the distribution of seeds around an individual tree in terms of an angular direction Θ and distance r, which we took to be independent of each other. Specifically, we took the angle to be uniform on 0 to 2π and the distance to have a Rayleigh distribution. The joint density that describes the number of expected seeds at a specific (r,Θ) has the form

$$f(r,\theta) = \frac{r\beta_t}{2\pi\sigma_t^2} exp\left\{-\frac{r}{2\sigma_t^2}\right\}, \qquad \text{eqn C2}$$

with β_t equal to fecundity (number of seeds per tree) and σ_t describing the width of dispersal kernel for the tree t. This specification can be shown to be equivalent to a dispersal kernel described by a rotationally symmetrical normal distribution centered at the tree, which is the form used by Clark *et al.* 1999 for red fir (*Abies magnifica* var. s*hastensis*). We modeled the number of seeds dispersed from every tree to every gridcell. The sum at each gridcell is the Seed Density.

We modeled β_t as a function of the basal area, constrained by observations that trees became reproductive with usually 1 cone at approximately 30cm DBH. By counting cones at tree tops in photos taken in different years, large trees (~90cm DBH) were estimated to have on average 100 cones. From additional photos and seed/cone counts, we estimated 550 seeds/cone. Both estimates

are commensurate with fecundity reported for red fir by Gordon [1970]. We used a linear relationship based on the basal area which is a quadratic relationship based on DBH:

$$\beta_t = a_o \text{ x } (0.5\ DBH_t)^2 + a_1, \qquad \text{eqn C3}$$

with a_o = 30.25 seeds/cm^2 and a_1 = – 6256.25 seeds.

We set the average dispersal distance parameter σ = 18.88 so that 95% of seeds fall within 46.2 meters of the parent tree [Clark *et al.* 1999] for the average height tree in the study site (30m). Because red fir cones only occur at the tops of the trees, the height of the tree should affect the width of the dispersal kernel, especially if strong winds occur. Thus, we adjust the dispersal distance parameter by tree height so that shorter trees have a slightly narrower dispersal kernel and taller trees have a wider one. Tree height, h_t, is estimated by a red fir specific allometric relationship: h_t = 1.0266 x $DBH_t^{0.81}$ [Westman 1987]. The tree specific dispersal kernel distance parameter is

$$\sigma_t = \sigma \text{ x } (1 + h_a \text{ x } (h_t - h_r) \ / \ h_r), \qquad \text{eqn C4}$$

where h_r = 0.5 x ($h_{t,max} - h_{t,min}$) and h_a = 0.2 for the base case.

As seed dispersal can be stand and year specific, due to both variable fecundity and weather conditions, we performed a sensitivity analysis comparing our base case as described above to a full factorial of (1) four fecundity levels, and (2) three dispersal kernel schemes as described in Table C3.

Table C3: Cases for Seed Density sensitivity analysis.

Factor	Case	Description
Fecundity and Dispersal Kernel	Base	Medium fecundity: a_o = 30.25 seeds/cm^2 and a_1 = –6256.25 seeds 550 seeds/cone, 1 cone for 30cm DBH tree, 100 cones for 90cm DBH Medium dispersal distance based on basal area: σ = 18.88 and h_a = 0.2 95% of seeds fall within 46.2 meters of 30m tall parent tree
Fecundity	Low F	Low fecundity: a_o = 13.11 seeds/cm^2 and a_1 = –2550 seeds 400 seeds/cone, 1 cone for 30cm DBH tree, 60 cones for 90cm DBH
	Var (L) F	Medium fecundity with low random noise: 0.8-1.2x adjustments
	High F	High fecundity: a_o = 54.06 seeds/cm^2 and a_1 = –11462 seeds 700 seeds/cone, 1 cone for 30cm DBH tree, 140 cones for 90cm DBH
	Var (H) F	Medium fecundity with high random noise: 0.5-1.5x adjustments
Dispersal kernel	Low D	Low dispersal distance based on basal area: σ = 12.26 and h_a = 0.2 95% of seeds fall within 30 meters of 30m tall parent tree
	Mid const D	Medium dispersal distance (constant): σ = 18.88 95% of seeds fall within 46.2 meters of 30m tall parent tree
	High D	High dispersal distance based on basal area: σ = 24.51 and h_a = 0.2 95% of seeds fall within 60 meters of 30m tall parent tree

The different parameterizations of the seed density model did not significantly affect the relative influence of seed density (Figure C13).

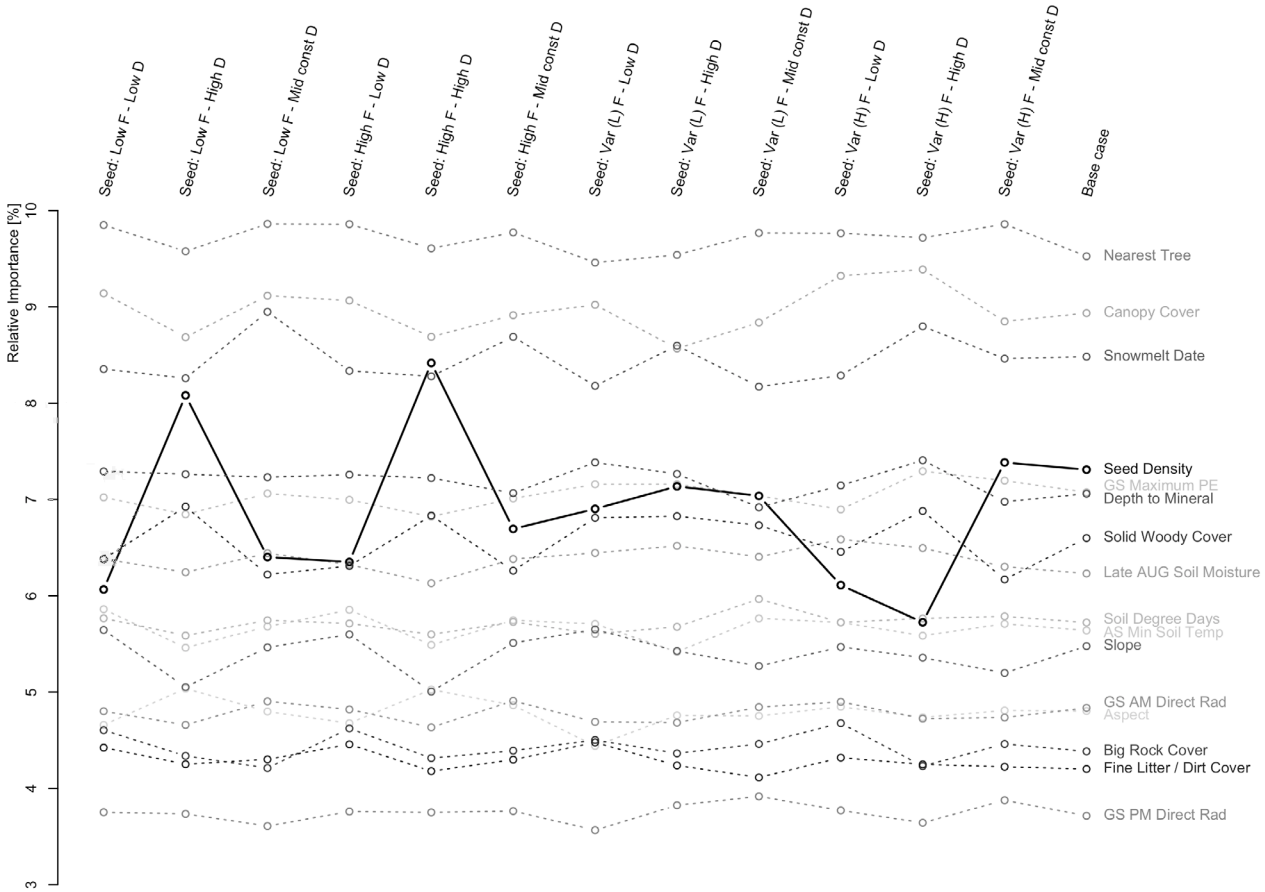


Figure C13: Relative importance of variables in explaining seedling occupancy patterns for different parameterizations of the Seed Density model. See chapter 3 for explanation of the seedling occupancy model.

C.1.5.5 Variable correlation

We eliminated GS Mean Soil Moisture, GS Mean PE, and GS Minimum PE as explanatory because of high correlations with the included soil moisture and PE variables. In addition, relative to the included soil moisture and PE variables, GS Mean Soil Moisture, GS Mean PE, and GS Minimum PE are less likely to cause ecophysiological stress. We examined pairwise correlations (Pearson's coefficient) between the remaining 20 variables (Figure C14) and identified 3 groups of highly correlated variables (correlation > 0.7): soil temperature (Soil Degree Days and AS Max Soil Temp), soil moisture (Early JUL and Late AUG Soil Moisture), and soil profile (Organic Layer Depth and Depth to Mineral). Additionally, Canopy Cover was correlated with Growing Season (GS) Diffuse Radiation at 0.99. We included only Canopy Cover because it is the direct measurement. From the 3 correlated pairs, we configured all possible combinations of variables forming 8 variable configurations which we used to explain seedling occupancy as described in chapter 3. Other variable pairs, like GS Maximum PE / Soil Degree Days (0.68), GS AM Direct Rad / Canopy Cover (0.6), GS Maximum PE / AS Max Soil Temp (0.7), are close to our cutoff at 0.7. We discuss potential effects of this in chapter 3 and below in section C.2.

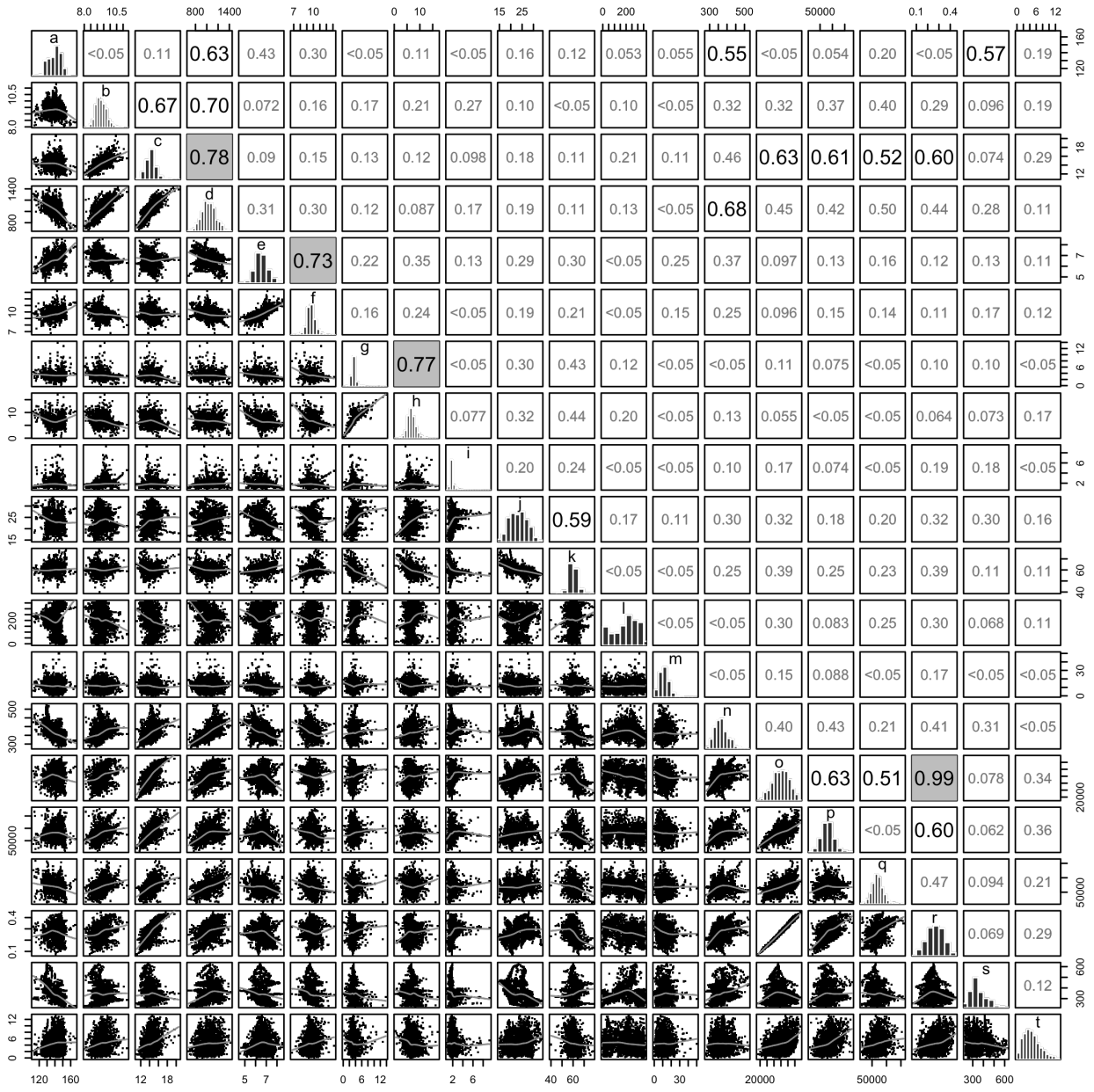


Figure C14: Correlation between all variables (labels in the diagonal histogram figures) based on a random sample of 2000 gridcell locations: (a) Snowmelt Date, (b) AS Min Soil Temp, (c) AS Max Soil Temp, (d) Soil Degree Days, (e) Late AUG Soil Moisture, (f) Early JUL Soil Moisture, (g) Organic Layer Depth, (h) Depth to Mineral, (i) Big Rock Cover, (j) Soil Woody Cover, (k) Fine Litter/Dirt Cover, (l) Aspect, (m) Slope, (n) GS Max PE, (o) GS Diffuse Rad, (p) GS AM Direct Rad, (q) GS PM Direct Rad, (r) Canopy Cover, (s) Seed Density, (t) Nearest Tree. For the upper panels, correlations greater than the 0.7 cutoff are shaded gray with black text; > 0.5 and <= 0.7 in black text; less than 0.5 in gray text. For the lower panel, the modeled relationship (gray) is the lowess function in R with f= 2/3.

C.1.6 Model selection

We used the following variable configuration to select the appropriate model formulation:

- Abiotic Variables: Snowmelt Date, AS Min Soil Temp, Soil Degree Days, Late AUG Soil Moisture, Depth to Mineral, Big Rock Cover, Solid Woody Cover, Fine Litter/Dirt Cover, Aspect, Slope, GS Maximum PE, GS AM Direct Rad, and GS PM Direct Rad;
- Biotic Variables: Canopy Cover, Seed Density, Nearest Tree.

We considered 5 model formulations: Spatial, Additive only, Interaction only with max interactions of 2, 3, and 4 depths (D2, D3, D4), Additive Spatial, and Interaction D4 Spatial, as described in chapter 3. We boosted each formulation, determining the optimal number of boosts using bootstrap validation with 25-folds. The negative log-likelihood of each of the optimal boosts can be used to assess the formulation performance [Hothorn *et al.* 2011], with lower values indicating better performance. The Interaction only formulations performed similarly (Figure C15). The addition of spatial information in the Interaction D4 Spatial models does not improve the Interaction only D4 formulation. Thus, we use the simplest of these, the Interaction only D2 formulation for simplicity in interpretation.

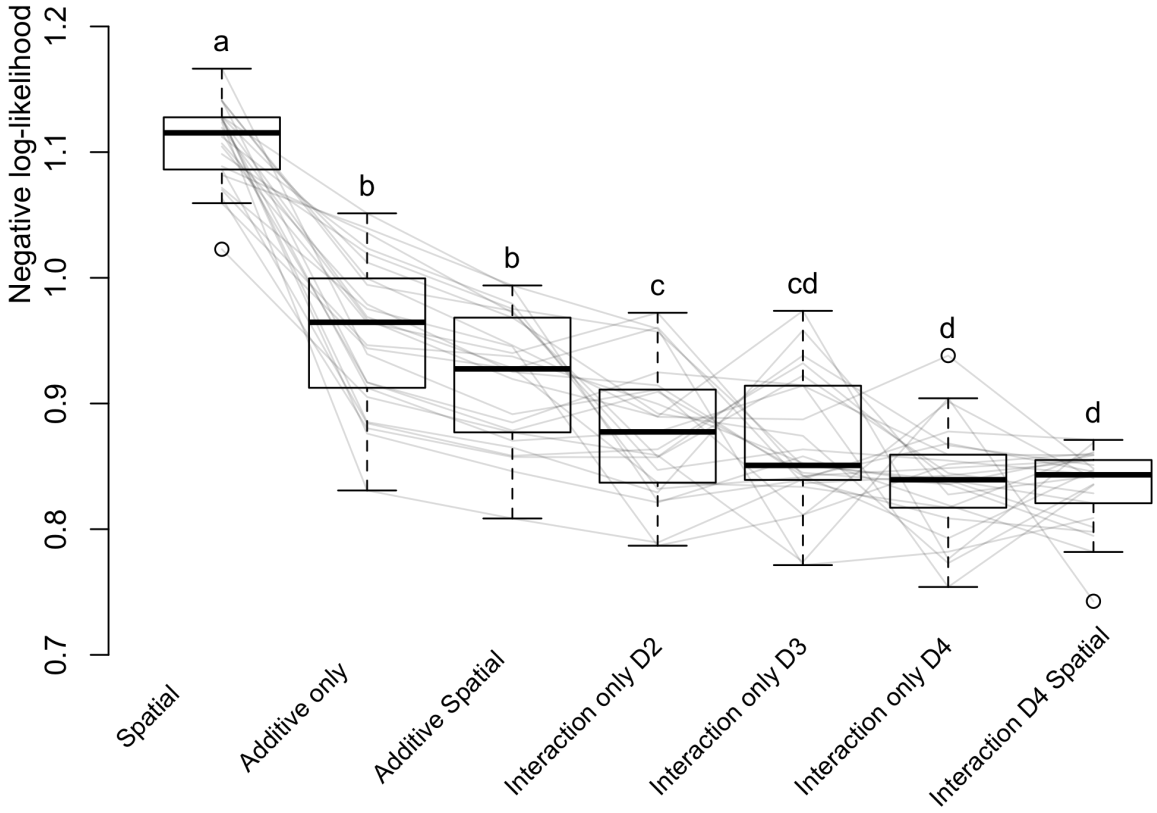


Figure C15: Model formulation comparison, with box edges indicating 25 and 75th quartiles, mean in solid black line. Lower negative log-likelihood values indicate better performance. Gray lines are the 25 bootstrapped model runs. Letters indicate significant difference between the model formulations.

C.2 Additional results

C.2.1 Marginal effects of variables on seedling occupancy

The marginal effects for many variables were similar for both seedling groups. In Figure C16, we show the marginal effects on seedling occupancy with both groups combined.

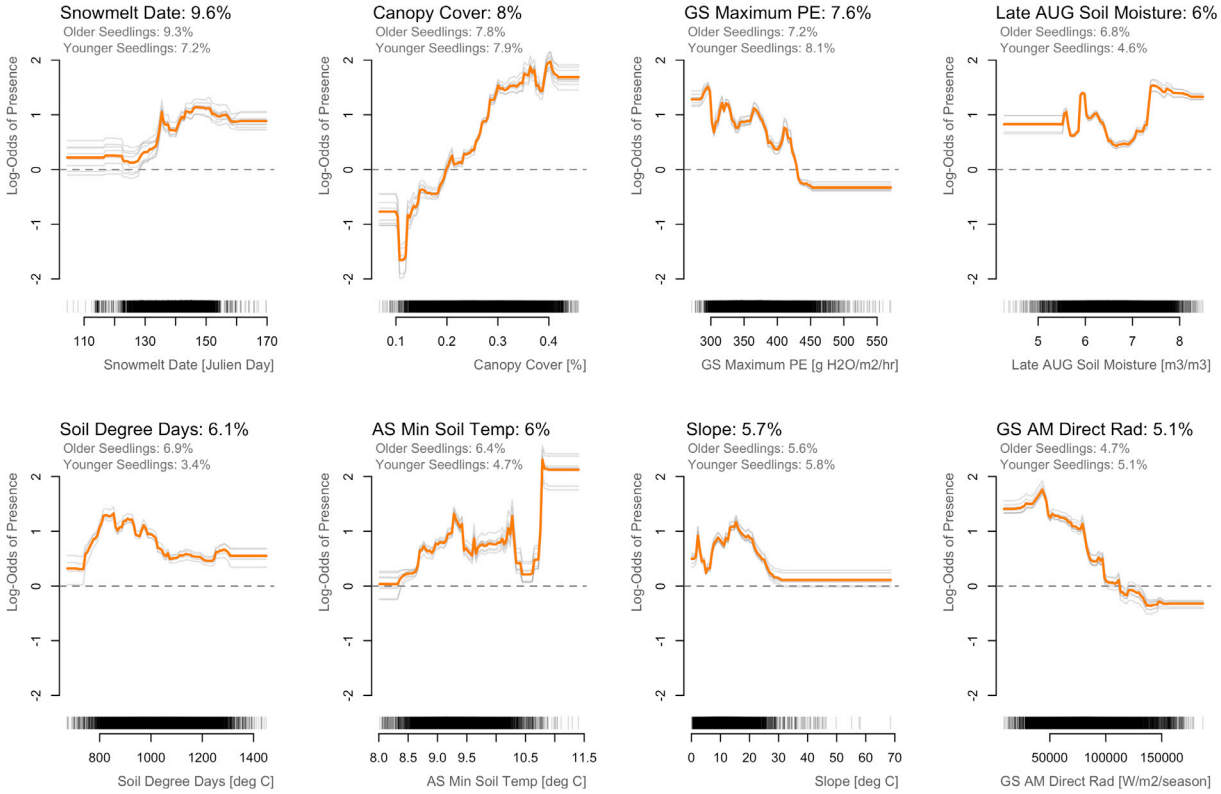


Figure C16: Marginal effects of selected variables the Older and Younger Seedling groups combined. Marginal effects for each variable combination are shown in gray and the mean effects are shown in orange (n=8 for all variables, excepting Late AUG Soil Moisture, Soil Degree Days, and AS Min Soil Temp which have n= 4). Variable representation in the study site is indicated by the graduated bar at the bottom; high representation (black) and low representation (white). Due to the nature of boosted classification tree models, these effects should be interpreted as loosely describing a trend [Merow *et al.* 2014] and care should be used when assessing responses at values with low representation.

C.2.2 Sensitivity of relative importance to variable configuration

We calculated the relative importance of each variable for all 8 variable configurations, for the Older and Younger Seedling groups. For the Older Seedlings (Figure C17a), there is a strong tradeoff in relative variable importance between Snowmelt Date and the Soil Temperature group variable. Related variables, GS Maximum PE, Canopy Cover, and AS Min Soil Temp, are not as affected as Snowmelt Date, suggesting that Snowmelt Date may represent the effects of temperature on seedling occupancy. However, it is unclear from this analysis whether the effect of Snowmelt Date is a purely temperature effect or is also coupled to water availability.

For the Younger Seedlings (Figure C17b), the included soil profile variable affects several other variables. The relative importance of Solid Woody Cover, Seed Density, Snowmelt Date, and GS

AM Direct Rad are all reduced when Depth to Mineral is included instead of Organic Layer Depth. The relative influence of Aspect on the other hand increases.

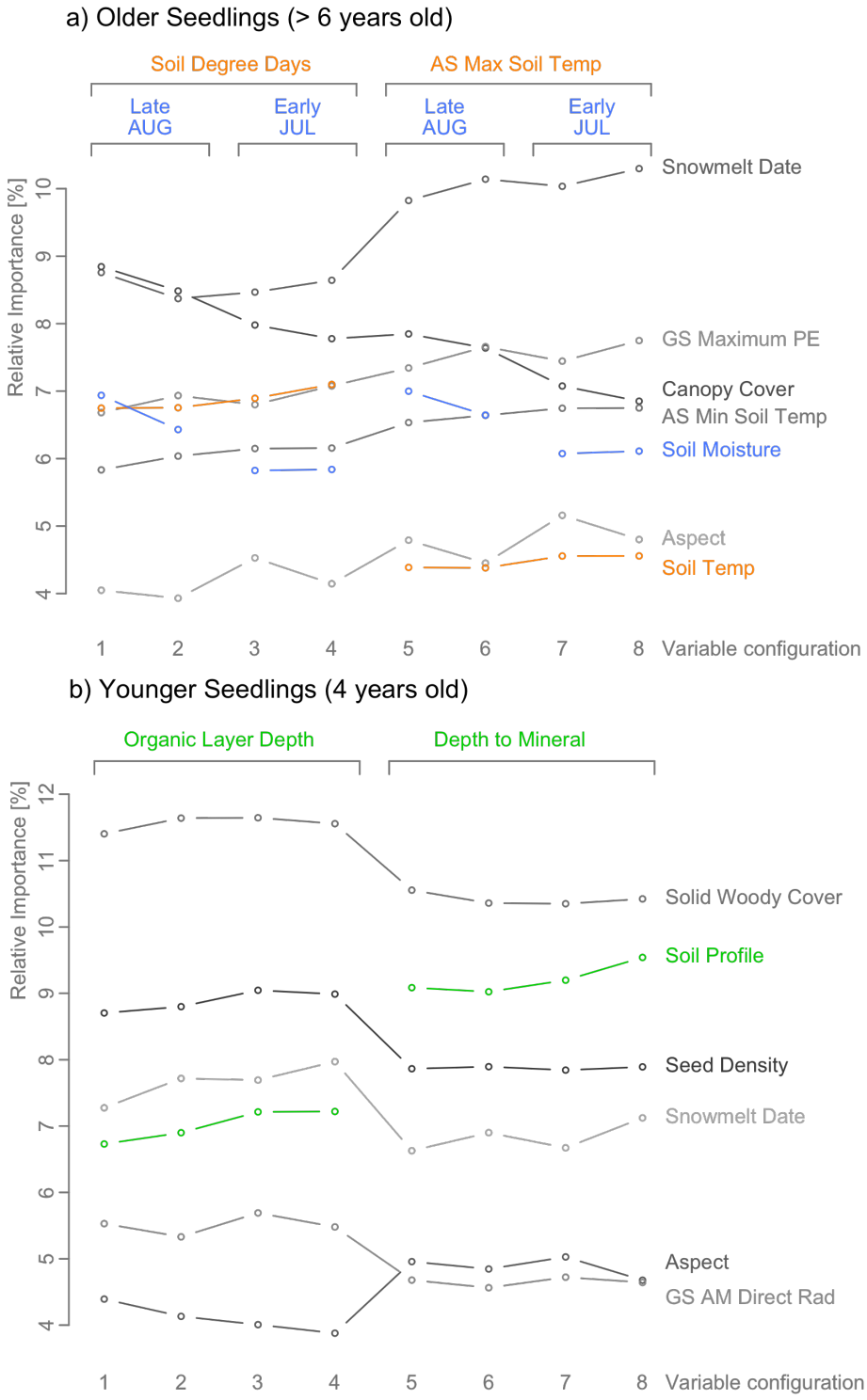


Figure C17: Selected relative importance of related variables for the 8 variable combinations along the x-axis. For the (a) Older Seedlings, soil temperature (orange) and soil moisture (blue) variables are highlighted to illustrate tradeoffs primarily with Snowmelt Date. For the (b) Younger Seedlings, soil profile (green) is highlighted to illustrate tradeoffs with other variables.

C.2.3 Mortality rates

We predicted habitat suitability in each gridcell location based on the tree seedling occupancy of seedlings that had survived the entire study period, *i.e.,* a seedling death occurring within the study period did not inform the model. Thus, we can assess the validity of the model by comparing observed mortality with predicted habitat suitability. We observed our expectation that mortality rates would decrease with increasing suitability. We present this finding in chapter 3 with Figure 3.6. We include an alternate visualization here in Figure C18. Instead of the number of seedlings on the y-axis, we show the number of gridcells with a presence at the beginning of the study period (2010). For both seedling groups, in locations with higher suitability, mortality within the majority of gridcells is not 100%; rather some seedlings survive. For Younger seedlings, gridcells with seedlings present in 2010 are fairly even across habitat suitability. Very high mortality rates (> 75%) decimate tree seedlings in unsuitable habitats (probability of presence < 50) so that very few had survived by the study end.

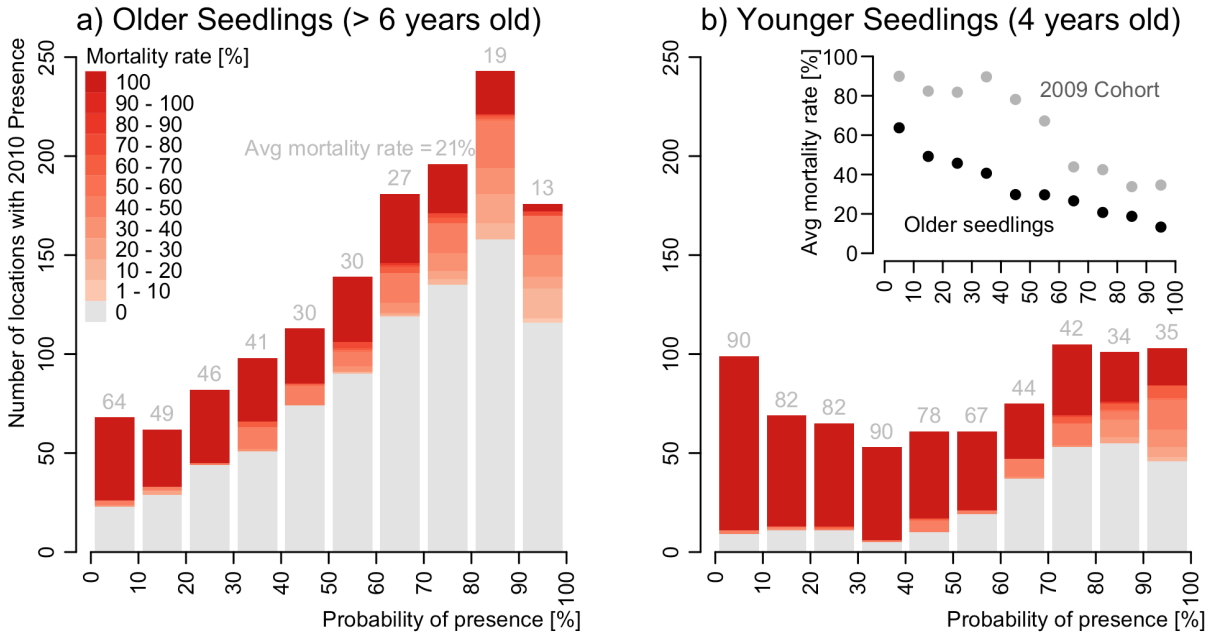


Figure C18: Per capita mortality rates for each gridcell with a seedling present at the beginning of the study period plotted by their predicted habitat suitability (probability of presence) for (a) Older and (b) Younger Seedlings. Each gridcell is colored by its mortality rate. The average mortality for the suitability interval is shown. Inset figure shows average mortality rate versus the habitat suitability (probability of presence).

C.3 References

Akima *et al. (*2013). Fortran code by H. Akima R, port by Albrecht Gebhardt, aspline function by Thomas Petzoldt interp2xyz, enhancements and corrections by Martin Maechler. akima: Interpolation of irregularly spaced data. R package version 0.5-11.

Clark, J.S., Silman, M., Kern, R., Macklin, E. & HilleRisLambers, J. (1999). Seed dispersal near and far: Patterns across temperate and tropical forests. *Ecology*, **80**, 1475–1494.

Delta-T (2014). User Manual for the Profile Probe type PR2. http://www.delta-t.co.uk. Accessed February 11, 2011.

Eschtruth, A.K. & Battles, J.J. (2008). Deer herbivory alters forest response to canopy decline caused by an exotic insect pest. *Ecological Applications*, **18**, 360–376.

Frazer, G.W., Canham, C.D., and Lertzman, K.P. (1999). Gap Light Analyzer (GLA), Version 2.0: Imaging software to extract canopy structure and gap light transmission indices from true-colour fisheye photographs, users manual and program documentation. Copyright © 1999: Simon Fraser University, Burnaby, British Columbia, and the Institute of Ecosystem Studies, Millbrook, New York.

Gonsamo, A., Walter, J-M.N. & Pellikka, P. (2011). CIMES: A package of programs for determining canopy geometry and solar radiation regimes through hemispherical photographs. *Computers and Electronics in Agriculture*, **79**, 207–215.

Gordon, D. T. 1970. Natural regeneration of white and red fir ... influence of several factors, PSW–58. USDA Forest Service.

Hothorn, T., Mueller, J., Schroeder, B., Kneib, T. & Brandl, R. (2011). Decomposing environmental, spatial, and spatiotemporal components of species distributions. *Ecological Monographs*, **81**, 329–347.

Kreylos, O., Bawden, G.W., and Kellogg, L.H. (2008). Immersive Visualization and Analysis of LiDAR Data, in: Bebis, G., et al. *ISVC 2008, Part I* LNCS 5358, Springer-Verlag Berlin Heidelberg, 846–855.

Macfarlane, C. (2011). Agricultural and Forest Meteorology. *Agricultural and Forest Meteorology*, **151**, 833–840.

Merow, C., Smith, M.J., Edwards, T.C., Jr, Guisan, A., McMahon, S.M., Normand, S., Thuiller, W., Wüest, R.O., Zimmermann, N.E. & Elith, J. (2014). What do we gain from simplicity versus complexity in species distribution models? *Ecography*, **37**, 1267–1281.

R Core Development Team. 2013. R: A language and environment for statistical computing. R Foundation for Statistical Computing, Vienna, Austria. URL http://www.R-project.org/

Westman, W.E. (1987). Aboveground biomass, surface area, and production relations of red fir (Abies magnified) and white fir (A. concolor). *Canadian Journal of Forest Research*, **17**, 311–319.

Appendix D: Supplemental information for Chapter 4

D.1 Terrestrial laser scanning field campaign

In choosing which instrumentation to use, I had to satisfy two requirements: (1) the instrument and associated equipment could be carried the 4.5 km (2.8 miles) and 300m (1000 ft) of elevation gain up and back from my field site and (2) more importantly, I needed someone with experience to train me or help me use it. Luckily, Toby, a fellow graduate student who first introduced me to the technology, was working with such an instrument and was available for hire. For these reasons, it was an easy decision to work with the I-Site 4400 instrument, but regardless, the capabilities of the instrument would structure the entire data collected. In this way, like the hemispherical photos, the data is theory-laden prior to collection. I also had to organize supporting equipment. We would need access to a total station with which we could accurately geo-reference the scanner locations and scan start directions, as well as a reference datum. I was able to borrow the USFS's total station (CTS-2, Topcon Positioning Systems, Inc., Tokyo, Japan) that I used to set up a reference datum while surveying the locations of 2,600 seedlings in the study site.

I could not scan my study site alone. First and foremost, I could not efficiently work all the instrumentation single-handedly; and secondly, I could never have transported all the equipment to the study site. Even with Toby, my field assistant, and myself, we each lugged roughly ~50+ pound backpacks up and back to the site. We planned a 5-day campaign: the first day we would pick up the scanner at the park entrance, followed by 3 days in the field scanning. The fifth day I would transport the scanner to a company rep in Sacramento.[1] It was a tight schedule because I could only afford 3 days of the equipment rental at $900/day — the educational rate — a large amount for a graduate student piecing together research funding[2].

On day 1, after picking up the equipment in a suitcase-sized Pelican case and driving almost to our base camp, we checked the equipment. We were missing a critical piece — a tribrach, the part that attaches the scanner to a tripod. We could not jerry rig this or complete the scans without it. Unfortunately, we were halfway up the mountain with no cell reception and it was 3pm. We scrambled to get to the USFS offices, where I was able to contact my USGS local support team. No luck. Perhaps fortuitously, I had met the Sequoia National Park Forester during the previous season when I was checking out the potential study possibilities. Once I tracked down his number, he thankfully answered his phone and suggested I call a small surveying company in a tiny town an hour and a half down the mountain. They had an old but functioning tribrach! This owner of the surveying company was hesitant to rent it to us, but eventually he agreed, leaving it outside his door after hours. I successfully made the 3-hour round trip that evening to acquire the critical piece. We were lucky to secure this piece in time to scan the next day.

---

[1] By driving the equipment to Sacramento, I saved $700 on overnight shipping and was not charged for a 4th day of rent.

[2] My USGS supporters paid for one day of scanning so that I could scan their adjacent 100m x 100m study site.

The first day of fieldwork we excitedly left camp with fresh legs, arriving at the field site at ~8am. We started right away, scanning as follows. Toby scouted the area determining potential scan locations. Having never used this equipment before, it was critical that we had his expertise at assessing how the scanner would see the forest. Recall that the scanner cannot see through solid objects so it takes skill and practice to set up a series of scanning locations that will capture the majority of surface features, especially in a complex system like a forest, whose trees, complex topography, and boulders create many occlusions. Toby also had to chose locations that had line of site to our total station reference sites, a series of 22 known, marked locations along the study plot that were already geo-referenced. The total station serves two purposes: geo-locating each scanner location in order to stitch the many scans together and setting the initial starting point of the scan. *I.e.,* at the beginning of each scan we pointed the scanner at the total station so it would start scanning in a known direction. Other scanners have different techniques for stitching scans together. None is necessarily better than another, but our reliance on the total station shaped the resulting point cloud representation. With my field assistant and I operating the total station and all three of us moving equipment along the study site, we quickly settled into a routine.

By around early-afternoon, we had 23 scans; however, our batteries were spent, and even worse, we had only traveled 100 of 600 meters along the study site. At this rate we would not finish scanning the entire site within the next 2 days. We headed down to the Wuk[3] so that we could look at a few of our scans on my 5-year old Micron PC. We stitched together ~10 scans, which pushed the PC's computational limits. We learned that we could space out our scanning while retaining enough resolution to capture the stand structure and fine topography, especially within the study site. We would sacrifice full scans of trees outside the study site[4] and instead aim to capture them at least from one side. This would minimally yield an arc of the tree trunk with which we could model as a circle to estimate the diameter at breast height (DBH) – the standard forestry measure of tree size. We would, however, not focus on capturing the canopy structure in detail. We also planned a new battery strategy. It entailed ultra conservative efforts to save the tablet interface battery (lowest screen brightness which made it even harder to view the screen in natural light), precision like teamwork between the three of us, and a midday trip down the mountain to recharge both the control tablet and the 2 scanner batteries. Additionally, we would start scanning at dawn — a 3:30am wake up call.

The next two days were no doubt two of the most challenging days of my life physically and mentally. We carried out our plan successfully, scanning 38 scans on day 2 covering 300m more of plot length and 29 scans on the third day completing the remaining 200m. The following are a few notable observations from the field effort. We finished scanning the 38th scan on the second day in complete darkness. Unlike us (the human operators), the scanner works perfectly fine without visible light. We were able to use our headlamps, reflecting off of the total station prism, to geo-reference the scanner location. Finally, at the end of the second, longest day, we returned after dark to a raging party at base camp, where the USFS trail crews were celebrating the end of their seasonal work. At day's end, the scanner batteries needed recharging. One battery recharged while we ate and readied other gear; I left the second battery charging overnight. We secured part of a table in a cabin housing the beer fridge by taping it off crime-scene style with duct tape and napkins reading "Do not put your beer here! Fragile equipment." I was relieved when all of the equipment was still there and functioning in the morning.

[3] Wuksachi Lodge in Sequoia National Park has free internet in the lobby plus nice tables at which to sit.

[4] I needed information about adult trees outside the study plot to model seed dispersal.

Appendix E: Supplemental information for the Conclusions

E.1 Coarse-scale air temperatures have mixed heterogeneity characteristics

For monthly aggregated metrics in CA and CO, heterogeneity is commensurate with climate change projections (Figure E1), with standard deviations ranging from ~1-2°C indicating ~4-8°C difference over 95% of the landscape. As we observed in fine-scale heterogeneity, the aggregated monthly metrics suggest less heterogeneity than observed in the daily values. Heterogeneity is more-or-less constant as average conditions warm, excepting the average monthly minimum temperature in CA, which increases as average conditions warm. These heterogeneity values and patterns are similar when looking at average monthly minimum temperature in the coolest growing season month (October) and average monthly maximum temperature in the warmest month (July), both common metrics used in projection tools (Figure E2). The relationship in CA for the average monthly maximum temperature during July (slope = 0.079 +/- 0.02 (95% CI); R^2 = 0.4), however, is nearly twice as high compared to that across all months (Figure E1a).

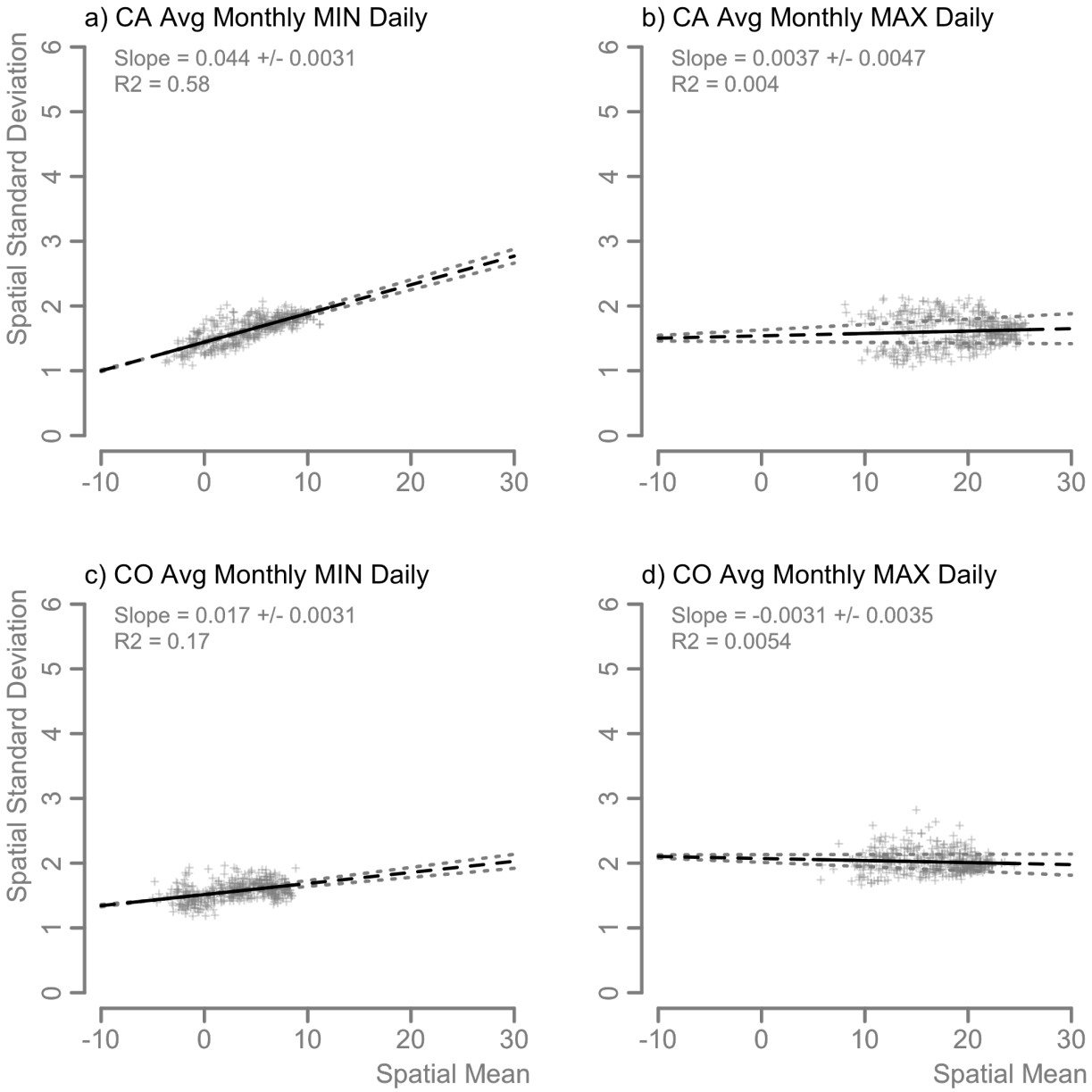


Figure E1: Air temperature heterogeneity (spatial standard deviation) versus average conditions (spatial mean) for average monthly minimum (a and c) and maximum (b and d) temperatures at mountainous elevations in Colorado Rockies, CO (c-d), and Californian Sierra Nevada, CA (a-b), during the typical growing season (May-Oct).

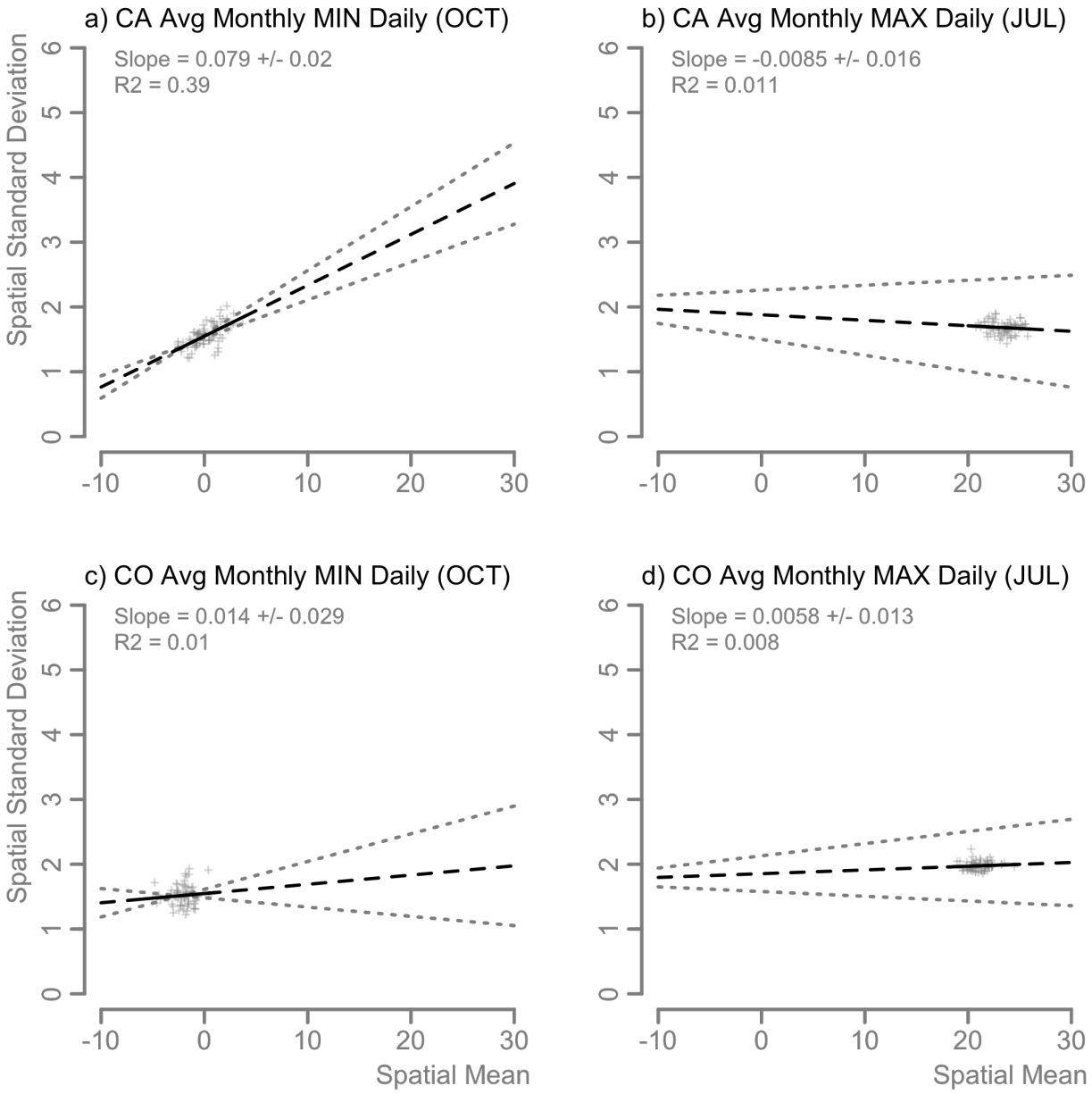


Figure E2: Air temperature heterogeneity (spatial standard deviation) versus average conditions (spatial mean) for average monthly (a and c) minimum temperature in the coolest growing season month (October) and (b snd d) maximum temperatures in the warmest month (July) at mountainous elevations in Colorado Rockies, CO (c-d), and Californian Sierra Nevada, CA (a-b).

E.2 Calculation of and additional results for analog energy input days

I used the NREL National Solar Radiation Database for Fresno, CA, the closest location to my SEKI study site in the California Sierra Nevada, for 1990 as an example year.[1] I first calculated the average amount of radiation received each day in W/m^2 using the Global Horizontal (GH)

[1] http://rredc.nrel.gov/solar/old_data/nsrdb/1961-1990/hourly/, accessed November 10, 2014

Radiation Data Value, which is the total amount of direct and diffuse solar radiation received on a horizontal surface. I then found the nearest day with an IR increase specified by the RCP scenario. As this observed value is the amount of radiation hitting the top of the vegetative canopy or soil surface, I adjusted the difference to account for an albedo of 0.2. I calculated both the forward and backward time to the nearest days. Figures E3–E5 show analog days for RCP2.6, 6, and 8.5.

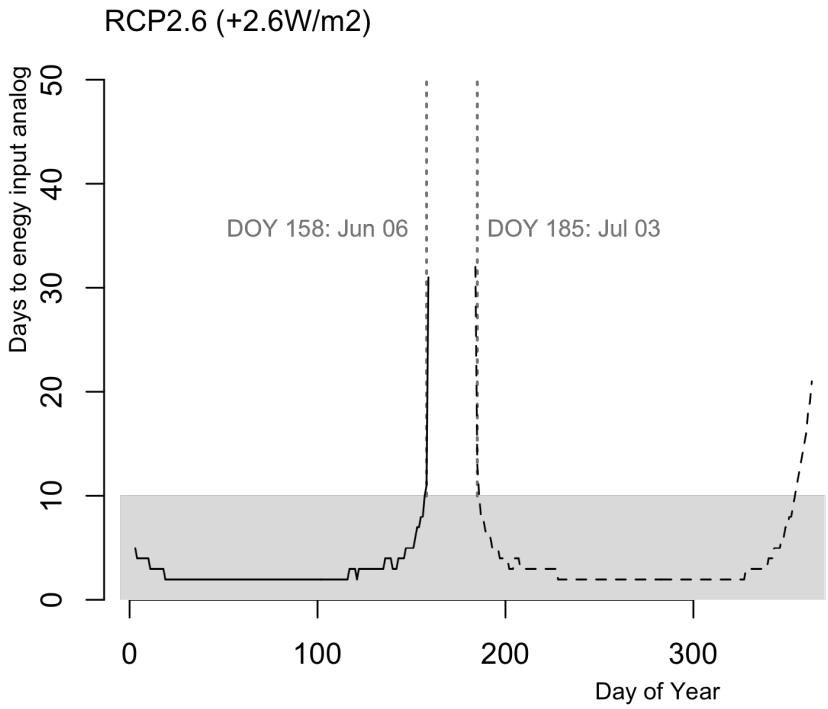


Figure E3: The number of days to an energy input analog for each day of year (Julian date) is shown for an energy difference of 2.6 W/m² (RCP2.6). Days forward to the analog are the solid line, and days backward are dashed. Analog days within 10 days (gray shade) are likely to have similar vegetative and soil moisture conditions. Data shown is an illustrative example from radiation observations at Fresno, CA, in 1990 with an albedo adjustment of 0.2.

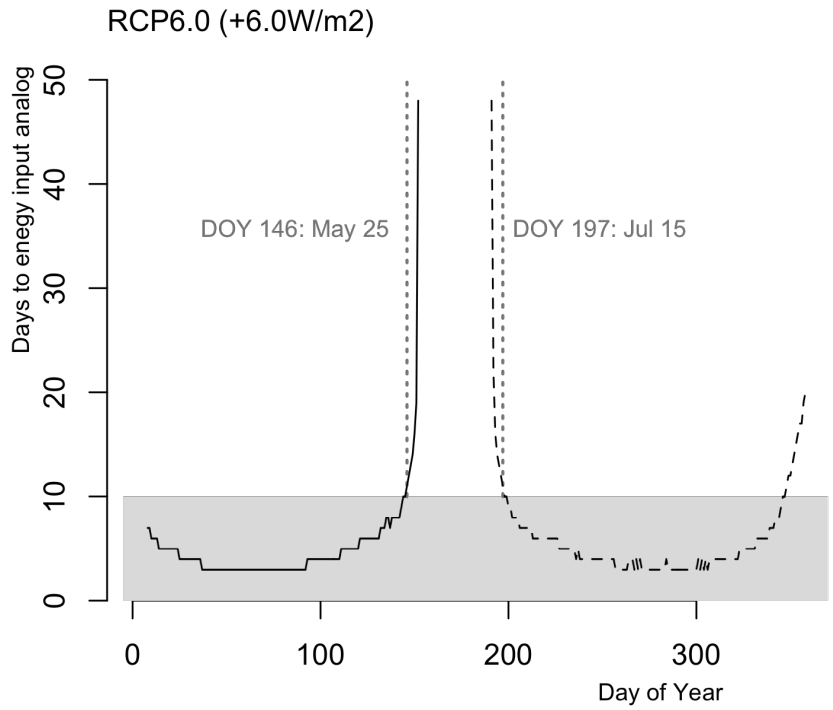


Figure E4: The number of days to an energy input analog for each day of year (Julian date) is shown for an energy difference of 6 W/m² (RCP6.0). Days forward to the analog are the solid line, and days backward are dashed. Analog days within 10 days (gray shade) are likely to have similar vegetative and soil moisture conditions. Data shown is an illustrative example from radiation observations at Fresno, CA, in 1990 with an albedo adjustment of 0.2.

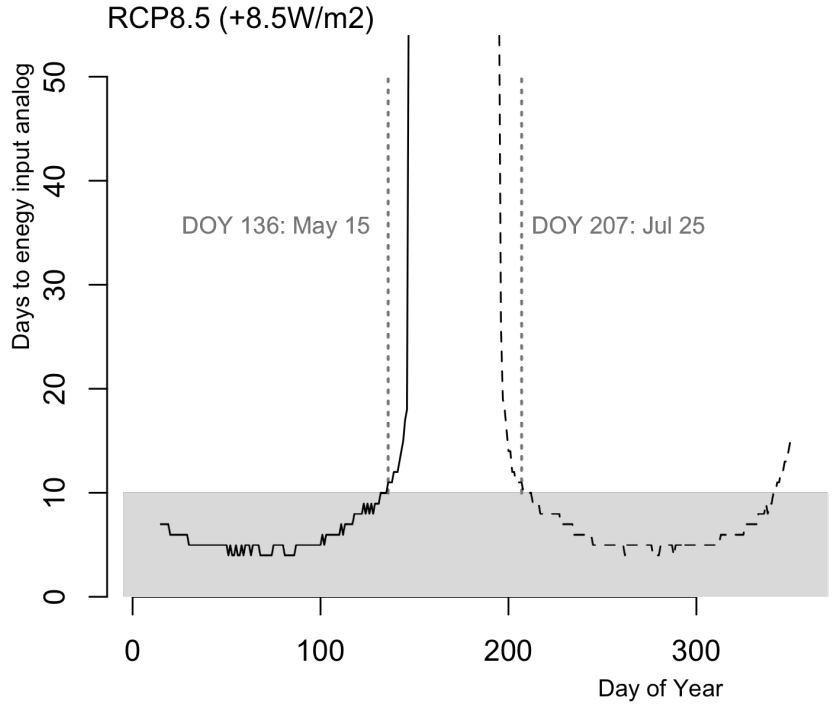


Figure E5: The number of days to an energy input analog for each day of year (Julian date) is shown for an energy difference of 8.5 W/m² (RCP8.5). Days forward to the analog are the solid line, and days backward are dashed. Analog days within 10 days (gray shade) are likely to have similar vegetative and soil moisture conditions. Data shown is an illustrative example from radiation observations at Fresno, CA, in 1990 with an albedo adjustment of 0.2.